

Electronic Thesis and Dissertation Repository

8-12-2022 12:00 PM

Using Craters to Study Carbon and Nitrogen Compounds on Icy Worlds

Joshua E. Hedgepeth, *The University of Western Ontario*

Supervisor: Neish, Catherine D., *The University of Western Ontario*

A thesis submitted in partial fulfillment of the requirements for the Doctor of Philosophy degree in Geophysics

© Joshua E. Hedgepeth 2022

Follow this and additional works at: <https://ir.lib.uwo.ca/etd>

Recommended Citation

Hedgepeth, Joshua E., "Using Craters to Study Carbon and Nitrogen Compounds on Icy Worlds" (2022). *Electronic Thesis and Dissertation Repository*. 8744.
<https://ir.lib.uwo.ca/etd/8744>

This Dissertation/Thesis is brought to you for free and open access by Scholarship@Western. It has been accepted for inclusion in Electronic Thesis and Dissertation Repository by an authorized administrator of Scholarship@Western. For more information, please contact wlsadmin@uwo.ca.

Abstract

Icy worlds have attracted a lot of attention from planetary scientists over the last century because they exhibit an array geophysical and chemical processes that both contrast and mirror those on terrestrial worlds. Nitrogen and carbon molecules drive some of the most unique processes on these icy worlds. The central focus of this thesis is to study the role of carbon and nitrogen rich molecules in different icy body environments, both geologically and chemically. These molecules drive fluvial and aeolian processes on Titan in the form of organic dunes and methane rain, and on Pluto, these molecules are present as volatile ices that go through cycles of deposition and sublimation. On both Pluto and Titan, these molecules also contribute to the formation of prebiotic compounds on the planet surfaces. These prebiotic compounds are often associated with the origin of life on Earth and may have provided the building blocks of life on icy worlds. I investigate both the geologic impact of these molecules and the evolution of the prebiotic chemistry when mixed with liquid water in an impact crater melt lens. Organics that mix into impact crater melt lens are shown to freeze throughout the depth of the melt sheet. The highest concentration is near the center, but it is likely that there will be large enough concentrations for the Dragonfly mission to sample. The concentration will vary, based on the buoyancy of the organic impurity. Hydrolysis can also delay when more complex organic molecules appear, but in most cases, I predict Dragonfly should be able to detect more complex organics within the first meter of the ice. I find that geologic impact of nitrogen and carbon molecules on Pluto creates a range of crater morphologies from entirely degraded to anomalously deep, and there does not appear to be a correlation between the surface age and the level of degradation. There is also a longitudinal relationship with the level of crater degradation, which may hint that Pluto underwent a significant change in conditions in its past (e.g., polar wander).

Keywords

Titan, Pluto, Surface Processes, Impact cratering, Volatiles, Organics Astrobiology

Summary for Lay Audience

Icy worlds have beautiful water ice surfaces that often hide a liquid ocean underneath. Some of the most majestic surfaces are those covered with a lot of unique chemistry such as carbon and nitrogen rich molecules. My work studies how these molecules shape the surfaces of these planets, and I also study how these molecules might fuel the origin of life itself. Titan, Saturn's largest moon, is covered in giant sand dunes made of organics, and its surface is covered with riverbeds and lakes made, not by water, but of liquid methane. On Pluto, the temperatures are so cold that molecules like methane freeze to form unstable ices that can slowly collect like snow or turn to gas. On both Pluto and Titan, the sun's light can transform these molecules into more complex prebiotic chemistry. Prebiotic chemistry is the stuff that scientists suspect led to the origin of life on Earth, so some scientists think icy worlds might have had their own origin of life because of it. I study how the surface is changing, and I study how the origin of life may have happened and where we could find evidence of it. Pluto's surface ranges from very old to very young. There are parts of Pluto that appear virtually new and other parts that are almost entirely erased. This shows that there is a wide range of things happening on Pluto that vary regionally; this contrasts with past work that showed Titan has few regions of ancient surface. For the origin of life, one of the best places to look is in impact craters where a large liquid water lake would have formed when the crater was new. Any evidence of the origin of life that forms in it is going to freeze into the frozen lake as it cools, with the highest concentration in the center. NASA's upcoming Dragonfly mission is going to Titan to sample one of these frozen impact lakes, and my results suggest they should be able to find at least some early signs of life-like molecules (like the amino acids found in life).

Co-Authorship Statement

Chapter 1 was prepared and written by myself, with two rounds of edits and suggestions by my advisor, Dr. C. Neish.

Chapter 2 was prepared and written by myself, with several round of edits and suggestions by my advisor, Dr. C. Neish. It also received edits and suggestions from the coauthors, J. Buffo, C. Chivers, and B. Schmidt. J. Buffo and C. Chivers provided guidance and aid in implementing the model, but the results were all produced and processed by myself. The work has been published in the Planetary Science Journal.

Hedgepeth, J.E., Buffo, J.J., Chivers, C.J., Neish, C.D. and Schmidt, B.E., 2022. Modeling the Distribution of Organic Carbon and Nitrogen in Impact Crater Melt on Titan. The Planetary Science Journal, 3(2), p.51.

Chapter 3 was prepared and written by myself, with two rounds of edits and suggestions by my advisor, Dr. C. Neish. J. Buffo and C. Chivers provided guidance and aid in implementing the model, but the results were all produced and processed by myself. C. Chivers updated the Chivers et al. (2021) model to incorporate hydrolysis, but I consulted with him on the approach that was taken for implementing the change.

Chapter 4 was prepared and written by myself, with several rounds of edits and suggestions by my advisor, Dr. C. Neish. It also received edits and suggestions from the coauthor V. Bray. C. Neish and V. Bray consulted in the analysis of the results, but I performed all the methodology and processing of the results.

Chapter 5 was prepared and written by myself, with one round of edits and suggestions by my advisor, Dr. C. Neish.

Acknowledgments

I would like to begin by thanking the Technologies for Exo-Planetary Science (TEPS) NSERC CREATE program and NSERC's New Frontiers in Research Fund for supporting this work. I have had the privilege to participate in the TEPS program since I was a Masters student. It has allowed for me to connect with the broader Canadian planetary science community in way that was not just educational, but a great opportunity to build friendships and connections that I will carry with me as I move forward in my academic career.

I would like to thank the Dragonfly Astrobiology and Surface Composition Working Group for feedback of our preliminary work. Furthermore, I would like to extend thanks to the entire Dragonfly team for the opportunity to work on the team as a student associate. It has helped foster my love of Titan, astrobiology, and planetary exploration. The Dragonfly team laid the groundwork that much of my work is built on. It is rewarding to be a part of such a massive endeavor, but there is also an immense pleasure to be doing this work and to connect with the Dragonfly team members themselves. They are all kind and inviting, stewarded by the phenomenal principal investigator, Dr. Zibi Turtle.

I would be remiss not to thank my advisor as well, Dr. Catherine Neish. She has guided me throughout my graduate career, allowing me to forge my own path and provided support when needed. She has allowed me to pursue the things that interested me most, even when there was no obvious benefit to my research. She fostered my love of astrobiology long before I knew it would be a central point of this work, but I suppose she was playing the long con, preparing me in ways even I didn't realize. Furthermore, she did all this in a productive and supportive manner. She provides her students dignity and respect—something that is sorely lacking by many in academia. She helped me realize my own potential and helped me discard my feelings of imposter syndrome. As the first person in my family to go to college, I never thought I would have what it took to get through graduate school. While I have put in the work needed to get here, we cannot ignore the importance and benefits of a good support system.

With that, I must also thank my undergrad advisor (and collaborator on my PhD work), Dr. Britney Schmidt. As important as Catherine has been in my development, my time with

Catherine was at a stage in my career where I was committed to pursuing a career in planetary science. When I first started working with Britney, I was going out on a limb. I left the field I had spent my entire undergrad studying (mechanical engineering) to venture into planetary science. I was not just unsure whether I was prepared for the change, I was unsure if my motivations were more than just a passing interest. I was at a very precarious stage in my life where I very easily could have gone down, what I recognize now, would have been a very unhappy path for myself. Britney was inviting and supportive. She fostered my love for planetary science, and she constantly communicated how great I was doing. I could have very easily been directed to a less supportive scientist, and I am immensely grateful to Britney for everything she did to help me transition into the planetary science community. In fact, she was a strong supporter of me continuing on to work with Catherine. She recognized that we would work well together, and she was right. Britney has continued to be supportive, encouraging me when I had the initial idea to study Titan melt lens, and even now as I venture into the work force, she continues to support me every way she can.

Of course, my work studying Titan's melt lens would not be possible without Dr. Jacob Buffo and Dr. Chase Chivers, both former students of Britney's. When I started this project, I was still wrestling with intense feelings of inadequacies and doubted whether I belonged in the planetary science community. Both Jacob and Chase have been nothing but supportive. They have been a pleasure to work with, patiently tolerating my barrage of questions and ideas relating to their work and my own. I am especially thankful to Jacob because he was one of Britney's graduate students when I started working with her in my undergrad, and, at the time, it was easy to compare myself and become intimidated. However, he only ever treated me as an equal, even when I was an undergrad. Collaborating with him has helped me appreciate my own value to the scientific community as he has transitioned from mentor to colleague. While Chase and I started graduate school at the same time, his support and kindness also helped me appreciate my own abilities as well.

I also want to thank Dr. Trina Ray and Dr. Scott Edgington because it was their public outreach, at a gaming convention no less, that ignited my interest in planetary science and

convinced me to reach out to Britney. I have always loved space, but it was hearing them speak about Cassini that made me decide to pursue planetary science.

I also must thank many of the teachers I had throughout grade school. These go far beyond my science teachers. In fact, most are not scientists. What they are, and were, is kind and supportive, fostering my love of learning, science, literature, and math. Thank you to all my teachers with a special thanks to: Rhonda Johnson, Stacy Holland, Caroline Oliver, and especially my 5th grade teacher, Lily Page, who forced me to repeat my 5th year, and in doing so, ironically sparked my love of learning and math.

Lastly, I would like to thank my family and closest friends for their support and companionship: Shannon Hibbard, Carolina Rodríguez Sánchez-Vahamonde, Jahnavi Shah, Brian Villamizar, Leah Sacks, the Neish-lab members, and many others as well.

I would also like to give special thanks to the friends I formed at Georgia Tech, who helped me feel welcome in the planetary science community: Julian and Mary McAdams, Amelia Winners, Raj Lal, Heather Chilton, Gabe Eggers, and many others.

Landmark Acknowledgement

I would like to acknowledge that the University of Western Ontario is located on the traditional lands of the Anishinaabek, Haudenosaunee, Lūnaapéewak and Attawandaron peoples. Western is on lands connected with the London Township and Sombra Treaties of 1796 and the Dish with One Spoon Covenant Wampum. This land has always been the home of these Indigenous Nations. We must continue to acknowledge their connection to the land we inhabit.

Table of Contents

Abstract.....	ii
Summary for Lay Audience.....	iii
Co-Authorship Statement.....	iv
Acknowledgments.....	v
Landmark Acknowledgement	vii
Table of Contents.....	viii
List of Tables	xii
List of Figures.....	xiii
Chapter 1.....	1
1 Introduction: Icy Worlds.....	1
1.1 A Brief History	1
1.2 Geologic History.....	3
1.2.1 Titan	4
1.2.2 Pluto	5
1.2.3 Summary.....	7
1.3 The Impact Cratering Process.....	8
1.3.1 Formation.....	8
1.3.2 Morphology.....	9
1.4 Impact Cratering as a Window into Surface Processes	11
1.4.1 Crater Dating.....	11
1.4.2 Forms of Crater Degradation	12
1.4.3 Measuring Crater Degradation.....	16
1.5 The Astrobiology of Icy Worlds.....	19
1.5.1 Subsurface Oceans	19

1.5.2	Cryovolcanism, Tectonics, and Other Endogenic Processes	21
1.5.3	Impact Cratering	23
1.5.4	Dragonfly	24
1.6	Summary	26
1.7	References.....	27
Chapter 2	48
2	Modeling the Distribution of Organic Carbon and Nitrogen in Impact Crater Melt on Titan	48
2.1	Introduction.....	48
2.2	Ice-melt Model.....	51
2.2.1	Initial Conditions	51
2.2.2	1D Ice Model	55
2.2.3	Application to Titan	59
2.3	Results and Discussion	64
2.3.1	1D Concentrations	64
2.3.2	2D Distributions.....	68
2.3.3	Implications and Future Work	73
2.3.4	Assumptions.....	76
2.4	Conclusions.....	78
2.5	References.....	80
Chapter 3	89
3	The role of hydrolysis in the emplacement of organic molecules into melt sheets on Titan	89
3.1	Introduction.....	89
3.1.1	Dragonfly	89
3.1.2	Sampling Biomolecules	90

3.1.3 Titan Melt Sheet.....	92
3.2 Methodology	94
3.2.1 Sea Ice Model	94
3.2.2 Modeling Hydrolysis	97
3.3 Results and Discussion	100
3.3.1 Glycine Distribution.....	100
3.3.2 Hydrolysis.....	105
3.3.3 Modeling Mixtures.....	109
3.4 Conclusions.....	110
3.5 References.....	112
Chapter 4.....	120
4 Impact Crater Degradation on Pluto	120
4.1 Introduction.....	120
4.1.1 Geologic History.....	122
4.1.2 Crater Modification.....	126
4.2 Methodology.....	131
4.2.1 Crater Mapping.....	131
4.2.2 Crater Morphology.....	132
4.3 Results.....	134
4.4 Discussion.....	139
4.4.1 The Mantling of the Venera and Hayabusa Groups.....	139
4.4.2 The Degraded Craters of Cthulhu Macula	141
4.4.3 The Anomalously Deep Craters of Cthulhu Macula and the Wright Group	142
4.4.4 The Lightly Degraded Terrains of Pluto.....	143
4.4.5 Summary.....	144

4.5	Conclusions.....	144
4.6	References.....	146
Chapter 5	155
5	Discussions and Conclusions.....	155
5.1	Discussion.....	155
5.1.1	The emplacement of organics into a freezing ice layer.	155
5.1.2	Impact Crater Degradation on Pluto.....	158
5.2	Future Work.....	161
5.2.1	Experimental studies on organics in a Titan melt sheet.....	161
5.2.2	Modeling impacts into heterogeneous ice layers.....	163
5.3	Conclusions.....	164
5.4	References.....	166

List of Tables

Table 2.1. All variables used in the text, along with their definition, values, and units.	58
Table 2.2. The constitutive equations developed by Buffo et al. (2020) with the corresponding constants used to fit to our results from the SF2 model. These equations are fit to the data for 1 ppt to 250 ppt. *Indicates values determined using extrapolation and averaging.	67
Table 3.1. The organic-specific variables used for modeling glycine and HCN in the SF2 and Chivers et al. (2021) models, along with their definition, values, and units. All other variables are unchanged from, and defined in, Hedgepeth et al. (2022).	95
Table 3.2. The constitutive equations developed by Buffo et al. (2020) with the corresponding constants used to fit to our glycine results from the SF2 model. Each equation represents a specific domain of the data set (Buffo et al., 2020; Chivers et al., 2021; Hedgepeth et al., 2022). The first equation represents the concentration as a function of depth. The second equation represents the shallow (or high thermal gradient) domain of the results as a function of thermal gradient. The third equation represents the deep (or low thermal gradient) domain of the results as a function of thermal gradient. These equations are fit to the data for 1 ppt (0.1%) to 210 ppt (21%, saturation point).	104
Table 4.1. Relative depth statistics by geologic group, ranked by estimated surface age (oldest to youngest). N is the number of craters in that group, R is the relative depth, avg is the average, std is the standard deviation measured using the ‘std’ function in MATLAB, and max is the maximum.	136

List of Figures

Figure 1.1. A schematic view of Titan's methane cycle modified from Lunine and Atreya (2008). Timescales are rough estimates. Methane clathrates or aquifers are a possible source of methane to maintain the atmosphere, cycling between the poles to form lakes (blue). Cycling begets rainfall (red), and methane is ionized by radiation to form organic hydrocarbons (purple) that settle out to potentially form the dunes (peach/coral).....	5
Figure 1.2. A cylindrical projection of Pluto from the “Pluto New Horizons LORRI MVIC - Global Mosaic” (300 mpp). It is overlain with outlines of its geologic terrains and a dashed circle of the position of the Sputnik impact. Figure from White et al. (2021).....	6
Figure 1.3. Crater parameters for a simple (A), complex (B), and multi-ringed basin (C) impact craters. Modified from Turtle et al. (2005).....	10
Figure 1.4. Modeling of an impact into basalt bedrock on Mars (brown) with water ice (blue) overlaying the bedrock at different thicknesses. Figure modified from Senft and Stewart (2008) to show 2 s and 200 s after impact. Thin ice layers mute the rim topography, and thicker ice layers cover the shallower basin that forms in the basalt bedrock.....	11
Figure 1.5. Impact crater degradation by aeolian deposition (left) and by fluvial erosion and deposition (right), as modeled on Mars. Figure modified from Forsberg-Taylor et al. (2004).	14
Figure 1.6. Simulation of the fluvial degradation of Isis crater on Ganymede, a proposed pristine analogue for the degraded crater Soi on Titan. The topography of the crater is presented through time, with the A-A' profile shown through time in the final box. Figure from Neish et al. (2016).....	14
Figure 1.7. a) Ksa crater seen in Cassini SAR images overlain by stereo topography. The rim (R) and floor (F) topography are used to statistically derive the rim and floor heights in past works. b) Ksa crater in stereo topography split into 8 profiles, spaced equally at azimuths between 0 and 180 degrees from the north-south axis. Figure from Hedgepeth et al. (2020).	18

Figure 1.8. An illustration of the European ocean, its ice crust, and the underlying rock-ocean interface. This illustration highlights a range of processes that contribute to the habitability of the Europa system. Figure from Hand et al. (2016)..... 20

Figure 1.9. Sotra Facula, a hypothesized cryovolcano, visualized in Cassini RADAR (a) and the same image overlaid with Cassini VIMS (b) showing where water (blue) is suspected to have mixed with organic dunes (brown) to produce the unknown composition (green). Figure from Neish et al. (2018)..... 22

Figure 1.10. Example cross-section of a complex crater on Titan with the crater ejecta is shown in green and the crater melt pond is shown in blue. The red box shows what a melt pond (of some height, h), may look like with a given surface temperature (T_s), melt temperature (T_m), and basal ice temperature (T_b). Figure is from Hedgepeth et al. (2022) with parameters equal to Titan conditions. 24

Figure 1.11. Synthetic aperture radar (SAR) image of Selk crater (left) with color-coded SARTopo (Stiles et al., 2009) and a yellow landing ellipse denoted in yellow. The linear traverse to the northeast from the landing ellipse (right) indicating the geologic features and their estimated topographies. Modified from Barnes et al. (2021)..... 25

Figure 2.1. Example cross-section of a complex crater on Titan. The crater ejecta is shown in green and the crater melt pond is shown in blue. The red box zooms in on one section of the melt pond of thickness h (m) overlain on a fractured bedrock of water-ice (white). Initial temperatures used in the model are shown for the melt (T_m), bedrock ice (T_b), and surface (T_s)..... 52

Figure 2.2. The SF2 model tracks the mushy water-ice interface (red box) within the finite region of space H (m) where each increment (dz) represents a volume average over some finite length (m). When the upper most increment of the water-ice interface reaches a critical porosity (here $\phi \leq 0.05$), the water-ice interface (H) shifts downward by one spatial increment (dz) and the concentration of the frozen increment ($\phi \leq 0.05$) is assumed to be trapped in the ice and remains constant throughout the remainder of the simulation. This process continues throughout the depth of the pond h (m), beginning at some interface depth d (m). The model

tracks the freeze front where buoyancy will drive impurities out of the ice. For salt, the model tracks the chamber roof's freezing front as imaged here, but for HCN the model is tracking the floor's upward propagating freeze front. In our work, the model runs bottom-up because HCN is less dense than water and ice, resulting in upward gravity drainage (see text for more details).

..... 61

Figure 2.3. (Top) A diagram illustrating the SF2 model outputs of the concentration of HCN entrained in ice at a given thermal gradient, visualized across a range of increasing concentrations in the melt (color coded). The points n_i show how the concentration of HCN trapped in ice will change as the freeze front progresses. (Bottom) We visualize four temporal steps of the $\sim 273\text{ K}$ water melt (blue) freezing into ice (white). As time (t_n) passes, the warmer ice insulates the melt, reducing the thermal gradient at the freeze front. Simultaneously, the concentration of HCN in the melt (C_n) is increasing. 63

Figure 2.4. Concentration of HCN (ppt) in the frozen melt pond, for initial concentrations of 1 ppt (0.1%, yellow) to 250 ppt (25%, dark blue), at different thermal gradients (a), and depths (b). The SF2 model results are shown with black points (they appear as disjointed lines because the spatial resolution is so fine). The analytical fits from Buffo et al. (2020) are applied to our data, where solid lines are fits formed using SF2 results, and dashed lines are formed by extrapolating from the lower concentration fits (see Table 2.2 and text). 66

Figure 2.5. Results of the Chivers et al. (2021) model showing how much HCN freezes into the ice with depth, measured through the center of the frozen melt sheet, for four different melt sheet thicknesses, (a) 10 m, (b) 25 m, (c) 50 m and (d) 100 m and for initial concentrations of 0.1% (1 ppt, dark blue line with 'x' at each point), 1.5% (15 ppt, light blue line), 2.5% (25 ppt, green dash line), 5% (50 ppt, yellow dotted line), and 7.50% (75 ppt, red double dash line). Results are taken for an 80 km crater..... 69

Figure 2.6. We use the Chivers et al. (2021) heat transfer model to calculate the final concentration distribution for an 80 km diameter crater (crater floor $\sim 55\text{ km}$) using an initial concentration of 1 ppt (0.1%) and an assumed melt pond of 100 m depth. On the left is the concentration of HCN in each element, in the middle is the temperature of each element, and on the right is the phase of each element (0 is frozen, 1 is liquid). The model uses the thermal

gradient on the interface boundary along with the constitutive equations of Table 2.2 to determine what the concentration will be upon freezing (see text for further explanation). .. 71

Figure 2.7. The time needed to freeze each element along the melt sheet depending on its thickness. Times are taken from the centermost grid cells of the melt sheet, for an 80 km crater starting with 1 ppt of HCN, where timescales are measured at spatial steps throughout the melt sheet that range from 1 m to 5 m (depending on the melt sheet thickness)..... 73

Figure 3.1. The concentration of glycine (ppt) in ice forming over an infinite ocean, for initial concentrations of 1 ppt (0.1%, yellow) to 210 ppt (21%, saturation point, dark blue), at thermal gradients (a), and depths (b) observed at the surface of Titan. The SF2 model results are shown with black points (they appear as disjointed lines because the spatial resolution is so fine). The analytical fits from Buffo et al. (2020) are applied to our data, where solid lines are fits formed using SF2 results (see Table 3.1) 102

Figure 3.2. The results of the Chivers et al. (2021) model showing the concentration of glycine frozen into the ice with depth. The melt sheet is modeled for initial glycine concentrations of 5 ppt (0.5%, blue dashed line), 10 ppt (1%, turquoise solid line), 50 ppt (5%, yellow double-dashed line), and 100 ppt (or 10%, red dotted line) and for melt thicknesses of 10 m, 50 m, 100 m, and 250 m. Results are taken for an 80 km diameter crater (with a crater floor that is ~55 km in diameter)..... 105

Figure 3.3. The Chivers et al. (2021) model is ran for HCN (top) and glycine (bottom) with an added mass flux representing the hydrolysis of HCN into glycine (i.e., mass is removed from the HCN model and added to the glycine model through time). We consider a range of half-lives from 1 year in blue to 50 years in orange, and a threshold concentration for HCN to hydrolysis into glycine of 0% (left), 50% (middle), and 100% (right) of the initial 25 ppt (2.5%) concentration. Results are taken for an 80 km diameter crater (with a crater floor of diameter ~55 km)..... 107

Figure 4.1. A cylindrical (top) and polar (bottom, *latitude* $\geq 50^\circ$) projection of Pluto from the “Pluto New Horizons LORRI MVIC - Global Mosaic” (300 mpp). It is overlain with red outlines of its geologic terrains as defined by White et al. (2021). Image courtesy New

Figure 4.2. Expected crater morphologies proposed for layered ice on Pluto, assuming different volatile ice layer thicknesses. The immediate post-impact morphologies are compared to the surface before impact and after short- and long-term degradation by escape erosion and relaxation. Note that “short” and “long” are relative terms, which vary based on the volatile ice (e.g., the long-term relaxation stage of N₂ will occur much faster than CH₄; Stern et al., 2015). Craters that form in a sufficiently thick volatile ice layer (i.e., $h > d$, where h is volatile ice thickness and d is crater depth) are assumed to form a traditional crater shape. Craters that form in thinner volatile ice layers are assumed to act like craters forming in water ice overlaying the much stronger basalt bedrock on Mars (see text for more details; Senft and Stewart, 2008). Escape erosion may degrade every crater, but it will most significantly affect craters that form into thicker volatile ice layers ($h > 0.5 * d$). For a moderate volatile thickness ($d > h > 0.5 * d$), the weaker volatile ice is expected to flow back and cover the more rigid water ice basin. Escape erosion would eventually reveal a shallower than normal water ice crater. For very thick volatile layers ($h > d$), escape erosion will act in conjunction with relaxation to degrade the crater..... 130

Figure 4.3. An example impact crater shown in the LORRI mosaic of Pluto overlaid with the DEM. The craters were identified by their circular shape, elevated rims, central peaks, flat floor, and ejecta (if present)..... 132

Figure 4.4. Crater topography is mapped using the 8-profile technique (top). An example topographic plot of profile A-A’, where the x axis is distance from the crater center (bottom). The red square identifies the rim, and the blue triangle indicates the crater floor..... 134

Figure 4.5. Global mosaic of Pluto’s complex impact craters ($D \geq 15 \text{ km}$) near the equator ($-50^\circ < \textit{Latitude} < 50^\circ$) colorized by relative depth where redder (higher R) are the most degraded and bluer craters are the most well-preserved. The map is shown without (top) and with (bottom) the geologic group boundaries. Crater diameters are proportional to circle size

but are not to scale. Note, craters with $R < 0$ are shown as 0 (see Figure 4.7 and text for details).
..... 137

Figure 4.6. Polar map (50°N to 90°N latitude) of Pluto's north pole with impact craters ($D \geq 15 \text{ km}$) mapped and colorized by relative depth. The map is shown without (left) and with (right) the geologic group boundaries. Redder (higher R) craters are the most degraded and bluer craters are the most well-preserved. Crater diameters are proportional to dot size but not to scale. 138

Figure 4.7. Relative depths of craters in the southeast region of Cthulhu Macula and the western region of the Wright group, with relative depths less than 0 shown to demonstrate the cluster of anomalously deep craters in this region 138

Chapter 1

1 Introduction: Icy Worlds

The planetary science community is fascinated with icy worlds. Over the last century, icy worlds have begun to receive more attention as we learn about their dynamic geomorphology and potential to harbor life (National Academies of Sciences, Engineering, and Medicine, 2018, 2022). They present an array of fascinating geologic, geophysical, and chemical processes that are both in stark contrast to terrestrial processes (e.g., viscous relaxation of icy topography, Parmentier and Head, 1981; Dombard and McKinnon, 2006) and remarkably similar to those observed on terrestrial worlds (e.g., dunes and rivers on Titan, Lorenz et al., 2006; Lorenz and Lunine, 2009; Le Gall et al., 2011; Burr et al., 2013; Neish et al., 2016). The central focus of this thesis is to study the role of carbon and nitrogen compounds in different icy body environments, both geologically and chemically. On the early Earth, carbon and nitrogen rich compounds likely played an essential role in the origin of life (Miller, 1953). These organic compounds may provide the building blocks of life on icy worlds across the solar system. These same organic compounds are intimately connected to the geology of icy worlds as well. In this chapter, I present a broad overview of icy worlds, to understand how each of these processes present themselves across the solar system.

1.1 A Brief History

Astronomers were unaware of the existence of icy worlds prior to the invention of telescopes capable of observing them. Telescopes revealed the structure of the solar system (Kepler, 1596, 1609), and as they improved, astronomers began to discover the icy bodies within it. Galileo Galilei revolutionized astronomy and discovered multiple worlds, including the icy satellites of Jupiter, aptly named the Galilean moons (Galilei, 1613). Galileo also discovered the rings of Saturn but mistook them for satellites. It was nearly 50 years later that Christiaan Huygens corrected Galileo's mistake and recognized that the satellites were in fact rings, and Huygens discovered Saturn's largest moon Titan (Huygens, 1659). Soon after, Giovanni Cassini would go on to discover several of Saturn's other icy satellites (Cassini, 1673). While little was known about the satellites, they proved

essential in Isaac Newton's understanding of gravity (Newton, 1687). It would be over a century before William Herschel and William Lassell would go on to identify multiple icy moons of Saturn, Uranus and Neptune (Herschel, 1785, 1787, 1790; Lassell 1847). Then in the early 1900s the search for Planet X (i.e., Pluto) would begin until it was ultimately discovered in 1930 by Clyde Tombaugh (Tombaugh, 1946). This discovery propelled the search for other distant objects, leading to Gerard Kuiper's proposal of the Kuiper Belt, a massive collection of volatile icy bodies beyond Neptune (Edgeworth, 1943; Kuiper, 1951). The existence of the Kuiper Belt would not be confirmed until late into the 20th century (Jewitt and Luu, 1993).

In the 20th century, the Pioneer and Voyager spacecrafts were sent into the outer solar system, giving the first close up glimpses of the icy moons (Hall, 1974; Smith et al., 1981, 1982). The mission was soon followed by a dedicated mission to Jupiter and the Galilean moons named Galileo (Meltzer, 2007). The next major mission was Cassini-Huygens, which sent a probe and orbiter to study the Saturn system, including Titan, Enceladus, and its other icy moons (European Space Agency, 1988; Matson et al., 2003). The Cassini-Huygens mission studied Saturn for nearly a decade and a half. A dedicated mission has yet to occur for the ice giants Uranus and Neptune, but in 2015, the New Horizons spacecraft revealed the beautiful and complex surface of Pluto (Stern et al., 2015a, 2017). The mission has since continued to study other bodies in the Kuiper belt, but its primary goal was to better understand Pluto.

Now, several major missions are heading to study the moons of Jupiter and Saturn within the next decade. Europa Clipper will build on the results of the Galileo mission to answer many of the questions that remain about Europa's ice shell (i.e., its thickness and dynamics) and habitability (Phillips and Pappalardo, 2014). JUICE is a mission by the ESA that is also returning to the Galilean moons to orbit Ganymede and study the Jupiter system at large (Grasset et al., 2013). Meanwhile, Dragonfly will build on the Cassini-Huygens Mission to understand Titan's prebiotic chemistry and the origin of life in the universe (Lorenz et al., 2018; Barnes et al., 2021). Other missions are on-going or in the works from a number of international agencies (e.g., JUNO, Bolton et al., 2017). These are likely only the beginning, with new missions to the outer solar system expected in the next decade (a

mission to Uranus received specific priority in the most recent Decadal Survey, National Academies of Sciences, Engineering, and Medicine, 2022).

Much has been learned about the icy worlds of the outer solar system in the last half a century. These moons went from being specks of light in the sky to dynamic worlds with unique histories. The ongoing missions illustrate how much is left to be discovered, but the missions up to now have revolutionized our understanding of these different worlds.

1.2 Geologic History

Each icy world is unique because the conditions on these worlds vary across the solar system. Ices that exist within the “ice line”, the point where water ice is stable at the surface, are localized regions where temperatures are abnormally low (e.g., the poles of Earth and Mars or the shadowed regions of Mercury, Byrne, 2009; Rubanenko et al., 2019). Beyond Jupiter, water ice becomes stable, but temperatures can vary due to heating (e.g., by tidal forces, Sotin et al., 2009). The further from the sun, however, temperatures continue to drop, and the properties of water ice change, affecting the geologic processes acting upon it. Beyond the ice giants, other volatile ices begin to form, further complicating the processes that are shaping the surface.

The geologic history is unique for each world because their environmental conditions and surface properties are different. The type of processes that occur on icy worlds are consistent, but the abundance and magnitude may vary. One major factor is tectonics and other endogenic crustal processes that lead to resurfacing (Figueredo and Greeley, 2004; Kattenhorn and Hurford, 2009). Another major process is viscous relaxation, or the flattening of large-scale topographic differences driven by gravity (Parmentier and Head, 1981; Dombard and McKinnon, 2006). There are, however, some especially unique worlds whose geologic histories are complicated by other contributing factors. In this work, I will explore two of these worlds: 1) Titan, because its carbon and nitrogen rich atmosphere creates a unique and complex system of processes, and 2) Pluto, because it has an abundance of carbon and nitrogen ices and organics across its surface that modifies the water ice bedrock in unique ways.

1.2.1 Titan

Saturn's largest moon, Titan, is unique for a range of reasons. It is the largest moon of Saturn (the second largest in the solar system, Zebker et al., 2009), it has a water ice ocean, shielded by ~100 km ice crust (Tobie et al., 2005, 2006), and is covered by a dense nitrogen rich atmosphere. This atmosphere is what allows for much of Titan's unique processes (Lunine and Atreya, 2008). The atmosphere is composed primarily of nitrogen (96%) with a significant fraction of methane (~4%) (Lindal et al., 1983; Tomasko et al., 2005). Overtime, cosmic and solar radiation ionizes and dissociates these primary molecules of Titan's atmosphere. Then, they recombine, and form longer chained complex organic and nitrogen bearing compounds. These are thought to further combine to form Titan's thick haze layer and rain down upon the surface (**Figure 1.1**, Thompson and Sagan, 1992; Lorenz et al., 2006; Soderblom et al., 2007; Le Gall et al., 2011; Barnes et al., 2015; Hörst, 2017).

These organics shape Titan's surface in two primary ways, through fluvial and aeolian processes. The organic particles (<microns in size) fall out of the Titan atmosphere to coat the surface (Lorenz et al., 2006; Janssen et al., 2016). In addition to this coating, large organic sand dunes span across Titan's equatorial region (Lunine and Lorenz, 2009). It is proposed that the organic haze particles may source the dunes (Lorenz et al., 2006; Soderblom et al., 2007; Le Gall et al., 2011), but the small (<microns in size) haze particles need to undergo additional steps to become the 100s of microns sized sand particles that are needed for the dunes to form (Lunine and Lorenz, 2009; Barnes et al., 2015).

In addition to the dunes, liquid methane (and possibly ethane) modifies the surface in the form of lakes and rivers (Stofan et al., 2007; Lorenz et al., 2008; Lunine and Atreya, 2008; Burr et al., 2013). More than 10% of the surface is covered in river networks (Lorenz et al., 2008; Burr et al., 2009, 2013). In fact, the Huygens probe landed in a likely riverbed or flood plain (Tomasko et al., 2005; Towner et al., 2006). While the plain was flat, some models estimate these rivers can be 100s of meters deep (Poggiali et al., 2016). These rivers are global with the largest population of methane is at the poles (Stofan et al., 2007). The methane cycle that creates these features simultaneously feeds the creation of the organics that form the dunes. This feedback loop degrades Titan's surface, leading to a young

surface (**Figure 1.1**) ($\leq 1 G. y.$, Neish and Lorenz, 2012; Hedgpeth et al., 2020). While Titan undergoes the same processes as other icy world (i.e., impact cratering, faulting, and cryovolcanism, Lopes et al., 2007, 2013; Hedgpeth et al., 2020; Burkhard et al., 2022), the evidence of these processes has been mostly degraded by the dunes and methane cycle (Hedgpeth et al., 2020).

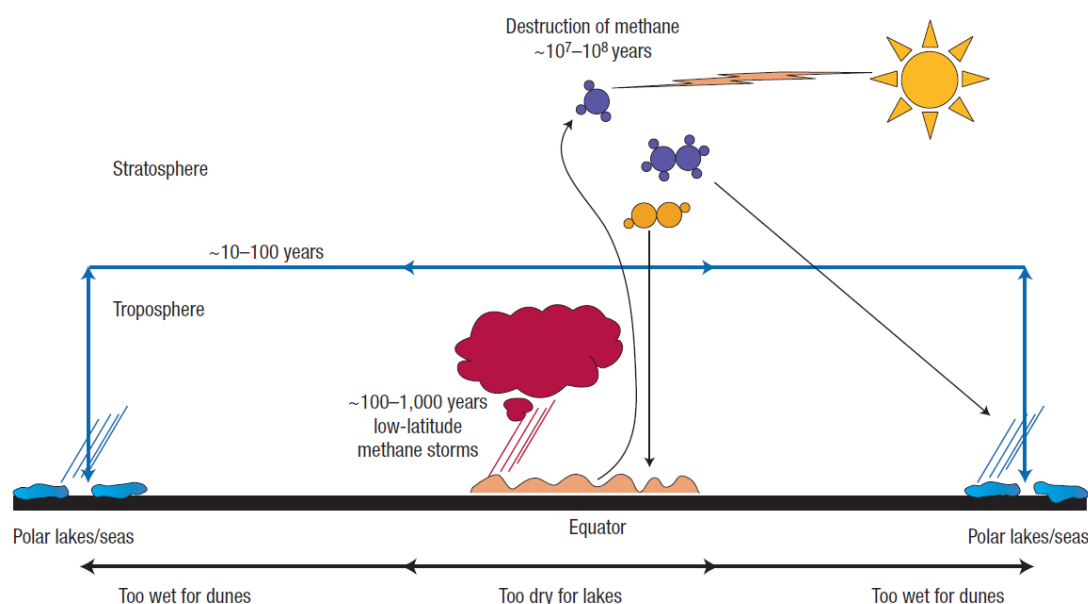


Figure 1.1. A schematic view of Titan's methane cycle modified from Lunine and Atreya (2008). Timescales are rough estimates. Methane clathrates or aquifers are a possible source of methane to maintain the atmosphere, cycling between the poles to form lakes (blue). Cycling begets rainfall (red), and methane is ionized by radiation to form organic hydrocarbons (purple) that settle out to potentially form the dunes (peach/coral).

1.2.2 Pluto

Little is known about the surface of most Kuiper belt objects. New Horizons is the only spacecraft to observe these objects up close, and it has only visited Pluto and its moons (in 2015) and 486958 Arrokoth (in 2019). However, Arrokoth and the other Kuiper belt objects are not as geologically active as Pluto given their small size (Porter et al., 2017). Like the other Kuiper belt objects, Pluto has an abundance of volatile ices and organic material that significantly affects the state of its surface (Bertrand and Forget, 2016; Binzel

et al., 2017; Forget et al., 2017; Grundy et al., 2018; Bertrand et al., 2018, 2019; Lewis et al., 2021). This has created a surface that ranges from very young, volatile-rich regions (e.g., Sputnik Planitia) to very old, volatile-poor regions (e.g., the dark, organic rich region known as Cthulhu Macula in the southern Burney group) (**Figure 1.2**) (Singer et al., 2021; White et al., 2021).

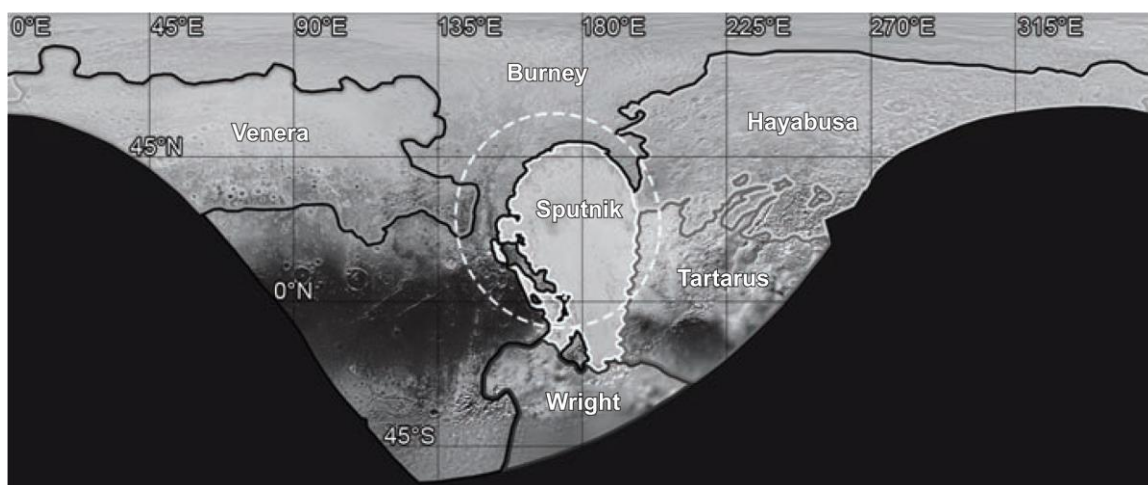


Figure 1.2. A cylindrical projection of Pluto from the “Pluto New Horizons LORRI MVIC - Global Mosaic” (300 mpp). It is overlain with outlines of its geologic terrains and a dashed circle of the position of the Sputnik impact. Figure from White et al. (2021).

The youngest terrains on Pluto are as young as 500 ky (McKinnon et al., 2016). Sputnik Planitia is filled with solid N_2 and CO that is estimated to be several kilometers thick, sufficient for convection in the pool of ice (McKinnon et al., 2016; Schenk et al., 2018). The next youngest region, the Wright group, is thought to be modified by cryovolcanism rather than the relaxation or erosion of its surface ices (Moore et al., 2016; Schenk et al., 2018; Nimmo and McKinnon, 2021; White et al., 2021; Singer et al., 2022). A rougher surface lies east of Sputnik Planitia in the Tartarus group with an age as young as 200 My old (Robbins et al., 2017; Singer et al., 2019, 2021; White et al., 2021). There is evidence of pitted terrain and sublimation erosion within these groups, but more extensive mantling (or layering) of volatile ices is found in Pluto’s oldest terrains.

Volatile ice layers are found in both Hayabusa and Venera groups. The Hayabusa group has muted topography and flat floors and valleys as strong evidence of long-term mantling of CH₄ ice in this region (Grundy et al., 2016; Howard et al., 2017b; Lewis et al., 2021; White et al., 2021). The mantle is estimated to have formed during Pluto's Middle Ages, with its precise age unclear (Howard et al., 2017b). The Venera group, east of Sputnik Planitia, also shows signs of long-term volatile ice mantling (White et al., 2021). Evidence suggests mantling was less extreme compared to the Hayabusa group, but it contains clear evidence of sublimation erosion (Howard et al., 2017b; White et al., 2021). Pluto's oldest group dates to near its formation (~4 Gy ago) and extends from the north pole to the south equatorial region (White et al., 2021). The southern Burney group contains Cthulhu Macula with few signs of modification and a thick dark layer of organic haze particles (Moore et al., 2016; Grundy et al., 2018; Schenk et al., 2018; Singer et al., 2019; Cruikshank et al., 2021; White et al., 2021; Earle et al., 2022). Fewer craters are found in the north than in Cthulhu Macula with evidence of past glaciation that likely occurred soon after the formation of Sputnik Planitia, when N₂ ice filled this putative impact basin (Bertrand and Forget, 2016; Moore et al., 2016; Howard et al., 2017a; White et al., 2019; Singer et al., 2019, 2021). Otherwise, volatile ice mantling seems likely, with modeling suggesting a net loss of volatile ice over the history of Pluto (Binzel et al., 2017; Bertrand et al., 2019).

1.2.3 Summary

Pluto and Titan are unique from other icy worlds in the solar system because of the additional complexity that arises from their abundance of nitrogen and carbon rich molecules. Icy moons like Enceladus and Europa have very active surfaces, with thin ice shells and possibly even rock-ocean interactions, and while this makes their surfaces young and their oceans of interest to astrobiologists, the same processes are possible on Titan and Pluto (McKinnon et al., 2021; White et al., 2021; Burkhard et al., 2022). However, these endogenic processes are curtailed on Titan and Pluto because of fewer heat sources that contribute to significantly different interior structures (Tobie et al., 2005, 2006; Nimmo et al., 2021). Endogenic processes likely played a larger role earlier in the lifespan of Titan and Pluto when the heat from formation was high (Canup et al., 2021; McKinnon et al.,

2021; Burkhard et al., 2022). However, these ancient features are less prominent today because the processes that arise from the abundance of carbon and nitrogen molecules erase them. This resurfacing is further reflected in the crater population that exists on Pluto and Titan compared to other worlds. A younger surface will have fewer craters, but the causes of crater degradation will be unique to the processes shaping the surface. Furthermore, the crater morphologies reflect the properties of the ice crust and a planetary body's interior (e.g., Passey and Shoemaker, 1982). It is, therefore, advantageous to investigate the crater population of these worlds more thoroughly.

1.3 The Impact Cratering Process

Impact craters are large depressions that form when celestial bodies impact the surface of another planetary body (Melosh, 1989). Impact cratering is ubiquitous across all worlds with solid surfaces, even those that show no evidence of it due to erosion or resurfacing. The abundance and morphology of a crater population reflects the physical and chemical properties of a planet, and it is thus an invaluable tool for understanding the processes on a planet's surface and interior.

1.3.1 Formation

Impact craters result from large projectiles colliding with a planetary surface at hypervelocities (10s of km/s) (Gault et al., 1968; Melosh, 1989; Osinski and Pierazzo, 2012). The impact process imparts high levels of energy into the surface, compressing and excavating the target material or bedrock (Osinski and Pierazzo, 2012; Osinski et al., 2012b). At impact, the surface is compressed as the kinetic energy of the projectile is converted to shock waves that propagate through the bedrock (Melosh, 2012). The shock wave propagates through the bedrock, dissipating with distance, but the impact imparts hundreds of GPa of pressure at its peak. At the highest levels of shock, bedrock vaporizes. As the shock wave dissipates, the bedrock is melted, and eventually, the bedrock is heated and fractured as the pressures diminish (Osinski et al., 2012a).

In a matter of seconds, the compression stage transitions into the excavation stage as the bedrock is moved up and out of the crater, in a ballistic trajectory that eventually re-impacts with the surface to form the ejecta (Osinski et al., 2012b). The crater may continue

to deform depending on the strength of the bedrock and the size of the crater. Larger complex craters experience significant crater collapse. Over longer timescales, target rock with weaker internal forces (i.e., having lower viscosity), will viscously relax on the order of 10s to 100s Ma depending on the viscosity of the bedrock which varies by composition and temperature (e.g., icy bodies; Dombard and McKinnon, 2006; Parmentier and Head, 1981).

1.3.2 Morphology

The three primary crater morphologies occur at increasing size (i.e., simple, complex and multi-ring basins, **Figure 1.3.**) (Melosh, 1989). Simple (bowl-like) craters create a parabolic profile. Complex craters reach a critical size that causes the walls to collapse and the interior to rebound, creating a crater with a flat floor, central uplift, and terraced walls. Multi-ring basins are the largest craters in the solar system and lack significant topography, identifiable mostly by their multi-ring nature. Realistically, these shapes are idealized, and crater morphologies vary even without modification from post degradational processes (e.g., due to preexisting topographic differences).

The morphology of craters may be further complicated when the impact bedrock is made of layers of significantly different material (**Figure 1.4;** Senft and Stewart, 2008). There are several terrestrial examples of stratified bedrock having no significant effect on the final crater morphology, but this is because the material properties do not differ significantly (e.g., Barringer crater; Shoemaker et al., 1974; Kring, 2007; Collins et al., 2008; Kenkmann et al., 2014). In contrast, modeling of crater formation into ice layers over rock on Mars and Earth suggests the material properties (principally the melting point) differ significantly enough to cause the final crater morphologies to change (Pierazzo et al., 1997; Senft and Stewart, 2008; Silber et al., 2021). The bedrock basalt is excavated and folded over the overlying ice layer (Senft and Stewart, 2008; Silber et al., 2021). When the ice layer is thin, the bedrock is exposed to form a traditional crater basin, but thicker ice layers flow back into the crater basin, potentially flattening its topography similar to marine impacts on Earth (and possibly Titan, Senft and Stewart, 2008; Neish and Lorenz, 2014; Silber et al., 2021; Bray et al., 2022).

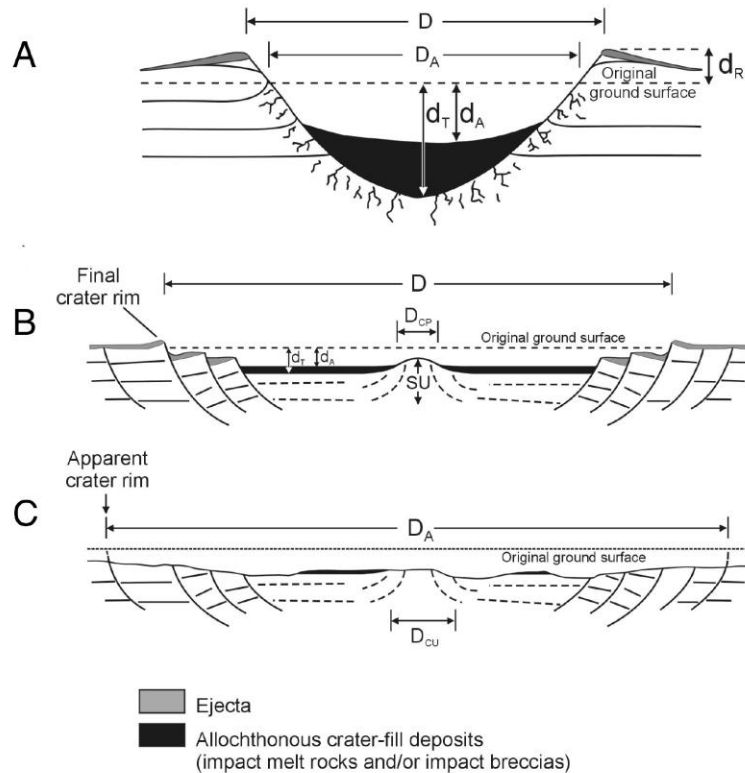


Figure 1.3. Crater parameters for a simple (A), complex (B), and multi-ringed basin (C) impact craters. Modified from Turtle et al. (2005).

The morphology of impact craters formed within stratified layers is important for icy worlds where different ice layers will exist. Craters that form on the icy moons of the gas giants are unlikely to present these morphologies (except for Titan where clathrates, wet sediment, and organic sedimentary layers also exist, Neish and Lorenz, 2014; Wakita et al., 2022). The moons that are likely to exhibit these morphologies are the moons of the ice giants (particularly Triton) and the Kuiper belt objects (Schenk et al., 2021). Pluto is known to have mantles (thick layers) of volatile ice on its surface now and in the past (Umurhan et al., 2021). More work is needed to understand crater formation into these layered ices. However, it is likely that stratified rock and ice-rock impacts on Earth and Mars are the two possible endpoints that stratified ice layers will follow during impact (Eluszkiewicz and Stevenson, 1990; Schenk and Zahnle, 2007; Schenk et al., 2021).

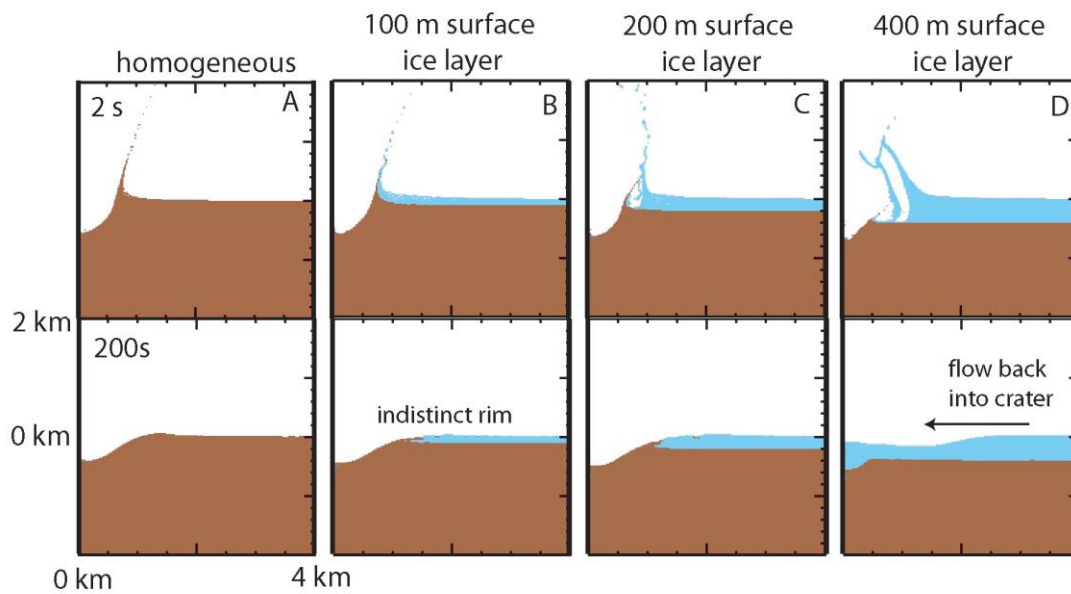


Figure 1.4. Modeling of an impact into basalt bedrock on Mars (brown) with water ice (blue) overlaying the bedrock at different thicknesses. Figure modified from Senft and Stewart (2008) to show 2 s and 200 s after impact. Thin ice layers mute the rim topography, and thicker ice layers cover the shallower basin that forms in the basalt bedrock.

1.4 Impact Cratering as a Window into Surface Processes

Impact cratering provides valuable constraints on the processes acting upon a planetary surface. Impact cratering provides a means to date the surface, and because the morphologies of impact craters are so well constrained, they also provide boundary conditions for the processes that act upon them.

1.4.1 Crater Dating

Understanding the geologic history of a planet requires constraints on the age of its surface. Dating of surfaces on Earth is possible through a variety of in-situ geologic studies (e.g., radiometric or relative stratigraphic dating; Kelley and Sherlock, 2013). Such studies are not easily implemented on other planets where we only have remote sensing data of a planetary surface (or in some cases, limited in situ data from rovers and landers). Direct aging of the Earth and Moon have constrained the history of these bodies, and

consequently, it has constrained the rate of impacts on their surfaces during this time (Hartmann, 1977; Neukum, 1983; Ivanov, 2001; Michael and Neukum, 2010). The impact rates are not the same in the outer solar system, but similar approaches have been done to constrain the rate of impacts in the outer solar system (e.g., Zahnle et al., 1998, 2003). By extension, the surface ages of the outer solar system planets can be ascertained (e.g., Singer et al., 2019, 2021). There are a myriad of processes that can drive resurfacing, and each process drives the degradation and depletion of the predicted crater population.

1.4.2 Forms of Crater Degradation

As resurfacing occurs, craters will exhibit a range of degradational stages. The total population of craters can provide estimates on the overall resurfacing rates, but crater morphologies can constrain how, and to what extent, processes modify the surface. In this subsection, we will review the mechanisms that modify crater morphologies on icy worlds within the solar system.

1.4.2.1 Viscous Relaxation

The forms of crater degradation are specific to each world, icy or otherwise. However, the most ubiquitous process that erases the surface topography on icy worlds is viscous relaxation (Parmentier and Head, 1981; Dombard and McKinnon, 2006; Stern et al., 2015b; Schurmeier and Dombard, 2018). Viscous relaxation is the slow creep of ice by gravity until it reaches an equilibrium state (Parmentier and Head, 1981). It is predominately a large-wavelength process (i.e., affects large features rather than small scale ones), but, overtime, even small-scale features can degrade. The rate at which the ice viscously relaxes is dependent on the material properties of the surface, which is itself temperature dependent (Dombard and McKinnon, 2006; Parmentier and Head, 1981). For that reason, viscous relaxation is not observed on rocky bodies because the viscosity of the rock is too high. This is also true for especially cold icy satellites where the low temperatures slow the rate of relaxation (e.g., Titan, Pluto, etc.), but even on especially cold worlds, relaxation can be instigated through various means. On Titan, sand deposition can produce sufficient insulation to enhance the viscous relaxation process (Schurmeier and Dombard, 2018). However, it is unlikely to play a significant role because the other

exogenic processes (i.e., fluvial and aeolian) will erase the feature before relaxation has time to take affect (Neish et al., 2013; 2016; Hedgepeth et al., 2020). On Pluto, less viscous material like volatile ices (i.e., methane or nitrogen) would still be affected by relaxation (Stern et al., 2015b). Even when the material is suspected to be too viscous to relax, localized heating events may arise to trigger significant relaxation (e.g., craters in Cthulhu Macula on Pluto, Nimmo and McKinnon, 2021; McKinnon et al., 2021). Moreover, nitrogen ice is known to act as an insulator in some parts of Pluto (e.g., Sputnik Planitia, McKinnon et al., 2016) which may also facilitate water ice relaxation.

1.4.2.2 Fluvial and Aeolian Processes

As previously noted, Titan is a special scenario where terrestrial-like erosion and deposition are occurring (**Figure 1.5**) (Neish et al., 2013, 2016; Hedgepeth et al., 2020). This is especially true in the poles where a large amount of liquid methane exists in the form of rivers, lakes, and seas (Stofan et al., 2007). Marine environments complicate crater identification by preventing the formation of many of their signature features, such as steep rims and deep depressions, as seen in terrestrial marine impacts (**Figure 1.6**) (Neish et al., 2016; Bray et al., 2022). Furthermore, there are distinct fluvial patterns in radar images of Titan, which demonstrate that fluvial erosion is a dominant feature there, even outside Titan's poles. Erosion will slowly erase the raised rims of the impact crater, and deposit sediment in the crater floor. Aeolian deposition of dune material in the crater cavity will also reduce the crater depth. When coupled with fluvial erosion, these processes may completely erase craters on Titan (Forsberg-Taylor et al., 2004; Neish et al., 2013, 2016; Hedgepeth et al., 2020).

No other icy moon is known to exhibit fluvial erosion. However, Pluto does show evidence of glaciation, which may have erosive affects (Howard et al., 2017a). For example, observations suggest N₂ ice glaciation in the high latitudes may have eroded water ice craters (Howard et al., 2017a). Pluto also has a thick organic layer in Cthulhu Macula that is suspected to be meters thick (Grundy et al., 2018; Cruikshank et al., 2021). The production and transport of the haze material on Pluto is not as extreme as on Titan, but evidence of material transport has been observed (Lorenz et al., 2006; Telfer et al., 2018). Furthermore, the volatile ices are known to migrate significantly over Pluto's orbit

(Bertrand et al., 2018, 2019), so volatile deposition may have a similar effect on the crater morphology to sediment infill on Titan (Earle et al., 2022).

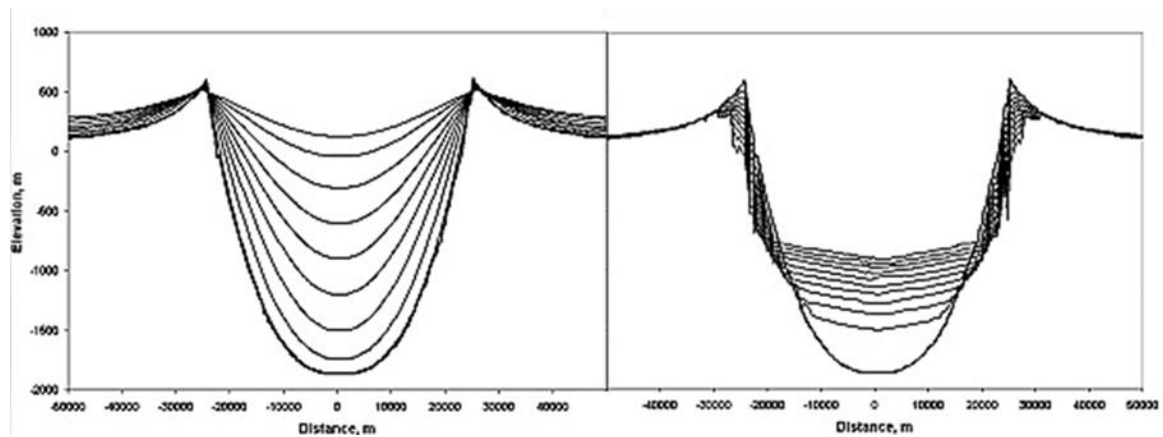


Figure 1.5. Impact crater degradation by aeolian deposition (left) and by fluvial erosion and deposition (right), as modeled on Mars. Figure modified from Forsberg-Taylor et al. (2004).

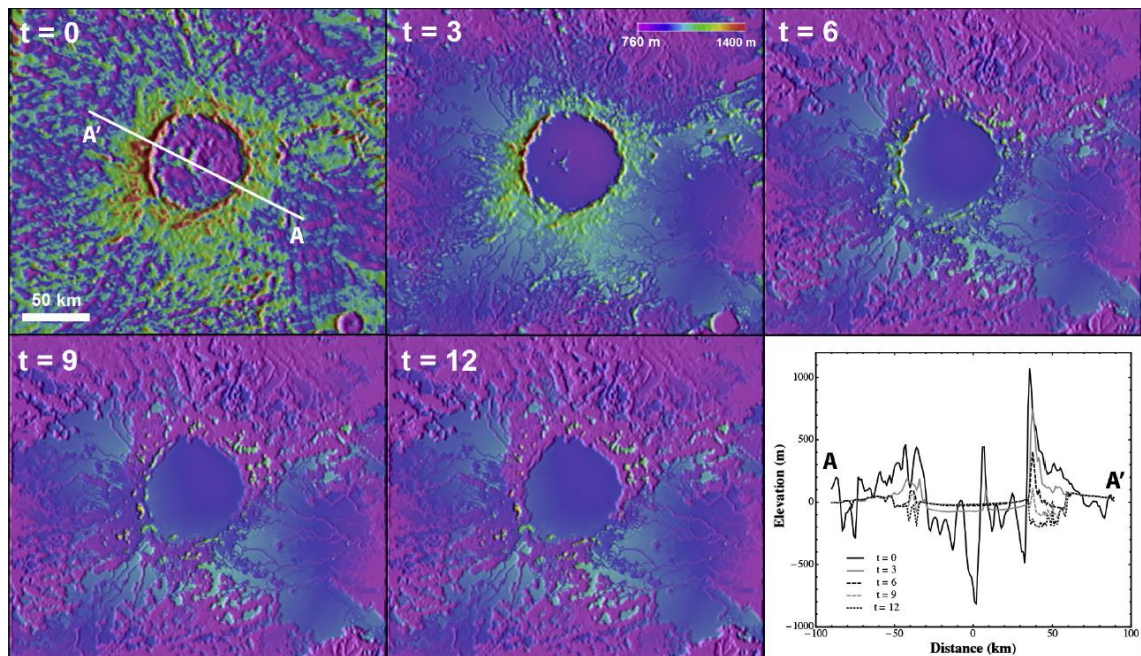


Figure 1.6. Simulation of the fluvial degradation of Isis crater on Ganymede, a proposed pristine analogue for the degraded crater Soi on Titan. The topography of the crater is presented through time, with the A-A' profile shown through time in the final box. Figure from Neish et al. (2016).

1.4.2.3 Cryovolcanism and Tectonics

Other forms of deposition are also possible on icy worlds. Cryovolcanism is another way that impact craters can become infilled and covered by fresh material (Cruikshank et al., 2019b). A good candidate on Titan is Sotra Facula (Lopes et al., 2007; Neish et al., 2018). Several potential cryovolcanoes have been identified on Pluto as well (Cruikshank et al., 2021; Nimmo and McKinnon, 2021; Singer et al., 2022). Pluto's most prominent cryovolcano, Wright Mons, dominates its geologic group with very few craters making it one of Pluto's youngest terrains (Singer et al., 2019, 2021, 2022; White et al., 2021). Cryovolcanism, or more aptly, plumes, are present on more active icy worlds as well (e.g., Europa and Enceladus, Postberg et al., 2018; Spencer et al., 2018). Other forms of cryovolcanism also occur with the formation of bands (long linear regions of fresh crust) on Europa, Enceladus, and even less geologically active worlds such as Ganymede (Head et al., 1999, 2002; Spencer et al., 2009; Sparks et al., 2017); this will more directly affect the crater population as the surface is completely renewed in places (Murchie et al., 1989; Bierhaus et al., 2005). Other forms of tectonics will modify the surface even when fresh material is not supplied (Parmentier et al., 1982; Squyres and Croft, 1986). For example, on Europa fresh ice is also supplied by diapirs or chaos terrain, which are regions of ice that have been broken up and mixed with fresh matrix material (i.e., ice or liquid) (Pappalardo et al., 1996; Schmidt et al., 2011).

1.4.2.4 Sublimation

A less common form of crater degradation is through sublimation. Water ice is stable on the surface of most icy moons (Poirier, 1982; Baragiola, 2003). However, as more volatile ices began to become stable, sublimation will play a larger role in surface modification (Watson et al., 1962; Clark et al., 2013). For example, nitrogen ice is abundant on Triton and Pluto (Quirico et al., 1999), and New Horizons has shown clear evidence of sublimation (Moore et al., 2017; Morison et al., 2021). While water ice is not significantly affected by sublimation, it has been suggested that water ice can be degraded through the cyclical deposition and sublimation of more volatile ices (e.g., in the north pole of Pluto) (Moore et al., 1996, 1999; Howard et al., 2017). Stern et al. (2015b) studied the role of sublimation (or escape erosion) and relaxation of craters on Pluto in N₂ and CH₄ ices. They

suggested a large population of craters would be destroyed by the two processes (Stern et al., 2015b; Moore et al., 2017; Bertrand et al., 2018, 2019).

1.4.3 Measuring Crater Degradation

Landscape evolution models are executed by assuming some initial surface topography (Coulthard, 2001; Tucker and Hancock, 2010). Crater morphologies provide excellent boundary conditions for such models because they require fewer assumptions about the initial topography of the system. Given that the initial topography of craters is well understood, studying crater morphology is a direct way of constraining how much the surface has evolved (e.g., Neish et al., 2013; Hedgepeth et al., 2020). Furthermore, sometimes the material properties of a planet may not be well constrained (e.g., Wakita et al., 2022). Reproducing observed crater morphologies is one way of constraining the conditions and/or material properties of the bedrock (e.g., Barlow, 2005; Neish and Lorenz, 2014; Wakita et al., 2022). Measuring the level of crater degradation improves our understanding of the processes acting on a surface, and it can provide global estimates of the overall modification of the surface.

1.4.3.1 Depth to Diameter Relationships

The most descriptive characteristic of a crater is its diameter. The diameter of a crater correlates to the approximate depth and overall morphology of a crater depending on the planet (Melosh, 1989). The transition between simple to complex and multi-ringed basins is dependent on surface properties and gravity (Schenk, 2002; Bray et al., 2012). Gravity is a driving factor behind the simple-complex transition diameter, but lithospheric structures and impact velocity also influence this transition depending on the thermal structure of the crust (Melosh, 1989; Turtle and Pierazzo, 2001; Schenk, 2002; Silber et al., 2017). Furthermore, the thermal structure affects how the shock wave travels through the bedrock; warmer material will be more ductile (plastically deforming) than brittle (faulting) (Ross and Schubert, 1989; Schenk, 2002). Each of these factors is reflected in the depth to diameter relationship.

The relationship between diameter and depth, and the transitions between crater shapes, are determined using the population of available craters (Pike, 1977; Robbins et

al., 2018). However, this relationship is not easily constrained without a wide selection of crater sizes to study, as on Titan (e.g., Neish and Lorenz, 2014; Hedgepeth et al., 2020). The crater morphology cannot be studied without the depth to diameter relationship because we do not have an initial morphology to compare the crater topography to, so analogues are used to infer the morphology of the pristine crater (eg., Hedgepeth et al., 2020; Neish et al., 2013). For example, Ganymede's similar size, composition, and internal structure is thought to be a good indicator that its crater population is representative of fresh craters on Titan. However, new modeling suggests the presence of methane clathrate on Titan could significantly alter the crater morphology, being much shallower than previously thought (Wakita et al., 2022).

Therefore, it is important to accurately characterize the diameter of a crater to accurately constrain the global trend of crater morphologies. Terrestrial (and Titan) craters undergo significant erosion that make it difficult to find the crater rim even with topographic information. Similarly, multi-ringed basins are hard to characterize even before erosion. In these cases, the best approach is to clearly identify the ambiguity required when interpreting a crater.

1.4.3.2 Crater Measurements

Crater morphologies are always idealized (Melosh, 1989); realistically, crater shapes are not uniform. Therefore, multiple measurements are best (Robbins et al., 2018). A statistical estimate of the crater morphology is recommended for the most holistic measurement of the crater properties (Robbins et al., 2018), but multiple line measurements have been shown to be a consistent approach as well (Bray et al., 2012; Hedgepeth et al., 2020).

Crater diameter is defined as the distance from each side of the crater rim (also called the apparent diameter; Turtle et al., 2005). The multiple profile approach uses multiple rim-to-rim measurements to determine the diameter by taking the average of the distances measured (Robbins et al., 2018). Erosion can alter the apparent diameter, but past work has suggested the difference is within the natural variance of the rim-to-rim diameter (Forsberg-Taylor et al., 2004; Hedgepeth et al., 2020). The variation in the rim-to-rim

diameter measurements on worlds with high erosion have been shown to be as high as 20% at times (Hedgepeth et al., 2020).

Crater depth is defined as the distance between the rim and the floor (Robbins et al., 2018). However, there are multiple ways of taking the rim-to-floor measurement. The more accurate approach is considered the statistical approach, which is an approach that uses all of the points within the crater topography to estimate the crater depth from the rim height and floor depth (**Figure 1.7a**, Neish et al., 2013; Robbins et al., 2018). The multiple profile approach uses the highest and lowest points on the rim and floor respectively (**Figure 1.7b**) (e.g., Bray et al., 2012; Hedgepeth et al., 2020). Variation can occur when using the statistical vs. the profile approach. The profile approach can also be complicated with degraded craters because the rim and floor positions are not as easily identified (e.g., Titan or Pluto). Furthermore, topographic resolution may affect the peak and lows of a crater profile, but past studies have suggested the difference is negligible when comparing measurements of topography with an order of magnitude lower resolution (Hedgepeth et al., 2020).

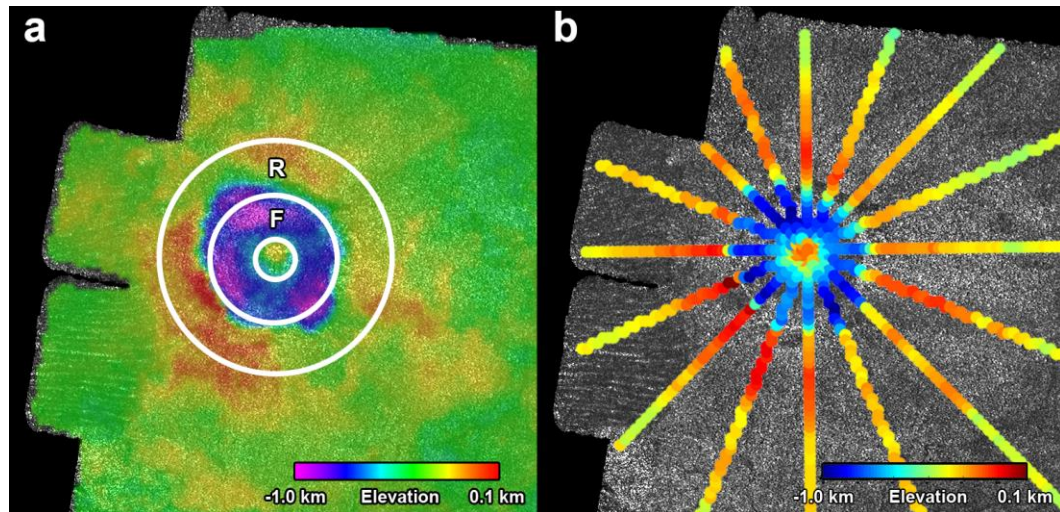


Figure 1.7. a) Ksa crater seen in Cassini SAR images overlain by stereo topography. The rim (R) and floor (F) topography are used to statistically derive the rim and floor heights in past works. b) Ksa crater in stereo topography split into 8 profiles, spaced equally at azimuths between 0 and 180 degrees from the north-south axis. Figure from Hedgepeth et al. (2020).

1.5 The Astrobiology of Icy Worlds

The rich geologic history of icy worlds makes them a fascinating point of study. However, interest in icy worlds has seen a huge rise in the last decade because of their potential to harbor life (e.g., National Academies of Sciences, Engineering, and Medicine, 2018, 2022). Habitability is often related to the stability of liquid water (or some solvent) on the surface of a planet (Hoehler et al., 2020). There is an abundance of subsurface water on icy worlds. Even moons as small as Europa ($D = 3120$ km) have more water than Earth under their ice shells (Schubert et al., 2009; Sohl et al., 2010). Furthermore, it has recently been shown that even worlds previously thought to be too cold may still have a liquid ocean (e.g., Pluto or Callisto, Nimmo and McKinnon, 2021; Spencer et al., 2021). Even without an ocean, temporary habitable zones are possible at the surface of icy satellites through cryovolcanism or impact cratering (e.g., Neish et al., 2018). In this section, we will review the wide breadth of astrobiological concepts within the field of icy worlds.

1.5.1 Subsurface Oceans

Most icy bodies begin with a liquid ocean, but the sustainability of that ocean will depend on the availability of heat sources (Sohl et al., 2010). The heat from formation may sustain an ocean for millions to billions of years, and radiogenic heating can prolong heating even further (e.g., Kimura and Kamata, 2020; Nimmo and McKinnon, 2021). Enceladus is often lauded as a fascinating source for the investigation of life because of its easily accessible ocean (i.e., via the plumes, Cable et al., 2021), but the source of its heat is still not fully understood (Hemingway et al., 2018; Nimmo et al., 2018). Tidal dissipation should lead to the inevitable loss of tidal heating on Enceladus (Roberts and Nimmo, 2008; Nimmo et al., 2018). Europa, in contrast, is in a unique state of resonance with its sister moons, which sustains its eccentric orbit to allow for long term stability of its ocean through tidal heating (Sotin et al., 2009). Europa is therefore likely the best candidate to host the long-term (and potentially ongoing) evolution of life (Hand et al., 2009, 2020). Enceladus is still intriguing because it has many of the characteristics that are suspected to make Europa habitable; in addition to its ocean, it is known to have hydrothermal plumes (Waite et al., 2017). These suggests that the ocean has resources that are fundamental to the formation of life (McKay et al., 2018). There is less direct evidence of these processes on

Europa (**Figure 1.8**) (i.e., hydrothermal plumes, Goodman et al., 2004; Lowell and DuBose, 2005). However, plumes could source life with the necessary nutrients to survive in the European Ocean (Hand et al., 2009, 2020; Zolotov and Kargel, 2009).

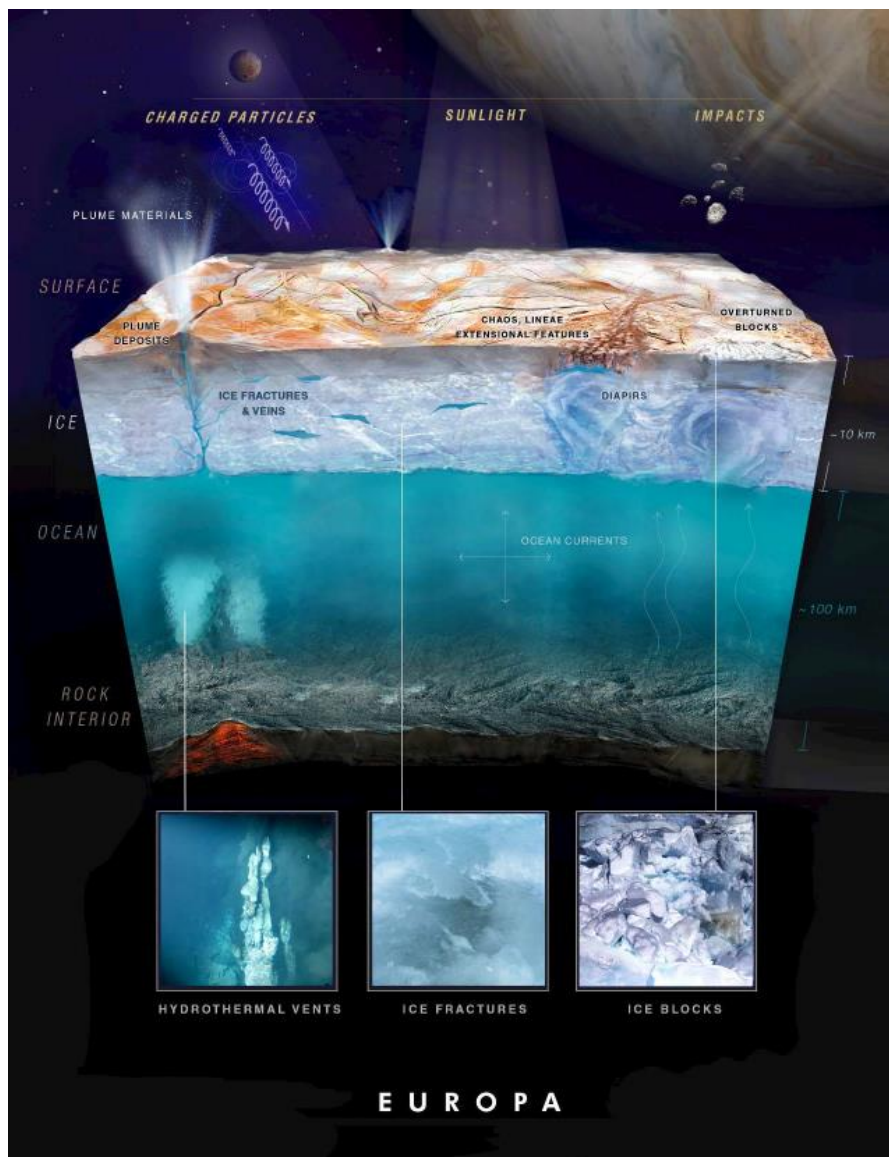


Figure 1.8. An illustration of the European ocean, its ice crust, and the underlying rock-ocean interface. This illustration highlights a range of processes that contribute to the habitability of the Europa system. Figure from Hand et al. (2016).

The oceans of less active worlds (i.e., those with fewer ice-ocean interactions) are still intriguing. That is especially true on worlds that are known to host large reservoirs of

organic material on their surface (e.g., Titan or Pluto, Thompson and Sagan, 1992; Hörst, 2017; Cruikshank et al., 2019a). Less active worlds are often separated from their silica core by a layer of high-pressure ices (e.g., Titan, Ganymede or Callisto, Sohl et al., 1992; Anderson et al., 2001; Kalousová and Sotin., 2020), but even oceans that are decoupled from their silicate core can still be sourced with the nutrients of life through resurfacing. Giant (100s of kilometers in diameter) impacts may provide the rare opportunity for the surface to mix with the subsurface ocean (e.g., Titan, Crósta et al., 2021). Furthermore, the oceans may have been seeded with nutrients earlier in their histories when the oceans were warmer and the crust possibly thinner (Tobie et al., 2005, 2006). The availability of resources early in the history of icy worlds like Titan or the Galilean moons are not well constrained, but these resurfacing mechanisms demonstrate that their oceans are still viable candidates to host past or present life.

1.5.2 Cryovolcanism, Tectonics, and Other Endogenic Processes

Outside of subsurface oceans, there are surface processes on icy satellites that also produce habitable environments. One major mechanism is cryovolcanism, which is the eruption of subsurface water (liquid or warm ice) from the interior of the body (Lopes et al., 2007; Spencer et al., 2009; Sparks et al., 2017; Cruikshank et al., 2019b; Singer et al., 2022). Cryovolcanism is not as easily achieved as terrestrial volcanism because the buoyancy differences that drive terrestrial volcanism act against cryovolcanism. Nevertheless, there are several features on icy bodies that show strong signs of cryovolcanism that may be caused by compositional or temperature differences in the ice (Lopes et al., 2007; Spencer et al., 2009; Sparks et al., 2017; Cruikshank et al., 2019b; Singer et al., 2022). Broadly speaking, the implications for astrobiology depend on how the cryovolcanic events formed, but in almost every case, cryovolcanism creates a habitable environment on the surface of icy bodies (Neish et al., 2006, 2018).

The origin of life (as we know it) requires the proper ingredients (CHNOPS) in addition to the presence of a solvent (Bains, 2004; Cockell, 2015). Therefore, worlds like Titan or Pluto are likely to be very conducive to the origin of life because of the thick (10s to 100s of meters) deposits of organic material that exist on their surfaces (Thompson and Sagan, 1992; Hörst, 2017; Cruikshank et al., 2019a). When mixed with liquid water, the

organics become oxygenated by hydrolysis producing biomolecular daughter products such as amino acids and nucleobases, the building blocks of life (McDonald et al., 1994; Neish et al., 2010; Cleaves et al., 2014; Cruikshank et al., 2019a). In fact, the VIMS (Visual and Infrared Mapping Spectrometer) instrument on the Cassini spacecraft observed a signature of a hypothesized cryovolcanic flow that contains an unknown composition that may have originated from the mixture of the water ice and surface organics (**Figure 1.9**) (Neish et al., 2006, 2018; Lopes et al., 2007, 2013). Similarly, cryovolcanism is proposed near the organic deposits on Pluto in Cthulhu Macula (Cruikshank et al., 2021).

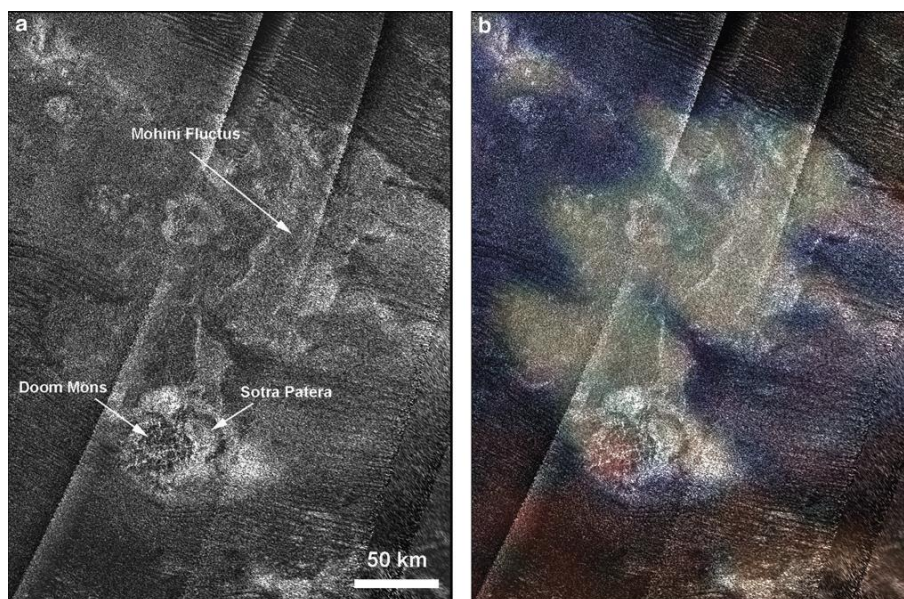


Figure 1.9. Sotra Facula, a hypothesized cryovolcano, visualized in Cassini RADAR (a) and the same image overlaid with Cassini VIMS (b) showing where water (blue) is suspected to have mixed with organic dunes (brown) to produce the unknown composition (green). Figure from Neish et al. (2018).

Cryovolcanic flows are one way for this type of chemistry to occur on Titan and Pluto, but cryovolcanism is not thought to be the most conducive environment for the origin of life on these surfaces (Neish et al., 2018). This is because they are generally thin (shorter lived) and possibly at temperatures well below 0°C, which would significantly reduce the rate biochemical reactions in the liquid (Sagan and Khare, 1979; Thompson and Sagan, 1992; Lorenz and Lunine, 1996; Lopes et al., 2007; Neish et al., 2008, 2010, 2018). The temperature of the flow will depend on where the material is sourced. For example, the

cryomagma may be sourced from within the crust driven by localized heating, or it may be sourced from the ocean which, on Titan, is likely below 0°C because ammonia is present (Lopes et al., 2007, 2013). Therefore, it is not the ideal place to study the origin of life. The source of the cryomagma also has important implications for the composition (both chemically and biologically) as the cryomagma may contain evidence of ocean life or be recycled crust. Other oceans, such as Europa's, may be warmer (~0°C, Melosh et al., 2004), but there is less prebiotic chemistry to react with on its surface.

Europa and Enceladus have much younger surfaces and are far more active (with resurfacing of the crust from ocean material) than more chemically rich worlds like Titan or Pluto (Squyres, 1983; Spencer et al., 2009, 2013). The nature of cryovolcanism on these worlds begins to blend into large scale tectonics, with the sourcing of large sections of new material (Head et al., 1999) or giant plumes from the interior (Hansen et al., 2006). Other features such as chaos terrain, diapirs, etc. present localized habitable zones that contribute to the recycling of the surface (Rathbun et al., 1998; Pappalardo and Barr, 2004; Schmidt et al., 2011). In this way, active worlds like Europa and Enceladus present a range of habitable environments for life to temporarily thrive, but because these worlds do not have the same abundance of prebiotic chemistry, their features are arguably much more useful as a window into the ocean habitability rather than studying the origin of life itself (e.g., Cable et al., 2021; MacKenzie et al., 2021). To investigate the origin of life, on Earth and beyond, impact craters, on organic rich ocean worlds, are likely the best places to study (Neish et al., 2018).

1.5.3 Impact Cratering

During impact, a high energy shock wave travels through the bedrock and imparts hundreds of GPa of pressure that compresses, moves, vaporizes and melts the bedrock (**Figure 1.10**) (Melosh, 1989; Osinski and Pierazzo, 2012; Osinski et al., 2012a). Modeling has suggested that impacts can form melt volumes hundreds of meters thick (Artemieva and Lunine, 2005), and the fraction of melt production (to total volume) increases with crater size (O'Brien et al., 2005). Furthermore, new modeling has suggested the presence of clathrates (i.e., water ice with methane or other carbon molecules trapped within the ice

lattice; Durham et al., 2003) could lead to significantly thicker melt sheets as well (Wakita et al., 2022).

Once formed, a melt sheet is a warm body of water that can easily last decades to possibly over a millennium before freezing solid (O'Brien et al., 2005). The temperature of the melt will reach boiling point (373 K) during impact which would promote the type of chemical reactions thought to be associated with the origin of life (Thompson and Sagan, 1992; Artemieva and Lunine, 2005; Neish et al., 2010). Therefore, impact craters are a natural laboratory for studying the origin of life, and while their lifespan may be trivial geologically, they span beyond anything that has been studied in a laboratory environment (Neish et al., 2008, 2010). This is one of the motivations for NASA's Dragonfly mission, going to Titan later this decade, where they will target Selk crater to sample its impact crater melt to better understand the origin of life (Lorenz et al., 2018, 2021; Neish et al., 2018).

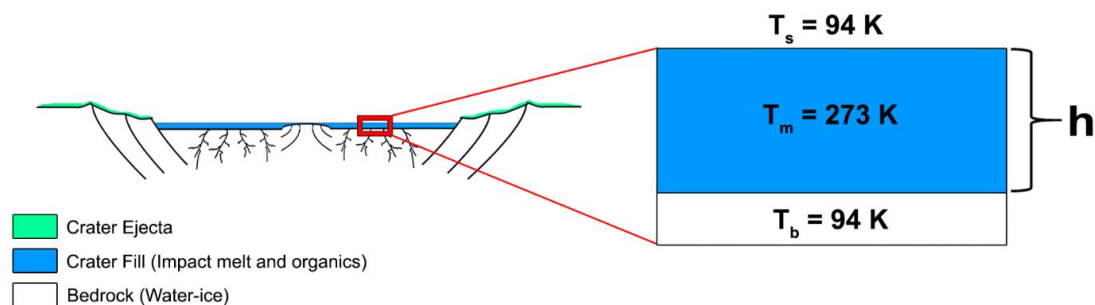


Figure 1.10. Example cross-section of a complex crater on Titan with the crater ejecta is shown in green and the crater melt pond is shown in blue. The red box shows what a melt pond (of some height, h), may look like with a given surface temperature (T_s), melt temperature (T_m), and basal ice temperature (T_b). Figure is from Hedgepeth et al. (2022) with parameters equal to Titan conditions.

1.5.4 Dragonfly

NASA's Dragonfly mission is sending a rotorcraft lander to investigate Titan. Dragonfly is a revolutionary approach to planetary science that takes advantage of Titan's dense atmosphere to navigate through flight (Lorenz et al., 2018). The Dragonfly science objectives are to: 1) investigate Titan's prebiotic chemistry, 2) investigate Titan's methane

cycle, 3) investigate Titan's geology, 4) study where and how water has mixed with organics, and 5) identify biosignatures that may have formed (Barnes et al., 2021). Dragonfly will address these objectives with a payload that contains: 1) a mass spectrometer (DraMS) with a drill for sampling (DrACO), 2) a gamma-ray and neutron spectrometer (DraGNS), 3) a geophysics and meteorology package (DraGMet), 4) and a camera suite (DragonCam) (Lorenz et al., 2018). Dragonfly will land southeast of Selk crater in the flat interdunes (**Figure 1.11**) (Barnes et al., 2021; Lorenz et al., 2021). The rotorcraft will make its way northeast, studying the dunes, ejecta will ultimately reach the crater melt in and around the crater itself.

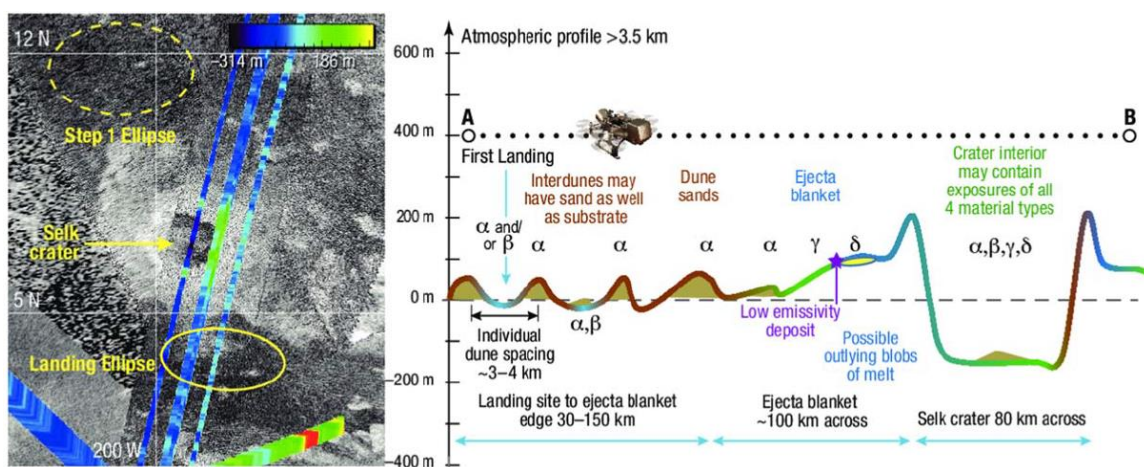


Figure 1.11. Synthetic aperture radar (SAR) image of Selk crater (left) with color-coded SARTopo (Stiles et al., 2009) and a yellow landing ellipse denoted in yellow. The linear traverse to the northeast from the landing ellipse (right) indicating the geologic features and their estimated topographies. Modified from Barnes et al. (2021)

1.6 Summary

This work will span three main chapters in addition to an Introduction (Chapter 1), and Discussion (Chapter 5). In this first chapter, I have introduced the background knowledge for the work I have done in the following chapters.

Chapter 2 is based on a paper published in the Planetary Science Journal, “Modeling the Distribution of Organic Carbon and Nitrogen in Impact Crater Melt on Titan” (Hedgepeth et al., 2022). In this work, we model how organic molecules may freeze into a melt lens on Titan, with HCN as a proxy for the organic molecules that exist on the surface of Titan.

Chapter 3 is based on a paper to be submitted to the Planetary Science Journal, “The role of hydrolysis in the emplacement of organic molecules into melt sheets on Titan.” This work builds on Chapter 2, modeling the freezing of glycine, a potential amino acid expected to form in a Titan melt pond. This work explores how different impurity buoyancies affects emplacement. It also explores how hydrolysis will change the melt properties of the mixture and how the rate of hydrolysis will affect Dragonfly’s ability to detect impurities.

Chapter 4 is based on a paper to be submitted to the Icarus, “Impact Crater Degradation on Pluto”. This work constrains the level of surface degradation across Pluto’s surface by examining the morphology of its impact craters.

In Chapter 5, I discuss the overall results of Chapters 2-4 and the broader implications on our understanding of icy worlds in the solar system. I also reflect on the overall implications of this work.

1.7 References

- Anderson, J.D., Jacobson, R.A., McElrath, T.P., Moore, W.B., Schubert, G. and Thomas, P.C., 2001. Shape, mean radius, gravity field, and interior structure of Callisto. *Icarus*, 153(1), pp.157-161.
- Artemieva, N. and Lunine, J.I., 2005. Impact cratering on Titan II. Global melt, escaping ejecta, and aqueous alteration of surface organics. *Icarus*, 175(2), pp.522-533.
- Bains, W., 2004. Many chemistries could be used to build living systems. *Astrobiology*, 4(2), pp.137-167.
- Baragiola, R.A., 2003. Water ice on outer solar system surfaces: Basic properties and radiation effects. *Planetary and Space Science*, 51(14-15), pp.953-961.
- Barlow, N.G., 2005. A review of Martian impact crater ejecta structures and their implications for target properties. *Large meteorite impacts III*, 384, pp.433-442.
- Barnes, J.W., Lorenz, R.D., Radebaugh, J., Hayes, A.G., Arnold, K. and Chandler, C., 2015. Production and global transport of Titan's sand particles. *Planetary Science*, 4(1), pp.1-19.
- Barnes, J.W., Turtle, E.P., Trainer, M.G., Lorenz, R.D., MacKenzie, S.M., Brinckerhoff, W.B., Cable, M.L., Ernst, C.M., Freissinet, C., Hand, K.P. and Hayes, A.G., 2021. Science goals and objectives for the Dragonfly Titan rotorcraft relocatable lander. *The Planetary Science Journal*, 2(4), p.130.
- Bertrand, T. and Forget, F., 2016. Observed glacier and volatile distribution on Pluto from atmosphere–topography processes. *Nature*, 540(7631), pp.86-89.
- Bertrand, T., Forget, F., Umurhan, O.M., Grundy, W.M., Schmitt, B., Protopapa, S., Zangari, A.M., White, O.L., Schenk, P.M., Singer, K.N. and Stern, A., 2018. The nitrogen cycles on Pluto over seasonal and astronomical timescales. *Icarus*, 309, pp.277-296.

- Bertrand, T., Forget, F., Umurhan, O.M., Moore, J.M., Young, L.A., Protopapa, S., Grundy, W.M., Schmitt, B., Dhingra, R.D., Binzel, R.P. and Earle, A.M., 2019. The CH₄ cycles on Pluto over seasonal and astronomical timescales. *Icarus*, 329, pp.148-165.
- Bierhaus, E.B., Chapman, C.R. and Merline, W.J., 2005. Secondary craters on Europa and implications for cratered surfaces. *Nature*, 437(7062), pp.1125-1127.
- Binzel, R.P., Earle, A.M., Buie, M.W., Young, L.A., Stern, S.A., Olkin, C.B., Ennico, K., Moore, J.M., Grundy, W., Weaver, H.A. and Lisse, C.M., 2017. Climate zones on Pluto and Charon. *Icarus*, 287, pp.30-36.
- Bolton, S.J., Lunine, J., Stevenson, D., Connerney, J.E.P., Levin, S., Owen, T.C., Bagenal, F., Gautier, D., Ingersoll, A.P., Orton, G.S. and Guillot, T., 2017. The Juno Mission. *Space Science Reviews*, 213(1), pp.5-37.
- Bray V. J., Schenk P. M., Melosh, H. J., Morgan, J. V., and Collins, G. S. 2012, Ganymede crater dimensions: Implications for central peak and central pit formation and development. *Icarus*, 217, 115–129, DOI: 10.1016/j.icarus.2011.10.004.
- Bray, V.J., Hagerty, J.J. and Collins, G.S. 2022, “False peak” creation in the Flynn Creek marine target impact crater. *Meteorit Planet Sci.* <https://doi.org/10.1111/maps.13822>
- Burkhard, L.M., Smith-Konter, B.R., Fagents, S.A., Cameron, M.E., Collins, G.C. and Pappalardo, R.T., 2022. Strike-slip faulting on Titan: Modeling tidal stresses and shear failure conditions due to pore fluid interactions. *Icarus*, 371, p.114700.
- Burr, D.M., Jacobsen, R.E., Roth, D.L., Phillips, C.B., Mitchell, K.L. and Viola, D., 2009. Fluvial network analysis on Titan: Evidence for subsurface structures and west-to-east wind flow, southwestern Xanadu. *Geophysical Research Letters*, 36(22).
- Burr, D.M., Taylor Perron, J., Lamb, M.P., Irwin III, R.P., Collins, G.C., Howard, A.D., Sklar, L.S., Moore, J.M., Ádámkóvics, M., Baker, V.R. and Drummond, S.A.,

2013. Fluvial features on Titan: Insights from morphology and modeling. *Bulletin*, 125(3-4), pp.299-321.
- Byrne, S., 2009. The polar deposits of Mars. *Annual Review of Earth and Planetary Sciences*, 37, pp.535-560.
- Cable, M.L., Porco, C., Glein, C.R., German, C.R., MacKenzie, S.M., Neveu, M., Hoehler, T.M., Hofmann, A.E., Hendrix, A.R., Eigenbrode, J. and Postberg, F., 2021. The science case for a return to Enceladus. *The planetary science journal*, 2(4), p.132.
- Canup, R.M., Kratter, K.M. and Neveu, M., 2021. On the origin of the Pluto system. *The Pluto System After New Horizons*, p.475.
- Cassini, J.D., 1673., A discovery of two new planets about Saturn made in the Royal Parisian Observatory by Signor Cassini, Fellow of both the Royal Societys, of England and France; English't out of French. *Philosophical Transactions of the Royal Society of London*, 8(92), pp.5178-5185.
- Clark, R.N., Carlson, R., Grundy, W. and Noll, K., 2013. Observed ices in the Solar System. *The science of solar system ices*, pp.3-46.
- Cleaves II, H.J., Neish, C., Callahan, M.P., Parker, E., Fernández, F.M. and Dworkin, J.P., 2014. Amino acids generated from hydrated Titan tholins: Comparison with Miller–Urey electric discharge products. *Icarus*, 237, pp.182-189.
- Cockell, C.S., 2020. *Astrobiology: understanding life in the universe*. John Wiley & Sons.
- Collins, G.S., Kenkmann, T., Osinski, G.R. and Wünnemann, K., 2008. Mid-sized complex crater formation in mixed crystalline-sedimentary targets: Insight from modeling and observation. *Meteoritics & Planetary Science*, 43(12), pp.1955-1977.
- Coulthard, T.J., 2001. Landscape evolution models: a software review. *Hydrological Processes*. 15, 165–173
- Crósta, A.P., Silber, E.A., Lopes, R.M.C., Johnson, B.C., Bjornes, E., Malaska, M.J., Vance, S.D., Sotin, C., Solomonidou, A. and Soderblom, J.M., 2021. Modeling the

formation of Menrva impact crater on Titan: Implications for habitability. *Icarus*, 370, p.114679.

Cruikshank, D.P., Materese, C.K., Pendleton, Y.J., Boston, P.J., Grundy, W.M., Schmitt, B., Lisse, C.M., Runyon, K.D., Keane, J.T., Beyer, R.A. and Summers, M.E., 2019a. Prebiotic chemistry of Pluto. *Astrobiology*, 19(7), pp.831-848.

Cruikshank, D.P., Umurhan, O.M., Beyer, R.A., Schmitt, B., Keane, J.T., Runyon, K.D., Atri, D., White, O.L., Matsuyama, I., Moore, J.M. and McKinnon, W.B., 2019b. Recent cryovolcanism in virgil fossae on Pluto. *Icarus*, 330, pp.155-168.

Cruikshank, D.P., Dalle Ore, C.M., Scipioni, F., Beyer, R.A., White, O.L., Moore, J.M., Grundy, W.M., Schmitt, B., Runyon, K.D., Keane, J.T. and Robbins, S.J., 2021. Cryovolcanic flooding in Viking Terra on Pluto. *Icarus*, 356, p.113786.

Dombard, A.J. and McKinnon, W.B., 2006. Elastoviscoplastic relaxation of impact crater topography with application to Ganymede and Callisto. *Journal of Geophysical Research: Planets*, 111(E1).

Durham, W.B., Kirby, S.H., Stern, L.A. and Zhang, W., 2003. The strength and rheology of methane clathrate hydrate. *Journal of Geophysical Research: Solid Earth*, 108(B4).

Earle, A.M., Binzel, R.P., Keane, J.T., Grundy, W.M., Howett, C.J.A., Olkin, C.B., Parker, A.H., Scipioni, F., Ennico, K., Stern, S.A. and Weaver, H.A., 2022. Tracing seasonal trends across Pluto's craters: New Horizons Ralph/MVIC results. *Icarus*, 373, p.114771.

Edgeworth, K.E., 1943. The evolution of our planetary system. *Journal of the British Astronomical Association*, 53, pp.181-188.

Eluszkiewicz, J. and Stevenson, D.J., 1990. Rheology of solid methane and nitrogen: applications to Triton. *Geophysical Research Letters*, 17(10), pp.1753-1756.

- European Space Agency, 1988. Cassini Saturn Orbiter and Titan Probe, Report on the Phase A Study,. ESA.
- Figueredo, P.H. and Greeley, R., 2004. Resurfacing history of Europa from pole-to-pole geological mapping. *Icarus*, 167(2), pp.287-312.
- Forget, F., Bertrand, T., Vangvichith, M., Leconte, J., Millour, E. and Lellouch, E., 2017. A post-new horizons global climate model of Pluto including the N₂, CH₄ and CO cycles. *Icarus*, 287, pp.54-71.
- Forsberg-Taylor, N.K., Howard, A.D. and Craddock, R.A., 2004. Crater degradation in the Martian highlands: Morphometric analysis of the Sinus Sabaeus region and simulation modeling suggest fluvial processes. *Journal of Geophysical Research: Planets*, 109(E5).
- Galilei, G., 1613. *Discourse on Floating Bodies*.
- Gault, D.E., Quaide, W.L., Oberbeck, V.R., 1968. Impact Cratering mechanics and structures, in: *Shock Metamorphism of Natural Materials*. Mono Book Corp., Baltimore, MD, pp. 87–99.
- Goodman, J.C., Collins, G.C., Marshall, J. and Pierrehumbert, R.T., 2004. Hydrothermal plume dynamics on Europa: Implications for chaos formation. *Journal of Geophysical Research: Planets*, 109(E3).
- Grasset, O., Dougherty, M.K., Coustenis, A., Bunce, E.J., Erd, C., Titov, D., Blanc, M., Coates, A., Drossart, P., Fletcher, L.N. and Hussmann, H., 2013. JUpiter ICy moons Explorer (JUICE): An ESA mission to orbit Ganymede and to characterise the Jupiter system. *Planetary and Space Science*, 78, pp.1-21.
- Grundy, W.M., Binzel, R.P., Buratti, B.J., Cook, J.C., Cruikshank, D.P., Dalle Ore, C.M., Earle, A.M., Ennico, K., Howett, C.J.A., Lunsford, A.W. and Olkin, C.B., 2016. Surface compositions across Pluto and Charon. *Science*, 351(6279), p.aad9189.

- Grundy, W.M., Bertrand, T., Binzel, R.P., Buie, M.W., Buratti, B.J., Cheng, A.F., Cook, J.C., Cruikshank, D.P., Devins, S.L., Dalle Ore, C.M. and Earle, A.M., 2018. Pluto's haze as a surface material. *Icarus*, 314, pp.232-245.
- Hall, C.F., 1974. Pioneer 10. *Science*, 183(4122), pp.301-302.
- Hand, K.P., Chyba, C.F., Priscu, J.C., Carlson, R.W. and Nealson, K.H., 2009. Astrobiology and the potential for life on Europa. *Europa*, pp.589-629.
- Hand, K., Murray, A. and Garvin, J., 2016. Europa lander mission. NASA, Tech. Rep JPL D-97667.
- Hand, K.P., Sotin, C., Hayes, A. and Coustenis, A., 2020. On the habitability and future exploration of ocean worlds. *Space science reviews*, 216(5), pp.1-24.
- Hansen, C.J., Esposito, L., Stewart, A.I.F., Colwell, J., Hendrix, A., Pryor, W., Shemansky, D. and West, R., 2006. Enceladus' water vapor plume. *Science*, 311(5766), pp.1422-1425.
- Hartmann, W.K., 1977. Relative crater production rates on planets. *Icarus* 31, 260–276.
- Head, J.W., Pappalardo, R.T. and Sullivan, R., 1999. Europa: Morphological characteristics of ridges and triple bands from Galileo data (E4 and E6) and assessment of a linear diapirism model. *Journal of Geophysical Research: Planets*, 104(E10), pp.24223-24236.
- Head, J., Pappalardo, R., Collins, G., Belton, M.J., Giese, B., Wagner, R., Breneman, H., Spaun, N., Nixon, B., Neukum, G. and Moore, J., 2002. Evidence for Europa-like tectonic resurfacing styles on Ganymede. *Geophysical Research Letters*, 29(24), pp.4-1.
- Hedgepeth, J.E., Neish, C.D., Turtle, E.P., Stiles, B.W., Kirk, R. and Lorenz, R.D., 2020. Titan's impact crater population after Cassini. *Icarus*, 344, p.113664.

- Hedgepeth, J.E., Buffo, J.J., Chivers, C.J., Neish, C.D. and Schmidt, B.E., 2022. Modeling the Distribution of Organic Carbon and Nitrogen in Impact Crater Melt on Titan. *The Planetary Science Journal*, 3(2), p.51.
- Hemingway, D., Iess, L., Tajeddine, R. and Tobie, G., 2018. The interior of Enceladus. *Enceladus and the icy moons of Saturn*, pp.57-77.
- Herschel, W., 1790. I. Account of the discovery of a sixth and seventh satellite of the planet Saturn; with remarks on the construction of its ring, its atmosphere, its rotation on an axis, and its spheroidal figure. *Philosophical Transactions of the Royal Society of London*, (80), pp.1-20.
- Herschel, W., 1787. XVI. An account of the discovery of two satellites revolving round the Georgian planet. *Philosophical Transactions of the Royal Society of London*, (77), pp.125-129.
- Herschel, W., 1785. XII. On the construction of the heavens. *Philosophical Transactions of the Royal Society of London*, (75), pp.213-266.
- Hoehler, T.M., Bains, W., Davila, A., Parenteau, M. and Pohorille, A., 2020. Life's requirements, habitability, and biological potential. *Planet. Astrobiol*, 13, p.37.
- Howard, A. D., Moore, J. M., Umurhan, O. M., et al. 2017a, Present and past glaciation on Pluto. *Icarus*, 287, 287–300.
- Howard, A. D., Moore, J. M., White, O. L., et al. 2017b, Pluto: Pits and mantles on uplands north and east of Sputnik Planitia. *Icarus*, 293, 218–230.
- Huygens, C., 1659. *Systema Saturnium (The System of Saturn)*. Adriaan Vlacq, The Hague.
- Ivanov, B.A., 2001. Mars/Moon cratering rate ratio estimates. *Space Science Reviews*, 96(1), pp.87-104.
- Jewitt, D. and Luu, J., 1993. Discovery of the candidate Kuiper belt object 1992 QB1. *Nature*, 362(6422), pp.730-732.

- Kalousová, K. and Sotin, C., 2020. Dynamics of Titan's high-pressure ice layer. *Earth and Planetary Science Letters*, 545, p.116416.
- Kattenhorn, S.A. and Hurford, T., 2009. Tectonics of Europa. *Europa*, pp.199-236.
- Kelley, S.P. and Sherlock, S.C., 2013. The geochronology of impact craters. *Impact cratering: Processes and products*, pp.240-253.
- Kepler, J., 1596. *Mysterium Cosmographicum*.
- Kepler, J., 1609. *Astronomia Nova*.
- Kenkmann, T., Poelchau, M.H. and Wulf, G., 2014. Structural geology of impact craters. *Journal of Structural Geology*, 62, pp.156-182.
- Kimura, J. and Kamata, S., 2020. Stability of the subsurface ocean of Pluto. *Planetary and Space Science*, 181, p.104828.
- Kring, D.A., 2007. Guidebook to the geology of barringer meteorite crater, arizona (aka Meteor Crater) (p. 150). Houston: Lunar and Planetary Institute.
- Kuiper, G.P., 1951. On the origin of the solar system. *Proceedings of the National Academy of Sciences*, 37(1), pp.1-14.
- Lassell, W., 1847. Observations of Neptune and his satellite. *Monthly Notices of the Royal Astronomical Society*, 7, p.307.
- Le Gall, A., Janssen, M.A., Wye, L.C., Hayes, A.G., Radebaugh, J., Savage, C., Zebker, H., Lorenz, R.D., Lunine, J.I., Kirk, R.L., Lopes, R.M.C., Wall, S., Callahan, P., Stofan, E.R., Farr, T., 2011. Cassini SAR, radiometry, scatterometry and altimetry observations of Titan's dune fields. *Icarus* 213, 608–624. <https://doi.org/10.1016/j.icarus.2011.03.026>
- Lewis, B.L., Stansberry, J.A., Holler, B.J., Grundy, W.M., Schmitt, B., Protopapa, S., Lisse, C., Stern, S.A., Young, L., Weaver, H.A. and Olkin, C., 2021. Distribution

and energy balance of Pluto's nitrogen ice, as seen by New Horizons in 2015. *Icarus*, 356, p.113633.

Lindal, G.F., Wood, G.E., Hotz, H.B., Sweetnam, D.N., Eshleman, V.R. and Tyler, G.L., 1983. The atmosphere of Titan: An analysis of the Voyager 1 radio occultation measurements. *Icarus*, 53(2), pp.348-363.

Lopes, R.M., Mitchell, K.L., Stofan, E.R., Lunine, J.I., Lorenz, R., Paganelli, F., Kirk, R.L., Wood, C.A., Wall, S.D., Robshaw, L.E. and Fortes, A.D., 2007. Cryovolcanic features on Titan's surface as revealed by the Cassini Titan Radar Mapper. *Icarus*, 186(2), pp.395-412.

Lopes, R.M., Kirk, R.L., Mitchell, K.L., LeGall, A., Barnes, J.W., Hayes, A., Kargel, J., Wye, L., Radebaugh, J., Stofan, E.R. and Janssen, M.A., 2013. Cryovolcanism on Titan: New results from Cassini RADAR and VIMS. *Journal of Geophysical Research: Planets*, 118(3), pp.416-435.

Lorenz, R.D. and Lunine, J.I., 1996. Erosion on Titan: Past and present. *Icarus*, 122(1), pp.79-91.

Lorenz, R.D., Wall, S., Radebaugh, J., Boubin, G., Reffet, E., Janssen, M., Stofan, E., Lopes, R., Kirk, R., Elachi, C. and Lunine, J., 2006. The sand seas of Titan: Cassini RADAR observations of longitudinal dunes. *Science*, 312(5774), pp.724-727.

Lorenz, R.D., Mitchell, K.L., Kirk, R.L., Hayes, A.G., Aharonson, O., Zebker, H.A., Paillou, P., Radebaugh, J., Lunine, J.I., Janssen, M.A. and Wall, S.D., 2008. Titan's inventory of organic surface materials. *Geophysical Research Letters*, 35(2).

Lorenz, R.D., Turtle, E.P., Barnes, J.W., Trainer, M.G., Adams, D.S., Hibbard, K.E., Sheldon, C.Z., Zacny, K., Peplowski, P.N., Lawrence, D.J. and Ravine, M.A., 2018. Dragonfly: A rotorcraft lander concept for scientific exploration at Titan. *Johns Hopkins APL Technical Digest*, 34(3), p.14.

Lorenz, R.D., MacKenzie, S.M., Neish, C.D., Le Gall, A., Turtle, E.P., Barnes, J.W., Trainer, M.G., Werynski, A., Hedgepeth, J. and Karkoschka, E., 2021. Selection

and characteristics of the Dragonfly landing site near Selk crater, Titan. *The Planetary Science Journal*, 2(1), p.24.

Lowell, R.P. and DuBose, M., 2005. Hydrothermal systems on Europa. *Geophysical Research Letters*, 32(5).

Lunine, J.I. and Atreya, S.K., 2008. The methane cycle on Titan. *Nature Geoscience*, 1(3), pp.159-164.

Lunine, J.I. and Lorenz, R.D., 2009. Rivers, lakes, dunes, and rain: Crustal processes in Titan's methane cycle. *Annual Review of Earth and Planetary Sciences*, 37, pp.299-320.

MacKenzie, S.M., Neveu, M., Davila, A.F., Lunine, J.I., Craft, K.L., Cable, M.L., Phillips-Lander, C.M., Hofgartner, J.D., Eigenbrode, J.L., Waite, J.H. and Glein, C.R., 2021. The Enceladus Orbilander mission concept: Balancing return and resources in the search for life. *The Planetary Science Journal*, 2(2), p.77.

McKay, C.P., Davila, A., Glein, C.R., Hand, K.P. and Stockton, A., 2018. Enceladus astrobiology, habitability, and the origin of life. *Enceladus and the icy moons of Saturn*, pp.437-452.

McKinnon, W.B. and Kirk, R.L., 2014. Triton. In *Encyclopedia of the solar system* (pp. 861-881). Elsevier.

McKinnon, W.B., Glein, C.R., Bertrand, T. and Rhoden, A.R., 2020. Formation, Composition, and History of the Pluto System: A Post-New-Horizons Synthesis. arXiv preprint arXiv:2011.14030.

Melosh, H.J., 1989. *Impact Cratering: A Geologic Process*, Oxford monographs on geology and geophysics. Oxford University Press.

Melosh, H.J., Ekholm, A.G., Showman, A.P. and Lorenz, R.D., 2004. The temperature of Europa's subsurface water ocean. *Icarus*, 168(2), pp.498-502.

- Melosh, H.J., 2012. The contact and compression stage of impact cratering. *Impact Cratering: processes and products*, pp.32-42.
- Meltzer, M., 2007. *Mission to Jupiter: A history of the Galileo project*, NASA STI (Vol. 13975). Recon Tech. Rep. N, 7.
- Michael, G.G., Neukum, G., 2010. Planetary surface dating from crater size–frequency distribution measurements: Partial resurfacing events and statistical age uncertainty. *Earth Planet. Sci. Lett.* 294, 223–229.
- McKinnon, W.B., Nimmo, F., Wong, T., Schenk, P.M., White, O.L., Roberts, J.H., Moore, J.M., Spencer, J.R., Howard, A.D., Umurhan, O.M. and Stern, S.A., 2016. Convection in a volatile nitrogen-ice-rich layer drives Pluto’s geological vigour. *Nature*, 534(7605), pp.82-85.
- McKinnon, W.B., Glein, C.R., Bertrand, T., and Rhoden, A.R., 2021. Formation, composition, and history of the Pluto system: A post-New Horizons synthesis. In *The Pluto System After New Horizons* (S. A. Stern, J. M. Moore, W. M. Grundy, L. A. Young, and R. P. Binzel, eds.), pp. 507–543. Univ. of Arizona, Tucson, DOI: 10.2458/azu_uapress_9780816540945-ch022.
- Michael, G.G. and Neukum, G., 2010. Planetary surface dating from crater size–frequency distribution measurements: Partial resurfacing events and statistical age uncertainty. *Earth and Planetary Science Letters*, 294(3-4), pp.223-229.
- Miller, S.L., 1953. A production of amino acids under possible primitive earth conditions. *Science*, 117(3046), pp.528-529.
- Moore, J.M., Mellon, M.T. and Zent, A.P., 1996. Mass wasting and ground collapse in terrains of volatile-rich deposits as a solar system-wide geological process: The pre-Galileo view. *Icarus*, 122(1), pp.63-78.
- Moore, J.M., Asphaug, E., Morrison, D., Spencer, J.R., Chapman, C.R., Bierhaus, B., Sullivan, R.J., Chuang, F.C., Klemaszewski, J.E., Greeley, R. and Bender, K.C.,

1999. Mass movement and landform degradation on the icy Galilean satellites: Results of the Galileo nominal mission. *Icarus*, 140(2), pp.294-312.
- Moore, J.M., McKinnon, W.B., Spencer, J.R., Howard, A.D., Schenk, P.M., Beyer, R.A., Nimmo, F., Singer, K.N., Umurhan, O.M., White, O.L. and Stern, S.A., 2016. The geology of Pluto and Charon through the eyes of New Horizons. *Science*, 351(6279), pp.1284-1293.
- Moore, J.M., Howard, A.D., Umurhan, O.M., White, O.L., Schenk, P.M., Beyer, R.A., McKinnon, W.B., Spencer, J.R., Grundy, W.M., Lauer, T.R. and Nimmo, F., 2017. Sublimation as a landform-shaping process on Pluto. *Icarus*, 287, pp.320-333.
- Morison, A., Labrosse, S. and Choblet, G., 2021. Sublimation-driven convection in Sputnik Planitia on Pluto. *Nature*, 600(7889), pp.419-423.
- Murchie, S.L., Head, J.W. and Plescia, J.B., 1989. Crater densities and crater ages of different terrain types on Ganymede. *Icarus*, 81(2), pp.271-297
- National Academies of Sciences, Engineering, and Medicine 2018, *Visions into Voyages for Planetary Science in the Decade 2013-2022: A Midterm Review* (Washington, DC: The National Academies Press), <https://doi.org/10.17226/25186>.
- National Academies of Sciences, Engineering, and Medicine, 2022. *Origins, Worlds, and Life: A Decadal Strategy for Planetary Science and Astrobiology 2023-2032*. doi: <https://doi.org/10.17226/26522>.
- Neish, C.D., Somogyi, A., Imanaka, H., Lunine, J.I. and Smith, M.A., 2008. Rate measurements of the hydrolysis of complex organic macromolecules in cold aqueous solutions: implications for prebiotic chemistry on the early Earth and Titan. *Astrobiology*, 8(2), pp.273-287.
- Neish, C.D., Somogyi, A. and Smith, M.A., 2010. Titan's primordial soup: formation of amino acids via low-temperature hydrolysis of tholins. *Astrobiology*, 10(3), pp.337-347.

- Neish, C.D. and Lorenz, R.D., 2012. Titan's global crater population: A new assessment. *Planetary and Space Science*, 60(1), pp.26-33.
- Neish, C.D., Kirk, R.L., Lorenz, R.D., Bray, V.J., Schenk, P., Stiles, B.W., Turtle, E., Mitchell, K., Hayes, A. and Cassini RADAR Team, 2013. Crater topography on Titan: Implications for landscape evolution. *Icarus*, 223(1), pp.82-90.
- Neish, C.D. and Lorenz, R.D., 2014. Elevation distribution of Titan's craters suggests extensive wetlands. *Icarus*, 228, pp.27-34.
- Neish, C.D., Molaro, J.L., Lora, J.M., Howard, A.D., Kirk, R.L., Schenk, P., Bray, V.J. and Lorenz, R.D., 2016. Fluvial erosion as a mechanism for crater modification on Titan. *Icarus*, 270, pp.114-129.
- Neish, C.D., Lorenz, R.D., Turtle, E.P., Barnes, J.W., Trainer, M.G., Stiles, B., Kirk, R., Hibbitts, C.A. and Malaska, M.J., 2018. Strategies for detecting biological molecules on Titan. *Astrobiology*, 18(5), pp.571-585.
- Neukum, G., 1984. Meteorite bombardment and dating of planetary surfaces (No. NASA-TM-77558).
- Newton, I., 1687. *Philosophiae Naturalis Principia Mathematica*. Londini, Jussu Societatis Regiae ac Typis Josephi Streater. Prostat apud plures Bibliopolas. Anno. [Pdf] Retrieved from the Library of Congress, <https://www.loc.gov/item/28020872/>.
- Nimmo, F., Barr, A.C., Behouňková, M. and McKinnon, W.B., 2018. The thermal and orbital evolution of Enceladus: observational constraints and models. *Enceladus and the icy moons of Saturn*, 475, pp.79-94.
- Nimmo, F. and McKinnon, W.B., 2021. Geodynamics of Pluto. *The Pluto System After New Horizons*, p.89.
- Osinski, G.R., Grieve, R.A., Marion, C. and Chanou, A., 2012a. Impact melting. *Impact Cratering-Processes and Products*.

- Osinski, G.R., Grieve, R.A. and Tornabene, L.L., 2012b. Excavation and impact ejecta emplacement. *Impact Cratering—Processes and Products*, pp.43-59.
- Osinski, G.R. and Pierazzo, E., 2012. Impact cratering: Processes and products. *Impact Cratering*, pp.1-20.
- Pappalardo, R.T., Reynolds, S.J. and Greeley, R., 1997. Extensional tilt blocks on Miranda: Evidence for an upwelling origin of Arden Corona. *Journal of Geophysical Research: Planets*, 102(E6), pp.13369-13379.
- Pappalardo, R.T. and Barr, A.C., 2004. The origin of domes on Europa: The role of thermally induced compositional diapirism. *Geophysical Research Letters*, 31(1).
- Parmentier, E.M. and Head, J.W., 1981. Viscous relaxation of impact craters on icy planetary surfaces: Determination of viscosity variation with depth. *Icarus*, 47(1), pp.100-111.
- Parmentier, E.M., Squyres, S.W., Head, J.W. and Allison, M.L., 1982. The tectonics of Ganymede. *Nature*, 295(5847), pp.290-293.
- Passey, Q.R. and Shoemaker, E.M., 1982. Craters and basins on Ganymede and Callisto- Morphological indicators of crustal evolution. *Satellites of Jupiter*, pp.379-434.
- Phillips, C.B. and Pappalardo, R.T., 2014. Europa Clipper mission concept: Exploring Jupiter's ocean moon. *Eos, Transactions American Geophysical Union*, 95(20), pp.165-167.
- Pierazzo, E., Vickery, A.M., and Melosh, H.J., 1997. A reevaluation of impact melt production. *Icarus*, 127(2), pp.408-423.
- Pike, R.J., 1977. Apparent depth/apparent diameter relation for lunar craters. In *Lunar and planetary science conference proceedings (Vol. 8, pp. 3427-3436)*.
- Poggiali, V., Mastrogiuseppe, M., Hayes, A.G., Seu, R., Birch, S.P.D., Lorenz, R., Grima, C. and Hofgartner, J.D., 2016. Liquid-filled canyons on Titan. *Geophysical Research Letters*, 43(15), pp.7887-7894.

- Poirier, J.P., 1982. Rheology of ices: a key to the tectonics of the ice moons of Jupiter and Saturn. *Nature*, 299(5885), pp.683-687.
- Porter, S., Verbiscer, A., Spencer, J.R., Weaver Jr, H.A., Buie, M.W., Benecchi, S., Olkin, C. and Stern, A., 2017, December. Constraints on the shapes and rotational states of the distant new horizons Kuiper Belt targets. In AGU Fall Meeting Abstracts (Vol. 2017, pp. P13F-07).
- Postberg, F., Clark, R.N., Hansen, C.J., Coates, A.J., Dalle Ore, C.M., Scipioni, F., Hedman, M. and Waite, J., 2018. Plume and surface composition of Enceladus. *Enceladus and the icy moons of Saturn*, pp.129-162.
- Quirico, E., Douté, S., Schmitt, B., de Bergh, C., Cruikshank, D.P., Owen, T.C., Geballe, T.R. and Roush, T.L., 1999. Composition, physical state, and distribution of ices at the surface of Triton. *Icarus*, 139(2), pp.159-178.
- Rathbun, J.A., Musser Jr, G.S. and Squyres, S.W., 1998. Ice diapirs on Europa: Implications for liquid water. *Geophysical research letters*, 25(22), pp.4157-4160.
- Robbins, S.J., Singer, K.N., Bray, V.J., Schenk, P., Lauer, T.R., Weaver, H.A., Runyon, K., McKinnon, W.B., Beyer, R.A., Porter, S. and White, O.L., 2017. Craters of the Pluto-Charon system. *Icarus*, 287, pp.187-206.
- Robbins, S.J., Watters, W.A., Chappelow, J.E., Bray, V.J., Daubar, I.J., Craddock, R.A., Beyer, R.A., Landis, M., Ostrach, L.R., Tornabene, L. and Riggs, J.D., 2018. Measuring impact crater depth throughout the solar system. *Meteoritics & Planetary Science*, 53(4), pp.583-637.
- Roberts, J.H. and Nimmo, F., 2008. Tidal heating and the long-term stability of a subsurface ocean on Enceladus. *Icarus*, 194(2), pp.675-689.
- Ross M. and Schubert G. (1989) Viscoelastic models of tidal heating in Enceladus. *Icarus*, 78, 90–101.

- Rubanenko, L., Venkatraman, J. and Paige, D.A., 2019. Thick ice deposits in shallow simple craters on the Moon and Mercury. *Nature Geoscience*, 12(8), pp.597-601.
- Sagan, C. and Khare, B.N., 1979. Tholins: Organic chemistry of interstellar grains and gas. *Nature*, 277(5692), pp.102-107.
- Schenk, P.M., 2002. Thickness constraints on the icy shells of the Galilean satellites from a comparison of crater shapes. *Nature*, 417(6887), pp.419-421.
- Schenk, P.M. and Zahnle, K., 2007. On the negligible surface age of Triton. *Icarus*, 192(1), pp.135-149.
- Schenk, P.M., Beyer, R.A., McKinnon, W.B., Moore, J.M., Spencer, J.R., White, O.L., Singer, K., Nimmo, F., Thomason, C., Lauer, T.R. and Robbins, S., 2018. Basins, fractures and volcanoes: Global cartography and topography of Pluto from New Horizons. *Icarus*, 314, pp.400-433.
- Schenk, P.M., Beddingfield, C.B., Bertrand, T., Bierson, C., Beyer, R., Bray, V.J., Cruikshank, D., Grundy, W.M., Hansen, C., Hofgartner, J. and Martin, E., 2021. Triton: Topography and Geology of a Probable Ocean World with Comparison to Pluto and Charon. *Remote Sensing*, 13(17), p.3476.
- Schmidt, B.E., Blankenship, D.D., Patterson, G.W. and Schenk, P.M., 2011. Active formation of 'chaos terrain' over shallow subsurface water on Europa. *Nature*, 479(7374), pp.502-505.
- Schubert, G., Sohl, F. and Hussmann, H., 2009. Interior of Europa. *Europa*, pp.353-367.
- Schurmeier, L.R., Dombard, A.J., 2018. Crater relaxation on Titan aided by low thermal conductivity sand infill. *Icarus* 305, 314–323.
<https://doi.org/10.1016/j.icarus.2017.10.034>
- Senft, L.E., and Stewart, S.T., 2008. Impact crater formation in icy layered terrains on Mars. *Meteoritics & Planetary Science*, 43, pp.1993-2013.

- Shoemaker, E.M., Kieffer, S.W. and Sutton, R.L., 1974. Guidebook to the geology of Meteor Crater, Arizona. Guidebook, pp.i-66.
- Silber, E. A., Osinski, G. R., Johnson, B. C., & Grieve, R. A. (2017). Effect of impact velocity and acoustic fluidization on the simple-to-complex transition of lunar craters. *Journal of Geophysical Research: Planets*, 122(5), 800-821.
- Silber, E. A., Johnson, B. C., Bjornnes, E., MacGregor, J. A., Larsen, N. K., & Wiggins, S. E. (2021). Effect of ice sheet thickness on formation of the Hiawatha impact crater. *Earth and Planetary Science Letters*, 566, 116972.
- Singer, K.N., McKinnon, W.B., Gladman, B., Greenstreet, S., Bierhaus, E.B., Stern, S.A., Parker, A.H., Robbins, S.J., Schenk, P.M., Grundy, W.M. and Bray, V.J., 2019. Impact craters on Pluto and Charon indicate a deficit of small Kuiper belt objects. *Science*, 363(6430), pp.955-959.
- Singer, K.N., Greenstreet, S., Schenk, P.M., Robbins, S.J. and Bray, V.J., 2021. Impact craters on Pluto and Charon and terrain age estimates. *The Pluto System After New Horizons*, p.121.
- Singer, K.N., White, O.L., Schmitt, B., Rader, E.L., Protopapa, S., Grundy, W.M., Cruikshank, D.P., Bertrand, T., Schenk, P.M., McKinnon, W.B. and Stern, S.A., 2022. Large-scale cryovolcanic resurfacing on Pluto. *Nature communications*, 13(1), pp.1-9.
- Smith, B.A., Soderblom, L., Beebe, R., Boyce, J., Briggs, G., Bunker, A., Collins, S.A., Hansen, C.J., Johnson, T.V., Mitchell, J.L. and Terrile, R.J., 1981. Encounter with Saturn: Voyager 1 imaging science results. *Science*, 212(4491), pp.163-191.
- Smith, B.A., Soderblom, L., Batson, R., Bridges, P., Inge, J.A.Y., Masursky, H., Shoemaker, E., Beebe, R., Boyce, J., Briggs, G. and Bunker, A., 1982. A new look at the Saturn system: The Voyager 2 images. *Science*, 215(4532), pp.504-537.
- Soderblom, L.A., Kirk, R.L., Lunine, J.I., Anderson, J.A., Baines, K.H., Barnes, J.W., Barrett, J.M., Brown, R.H., Buratti, B.J., Clark, R.N. and Cruikshank, D.P., 2007.

Correlations between Cassini VIMS spectra and RADAR SAR images: Implications for Titan's surface composition and the character of the Huygens Probe Landing Site. *Planetary and Space Science*, 55(13), pp.2025-2036.

Sohl, F., Choukroun, M., Kargel, J., Kimura, J., Pappalardo, R., Vance, S. and Zolotov, M., 2010. Subsurface water oceans on icy satellites: Chemical composition and exchange processes. *Space Science Reviews*, 153(1), pp.485-510.

Sotin, C., Tobie, G., Wahr, J., McKinnon, W.B., McKinnon, W.B. and Khurana, K.K., 2009. Tides and tidal heating on Europa. *Europa*, 11.

Sparks, W.B., Schmidt, B.E., McGrath, M.A., Hand, K.P., Spencer, J.R., Cracraft, M. and Deustua, S.E., 2017. Active cryovolcanism on Europa?. *The Astrophysical Journal Letters*, 839(2), p.L18.

Spencer, J.R., Barr, A.C., Esposito, L.W., Helfenstein, P., Ingersoll, A.P., Jaumann, R., McKay, C.P., Nimmo, F. and Waite, J.H., 2009. Enceladus: An active cryovolcanic satellite. In *Saturn from Cassini-Huygens* (pp. 683-724). Springer, Dordrecht.

Spencer, J.R. and Nimmo, F., 2013. Enceladus: An active ice world in the Saturn system. *Annu. Rev. Earth Planet. Sci*, 41(1), pp.693-717.

Spencer, J.R., Nimmo, F., Ingersoll, A.P., Hurford, T.A., Kite, E.S., Rhoden, A.R., Schmidt, J. and Howett, C.J.A., 2018. Plume origins and plumbing: from ocean to surface. *Enceladus and the icy moons of Saturn*, pp.163-174.

Spencer, J., Beyer, R.A., Robbins, S.J., Singer, K.N. and Nimmo, F., 2021. The geology and geophysics of Charon. *The Pluto System After New Horizons*, p.395.

Squyres, S.W. and Croft, S.K., 1986. The tectonics of icy satellites. In *IAU Colloq. 77: Some Background about Satellites* (pp. 293-341).

Squyres, S.W., Reynolds, R.T., Cassen, P.M. and Peale, S.J., 1983. Liquid water and active resurfacing on Europa. *Nature*, 301(5897), pp.225-226.

- Stern, S.A., Bagenal, F., Ennico, K., Gladstone, G.R., Grundy, W.M., McKinnon, W.B., Moore, J.M., Olkin, C.B., Spencer, J.R., Weaver, H.A. and Young, L.A., 2015a. The Pluto system: Initial results from its exploration by New Horizons. *Science*, 350(6258), p.1815.
- Stern, S.A., Porter, S. and Zangari, A., 2015b. On the roles of escape erosion and the viscous relaxation of craters on Pluto. *Icarus*, 250, pp.287-293.
- Stern, S.A., Grundy, W., McKinnon, W.B., Weaver, H.A. and Young, L.A., 2017. The Pluto system after new horizons. arXiv preprint arXiv:1712.05669.
- Stiles, B.W., Hensley, S., Gim, Y., Bates, D.M., Kirk, R.L., Hayes, A., Radebaugh, J., Lorenz, R.D., Mitchell, K.L., Callahan, P.S. and Zebker, H., 2009. Determining Titan surface topography from Cassini SAR data. *Icarus*, 202(2), pp.584-598.
- Stofan, E.R., Elachi, C., Lunine, J.I., Lorenz, R.D., Stiles, B., Mitchell, K.L., Ostro, S., Soderblom, L., Wood, C., Zebker, H. and Wall, S., 2007. The lakes of Titan. *nature*, 445(7123), pp.61-64.
- Telfer, M.W., Parteli, E.J., Radebaugh, J., Beyer, R.A., Bertrand, T., Forget, F., Nimmo, F., Grundy, W.M., Moore, J.M., Stern, S.A. and Spencer, J., 2018. Dunes on Pluto. *Science*, 360(6392), pp.992-997.
- Thompson, W.R. and Sagan, C., 1992, April. Organic chemistry on Titan-surface interactions. In *Symposium on Titan* (Vol. 338, pp. 167-176).
- Tobie, G., Grasset, O., Lunine, J.I., Mocquet, A. and Sotin, C., 2005. Titan's internal structure inferred from a coupled thermal-orbital model. *Icarus*, 175(2), pp.496-502.
- Tobie, G., Lunine, J.I. and Sotin, C., 2006. Episodic outgassing as the origin of atmospheric methane on Titan. *Nature*, 440(7080), pp.61-64.
- Tomasko, M.G., Archinal, B., Becker, T., Bézard, B., Bushroee, M., Combes, M., Cook, D., Coustenis, A., De Bergh, C., Dafoe, L.E. and Dose, L., 2005. Rain, winds and

haze during the Huygens probe's descent to Titan's surface. *Nature*, 438(7069), pp.765-778.

Tombaugh, C.W., 1946. The search for the ninth planet, Pluto. Leaflet of the Astronomical Society of the Pacific, 5, p.73.

Towner, M.C., Garry, J.R.C., Lorenz, R.D., Hagermann, A., Hathi, B., Svedhem, H., Clark, B.C., Leese, M.R. and Zarnecki, J.C., 2006. Physical properties of Titan's surface at the Huygens landing site from the Surface Science Package Acoustic Properties sensor (API-S). *Icarus*, 185(2), pp.457-465.

Tucker, G.E. and Hancock, G.R., 2010. Modelling landscape evolution. *Earth Surface Processes and Landforms*, 35(1), pp.28-50.

Turtle, E.P. and Pierazzo, E., 2001. Thickness of a European ice shell from impact crater simulations. *Science*, 294(5545), pp.1326-1328.

Turtle, E.P., Pierazzo, E., Collins, G.S., Osinski, G.R., Melosh, H.J., Morgan, J.V. and Reimold, W.U., 2005. Impact structures: What does crater diameter mean. *Large meteorite impacts III*, 384, pp.1-24.

Waite, J.H., Glein, C.R., Perryman, R.S., Teolis, B.D., Magee, B.A., Miller, G., Grimes, J., Perry, M.E., Miller, K.E., Bouquet, A. and Lunine, J.I., 2017. Cassini finds molecular hydrogen in the Enceladus plume: evidence for hydrothermal processes. *Science*, 356(6334), pp.155-159.

Wakita, S., Johnson, B.C., Soderblom, J.M., Shah, J. and Neish, C.D., 2022. Methane-saturated layers limit the observability of impact craters on Titan. *The Planetary Science Journal*, 3(2), p.50.

Watson, K., Murray, B.C. and Brown, H., 1962. The stability of volatiles in the solar system. *Icarus*, 1(1-6), pp.317-327.

White, O.L., Moore, J.M., Howard, A.D., McKinnon, W.B., Keane, J.T., Singer, K.N., Bertrand, T., Robbins, S.J., Schenk, P.M., Schmitt, B. and Buratti, B.J., 2019.

Washboard and fluted terrains on Pluto as evidence for ancient glaciation. *Nature Astronomy*, 3(1), pp.62-68.

White, O.L., Moore, J.M., Howard, A.D., Schenk, P.M., Singer, K.N., Williams, D.A. and Lopes, R.M.C., 2021. The geology of Pluto. *The Pluto System After New Horizons*, p.55.

Zahnle, K., Dones, L., Levison, H.F., 1998. Cratering Rates on the Galilean Satellites. *Icarus* 136, 202–222. <https://doi.org/10.1006/icar.1998.6015>

Zahnle, K., Schenk, P., Levison, H., Dones, L., 2003. Cratering rates in the outer Solar System. *Icarus* 163, 263–289. [https://doi.org/10.1016/S0019-1035\(03\)00048-4](https://doi.org/10.1016/S0019-1035(03)00048-4)

Zebker, H.A., Stiles, B., Hensley, S., Lorenz, R., Kirk, R.L. and Lunine, J., 2009. Size and shape of Saturn's moon Titan. *Science*, 324(5929), pp.921-923.

Zolotov, M.Y. and Kargel, J.S., 2009. On the chemical composition of Europa's icy shell, ocean, and underlying rocks (Vol. 431). Tucson: University of Arizona Press.

Chapter 2

2 Modeling the Distribution of Organic Carbon and Nitrogen in Impact Crater Melt on Titan¹

2.1 Introduction

Titan is one of the most chemically rich places in the solar system. It houses a dense nitrogen rich atmosphere with small amounts of methane (Lindal et al., 1983; Tomasko et al., 2005). This introduces a unique complexity to Titan's chemistry and geology (Malaska et al., 2020; Hörst, 2017). Solar and cosmic radiation constantly dissociate the molecules in Titan's atmosphere, and, over time, the carbon, hydrogen and nitrogen recombine to form a range of complex organic compounds referred to as tholins (Sagan and Khare, 1979; Sagan and Thompson, 1984; Krasnopolsky et al., 2014). These tholins are the source of Titan's haze, layers of large molecules that scatter and absorb visible light and prevent most of it (~90%) from reaching the surface (Tomasko et al., 2005; Hörst, 2017). Any chemical arrangement that can form likely does, producing molecules with the general formula $C_xH_yN_z$ (Khare et al., 1986). Indeed, Titan possesses an abundance of organic molecules, the most prevalent of these being ethane (C_2H_6), acetylene (C_2H_2), propane (C_3H_8), ethylene (C_2H_4), and hydrogen cyanide (HCN) (Hörst, 2017). Furthermore, Titan's surface pressure is very similar to Earth's (1.5 bar vs 1 bar), and with temperatures of 94 K, methane is stable as both a gas and a liquid at the surface (Kouvaris and Flasar, 1991). This produces a methane hydrological cycle that contributes to Titan's surface degradation (Neish et al., 2013, 2016, 2018; Hedgepeth et al., 2020)

It is possible that Earth's early atmosphere was similar to Titan's present atmosphere (Trainer et al., 2006; He and Smith, 2014). In 1953, the Miller-Urey experiment showed how conditions similar to Titan (an atmosphere rich in reducing molecules) could produce important amino acids relevant to life (Miller, 1953). Later work demonstrated that similar amino acids could be produced in simulated Titan conditions

¹ Hedgepeth, J.E., Buffo, J.J., Chivers, C.J., Neish, C.D. and Schmidt, B.E., 2022. Modeling the Distribution of Organic Carbon and Nitrogen in Impact Crater Melt on Titan. *The Planetary Science Journal*, 3(2), p.51.

(McDonald et al., 1994; Neish et al., 2010; Cleaves, et al., 2014). Thus, understanding the processes occurring in Titan's atmosphere and on its surface may help us understand how life on Earth could have transitioned from abiotic chemistry to biology. Large quantities of organic compounds exist on Titan's surface in the form of sand dunes and methane lakes (Lorenz et al., 2008); the dunes alone cover ~40% of the equatorial regions (Lorenz et al., 2006; Lorenz, 2014). While the exact composition of the sand dunes is not well constrained, the consensus is that they are sourced from Titan's atmosphere and are organic in nature (Soderblom et al., 2007; Barnes et al., 2015; Janssen et al., 2016). These organics make Titan a natural laboratory for prebiotic chemistry. Neish et al. (2010) showed that Titan tholins produce amino acids when exposed to liquid water at room temperature. Titan has an abundance of water in the form of ice, but frigid surface temperatures (~94 K) would impede any long-term life from taking hold (Clarke 2014). However, there exist a number of geophysical processes which may permit opportunities for Titan's tholins to mix with liquid water (Thompson and Sagan, 1992; Neish et al., 2018).

Impact craters on Titan are potentially the most suitable geologic features to facilitate prebiotic chemical reactions of tholins in liquid water (Neish et al., 2018; Crósta et al., 2021). Impact craters deliver massive amounts of energy and melt the bedrock ice at the site of the impact (Osinski et al., 2011). On Titan, this process would produce warm liquid water (>273 K), and depending on the size of the crater, could take hundreds to thousands of years to refreeze, far exceeding the time scales that can be examined in a laboratory (Thompson and Sagan, 1992; Artemieva and Lunine, 2005; O'Brien et al., 2005; Neish et al., 2018). Other mechanisms like cryovolcanos may contain water magma chambers that are sufficiently large to remain liquid over similar time scales, but the lava flows that reach the surface (where the organics are located) would be much shorter lived (Neish et al., 2006). Furthermore, cryovolcanic processes on Titan are likely to be rare, and the cold, ammonia-laced fluid erupted from depth is less conducive to the fast chemical reactions needed to produce biological molecules before the water source freezes (Thompson and Sagan, 1992; Lorenz, 1996; Lopes et al., 2007; Neish et al., 2008, 2010, 2018). Therefore, impact craters are likely the most important astrobiological target on Titan as advanced prebiotic chemistry could have occurred in their temporarily liquid melt sheets.

Titan's biological potential is the primary motivation behind the newly selected Dragonfly mission (Lorenz et al., 2018). Dragonfly is a rotorcraft lander selected to be NASA's fourth New Frontiers mission. Dragonfly will directly sample and analyze the chemistry frozen in Titan's surface ice as well as its atmosphere, including at Selk crater (Lorenz et al., 2018,2021). Selk crater was chosen as a target because it is one of the larger craters on Titan, offering a maximal timespan for chemistry to evolve in its putatively thicker melt deposit (Neish et al., 2018). It is unclear how organic impurities might become trapped in the residual melt and overlying ice as it freezes, however longer timescales are likely the most conducive to the chemical evolution of life (Wald, 1954). This suggests that the most astrobiologically interesting samples will be found in the deep interior of the melt layer, where the water freezes last.

There are 90 suspected impact craters identified on Titan, many of which exhibit high levels of degradation (Hedgepeth et al., 2020). Of particular importance for the present study is naturally forming methane rivers which are known to incise into Titan craters (Neish et al., 2016, 2018; Hedgepeth et al., 2020). These rivers will incise into the frozen melt sheet, depositing ice (and the material trapped in it) in alluvial fans and exposing the interior of the melt deposits along the walls of the riverbed. The alluvial fans and exposed riverbed walls are two direct ways of accessing potentially prebiotic molecules with a landed asset on Titan (Neish et al., 2018). In addition to its size, Selk's depth to diameter ratio indicates that it is relatively fresh and is therefore less likely to be buried in a large amount of aeolian or fluvial deposited sediment (Neish et al., 2018; Hedgepeth et al., 2020). However, its relative depth suggests it is still more than 40% degraded relative to a fresh crater, and its rim heights are generally lower than expected (but within error; Hedgepeth et al., 2020). This is consistent with some fluvial erosion, but it should be noted, no fluvial features are discernable in RADAR or ISS (Imaging Science Subsystem) data, given their limited resolutions. However, evidence of fluvial erosion has been proposed in VIMS data (Soderblom et al., 2010).

In this work, we seek to determine where the products of aqueous prebiotic chemistry are most likely to be located within impact melt sheets on Titan. We use terrestrial sea ice as an endmember analogue for the freezing of organic molecules within

impact craters on Titan. Terrestrial studies have investigated sea ice biogeochemistry, but these results are inherently skewed toward biologic processes so are unlikely to be a good predictor for organics in Titan melt ponds (Collins et al., 2008; Santibáñez et al., 2019). Terrestrial sea ice naturally rejects most impurities as it freezes (Hobbs, 1974), but the physics that control how much is rejected are dependent on the thermal gradient at the solidification interface, as well as the concentration, and chemistry of the brine mixture (Hunke et al., 2011; Buffo et al., 2018, 2020). Therefore, it cannot be assumed that organic molecules on Titan will follow the same pattern as terrestrial impurities, because it has a different chemistry (organics vs. salt) and the ambient temperature is much lower (94 K vs 273 K), leading to significantly different density and thermal gradient extremes. However, once a thin layer (~10 m) of ice covering the melt sheet forms, the thermal gradients in impact melt sheets on Titan become comparable to those in terrestrial sea ice. For Dragonfly to adequately sample the frozen melt for prebiotic (or possibly biologic) products, the team must understand the geologic history of the water-organic mixture at Selk crater. Here, we constrain how much HCN will become trapped in the ice versus rejected into the remaining liquid reservoir under the conditions predicted for fresh impact crater melts on Titan. We use the planetary ice model SlushFund2.0-v2 (SF2) (Buffo et al., 2020) and a heat transfer model (Chivers et al. 2021) to track the concentrations of molecular impurities, both within the ice and the residual melt, as the melt pond refreezes, providing improved estimates of organic material distribution in Titan environments for future planetary exploration.

2.2 Ice-melt Model

2.2.1 Initial Conditions

During the impact cratering process, extreme levels of energy compress and excavate the target material (Melosh, 1989; Osinski and Pierazzo, 2013). Hundreds of GPa of pressure is converted to heat and kinetic energy, vaporizing and melting the bedrock ice (Melosh, 1989). Artemieva and Lunine (2005) estimated a 10 km crater would have a 100 – 200 m thick melt pond and that larger craters will produce melt at ~2-5% of the total volume of a crater. This means Selk crater ($D \cong 84$ km) would have a melt pond ~80 m in depth (Bray et al., 2012; Hedgepeth et al., 2020). O'Brien et al. (2005) were more liberal

with their estimation of melt production, scaling up the ~3% melt volume estimate of Artemieva and Lunine (2005) to ~7%, which may produce melt ponds 100-200 m in depth for a crater of Selk's size (**Figure 2.1**). This may be a reasonable estimate considering lunar models predict that larger impact craters produce larger melt volume fractions, with nearly an order of magnitude higher volume fraction for 100 km craters than 10 km craters (Cintala and Grieve, 1998). Furthermore, Elder et al. (2012) estimated melt volumes of ~10% for a crater of Selk's size on Ganymede, supporting the higher estimate from O'Brien et al., (2005). This is an ideal situation, though; in reality, the icy substrate will become fractured by impact, allowing for drainage of the denser water into the subsurface ice (Elder et al., 2012). Elder et al. (2012) estimated that crater melt ponds on icy satellites will be significantly shallower than the estimates of O'Brien et al. (2005), with only larger craters (> 50 km) being able to retain substantial melt.

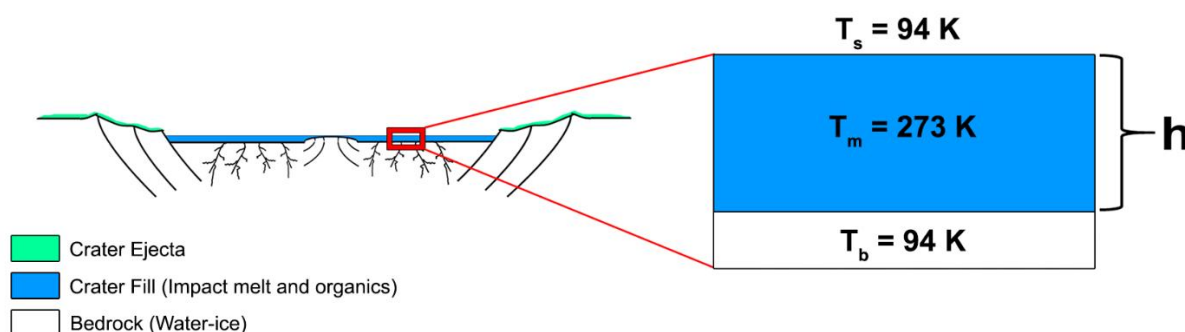


Figure 2.1. Example cross-section of a complex crater on Titan. The crater ejecta is shown in green and the crater melt pond is shown in blue. The red box zooms in on one section of the melt pond of thickness h (m) overlain on a fractured bedrock of water-ice (white). Initial temperatures used in the model are shown for the melt (T_m), bedrock ice (T_b), and surface (T_s).

The thickness of an impact crater melt pond will depend on the crater shape, which changes depending on its size. Small, simple craters form bowl like shapes, but larger, complex craters will experience rebound in the center and collapse (Osinski et al., 2011). The largest craters collapse so severely that they become basins (Melosh, 1989). On Titan, the transition diameter from simple to complex craters is smaller than most of the observed craters (~5 km), assuming Titan craters form with the same crater morphology as those on

Ganymede (Schenk, 2002). The only basin crater observed on Titan is Menrva at ~400 km in diameter. Unlike simple bowl-shaped craters, complex craters typically have flat floors, especially on icy moons (Schenk 2002; Neish et al., 2013). Therefore, the melt ponds can be considered effectively cylindrical in shape (but it may be more of a torus if a central uplift is present).

In terms of organic material, Artemieva and Lunine (2005) estimate the loss of ~90% of the original surface organics in the impact cratering event, with the remaining 10% mixing with the water and sustaining minimal damage from the impact. However, the damage by the impact may have more severe effects on some molecules than others (Pierazzo and Chyba, 1999). For our application, we examine the organic molecule HCN, motivated by its relative abundance on Titan (Krasnopolsky et al., 2014) and its well-studied chemistry (Haynes, 2011). However, HCN will vaporize at ~247.5 K and regions of the melt may range from -203 K to 498 K (Artemieva and Lunine 2005). How much of the melt pond is above its vaporization temperature, and for how long, will determine whether HCN is retained. HCN has been estimated to compose 4%-10% of the material condensed to Titan's surface (Vuitton et al., 2014). Nearly half of the equatorial region is covered with, on average, 30 m of sand dunes, which are suspected to be composed of organics (Lorenz et al., 2008; Hörst, 2017). If we assume this is a good estimate of the dune height in the region of Selk crater when it formed, we can estimate the total volume of dune material that mixed into the Selk melt pond as the volume of a cylinder,

$$V_{dunes} = \pi * r_{crater}^2 * h_{dunes} \quad \text{Equation 2.1}$$

where $r_{crater} = 40 \text{ km}$, and $h_{dunes} = 30 \text{ m}$. Then the final concentration of dunes within the melt sheet can be estimated as,

$$C_{dune} = \frac{V_{dunes}}{V_{melt}} * 10\% \quad \text{Equation 2.2}$$

where only 10% of the dunes are expected to make it into the melt unshocked (Artemieva and Lunine, 2005) and V_{melt} varies based on crater size. For an 80 km crater with 7% melt production (~100 m thick), the concentration of dunes in the melt pond is ~7%. If we assume a conservative concentration (4%) of HCN within the dune material, the

concentration of HCN in the melt would be ~0.25%, or ~2.5% for a much thinner melt sheet (10 m). As the melt sheet freezes and impurities are rejected back into the fluid, concentrations can reach as high as 25% depending on the initial conditions used. We therefore use the SF2 model to study a range of HCN concentrations from 0.1% to 25% by weight (1-250 parts per thousand, or ppt) for melt sheet thicknesses of 10 to 250 m.

However, HCN will not be the only organic molecule present in the melt pond. HCN, as with many other compounds, will quickly undergo hydrolysis into its oxygenated daughter products (e.g., amino acids and nucleobases) at a rate that varies by temperature and pH (Ferris et al., 1978; McDonald et al., 1994; Neish et al., 2010; Hörst et al., 2012; Ruiz-Bermejo et al 2021). HCN's half-life (the time it takes for ½ of it to evolve into its daughter products) is reduced from weeks to minutes by increasing the temperature from 60 °C to 120°C, but if the pH drops below 7, the half-life can go to as high as 100 yrs (Miyakawa et al., 2002). Extrapolating the results of Miyakawa et al. (2002) to temperatures that we would expect in Titan's melt sheet, we would expect half-lives on the order of years at high pHs (≥ 8) and up to centuries for low pHs (≤ 7); these rates are consistent with other low temperature hydrolysis measurements for HCN (Sanchez et al, 1966; Neish et al., 2008, 2009). Therefore, HCN's daughter products would likely dominate the chemistry deeper into the melt sheet and change the chemical properties of the melt in the process.

We therefore acknowledge that tracing organic compounds in the melt sheet is not as simple as modeling just HCN. Other compounds are present, and the total amount of HCN will be reduced with time as it hydrolyzes into different compounds. Therefore, our results are not entirely representative of what Dragonfly is going to observe. Instead, we use HCN as a tracer for the other organic molecules in the melt sheet. Our work is intended as a first order approximation of the freezing process, guiding us to the best place(s) within the melt pond to investigate with Dragonfly. We have modeled at melt concentrations of HCN that are as low as the lowest predicted initial concentrations (~0.1%), to as high a concentration we would expect in the thickest, deepest part of the melt sheet where the rejected material will concentrate with time (10-25%).

2.2.2 1D Ice Model

We use two models to predict the distribution of organics in a Titan melt sheet. We use the 1D multiphase reactive transport model (SF2) of Buffo et al. (2020) to determine the concentration of organics that will freeze into ice of a solidifying Titan impact melt deposit. The outputs of the SF2 model creates a series of approximations that are fed into the second model, a 2D thermophysical model of Chivers et al. (2021) (see **Section 2.2.3**). SF2 is adapted from the sea ice model of Buffo et al. (2018) to accommodate diverse ocean chemistries and planetary thermal environments. Reactive transport modeling is a powerful tool used to simulate physical, chemical and biological processes at a range of spatial and temporal scales (Steeffel et al., 2005). SF2 solves the heat and mass conservation equations governing a reactive porous media using the finite difference method. It employs the enthalpy method to simulate the phase evolution of the system.

In prior work, Buffo et al. (2018) developed a sea ice model that incorporated advection-reaction-diffusion processes using the theory of mushy layers for ice-ocean systems (Worster 1992, 1997; Feltham et al., 2006; Hunke et al., 2011) coupled with parameterized one-dimensional density driven convection. The model takes a continuum approach and spatially averages state variables across discretization cells and employs the enthalpy method of Huber et al. (2008) to iteratively calculate the liquid fraction of each cell. The *mushy layer theory* (Feltham et al., 2006) guarantees the conservation of heat and mass. “Mushy” refers to a system in which multiple components or phases coexist. It allows for different regimes (ice, brine, ice+brine) to be described with the same set of equations.

$$\bar{\rho}c \frac{\partial T}{\partial t} = \frac{\partial}{\partial z} \left(\bar{k} \frac{\partial T}{\partial z} \right) - \rho_{ice} L \frac{\partial \phi}{\partial t} \quad \text{Equation 2.3}$$

$$\phi \frac{\partial S_{br}}{\partial t} = \frac{\partial}{\partial z} \left(\bar{D} \frac{\partial S_{br}}{\partial z} \right) - \frac{\rho_{ice}}{\rho_{br}} S_{br} \frac{\partial \phi}{\partial t} \quad \text{Equation 2.4}$$

Here, ρ is density, T is temperature, t is time, z is the vertical coordinate, k is thermal conductivity, L is the latent heat of fusion for the water to ice phase transformation, ϕ is the liquid fraction, S is HCN concentration, and D is HCN diffusivity. Subscripts *ice* and *br* refer to characteristics of the ice and brine components of the cell, respectively, and

variables with an over bar are volumetrically averaged quantities. That is, they are averaged using the respective amounts of ice and brine in the mixture, using the current liquid fraction (ϕ) (e.g., a hypothetical value y would be averaged, $\bar{y} = \phi y_{br} + (1 - \phi)y_{ice}$). All variables and their values can be found in **Table 2.1**.

In their basic forms, **Equation 2.3** is an expression of heat conservation, and **Equation 2.4** is an expression of HCN conservation. **Equation 2.4** tracks the bulk change in the diffusion of the solute (where $D_{ice} = 0$), and the concentration of the solute by a phase change. The work of Buffo et al. (2018) was adapted to model the European ice and ocean boundary (Buffo et al., 2020). The key modification Buffo et al. (2020) made to their 2018 model was to ignore rejection of salt by volumetric changes that occur during freezing in the mushy layer. In terrestrial sea ice, volumetric changes were shown to play a negligible role in the rejection of salt (Buffo et al., 2020); the primary factor controlling salt removal is gravity drainage (Hunke et al., 2011).

Thus, we move forward with two partial differential equations that contain three unknowns (T, S, ϕ). We therefore need another constraint to solve this system of equations. Buffo et al. (2018) use the enthalpy method (e.g., see Huber et al. (2008)) to calculate the liquid fraction (ϕ) of each cell.

$$H = c_{ice}T + L\phi \quad \text{Equation 2.5}$$

$$\phi = \begin{matrix} 0 \\ (H - H_s)/L \\ 1 \end{matrix} \quad \text{if } \begin{matrix} H < H_s = c_{ice}T_m \\ H_s \leq H \leq H_s + L \\ H > H_s + L \end{matrix} \quad \text{Equation 2.6}$$

Here, H is enthalpy, T_m is the melting temperature, c is specific heat capacity, and H_s is the enthalpy if the cell was completely frozen (enthalpy of solid ice). The model iterates **Equations 2.5** and **2.6** with **Equations 2.3** and **2.4** until the T, S , and ϕ converge before moving onto the next time step of the simulation.

As water freezes, the solute will concentrate, and a density difference will be created in the form of a concentration gradient. Buffo et al. (2018) describes this using the

approach of Griewank and Notz (2013)'s 1-D model of gravity drainage by finding the amount of vertical brine transported by convection (br_j^\downarrow).

$$br_j^\downarrow = \alpha(Ra_j - Ra_c)dz^3 dt = \alpha \left(\frac{g\rho_{sw}\beta\Delta S_j\tilde{\Pi}_j h_j}{\kappa\mu} - Ra_c \right) dz^3 dt \quad \text{Equation 2.7}$$

Here, α is a constant of proportionality optimized by Griewank and Notz (2013), Ra_j is the Rayleigh number of the j th layer, Ra_c is the critical Rayleigh number, dz and dt are the spatial and temporal discretization sizes, g is the acceleration due to gravity, ρ_{sw} is the density of meltwater, β is a density coefficient describing the relationship between density and concentration, ΔS_j is the difference in concentration of the brine from ambient seawater, h_j is the height of the j th layer above the basal surface of the ice, κ is the thermal diffusivity of seawater, μ is the kinematic viscosity of seawater, and $\tilde{\Pi}_j$ is the minimum permeability of any layer between the j th layer and the basal ice surface. It is found using the permeability function given by Griewank and Notz (2013).

In essence, **Equation 2.7** is a measure of how much an element exceeds the critical Rayleigh number, which triggers the brine transport. The localized differences in the Rayleigh number fuels convection, which is the dominant process in the desalinization of sea ice (Buffo et al., 2018, 2020). The brine transport changes the concentration (S) and temperature (T) that feeds into the conservation equations of the Mushy Layer Model. Note that we assume constants optimized for sea ice by Griewank and Notz (2013) are adequate for our study, and that the thermal diffusivity and viscosity are approximately the same as sea water (**Table 2.1**). As water freezes, impurities are concentrated within the residual liquid fraction (pore space) of the two-phase interfacial layer. In terrestrial sea ice, this translates to pockets and veins of concentrated brines (Buffo et al., 2018).

Table 2.1. All variables used in the text, along with their definition, values, and units.

Symbol	Definition	Value	Units
α	1-D advection coefficient	1.56×10^{-1}	-
br_j^{\downarrow}	Vertical brine transported	Calculated	kg
β	Density coefficient	3.139×10^{-4}	$kg ppt^{-1}$
c_{br}	Brine heat capacity	Calculated	-
c_{ice}	Water ice heat capacity	2000	$J kg^{-1} K^{-1}$
dt	Time discretization	1 - 10,000	s
dz	Spatial discretization	.01 - .025	m
D	HCN diffusivity	Calculated ^a	$m^2 s^{-1}$
H	Enthalpy	Calculated	$J kg^{-1}$
H_c	Enthalpy of solid cell	Calculated	$J kg^{-1}$
g	Acceleration due to gravity	1.352	ms^{-2}
h	Distance to interface	Varies	m
H	Melt pond thickness	Varies	m
k_{HCN}	HCN thermal conductivity	0.2256	$Wm^{-1}K^{-1}$
k_{br}	Brine thermal conductivity	Calculated	$Wm^{-1}K^{-1}$
k_{ice}	Water ice heat conductivity	2.0	$Wm^{-1}K^{-1}$
κ	Thermal diffusivity	Varies ^a	$m^2 s^{-1}$
L	Latent heat of fusion (ice)	334,774	Jkg^{-1}
μ	Kinematic viscosity	1.55×10^{-3} ^a	$m^2 s^{-1}$
ϕ	Liquid fraction	Calculated	-
ϕ_c	Critical porosity	0.05 ^a	-
ρ_{br}	Brine density	Varies	$kg m^{-3}$
ρ_{ice}	Water ice density	917	$kg m^{-3}$
Π	Permeability	Calculated ^a	m^2
Ra	Rayleigh number	Calculated	-
Ra_c	Critical Rayleigh number	1.01×10^{-2}	-
S	Concentration	Calculated	ppt
T	Temperature	Calculated	K
T_m	Melting temperature	94	K
t	Time	-	s
w	Brine velocity	0	ms^{-1}
ρ_{HCN}	HCN Liquid density	687 ^b	$kg m^{-3}$
$T_{melt,HCN}$	HCN Melting temperature	259.85 ^b	K
$T_{boil,HCN}$	HCN Boiling temperature	298.75 ^b	K
c_{HCN}	HCN Heat capacity	2.612×10^3 ^b	$J kg^{-1} K^{-1}$
k_{HCN}	HCN Heat conductivity	2.28×10^{-9} ^b	$Wm^{-1}K^{-1}$

^aAssumes the value is the same, or calibrated for, sea ice (Buffo et al., 2018, 2020).

^bProperties of HCN at 1 atm and ~20°C are from limited experimental data (MatWeb 2018; Rumble 2020).

2.2.3 Application to Titan

The 1D SF2 model described above uses active interface tracking of the temperature and chemistry of the mushy layer in finite increments (**Figure 2.2**). It focuses on the active two-phase region at the water-ice interface ($H = 1$ m). As each increment (e.g., $dz = 1$ cm) in the active layer freezes (reaches a critical porosity that is estimated from terrestrial ice studies (Buffo et al., 2018)) it is removed from the domain and catalogued while a new increment with ambient liquid water reservoir properties is added to the bottom of the domain. Once an increment of the mushy layer reaches critical porosity ($\phi \leq 5\%$), the ice is assumed to be frozen enough such that all the liquid brine, trapped in pockets and veins, is closed off from the underlying liquid. The impurities become fixed in the ice, and the 1 m mushy layer moves down to the next increment of the melt pond. While Titan's conditions reach more extreme temperatures than the terrestrial sea ice the model was initially designed for, the temperatures within the mushy layer are likely comparable with terrestrial ice (~ 273 K).

In sea ice, the removal of salt from the forming ice layer is gravity driven and due to buoyancy differences between the denser interstitial brine and the underlying ocean (Buffo et al., 2018, 2020). Unlike salt, HCN is less dense than water and ice (**Table 2.2**; Haynes, 2011). This relationship will invert the system such that impurities are buoyantly removed at the base of the melt pond, while at the top, gravity will not drive the removal of impurities (Chivers et al., 2021). Similar scenarios have been studied in terrestrial magma chambers, where low density melt is concentrated in the porous roof magma-rock interface during solidification (Worster, 1990). We propose that HCN in a Titan melt pond would follow the same pattern as less dense impurities in terrestrial lavas because of its buoyancy within water and ice, with HCN becoming entrapped in the ice at the top freeze front. HCN's density relationship with water and ice suggests that as a melt pond freezes from all directions, the HCN dynamics will operate differently at the bottom and upper interface. A key feature of our impact melt system is that it is a closed finite body of water, similar to the proposed pockets of water thought to cause chaos terrain on Europa (Schmidt 2011; Buffo et al., 2020; Chivers et al., 2021). SF2 assumes the mushy layer is atop an infinite ocean and that the rejected impurities will never significantly affect the bulk

concentration of the ocean, however the bulk concentration of a melt pond will become progressively more concentrated as it freezes. SF2 provides an estimate of impurities frozen into the ice for a range of temperature gradients (or depths) at a given concentration of HCN in the melt. Each profile is effectively the concentration of HCN that would freeze into sea ice forming over an infinite ocean. Therefore, we produced multiple impurity entrainment vs. thermal gradient relationships at a range of melt HCN concentrations to encapsulate the evolving conditions (i.e., thermal gradients and melt concentrations) of the melt pond as it freezes (**Figure 2.3**).

These results are incorporated into a 2D thermophysical model by creating a relationship between the impurity entrainment and thermal gradient at the time of freezing. The SF2 results are produced in increments of ≥ 5 m sections of the melt pond over a broad range of depths and thermal gradients sufficient to infer a complete relationship between the impurity entrainment and the depths or thermal gradients anticipated in Titan impact crater melt sheets. We solve the 2D heat transfer model by coupling it with the SF2 results. We fit impurity entrainment results to complete profiles using a set of constitutive equations produced by Buffo et al. (2020) to construct quasi-analytical concentration dependencies that can be utilized without explicit simulations (**Table 2.2**). We then reproduced the results for a range of initial concentrations of HCN in the melt. This accounts for the changing fluid concentration as the melt pond freezes, which is necessary to produce an impurity entrainment relationship for Titan crater melt ponds as opposed to an infinite ocean. The 2D heat transfer model uses the impurity entrapment-thermal gradient profiles, interpolating between them using a linear least squares method to create a reference to track how much impurity is entrained into the ice in a closed system like a melt pond. This reference is crucial in tracking how much impurity is entrained in the ice because the thermal gradient at the freeze front and the impurity concentration in the melt changes as the melt pond freezes, and both variables are inextricably linked to how much impurity is entrapped in the ice (**Figure 2.3**)

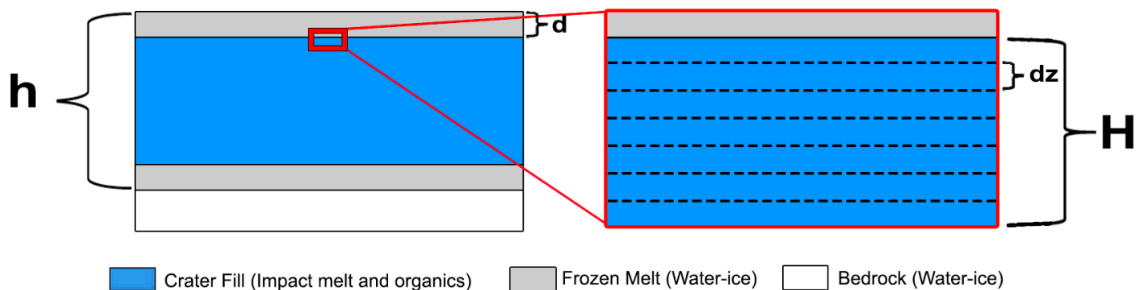


Figure 2.2. The SF2 model tracks the mushy water-ice interface (red box) within the finite region of space H (m) where each increment (dz) represents a volume average over some finite length (m). When the upper most increment of the water-ice interface reaches a critical porosity (here $\phi \leq 0.05$), the water-ice interface (H) shifts downward by one spatial increment (dz) and the concentration of the frozen increment ($\phi \leq 0.05$) is assumed to be trapped in the ice and remains constant throughout the remainder of the simulation. This process continues throughout the depth of the pond h (m), beginning at some interface depth d (m). The model tracks the freeze front where buoyancy will drive impurities out of the ice. For salt, the model tracks the chamber roof's freezing front as imaged here, but for HCN the model is tracking the floor's upward propagating freeze front. In our work, the model runs bottom-up because HCN is less dense than water and ice, resulting in upward gravity drainage (see text for more details).

As previously outlined, we studied a range of concentrations from 0.1% to 25%. However, the model was unable to converge at higher concentrations ($>7.5\%$) and at low thermal gradients (< 10 K/m) for moderate concentrations (5% - 7.5%). Without these results, we could not construct full profiles using the constitutive equations (**Table 2.2**); these are necessary in tracking a 2D closed system where a range of concentrations will exist. Therefore, we extrapolated from the results at lower concentrations ($\leq 7.5\%$).

There are three areas where extrapolation is performed: the linear thermal gradient domain, the shallow thermal gradient domain, and the entire depth domain (**Figure 2.4**). First, the linear domain is clearly distinguishable in the results for the lower initial concentrations (**Figure 2.4a**). Because the modeled concentrations converge at these lower

thermal gradients, we assume the larger initial concentration profiles converge onto this line too. Therefore, their constants in the constitutive equation are taken to be the average of the constants derived from the lower concentrations. This extrapolation was done for all concentrations $\geq 5\%$ (**Figure 2.4a**). Second, the shallow domain was best constrained using a linear extrapolation, done for all concentrations $\geq 15\%$. The depth relationship is defined by a single constitutive equation, and it was best constrained using a power law extrapolation, where the extrapolation is performed for initial concentrations $\geq 7.5\%$ (**Figure 2.4b**).

We couple these results using the constitutive equations (**Table 2.2**) with a 2D heat transfer model in a stand-alone code built by Chivers et al. (2021) to simulate a simple closed system melt sheet. The Chivers et al. (2021) model is a finite difference model representing a rectangular (cylindrical) melt sheet that tracks the transfer of heat, phase change, and chemistry as the melt sheet freezes. As each element freezes, the model references the SF2 results that correspond to the liquid melt concentration and the thermal gradient of the cell at the time of freezing. The Chivers et al. (2021) model uses this to account for how much HCN is frozen into the ice at the bottom ice-liquid interface, and the rejected HCN increases the liquid melt concentration. As each cell freezes at the upper ice-liquid interface, the model assumes that the amount of HCN that will be trapped in the ice is the same as the liquid melt concentration at the point of freezing. Unlike the SF2 model, the Chivers model uses a temperature dependent ice conductivity to account for the large-scale variations of ice temperatures that exist across the entire model domain, which can become ~ 5 times larger at ambient Titan temperatures than at the melting point of ice (Ahmad and Phillips, 1987).

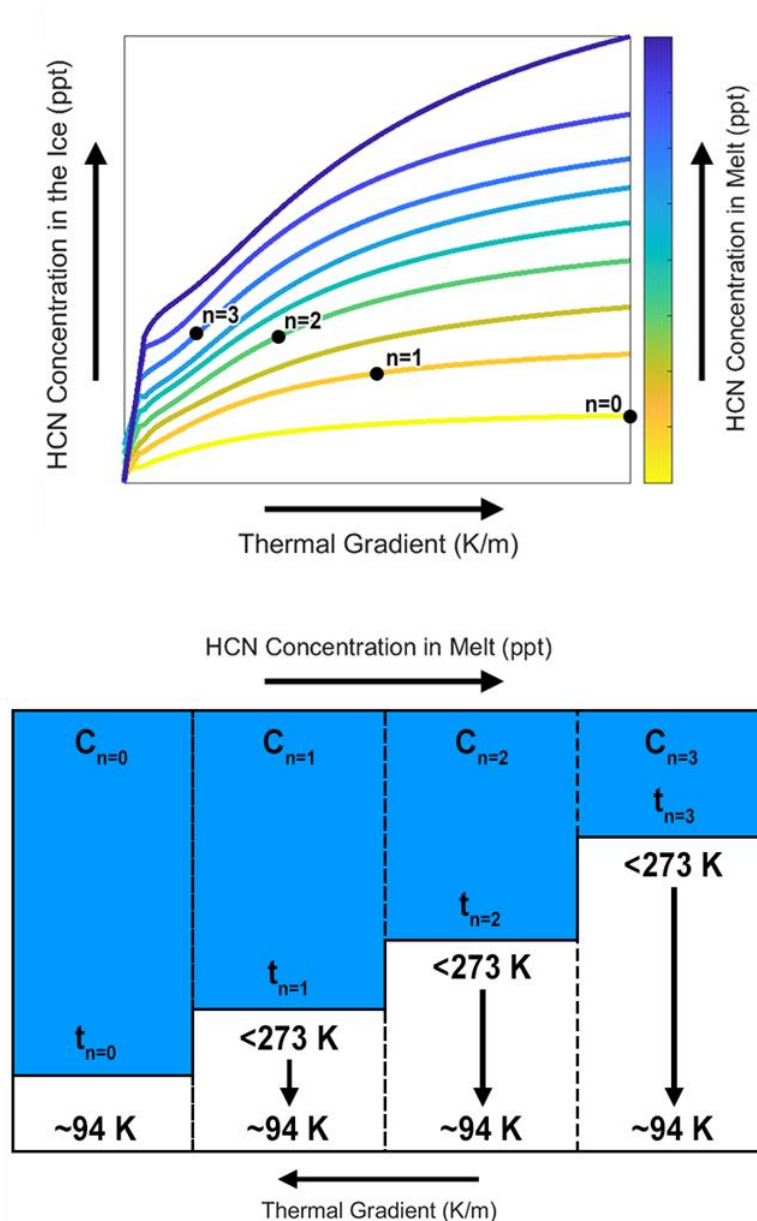


Figure 2.3. (Top) A diagram illustrating the SF2 model outputs of the concentration of HCN entrained in ice at a given thermal gradient, visualized across a range of increasing concentrations in the melt (color coded). The points n_i show how the concentration of HCN trapped in ice will change as the freeze front progresses. (Bottom) We visualize four temporal steps of the $\sim 273\text{ K}$ water melt (blue) freezing into ice (white). As time (t_n) passes, the warmer ice insulates the melt, reducing the thermal gradient at the freeze front. Simultaneously, the concentration of HCN in the melt (C_n) is increasing.

We model a closed 2D melt pond of an 80 km diameter crater (~55 km floor, Bray et al., 2012) mixed with HCN using the same initial conditions as in the SF2 model (**Figure 2.5**). We ran the model for melt sheets of 10 m to 100 m thickness and an initial concentration of HCN ranging from 0.1% to 7.5% by weight HCN, where the highest concentrations in the melt will reach 25% as the melt freezes. The thicker 250 m melt sheet was modeled at just 0.1% because larger initial values caused the melt concentration to exceed 25% as the melt lens shrinks; this is the maximum concentration that we studied with the SF2 model. The heat transfer model begins with 1-10 m of ice frozen at the roof of the melt pond. We do this to avoid the extreme conditions encountered in this region of the melt sheet, which are likely to be chaotic and difficult to model. This initiates the model with a thin layer of ice insulating the melt sheet, assuming that once this ice layer exists, the model will proceed to freeze via conduction.

2.3 Results and Discussion

2.3.1 1D Concentrations

We have created a complete profile of how much HCN will freeze into a solidified water ice melt pond for an array of melt concentrations between 1 ppt (0.1%) and 250 ppt (25%) (**Figure 2.4**). We fit our results to the constitutive equations of Buffo et al., (2020) (**Table 2.2**). These constitutive equations provide a complete profile of bulk HCN in the ice across the melt pond depth for variable temperature gradients (at the instance of freezing). Note that our fits are not perfect; they become less precise at higher thermal gradients and concentrations. The observed imprecision in the fits is not related to the model's physical assumptions, but rather its ability to be fit to the constitutive equations at the extremes found on other worlds. Furthermore, these extremes are occurring at the boundaries of our model (i.e., the highest concentrations occur near the end of the melt pond's evolution and the highest thermal gradients occur at the very beginning of the melt pond's evolution). The intermediate stages are likely to be the most reliable because the thermal gradients are far less extreme and more akin to those in terrestrial environments. Fortunately, this is the region of most interest to Dragonfly because any biomolecules trapped in the upper portions of the melt sheet would have had very little time to evolve into something chemically and astrobiologically interesting. Our fits are also less precise

for the domain where the amount of HCN that is trapped in the ice forms a linear relationship with the thermal gradient (**Table 2.2**). The transition into the linear domain appears to occur at progressively higher thermal gradients for higher melt concentrations. The results at higher concentrations ($> 7.5\%$) are largely extrapolated, as detailed in Section 2.2.3, but these profiles are mostly relevant in the deep interior of the melt sheet as it freezes. The point at which the melt sheet reaches said concentrations will depend on the initial concentration and the melt thickness (**Figure 2.5 and 2.6**). The primary purpose of the extrapolated profiles is to provide an estimate for these large HCN melt concentrations, which only exist in a small region of the melt sheet, but the results in regions of lower concentration are more reliable.

Our results from the SF2 model exhibit clear trends. As expected, higher bulk concentrations will lead to a higher concentration of HCN trapped in the ice. The magnitude of this difference is largest at the highest thermal gradients. We observe that higher HCN concentrations in the liquid melt result in a higher concentration in the ice, but all the concentration profiles soon begin to converge to ~ 1 ppt and below at the lower thermal gradients (more ice insulating the melt). With HCN as the impurity, the SF2 model tracks the HCN entrainment of the freeze front at the base of the crater, and, as stated in Section 2.2.3, buoyancy is assumed to hold the HCN in place at the top interface of the melt pond, resulting in ice compositions that reflect that of the underlying melt.

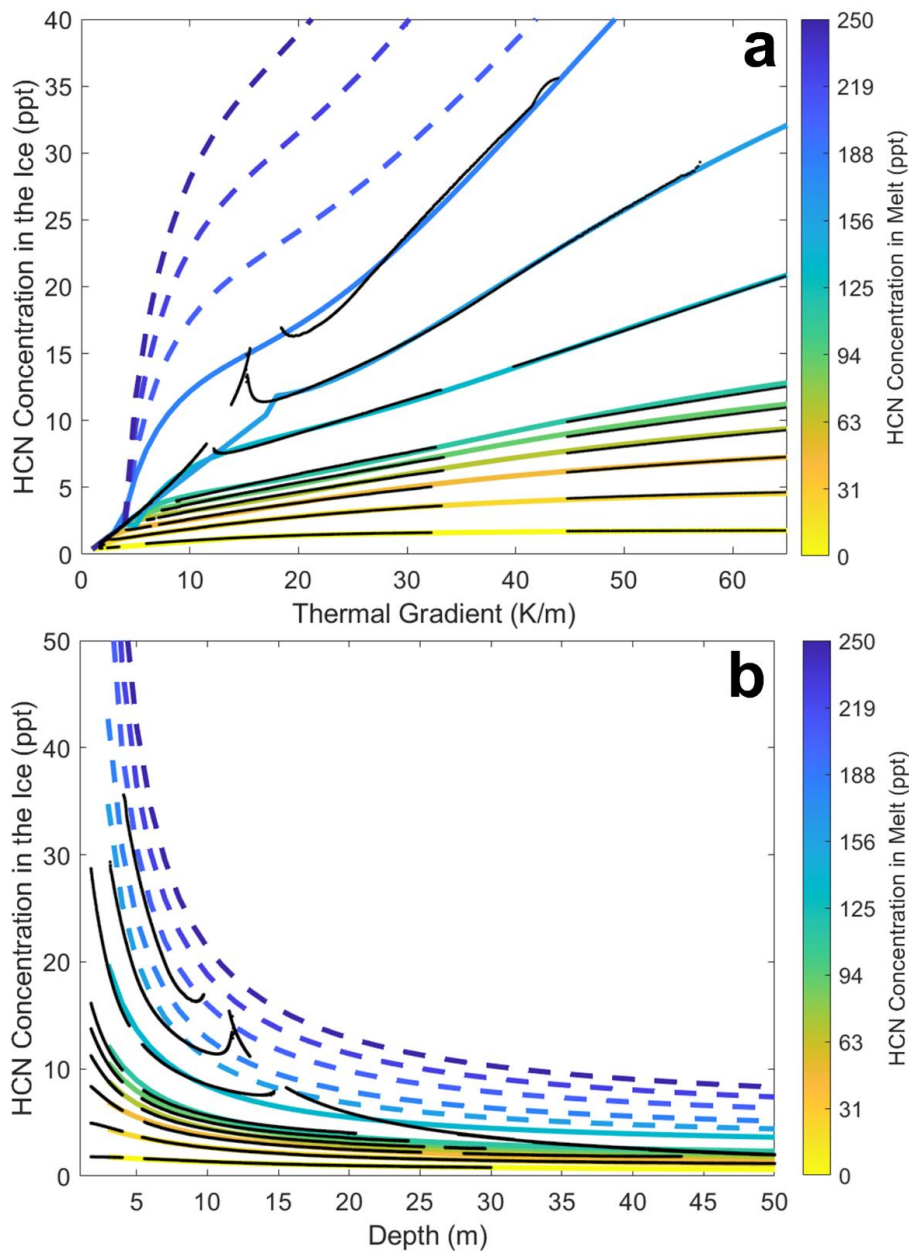


Figure 2.4. Concentration of HCN (ppt) in the frozen melt pond, for initial concentrations of 1 ppt (0.1%, yellow) to 250 ppt (25%, dark blue), at different thermal gradients (a), and depths (b). The SF2 model results are shown with black points (they appear as disjointed lines because the spatial resolution is so fine). The analytical fits from Buffo et al. (2020) are applied to our data, where solid lines are fits formed using SF2 results, and dashed lines are formed by extrapolating from the lower concentration fits (see Table 2.2 and text).

Table 2.2. The constitutive equations developed by Buffo et al. (2020) with the corresponding constants used to fit to our results from the SF2 model. These equations are fit to the data for 1 ppt to 250 ppt. *Indicates values determined using extrapolation and averaging.

Constitutive Equations	a	b	c	d
$S_{tot}(z) = a + \frac{b}{c - z}$	$a_1 = 0.1674$ $a_5 = 00.4654$ $a_{10} = 0.6802$ $a_{15} = 0.9876$ $a_{20} = 1.120$ $a_{25} = 1.328$ $a_{50} = 2.346$ $a_{75} = 2.849^*$ $a_{100} = 3.348^*$ $a_{150} = 4.166^*$ $a_{200} = 4.838^*$ $a_{250} = 5.417^*$	$a_1 = -27.98$ $a_5 = -35.87$ $a_{10} = -43.35$ $a_{15} = -43.64$ $a_{20} = -49.62$ $a_{25} = -51.15$ $a_{50} = -65.06$ $a_{75} = -76.75^*$ $a_{100} = -87.61^*$ $a_{150} = -107.1^*$ $a_{200} = -124.6^*$ $a_{250} = -140.8^*$	$a_1 = -14.26$ $a_5 = -6.127$ $a_{10} = -3.960$ $a_{15} = -2.535$ $a_{20} = -2.242$ $a_{25} = -1.710$ $a_{50} = -0.7333$ $a_{75} = 0.5926^*$ $a_{100} = 0.7731^*$ $a_{150} = 0.9729^*$ $a_{200} = 1.086^*$ $a_{250} = 1.343^*$	
$S_{tot} \left(\frac{\partial T}{\partial z} \right) = a + b \frac{\partial T}{\partial z}$	$a_1 = 0.3317$ $a_5 = 0.03900$ $a_{10} = -0.1483$ $a_{15} = -0.1847$ $a_{20} = -0.2948$ $a_{25} = -0.2805$ $a_{50} = -0.2533^*$ $a_{75} = -0.2533^*$ $a_{100} = -0.2533^*$ $a_{150} = -0.2533^*$ $a_{200} = -0.2533^*$ $a_{250} = -0.2533^*$	$a_1 = 0.0625$ $a_5 = 0.3587$ $a_{10} = -0.1483$ $a_{15} = 0.6002$ $a_{20} = 0.6427$ $a_{25} = 0.6387$ $a_{50} = 0.6272^*$ $a_{75} = 0.6272^*$ $a_{100} = 0.6272^*$ $a_{150} = 0.6272^*$ $a_{200} = 0.6272^*$ $a_{250} = 0.6272^*$		
$S_{tot} \left(\frac{\partial T}{\partial z} \right) = a + \frac{b \left(\frac{\partial T}{\partial z} + c \right)}{1 + \frac{\partial T}{\partial z}} \left[1 - \exp \left(- \frac{d}{\frac{\partial T}{\partial z}} \right) \right]$	$a_1 = 1.982$ $a_5 = 5.942$ $a_{10} = 10.79$ $a_{15} = 15.77$ $a_{20} = 20.63$ $a_{25} = 26.60$ $a_{50} = 60.70$ $a_{75} = 76.24$ $a_{100} = 167.2$ $a_{150} = 223.6^*$ $a_{200} = 301.4^*$ $a_{250} = 379.1^*$	$a_1 = -59.30$ $a_5 = -4.028$ $a_{10} = -7.847$ $a_{15} = -11.79$ $a_{20} = -15.61$ $a_{25} = -20.47$ $a_{50} = -49.17$ $a_{75} = -71.31$ $a_{100} = -147.40$ $a_{150} = -193.8^*$ $a_{200} = -262.2^*$ $a_{250} = -300.7^*$	$a_1 = -2.381$ $a_5 = 1.885$ $a_{10} = 1.761$ $a_{15} = 1.766$ $a_{20} = 1.866$ $a_{25} = 1.936$ $a_{50} = 2.145$ $a_{75} = -0.3654$ $a_{100} = 1.566$ $a_{150} = 1.784^*$ $a_{200} = 1.771^*$ $a_{250} = 1.748^*$	$a_1 = 0.2337$ $a_5 = 27.05$ $a_{10} = 38.29$ $a_{15} = 49.80$ $a_{20} = 58.65$ $a_{25} = 70.89$ $a_{50} = 103.4$ $a_{75} = 65.06$ $a_{100} = 94.20$ $a_{150} = 96.89^*$ $a_{200} = 97.64^*$ $a_{250} = 98.09^*$

2.3.2 2D Distributions

The freeze fronts create insulating ice layers that grow, slowing the cooling process. However, the upper ice layer will not insulate as effectively as the ice at the base of the melt pond, causing the upper boundary of the melt pond to freeze faster than the lower boundary. Furthermore, the base crustal ice is likely to be warmer than the background temperature (94 K) because of the residual heat left over from the impact, but we assumed the basal ice was the same temperature as the background for this initial study. Consequently, the melt pond's final, most concentrated fluid solidifies just below the geometric center of the melt pond (as previous studies have suggested, e.g., Chivers et al., 2021; Thompson and Sagan, 1992), offset by ~25% of the melt sheet thickness in every run (**Figure 2.5 and 2.6**). While this region exhibits the highest concentration of HCN, ~70% of the total HCN content is still stored in the top half of the melt sheet. The position of this peak will shift depending on how much the basal ice is heated from the impact process, but it will also shift as the freezing temperature changes (i.e., gets lower at higher concentrations). The effect of melting temperature is observed at the highest initial concentrations of HCN; melt sheets of 50 m and 100 m thickness peak slightly deeper for initial concentrations of 5% and 7.5%. In these cases, the melt sheet is sufficiently concentrated such that the lower melting temperature prolongs the freezing process.

HCN preferentially freezes into the ice in the upper boundary, and the concentration of HCN increases with depth as HCN is removed from the lower boundary. Conversely, the bottom boundary sees a small spike in HCN trapped in the ice before its concentration drops significantly. That is because the initial conditions assume the underlying ice is 94 K, but realistically, the thermal gradient would be much lower because of residual heat from the impact. Therefore, our results are a lower bound for the lifetime of the melt pond because warmer ice will insulate the melt pond prolonging the time it takes to freeze. Furthermore, higher thermal gradients will lead to more HCN freezing into the melt ponds basal ice, so the upper profile of HCN concentrated in the ice is a lower bound for the amount of HCN Dragonfly is likely to find in the ice. However, the increase in HCN in the basal ice that results from higher thermal gradients is negligible relative to the concentrations observed near the surface.

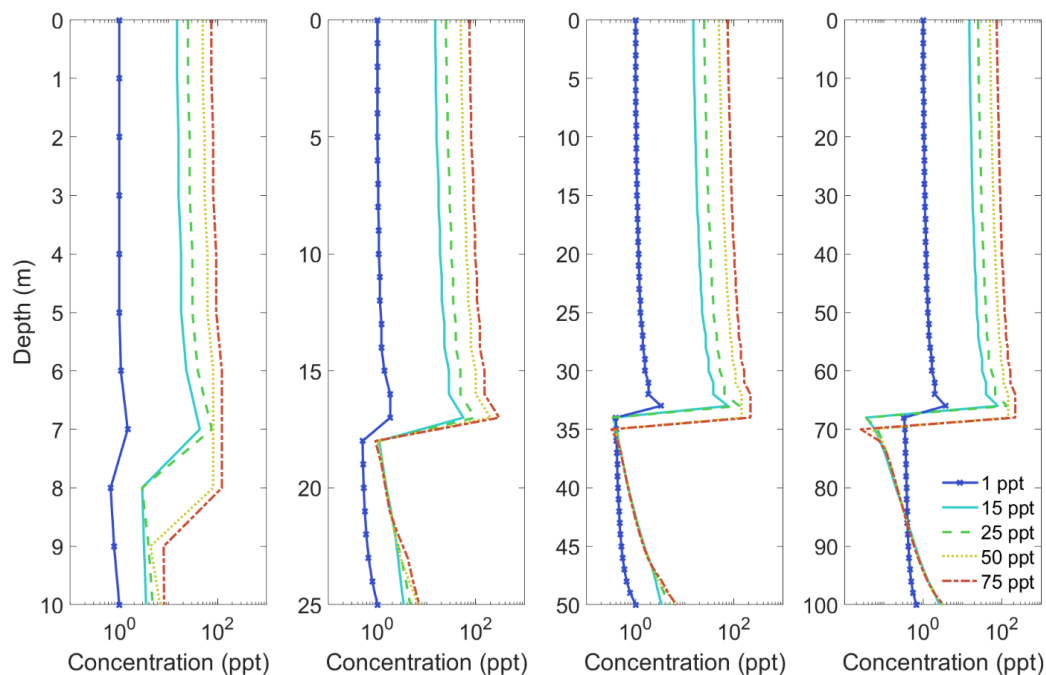


Figure 2.5. Results of the Chivers et al. (2021) model showing how much HCN freezes into the ice with depth, measured through the center of the frozen melt sheet, for four different melt sheet thicknesses, (a) 10 m, (b) 25 m, (c) 50 m and (d) 100 m and for initial concentrations of 0.1% (1 ppt, dark blue line with ‘x’ at each point), 1.5% (15 ppt, light blue line), 2.5% (25 ppt, green dash line), 5% (50 ppt, yellow dotted line), and 7.50% (75 ppt, red double dash line). Results are taken for an 80 km crater.

The lower boundary faces two conflicting environmental pressures. 1) A drop in the thermal gradient will decrease how much HCN brine freezes into the ice, but 2) the increasing bulk concentration will increase how much HCN brine freezes into the ice. Our SF2 results (**Figure 2.4**) suggest that an increase in the initial concentration of HCN would have a significant effect on how much HCN freezes into the ice for the first several meters of the melt sheet or up to ~ 5 K/m thermal gradients. At thermal gradients below ~ 5 K/m, the initial concentration appears to matter much less, as the concentration in the ice across different initial conditions begins to converge. This trend is observed in the results of the Chivers et al. (2021) model as well. The higher initial concentrations of HCN produce a slightly higher concentration of HCN trapped in the ice at the bottom of the melt pond (where the SF2 model is applied), but the more the melt sheet freezes, the smaller the

thermal gradients become such that less HCN is trapped in the ice. In the inner most region of the melt sheet we see that a higher initial concentration of HCN in the melt produces profiles of HCN concentration in the ice that overlap (and drop below) profiles of lower initial HCN concentration in the melt (**Figure 2.6**), but this is not representative of reality. It is unlikely that higher impurity concentrations in the melt would entrain less impurity in the ice.

These unrealistic results derive from how we construct and apply the trend lines for each concentration profile. Each profile converges upon the same linear concentration line (**Figure 2.4a**) at low thermal gradients. The higher the initial concentration, the sooner the profile reaches that linear region. The linear fits we use are only applicable for a specific region (up to ~15 m) beyond which they breakdown. These fits allow us to track the concentration until it reaches critical minimum concentration, and while we see the concentration profiles dip below our lowest initial concentration line (1 ppt), it is safe to assume the fit is only applicable until it reaches the lowest concentration line where it would converge with the profile.

For example, the lowest initial melt concentration profile that we study is 1 ppt (0.1%) concentration. In our thickest melt sheet (100 m), this concentration profile decreases at a much slower rate than the higher concentrations, reaching, at its lowest point, about 30% of the initial concentration. In this region of very low thermal gradients, the highest initial concentrations begin to produce concentrations in the ice as low as melt with an initial concentration of 1 ppt; this is the point where the higher concentration linear fits cease to be applicable. This suggests that at very low concentrations, very little material will be rejected, even with the lowest of thermal gradients. Logically, this is to be expected as lower concentrations lead to smaller density differences and thus smaller forces driving the movement of HCN within the forming ice lattice. Therefore, HCN may freeze at $1/3^{\text{rd}}$ its initial concentration (0.25% - 2.5%); if HCN hydrolyses into more complex biomolecules, these daughter products may freeze near their initial concentration given they would be a fraction as abundant as HCN (at least for melt sheets <50 m). However, it should be noted that volumetric effects become a bigger factor as concentrations have an increasingly negligible effect on the density of the melt.

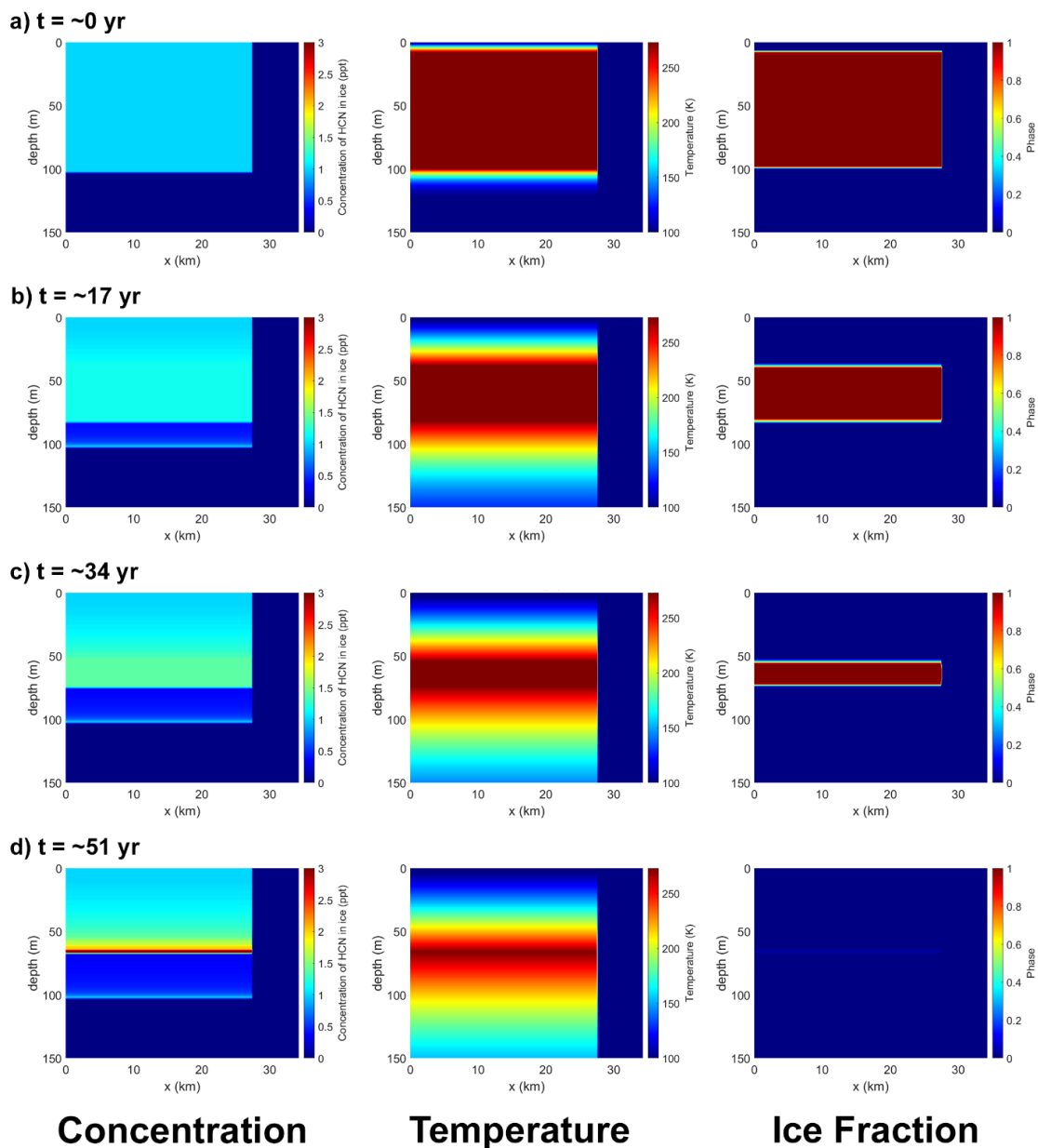


Figure 2.6. We use the Chivers et al. (2021) heat transfer model to calculate the final concentration distribution for an 80 km diameter crater (crater floor ~ 55 km) using an initial concentration of 1 ppt (0.1%) and an assumed melt pond of 100 m depth. On the left is the concentration of HCN in each element, in the middle is the temperature of each element, and on the right is the phase of each element (0 is frozen, 1 is liquid). The model uses the thermal gradient on the interface boundary along with the constitutive equations of Table 2.2 to determine what the concentration will be upon freezing (see text for further explanation).

In a bulk scenario, where the total concentration of organics is much larger (~7%), more material will be rejected if the organics are assumed to act as a whole (rather than segregate). However, the lowest concentrations in the ice still seem to be ~0.03% (0.3 ppt), well within the parts per trillion that Dragonfly will need for its investigation.

The results in **Figure 2.6** is for the Chivers 2D heat transfer model, which accounts for lateral heat transfer. However, the x-axis (radius of the melt pond, ~55 km) is orders of magnitude larger than the y-axis (depth of the melt pond, 50-250 m) (see Chivers et al. (2021) for more on heat loss in the x-direction). Therefore, the horizontal freezing is not overly apparent in **Figure 2.6**, but if you look at the ice fraction column you can see the corners begin to curve in. Our measured freezing timescales of 10s to 100s of years is consistent with previous timescale estimates for the freezing of a melt sheet at the thicknesses we modeled (**Figure 2.5 and 2.7**) (O'Brien et al., 2005; Artemieva and Lunine, 2005). However, our largest freezing timescales are much smaller than the most liberal estimates of O'Brien et al. (2005); they consider larger depths (up to $d/D = 0.05$) and volume fractions (up to 20%) than we deem reasonable. Their estimates would lead to depths multiple kilometers deep for the largest craters, but there is evidence that the depths of large craters on icy worlds reach a limit where relaxation produces shallower craters (Schenk, 2002). In addition, they neglect the significant drainage into the underlying fractured bedrock ice that will likely occur, thinning the melt sheets (Elder et al., 2012). With a conservative depth to diameter ratio ($d/D = 0.01$, as opposed to the slightly higher estimate we used in Section 2.2.1 from Bray et al., 2012) and volume fraction ($f = 2 - 5\%$), a crater the size of Selk would produce a melt pond 60 m in depth (excluding any drainage), resulting in a freezing timescale of ~10 yrs. If we are more liberal with the volume fraction ($f \cong 15\%$), a crater the size of Selk would produce a melt pond ~350 m in depth and freezing timescales of up to ~600 yrs. However, we focused on melt sheets no thicker than 250 m, as thicker melt ponds are unlikely to persist given the effects of drainage (**Figure 2.7**) (Elder et al, 2012). The timescales of each melt sheet thickness become progressively longer but retain the same pattern of freezing when presented with the same initial conditions.

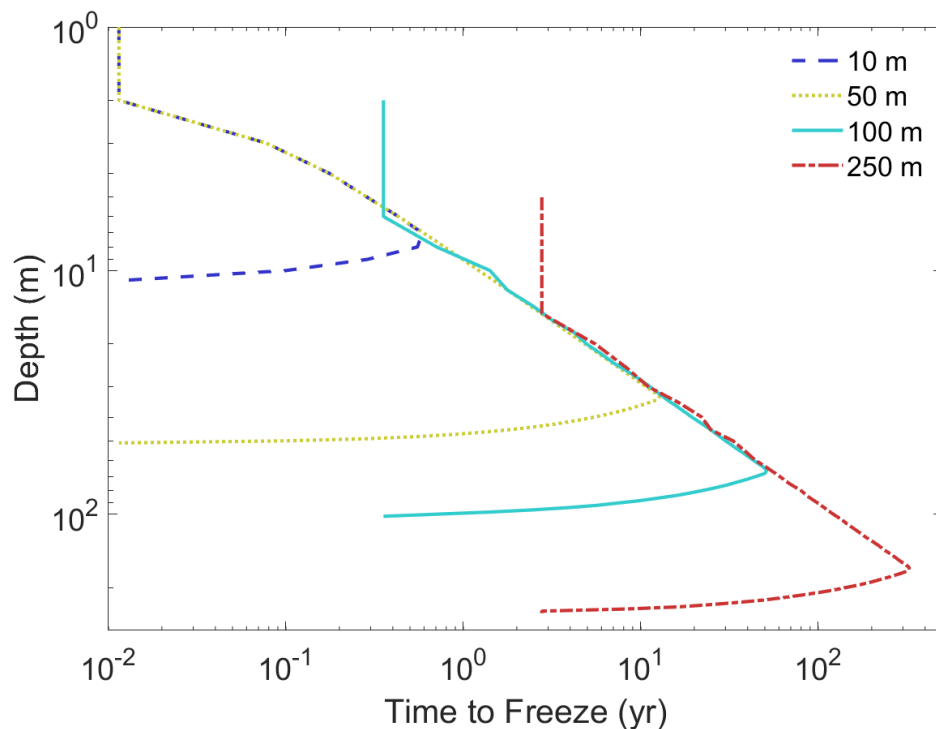


Figure 2.7. The time needed to freeze each element along the melt sheet depending on its thickness. Times are taken from the centermost grid cells of the melt sheet, for an 80 km crater starting with 1 ppt of HCN, where timescales are measured at spatial steps throughout the melt sheet that range from 1 m to 5 m (depending on the melt sheet thickness).

2.3.3 Implications and Future Work

Our results suggest that Dragonfly should be able to access HCN at the top of the melt sheet in concentrations similar to those present at the point of its formation (assuming the melt pond is thoroughly mixed). Of course, these results do not account for the hydrolysis of HCN, but rather uses it as a representative tracer for its byproducts. The byproducts of HCN aqueous chemistry may freeze into the ice in a different manner; our results suggest density would dictate the path they follow. If a particular byproduct of HCN has an inverse density relationship, the ratio of HCN to its byproduct may be lower than what is expected through aqueous reactions because the denser byproduct will freeze into the ice at lower concentrations than HCN. Based on the half-lives discussed in Section 2.2.1, it is unlikely that HCN's daughter products will dominate a melt sheet less than ~50

m thick, and potentially as thick as 100 m depending on the pH, because the half-life of HCN in the best case is on the order of 100s of years (**Figure 2.7**; Miyakawa et al., 2002). HCN may continue to segregate as we have predicted, while the daughter products act independently in the mushy layer freezing process. In this case, the trends we present are still accurate, but the magnitude of the concentration in the ice would be lower than we predict. Alternatively, such a mixture of compounds may not segregate at all, but instead be governed by its bulk properties, with much broader implications for the distribution of impurities within the melt sheet.

As HCN hydrolyzes and becomes less concentrated, its chemical properties would become decreasingly relevant to the physics of the SF2 model. Once the melt sheet has remained liquid beyond HCN's half-life, the chemical properties of its daughter products will dominate the physics. Therefore, our results are the least reliable beyond this point (perhaps as quickly as a few years and almost certainly after centuries). The most drastic difference would be if its daughter products (e.g., glycine) are denser than HCN and water, thus inverting the forces that drive how much, and where, impurity freezes into the ice. In such a scenario, the current pattern of organic distribution with a large segregation of organics in the top half and orders of magnitude less concentration of organics in the bottom half would still be present, but once HCN's daughter product becomes dominant (closer to the melt sheet's center), the same pattern would be reproduced but mirrored (much like salt, Chivers et al., 2021). Eventually, the two freeze fronts would meet and the concentration would spike at the center. Realistically, this transition could happen as early as 10 m below the surface (with the fastest hydrolysis) or to as deep as 100 m into the surface (for slower rates). This is within the region Dragonfly may be able to access. Therefore, the team should be prepared for this potential reality.

An additional complication may arise as the HCN hydrolyzes into potentially more dense daughter products. Going from HCN's buoyant density to a denser daughter product might introduce a period where the bulk melt density is near that of water. In this case, buoyancy driven rejection of impurities may become less important than volumetric phase change driven expulsion. These are ignored in our work because it has been shown that volumetric changes are negligible to those driven by density differences (Griewank and

Notz, 2013; Buffo et al 2018, 2020), but if buoyancy differences don't exist, volumetric changes may become more important in the diffusion of impurities out of the ice.

There are further limitations to this work that must be considered as well. It is difficult to make precise approximations of the near surface concentration of chemical impurities in the ice because of the chaotic nature of the freezing process in this region. Naturally formed methane rivers on Titan could incise deeper into the melt sheet, where the freezing conditions were less extreme, and the SF₂ model would provide a more accurate numerical solution. Selk crater was chosen, in part, because of its relative freshness (Neish et al., 2018), but there is evidence to suggest erosion plays an ongoing role in the degradation of Titan's impact craters (Soderblom et al., 2010; Neish et al., 2013; Werynski et al., 2019; Hedgepeth et al., 2020; Solomonidou et al., 2020). Erosion will help to expose subsurface material, creating easily accessible samples for Dragonfly to target (Neish et al., 2018). However, sediment covering the melt sheet may still impede Dragonfly's access to these samples (Neish et al., 2013). If rivers do not incise in the frozen melt pond, or incise very little, the aqueous chemistry found near the surface of the melt sheet could only have evolved on very short time scales (minutes to hours), limiting its potential to evolve into more complex biochemistry (Neish et al., 2006; 2018).

Overall, we predict that the best samples for Dragonfly to target would be near the center depth of the melt sheet. Ignoring other chemistry, the region of maximum HCN concentration does not appear to shift based on different initial HCN concentrations or melt sheet thicknesses (although the absolute depth of this region will vary with the initial thickness of the melt sheet, which is unknown). The easiest location to access samples would be in any available river plains, where portions of the melt sheet may have eroded (Neish et al., 2018). Our results suggest even in low HCN concentrations (0.1%), there is likely to be plenty of HCN for Dragonfly to sample. However, the dynamics that govern the emplacement will likely complicate as HCN undergoes hydrolysis during freezing, potentially changing what may be observed. However, our results suggest even in the lowest of concentrations, there is likely to be plenty of HCN in the ice to sample with Dragonfly's instruments. Whether this is true for its daughter products requires further study.

2.3.4 Assumptions

This work offers a suggestion of how much organic material Dragonfly will likely find in the melt sheet associated with Selk crater, but there are several assumptions that are associated with this work. The most important assumption is that the planetary ice model SF2 is applicable for alternate chemistries and environments other than those of terrestrial sea ice. Overall, we deem this to be a good assumption because the fundamental physics governing ice-brine environments will not change across the solar system. However, the extreme conditions found at Titan do make it more difficult to find a numerical solution, but only for a thin layer at the surface. A necessary part of adapting this model to Titan is the assumption that some of the unique parameters taken from sea ice research are the same for Titan (**Table 2.1**) (Golden et al., 2007; Maus et al., 2020). Even in the terrestrial sea ice community, some of these parameters (e.g., permeability) are still heavily debated (Golden et al., 2007).

Furthermore, we assume our system is analogous to terrestrial sea ice, but as previously stated, the temperatures drop below those found in terrestrial sea ice. This would affect the SF2 model in its initial stages, but that is only because we assume the basal ice begins at background temperatures (i.e., 94 K). Once the temperatures adjust from the extreme initial conditions, the temperatures within the mushy layer will not vary nearly as significantly, and the assumption of a constant conductivity of ice will have a much smaller impact. The 2D heat transfer model accounts for temperature dependent conductivities (Chivers et al., 2021), but our initial parameters still assume the basal ice is at the background temperature (94 K). **Figures 2.6 and 2.7** show that the top boundary freezes at a rate almost twice that of the base of the melt sheet. This suggests that the time scales may extend another decade or more from what we predict, depending on the level of heating the ice experiences from impact. It also suggests the impurities may concentrate further down into the melt sheet. This is because the upper freeze front will continue at the same rate that we observed but the warmer basal ice will slow the progression of the lower freeze front. The impact is also likely to lead to initial melt temperatures well above the freezing point of water. This would produce higher thermal gradients (and therefore, higher impurity entrainment) and longer timescales over which the freezing will occur. Overall,

we anticipate that the temperature assumptions we made in this work represent a lower limit on the actual freezing timescales encountered on Titan.

Even though the conditions in a Titan melt sheet are not extreme compared to those of terrestrial sea ice for most of the model, the SF2 model still faced limits in how well it could model the scenarios we gave it. This does not seem to be a physical problem, however. The limitations we observed appear to be specific to HCN's chemical properties, and as the initial concentration is increased, the problems are exacerbated. The combination of HCN's lower melting temperature ($\sim -13\text{C}$) with its specific heat ($2612 \frac{\text{J}}{\text{kg}\cdot\text{K}}$) at the extremely low thermal gradients within the melt sheet make it progressively more difficult for the model to converge. This limited our SF2 model runs to relatively high thermal gradients and relatively low concentrations. It should be noted that most of the concentrations of interest (0.1% to 7%) produced results which converged even at low thermal gradients. The extrapolation to higher concentrations was needed for the Chivers et al. (2021) model to simulate the melt when it reaches these concentrations. While we do not put strong weight into the extrapolations, they do serve the purpose of producing a more cohesive picture. Further, while the region where the melt concentrations rely on extrapolated SF2 results may be the least accurate, these are also the regions that are of least interest. That is because they are less accessible to Dragonfly, and if they are accessed, we can at least say that there will be ample organic samples for Dragonfly to analyze. Outside of this region, the extrapolation is less important.

Our work also assumes a well-mixed pond. This may be true during its energetic origin, but the initial energy of the system will dissipate with time. It is possible that large scale convection may continue to mix the melt pond, as observed in terrestrial magma chambers (Sparks et al., 1984; Turner and Campbell, 1986), and the model of Chivers et al. (2021) assumes this type of convection will be enough to keep the melt sheet well-mixed.

Another assumption is that HCN will be present and is not lost during the initial stages of impact cratering, where temperatures may exceed the vaporization point of water (373K). This is above the vaporization point of HCN (299K). The SF2 model cannot

account for gases in the melt, and this problem is not unique to HCN. This points to the larger problem of the modification and destruction of organics that may occur during impact (Artemieva and Lunine, 2005). The destruction or loss of HCN will largely affect the initial concentration of HCN in the melt pond, and the high pressures and temperatures experienced during impact may alter the chemistry as well (Pierazzo and Chyba, 1999; Blank et al., 2001). Therefore, the estimates we give for HCN are likely an upper bound, and HCN's half-life may be significantly smaller for the much warmer temperature conditions. Therefore, the daughter products may become a bigger factor in the melt sheet sooner than we predicted.

We have assumed that HCN will act as a proxy for the bulk mixture of material, and we have discussed significantly how the presence of its daughter products (and other chemistry) would complicate this process. This relates not just to the traditional mushy layer problem being solved in this work but to other chemical processes we do not consider. For example, HCN will begin to dissociate when in high pH conditions, which is also when rates of hydrolysis are known to be especially high (Miyakawa et al., 2002; Gail et al., 2011). The final pH of the melt solution will depend on the other compounds present in the melt, and it will determine the stability and rate of hydrolysis of HCN, as well as for the other molecules that are present. Therefore, when we discuss the distribution of HCN, it is more accurately thought of as a first order approximation of the distribution of buoyant organic molecules within the melt sheet. Future studies are needed to determine the full breadth of factors that will influence the final distribution of biomolecules in Titan's frozen melt ponds.

2.4 Conclusions

We use the planetary ice model of Buffo et al. (2020) to constrain the spatial distribution of HCN (and by extension, other organic compounds) trapped within a freezing crater melt pond on Titan. We found that HCN will become entrained in the upper boundary of the melt sheet at the initial concentration of the melt reservoir, and HCN will be removed from the lower boundary due to density differences with water. As the system freezes, HCN will concentrate in the remaining fluid of the melt sheet, becoming most concentrated at a depth of ~75% of the total melt sheet thickness. This portion of the melt sheet is likely to

contain the most evolved aqueous chemistry, because it remains liquid for the longest time, but it is also the region where HCN becomes a less accurate representation of how impurities will act. Our results offer constraints for Dragonfly to use to predict how many organic molecules it will find frozen into the melt sheet at any depth. Furthermore, our results can be utilized to link near-surface sample observations to deeper reservoir properties to better understand the history of the melt sheet and the initial conditions when it formed. Finally, the freezing timescales we found will aid in our understanding of the extent to which prebiotic chemistry could have evolved within the freezing melt sheet. This is critical for understanding the astrobiological potential of Titan and provides necessary context to the samples Dragonfly will collect.

2.5 References

- Ahmad, N., and Phillips, W.A., 1987. Thermal conductivity of ice and ice clathrate. *Solid state communications*, 63(2), pp.167-171.
- Artemieva, N., Lunine, J.I., 2005. Impact cratering on Titan II. Global melt, escaping ejecta, and aqueous alteration of surface organics. *Icarus* 175, 522–533. <https://doi.org/10.1016/j.icarus.2004.12.005>
- Barnes, J.W., Lorenz, R.D., Radebaugh, J., Hayes, A.G., Arnold, K., and Chandler, C., 2015. Production and global transport of Titan's sand particles, *Planet. Sci.* 4, 1. doi:10.1186/s13535-015-0004-y.
- Blank, J.G., Miller, G.H., Ahrens, M.J., Winans, R.E., 2001. Experimental Shock Chemistry of Aqueous Amino Acid Solutions and the Cometary Delivery of Prebiotic Compounds. *Origins of Life and Evolution of the Biosphere* 31, 15-21.
- Bray, V.J., Schenk, P.M., Melosh, J., H., Morgan, J.V., Collins, G.S., 2012. Ganymede crater dimensions – Implications for central peak and central pit formation and development. *Icarus* 217, 115–129. <https://doi.org/10.1016/j.icarus.2011.10.004>
- Buffo, J., Schmidt, B., and Huber, C., Walker, C., 2020. Entrainment and dynamics of ocean-derived impurities within Europa's ice shell. *Journal of Geophysical Research*. <https://doi.org/10.1002/essoar.10502079.2> .
- Buffo, J., Schmidt, B., and Huber, C., 2018. Multiphase reactive transport and platelet ice accretion in the sea ice of McMurdo sound, Antarctica. *Journal of Geophysical Research: Oceans* 123, 324-345.
- Chivers, C. J., Buffo, J. J., & Schmidt, B. E. (2021). Thermal and chemical evolution of small, shallow water bodies in Europa's ice shell. *Journal of Geophysical Research: Planets* 126. <https://doi.org/10.1029/2020JE006692>.
- Clarke, A., 2014. The thermal limits to life on Earth. *International Journal of Astrobiology* 13, 141-154. doi:10.1017/S1473550413000438

- Cleaves, H. J., Neish, C., Callahan, M. P., Parker, E., Fernández, F. M., and Dworkin, J. P. (2014). Amino acids generated from hydrated Titan tholins: Comparison with Miller-Urey electric discharge products. *Icarus* 237:182–189.
- Coates, J.E., and Hartshorne, N.H., 1931. Studies on Hydrogen Cyanide. Part III. The Freezing Points of Hydrogen Cyanide-Water Mixtures. *Journal of Chemistry Society*, 657-665.
- Collins, R.E., Carpenter, S.D., Deming, J.W., 2008. Spatial heterogeneity and temporal dynamics of particles, bacteria, and pEPS in Arctic winter sea ice. *J. Marine Syst.* 74, 902-917.
- Crósta, A.P., Silber, E.A., Lopes, R.M.C., Johnson, B.C., Bjornes, E., Malaska, M.J., Vance, S.D., Sotin, C., Solomonidou, A. and Soderblom, J.M., 2021. Modeling the formation of Menrva impact crater on Titan: Implications for habitability. *Icarus*, 370, p.114679.
- Elder, C.M., Bray, V.J. and Melosh, H.J., 2012. The theoretical plausibility of central pit crater formation via melt drainage. *Icarus* 221(2), 831-843.
- Feltham, D., Untersteiner, N., Wettlauger, J.S., Worster, M.G. , 2006. Sea ice is a mushy layer. *Geophysical Research Letters* 33, L14501. doi:10.1029/2006GL026290.
- Gail, E., Gos, S., Kulzer, R., Lorösch, J., Rubo, A., Sauer, M., Kellens, R., Reddy, J., Steier, N. and Hasenpusch, W., 2011. Cyano Compounds, Inorganic. In *Ullmann's Encyclopedia of Industrial Chemistry*, (Ed.). https://doi.org/10.1002/14356007.a08_159.pub3
- Golden, K.M., Eicken, H., Heaton, A.L., Miner, J., Pringle, D.J., and Zhu, J., 2007. Thermal evolution of permeability and microstructure in sea ice. *Geophysical Research Letters* 34, L16501. <https://doi.org/10.1029/2007GL030447>
- Griewank, P.J. and Notz, D., 2013. Insights into brine dynamics and sea ice desalination from a 1-D model study of gravity drainage. *Journal of Geophysical Research: Oceans* 118, 3370-3386.

- Haynes, W.M., 2011. CRC Handbook of Chemistry and Physics, (Internet Version 2011). Taylor Francis Group: Boca Raton, FL.
- He, C., Smith, M.A., 2014. Identification of nitrogenous organic species in Titan aerosols analogs: Implication for prebiotic chemistry on Titan and early Earth, *Icarus* 238, 86-92, <https://doi.org/10.1016/j.icarus.2014.05.012>.
- Hedgpeeth, J.E., Neish, C.D., Turtle, E.P., Stiles, B.W., Kirk, R., & Lorenz, R.D., 2020. Titan's impact crater population after Cassini. *Icarus* 344, 113664. <https://doi.org/10.1016/j.icarus.2020.113664>.
- Hobbs, P.V., 1974. Ice physics. Oxford, Clarendon Press xvii, 837. *Journal of Glaciology* 17, 155-156. doi:10.3189/S0022143000030847.
- Hörst, S.M., 2017. Titan's atmosphere and climate. *Journal of Geophysical Research: Planets* 122, 432–482. <https://doi.org/10.1002/2016JE005240>.
- Hörst, S.M., Yelle, R.V., Buch, A., Carrasco, N., Cernogora, G., Dutuit, O., Quirico, E., Sciamma-O'Brien, E., Smith, M.A., Somogyi, A., Szopa, C., Thissen, R., and Vuitton, V., 2012. Formation of amino acids and nucleotide bases in a Titan atmosphere simulation experiment. *Astrobiology* 12: 809–817.
- Huber, C., Parmigiani, A., Chopard, B., Manga, M., & Bachmann, O., 2008. Lattice Boltzmann model for melting with natural convection. *International Journal of Heat and Fluid Flow* 29, 1469–1480. <https://doi.org/10.1016/j.ijheatfluidflow.2008.05.002>.
- Hunke, E.C., Notz, D., Turner, A.K., and Vancoppenolle, M., 2011. The multiphase physics of sea ice: A review for model developers. *The Cryosphere* 5(4), 989–1009. <https://doi.org/10.5194/tc-5-989-2011>.
- Janssen, M.A., Le Gall, A., Lopes, R.M., Lorenz, R.D., Malaska, M.J., Hayes, A.G., Neish, C.D., Solomonidou, A., Mitchell, K.L., Radebaugh, J., Keihm, S.J., Choukroun, M., Leyrat, C., Encrenaz, P.J., Mastrogiuseppe, M., 2016. Titan's surface at 2.18-cm wavelength imaged by the Cassini RADAR radiometer: Results and

interpretations through the first ten years of observation. *Icarus* 270, 443–459.
<https://doi.org/10.1016/j.icarus.2015.09.027>

Khare, B.N., Sagan, C., Ogino, H., Nagy, B., Er, C., Schram, K.H., and Arakawa, E.T., 1986. Amino Acids Derived from Titan Tholins, *Icarus*, 68, 176-184.

Kouvaris, L.C., Flasar, F.M., 1991. Phase equilibrium of methane and nitrogen at low temperatures: Application to Titan. *Icarus* 91, 112–124.
[https://doi.org/10.1016/0019-1035\(91\)90131-C](https://doi.org/10.1016/0019-1035(91)90131-C).

Krasnopolsky, V.A., 2014. Chemical composition of Titan's atmosphere and ionosphere: Observations and the photochemical model. *Icarus* 236, 83-91.
<https://doi.org/10.1016/j.icarus.2014.03.041>.

Lindal, G.F., Wood, G.E., Hotz, H.B., Sweetnam, D.N., Eshleman, V.R., Tyler, G.L., 1983. The atmosphere of Titan: An analysis of the Voyager 1 radio occultation measurements. *Icarus* 53, 348–363. [https://doi.org/10.1016/0019-1035\(83\)90155-0](https://doi.org/10.1016/0019-1035(83)90155-0).

Lopes, R. M.C., Mitchell, K.L., Stofan, E.R., et al., 2007. Cryovolcanic features on Titan's surface as revealed by the Cassini Titan Radar Mapper, *Icarus* 186, 395–412, [doi:10.1016/j.icarus.2006.09.006](https://doi.org/10.1016/j.icarus.2006.09.006).

Lorenz, R.D., Wall, S., Radebaugh, J., Boubin, G., Reffet, E., Janssen, M., Stofan, E., Lopes, R. M.C., Kirk, R.L., Elachi, C., Lunine, J., Mitchell, K., Paganelli, F., Soderblom, L., Wood, C., Wye, L., Zebker, H., Anderson, Y., Ostro, S., Allison, M., Boehmer, R., Callahan, P., Encrenaz, P., Ori, G. G., Francescetti, G., Gim, Y., Hamilton, G., Hensley, S., Johnson, W., Kelleher, K., Muleman, D., Picardi, G., Posa, F., Roth, L., Seu, R., Shaffer, S., Stiles, B., Vetrella, S., Flamini, E., West, R., 2006. The Sand Seas of Titan: Cassini RADAR Observations of Longitudinal Dunes. *Science* 312, 724–727. <https://doi.org/10.1126/science.1123257>

Lorenz, R.D., Mitchell, K.L., Mitchell, K.L., Kirk, R.L., Hayes, A.G., Aharonson, O., Zebker, H.A., Paillou, P., Radebaugh, J., Lunine, J.I., Janssen, M.A., Wall, S.D.,

- Lopes, R.M., Stiles, B., Ostro, S., Mitri, Giuseppe, Stofan, E.R., 2008. Titan's inventory of organic surface materials. *Geophys. Res. Lett.* 35, doi:10.1029/2007GL032118. L02206
- Lorenz, R.D., MacKenzie, S.M., Neish, C.D., Le Gall, A., Turtle, E.P., Trainer, M.G., Barnes, J.W., Werynski, A., Hedgepeth, J., Karkoschka, E., 2021. Selection and Characteristics of the Dragonfly Landing Site near Selk Crater, Titan. *Planetary Science Journal*.
- Lorenz, R.D., Lunine, J.I., 1996. Erosion on Titan: Past and present. *Icarus* 122, 79–91.
- Lorenz, R.D., Turtle, E.P., Barnes, J.W., Trainer, M.G., Adams, D.S., Hibbard, K.E., Sheldon, C.Z., Zancy, K. Peplowski, P.N., Lawrence, D.J., and Ravine, M.A., 2018. Dragonfly: A rotorcraft lander concept for scientific exploration at Titan. *Johns Hopkins APL Technical Digest*, 34(3), p14.
- Lorenz, R.D., Zimbelman, J.R., 2014. *Dune Worlds: How Windblown Sand Shapes Planetary Landscapes*, 1st ed. Springer-Verlag Berlin Heidelberg.
- Malaska, M.J., Radebaugh, J., Lopes, R.M., Mitchell, K.L., Verlander, T., Schoenfeld, A.M., Florence, M.M., Le Gall, A., Solomonidou, A., Hayes, A.G. and Birch, S.P., et al., 2020. Labyrinth terrain on Titan. *Icarus*, 344, 113764.
- MatWeb, 2018. Hydrogen Cyanide, HCN - MatWeb. http://www.matweb.com/search/datasheet_print.aspx?matguid=95207a948b2c4d6ab6bed897a6c0a0d4&n=1 (accessed 2018)
- Maus, S., Schneebeli, M., and Wiegmann, A., 2020. An X-ray micro-tomographic study of the pore space, permeability and percolation threshold of young sea ice. *The Cryosphere Discuss.*, <https://doi.org/10.5194/tc-2020-288>.
- McDonald, G.D., Corlies, P., Wray, J.J., Horst, S.M., Hofgartner, J.D., Liuzzo, L.R., Buffo, J., and Hayes, A. G., 2015. Altitude-dependence of Titan's methane transmission windows: Informing future missions. In: 46th Lunar and Planetary Science Conference Abstracts, The Woodlands, Texas, USA.

- Melosh, H.J., 1989. *Impact Cratering: A Geologic Process*, Oxford monographs on geology and geophysics. Oxford University Press.
- Miller, S.L., 1953. A production of amino acids under possible primitive earth conditions. *Science* 117, 528-529.
- Miyakawa, S., James Cleaves, H. & Miller, S.L. The Cold Origin of Life: A. Implications Based On The Hydrolytic Stabilities Of Hydrogen Cyanide And Formamide. *Orig Life Evol Biosph* 32, 195–208 (2002). <https://doi.org/10.1023/A:1016514305984>
- Neish, C.D., Lorenz, R.D., O'Brien, D.P., and the Cassini RADAR Team, 2006. The potential for prebiotic chemistry in the possible cryovolcanic dome Ganesa Macula on Titan. *Int J Astrobiol* 5, 57–65.
- Neish, C.D., Somogyi, A., et al., 2008. Rate measurements of the hydrolysis of complex organic macromolecules in cold aqueous solutions: Implications for prebiotic chemistry on the early Earth and Titan. *Astrobiology* 8 (2), 273–287.
- Neish, C.D., Somogyi, A., and Smith, M.A., 2009. Low temperature hydrolysis of laboratory tholins in ammonia-water solutions: implications for prebiotic chemistry on Titan. *Icarus* 201, 412–421.
- Neish, C.D., Somogyi, A., and Smith, M.A., 2010. Titan's primordial soup: formation of amino acids via low-temperature hydrolysis of tholins. *Astrobiology* 10, 337–347.
- Neish, C.D., Kirk, R.L., Lorenz, R.D., Bray, V.J., Schenk, P., Stiles, B.W., et al., 2013. Crater topography on Titan: implications for landscape evolution. *Icarus* 223, 82–90.
- Neish, C.D., Molaro, J.L., Lora, J.M., Howard, A.D., Kirk, R.L., Schenk, P., Bray, V.J., Lorenz, R.D., 2016. Fluvial erosion as a mechanism for crater modification on Titan. *Icarus* 270, 114–129. <https://doi.org/10.1016/j.icarus.2015.07.022>
- Neish, C.D., Lorenz, R.D., Turtle, E.P., Barnes, J.W., Trainer, M.G., Stiles, B., et al., 2018. Strategies for detecting biological molecules on Titan. *Astrobiology* 18, 571-585.

- O'Brien, D.P., Lorenz, R.D., and Lunine, J.I. (2005) Numerical calculations of the longevity of impact oases on Titan. *Icarus* 173:243–253.
- Osinski, G.R., & Pierazzo, E., 2013. Impact cratering: Processes and products. *Impact Cratering*, 1-20.
- Osinski, G.R., Tornabene, L.L., and Grieve, R.A. 2011. Impact ejecta emplacement on terrestrial planets. *Earth and Planetary Science Letters*, 310, 167-181.
- Pierazzo, E. and Chyba, C.F., 1999. Amino acid survival in large cometary impacts. *Meteoritics & Planetary Science* 34(6), 909-918.
- Ruiz-Bermejo, M.; de la Fuente, J.L.; Pérez-Fernández, C.; Mateo-Martí, E. A Comprehensive Review of HCN-Derived Polymers. *Processes* 2021, 9, 597. <https://doi.org/10.3390/pr9040597>
- Rumble, J.R. (2020). *CRC Handbook of Chemistry and Physics*, 101st Edition (Internet Version 2020). Taylor Francis Group: Boca Raton, FL.
- Sagan, C., and Khare, B.N., 1979. Tholins—Organic chemistry of interstellar grains and gas, *Nature* 277, 102–107, doi:10.1038/277102a0.
- Sagan, C., and Thompson, W.R., 1984. Production and condensation of organic gases in the atmosphere of Titan, *Icarus*, 59, 133–161, doi:10.1016/0019-1035(84)90018-6.
- Sanchez, R.A., Ferris, J.P., and Orgel, L.E. (1966) Conditions for purine synthesis: did prebiotic synthesis occur at low temperatures? *Science* 153, 72–73.
- Santibáñez, P.A., Michaud, A.B., Vick-Majors, T.J., D'Andrilli, J., Chiuchiolo, A., Hand, K.P., and Priscu, J.C., 2019. Differential incorporation of bacteria, organic matter, and inorganic ions, into lake ice during ice formation.
- Schenk, P.M., 2002. Thickness constraints on the icy shells of the Galilean satellites from a comparison of crater shapes 417, 3.

- Schmidt, B.E., Blankenship, D.D., Patterson, G.W. and Schenk, P.M., 2011. Active formation of 'chaos terrain' over shallow subsurface water on Europa. *Nature*, 479(7374), pp.502-505.
- Soderblom, L.A., et al., 2007. Correlations between Cassini VIMS spectra and RADAR SAR images: Implications for Titan's surface composition and the character of the Huygens Probe landing site, *Planet. Space Sci.* 55, 2025–2036, doi:10.1016/j.pss.2007.04.014.
- Soderblom, J.M., Brown, R.H., Soderblom, L.A., Barnes, J.W., Jaumann, R., Mouélic, S.L., Sotin, C., Stephan, K., Baines, K.H., Buratti, B.J., 2010. Geology of the Selk crater region on Titan from Cassini VIMS observations. *Icarus* 208, 905–912. <https://doi.org/10.1016/j.icarus.2010.03.001>
- Sparks, R.S.J., Huppert, H.E., and Turner, J. S., 1984. The fluid dynamics of evolving magma chambers. *Philosophical Transactions of the Royal Society of London. Series A, Mathematical and Physical Sciences* 310(1514), 511-534.
- Steeffel, C., DePaolo, D., Lichtner, P., 2005. Reactive transport modeling: An essential tool and a new research approach for the Earth sciences. *Earth and Planetary Science Letters* 240, 539-558.
- Thompson, W.R. and Sagan, C. (1992). Organic chemistry on Titan: surface interactions. In: *Proceedings of the Symposium on Titan, 9–12 September 1991, Toulouse, France*. ESA SP-338, pp. 167–176.
- Tomasko, M.G., Archinal, B., Becker, T., Be'zard, B., Bushroe, M., Combes, M., et al., 2005. Rain, winds and haze during the Huygens probe's descent to Titan's surface. *Nature* 438: 765–778.
- Trainer, M.G., Pavlov, A.A., DeWitt, H.L., Jimenez, J.L., McKay, C.P., Toon, O.B., and Tolbert, M.A., 2006. Organic haze on Titan and the early Earth. *Proceedings of the National Academy of Sciences* 103(48), 18035-18042.

- Turner, J.S., and Campbell, I.H., 1986. Convection and mixing in magma chambers. *Earth-Science Reviews* 23(4), 255-352.
- Vuitton, V., O. Dutuit, M. A. Smith, and N. Balucani, 2014. Chemistry of Titan's Atmosphere, in *Titan*, edited by I. Müller-Wodarg et al., Cambridge Univ. Press, Cambridge, U. K., 224– 271.
- Wald, G., 1954. The Origin of Life. *Scientific American* 191, 44-53.
- Werynski, A., Neish, C.D., Le Gall, A., Janssen, M.A., and Cassini RADAR Team., 2019. Compositional variations of Titan's impact craters indicates active surface erosion. *Icarus*, 321, 508-521.
- Worster, M.G., 1992. The dynamics of mushy layers. In *Interactive dynamics of convection and solidification* (pp. 113-138). Springer, Dordrecht.
- Worster, M.G., 1997. Convection in mushy layers. *Annual Review of Fluid Mechanics* 29, 91-122.
- Worster, M.G., 1990. Structure of a convecting mushy layer. *Appl. Mech. Rev.* 43, S59-S62, <https://doi.org/10.1115/1.3120852>.

Chapter 3

3 The role of hydrolysis in the emplacement of organic molecules into melt sheets on Titan

3.1 Introduction

NASA is sending the Dragonfly mission to Titan to investigate its chemistry (prebiotic and biomolecular), methane cycle, and geology (Barnes et al., 2021). Titan has a dense, nitrogen-rich atmosphere with small amounts of methane (2%) that leads to complex chemistry and geology (Lindal et al., 1983; Kouvaris and Flasar, 1991; Tomasko et al., 2005; Tobie et al., 2006; Hörst, 2017). Cosmic radiation ionizes and dissociates the methane and nitrogen in Titan's atmosphere, and over time, complex organic molecules form with the general formula $C_xH_yN_z$ (Sagan and Thompson, 1984; Krasnopolsky et al., 2014). Signature among these molecules are the complex organics called tholins that are thought to have played a role in the origin of life (Sagan and Khare, 1979; Sagan and Thompson, 1984; Krasnopolsky et al., 2014). The atmosphere of the early Earth is thought to have undergone similar photochemical processes, which created a reservoir of prebiotic molecules that may have sparked the origin of life when mixed with Earth's liquid water (Miller, 1953; Wald, 1954; Trainer et al., 2006; He and Smith, 2014). Therefore, Titan is a natural laboratory for studying the origin of life on the early Earth and other worlds (McDonald et al., 1994; Neish et al., 2010; Cleaves, et al., 2014).

3.1.1 Dragonfly

The primary motivation behind NASA's new mission, Dragonfly, is to investigate Titan's prebiotic chemistry (Lorenz et al. 2018; Barnes et al., 2021). It will investigate the composition of the organic molecules that exist on Titan. There is evidence of organics exist on Titan's surface in several forms: 1) as the hydrocarbon lakes, rivers, and rain (Lorenz et al., 2008), 2) as a thin (10s of centimeters) coating across Titan's surface (Janssen et al., 2016), 3) as large sand dunes of organics across the equatorial region (Lorenz et al., 2006; Lorenz and Zimbelman, 2014), and 4) potentially as oxygenated molecules that mixed with temporarily liquid bodies of water (e.g., Thompson & Sagan 1992; Lopes et al., 2007; Neish et al., 2006, 2018). To investigate Titan's prebiotic chemistry, the mission will land in the dunes south of Selk crater, where temporarily liquid

bodies of water (in the form of impact melt) may have mixed with the surface organics to produce more complex biomolecules (Artemieva and Lunine, 2005; O'Brien et al., 2005; Hedgepeth et al., 2022). Past work has demonstrated that when Titan's organics are exposed to oxygen (i.e., through liquid water on Titan) biomolecules like amino acids begin to form (Neish et al., 2010; Hörst et al., 2012; Cleaves et al., 2014).

Dragonfly will be targeting the liquid melt that forms during the impact cratering process (Artemieva and Lunine, 2005; O'Brien et al., 2005; Neish et al., 2018; Barnes et al., 2021; Lorenz et al., 2021; Hedgepeth et al., 2022). An impact crater is formed when a celestial object impacts a planetary body imparting huge amounts of energy that excavates, vaporizes, and melts the impacted bedrock (Melosh, 1989; Osinski et al., 2011). The liquid melt will be warm (>273 K) with modeling suggesting it will reach the boiling point, with parts of it vaporizing at temperatures of up to 773 K (Artemieva and Lunine, 2005). This environment will remain liquid for decades, possibly up to centuries or millennia before freezing (O'Brien et al., 2005; Hedgepeth et al., 2022). These warm temperatures will facilitate a more active chemical environment compared to the colder, ammonia-laced liquid in Titan's interior ocean (Neish et al., 2006, 2018; Lopes et al., 2007). Selk crater is one of nearly a hundred craters on Titan (Neish et al., 2013; Hedgepeth et al., 2020), but Dragonfly has chosen Selk crater because of its 1) large size, which leads to more melt production, 2) relative freshness, which would limit the covering of the melt by sand deposition, and 3) limitations in orbital dynamics (Neish et al., 2013, 2018; Hedgepeth et al., 2020; Barnes et al., 2021; Lorenz et al., 2021). However, the samples that Dragonfly can target will be limited by the extent to which fluvial erosion has exposed Selk's buried melt deposits.

3.1.2 Sampling Biomolecules

Studies of terrestrial impact craters have demonstrated how subsurface impact crater melt deposits can become accessible through fluvial incision by rivers (Neish et al., 2018). Selk's depth to diameter ratio indicates that it is not buried by large amounts of sediments, but there is still evidence of sand dunes on the floor of Selk in Cassini data (Neish et al., 2018; Lorenz et al., 2021). The level of fluvial erosion in Selk crater is not well constrained. An indirect method of measuring fluvial erosion is by studying crater rim heights because they are primarily degraded by fluvial erosion (Forsberg-Taylor et al.,

2004). Selk's rim heights are just within the lowest estimates of rim heights expected for similarly sized craters on Ganymede (Hedgepeth et al., 2020), so it is unlikely that significant fluvial erosion has occurred there (Neish et al., 2016). Nevertheless, fluvial features have been identified in the Visible and Infrared Mapping Spectrometer (VIMS) data within Selk's ejecta blanket (Soderblom et al., 2010). If fluvial erosion has caused the incision of the crater floor, subsurface melt material will be exposed, and portions of it will be deposited in the smooth valley at the bottom of the river (Neish et al., 2018). If such rivers exist in Selk's interior, Dragonfly will have an easy path to access the biomolecules that form in the crater melt. However, the final target that Dragonfly chooses must take into account the physical and chemical evolution of the ice that it samples (Hedgepeth et al., 2022).

Each melt sample will have a unique thermal history that will determine how organic molecules react in the aqueous solution and are emplaced into the ice. Hedgepeth et al. (2022) assumed that the emplacement of organics into the freezing melt sheet will follow the same physics that controls the removal of salt from sea ice on Earth and other ocean worlds (Hobbs, 1974; Buffo et al., 2018, 2020, 2021; Chivers et al., 2021). The process is driven by buoyancy differences between the impurity (e.g., salt or organics) and the surrounding water (Buffo et al., 2018, 2020, 2021; Chivers et al., 2021; Hedgepeth et al., 2022). A melt lens on Titan, like a melt lens on Europa (e.g., Schmidt et al., 2011; Chivers et al., 2021), will freeze inwards from the top and bottom creating two freeze fronts. Buoyancy creates two contrasting patterns: 1) buoyancy drives most (but not all) of the impurity out of the ice, and 2) buoyancy forces prevent the impurity from diffusing out of the forming ice lattice (Buffo et al., 2018, 2020, 2021; Chivers et al., 2021; Hedgepeth et al., 2022). Hedgepeth et al. (2022) demonstrated that even the most conservative estimates of the bulk organic concentrations in the melt sheet should be detectable by Dragonfly (i.e., ≥ 500 parts per billion, ppb, Grubisic et al., 2021). However, specific molecules may be harder to identify, particularly complex biomolecules that take time to form within the freezing melt sheet.

3.1.3 Titan Melt Sheet

Hedgepeth et al., (2022) modeled the emplacement of HCN into a freezing melt lens on Titan using the planetary ice model SlushFund2.0-v2 (SF2) (Buffo et al., 2020). They treated HCN as representative of the larger population of organics that will exist within the Selk melt lens, but the reality is that other organics will exist with different chemical properties. Furthermore, the system will actively evolve via hydrolysis from the initial prebiotic chemistry (e.g., HCN) into their biomolecular daughter products (Neish et al., 2010; Hörst et al., 2012; Cleaves et al., 2014). Modeling complex mixtures of organics requires constraints on the properties of the aqueous mixture (Buffo et al., 2020). For example, the freezing temperature of water changes for different aqueous mixtures (e.g., HCN and glycine each have different freezing points in water, Coates and Hartshorne, 1931; El-Sharkway et al., 1992). Extensive laboratory work is required to adequately characterize the chemical mixture in a true Titan melt sheet (both initially and as it evolves). Until such work is done, it is not practical to attempt to model such advanced scenarios. However, it is still possible to explore the impact of specific chemical variables like buoyancy and the rate of hydrolysis.

Specific variables can be studied by assuming a specific, unchanging, chemistry in the same way HCN was used to create a first order estimate for the larger population of carbon and nitrogen rich organic molecules on Titan by Hedgepeth et al. (2022). HCN provided a good contrast to the sea ice models because it was less dense than water and ice compared to the denser salt in sea ice (Buffo et al., 2018, 2020, 2021; Chivers et al., 2021; Hedgepeth et al., 2022). In a realistic melt pond, the bulk chemical properties of the aqueous mixture will be determined by what chemistry is present; slight variations in properties (e.g., specific heat and conductivity) will affect how much impurity is trapped within the ice. That is a level of precision that cannot be achieved without more laboratory work and direct measurement of the Titan surface chemistry. However, the broader pattern of emplacement (i.e., orders of magnitude more impurity in the top or bottom section of the melt lens) can be constrained using the bulk mass density of the impurities (Chivers et al., 2021; Hedgepeth et al., 2022). Therefore, the most extreme system may be thought to begin with a mixture of organics that are more buoyant like HCN (as many Titan organics

are, Hörst, 2017) that become denser as biomolecules begin to form. The point in time at which the biomolecules become abundant enough to be detected by Dragonfly will depend on how fast the parent products (i.e., the prebiotic molecules) undergo hydrolysis into the daughter products (i.e., the biomolecules). Furthermore, the relative abundance of parent to daughter products will be a key indicator of how the chemical properties of the aqueous mixture are evolving. A better understanding of how parent products evolve into the daughter products will constrain how the daughter products (i.e., the biomolecules that Dragonfly is interested in sampling) will be trapped into the ice.

In this work, we explore the chemical evolution of a freezing melt lens on Titan. We build on the work of Hedgepeth et al. (2022) to model the effect hydrolysis has on the emplacement of organics into a solidified water ice melt sheet on Titan. We treat HCN as representative of the parent population and consider glycine as representative of the daughter product population. We are following the methodology of Hedgepeth et al. (2022) to track the emplacement of glycine as ice freezes using the SlushFund2.0-v2 (SF2) model (Buffo et al., 2020). We use the results of the SF2 model within the 2D thermophysical model of Chivers et al. (2021) to produce the distribution of glycine in a Titan melt sheet. We then modify the Chivers et al. (2021) model to provide a mass sink and source to account for the decay and production of the parent and daughter products through hydrolysis, respectively. The distribution of glycine provides a useful contrast to the distribution of HCN, as it is a less buoyant (or denser than water) impurity. The emplacement of glycine and HCN will be further affected as hydrolysis removes HCN to produce glycine. The rate of hydrolysis may affect how quickly the biomolecular products become detectable, so we consider the detectability of glycine for a range of hydrolysis rates to identify when and where it will be detectable by Dragonfly. Furthermore, we consider how the bulk properties of the melt will evolve as the system becomes more dominated by the daughter products.

3.2 Methodology

3.2.1 Sea Ice Model

We use the same 1D multiphase reactive transport model (SF2) employed by Hedgepeth et al. (2022) to determine the impurity concentration profile of organics in a Titan impact melt lens. The model is created to study the evolution of aqueous chemistry in a liquid body with a progressing freeze front. The model employs the use of a reactive transport model to simulate physical, chemical, and biological processes for discrete spatial and temporal scales (Steefal et al., 2005). The model is built on the mushy layer theory that is often used to study ice-ocean systems where multiple phases of ice exist (Worster 1992, 1997; Feltham et al. 2006; Hunk et al., 2011; Buffo et al., 2018). The model incorporates advection-reaction-diffusion processes to conserve the evolution of heat and mass within the system. The change in phase is determined using the enthalpy method first proposed by Huber et al. (2008). The mass flow is determined to be driven by density differences between the surrounding water and the impurities in the system (Griewank and Notz, 2013; Buffo et al., 2018). Other forces will facilitate mass flow in the system (e.g., volumetric changes or temperature differences within the mushy layer), but past work has demonstrated that the effect of these are negligible to the density driven forces produced between the impurity and the surrounding water (Buffo et al., 2020).

The freezing process occurs by concentrating impurities within the residual liquid that exists within the pore spaces in the forming ice lattice (Weissenberger et al., 2019). These create brine channels within which the impurity rich liquid, typically referred to as brine in sea ice, is driven by the forces that the SF2 model is tracking (Buffo et al., 2018, 2020). Once a critical porosity is reached, the pores are assumed to be cut off from the remaining liquid layer; we assume the same critical porosity as for sea ice ($\phi \leq 5\%$, **Table 3.1**) (Buffo et al., 2018; Hedgepeth et al., 2022). The concentration profile that the SF2 model produces are volumetric averages of these concentrated veins throughout the depth of the ice. Therefore, the discrete increments must be large enough to encapsulate the veins but small enough to accurately average the distribution of organics (e.g., $dz = 1$ cm). The SF2 model can estimate the distribution impurities for any thickness of ice over an ocean sufficiently large that the rejection of impurities from the ice does not affect the bulk

concentration within the ocean. We model a Titan melt sheet by using the SF2 outputs in the Chivers et al. (2021) thermophysical model to track the impurities in a 2D melt sheet, using the same approach as Hedgepeth et al. (2022).

Table 3.1. The organic-specific variables used for modeling glycine and HCN in the SF2 and Chivers et al. (2021) models, along with their definition, values, and units. All other variables are unchanged from, and defined in, Hedgepeth et al. (2022).

Symbol	Definition	Glycine	HCN	Units
ρ	Liquid density	1267 ^a	687 ^a	$kg\ m^{-3}$
T_{melt}	Melting temperature	535.15 ^a	259.85 ^a	K
T_{boil}	Boiling temperature	563.15 ^b	298.75 ^a	K
c	Heat capacity	1.253×10^3 ^c	2.612×10^3 ^d	$J\ kg^{-1}K^{-1}$
k	Heat conductivity	2.28×10^{-9} ^c	2.28×10^{-9} ^d	$Wm^{-1}K^{-1}$

^aHaynes (2011).

^bCompound decomposes at this point (Kerr, 1999).

^cEl-Sharkawy et al., (1992).

^dRumble (2020).

The Chivers et al. (2021) model is a 2D thermophysical model that tracks the evolution of a liquid body, within (or on top of) an icy crust. As the body freezes, impurities are assumed to freeze into the ice at a rate determined using the SF2 outputs. The SF2 model outputs the concentration of organics into the ice at a specific thermal gradient and melt concentration. Therefore, a catalog of results is created using the SF2 model by relating the emplacement concentration to the thermal gradient and the melt concentration. We are effectively using the SF2 model to consider a range of ocean concentrations, where no one ice-ocean profile represents an actual melt sheet profile, but within the range of ocean profiles exists all the possible conditions that will exist within the melt sheet (i.e., all possible melt concentrations and thermal gradients). The Chivers model does not reproduce the mushy layer physics of the SF2 model. Rather, it is a heat transfer model that only tracks the movement of heat and changes of phase within each element of the melt sheet. It infers how much of the organic impurities freeze into the ice based on the organic concentration in the melt and the thermal gradient on the element when it freezes. As the melt sheet freezes, the warm melt lens is insulated from the colder ice, reducing the thermal

gradient. Simultaneously, as ice freezes, excess impurity is concentrated into the remaining melt. The SF2 results are imported using a set of constitutive equations that were produced by Buffo et al. (2020) to construct quasi-analytical concentration dependencies that can be utilized without explicit simulations.

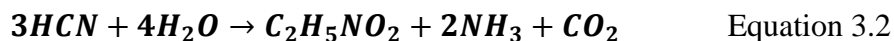
We begin by studying the concentration of glycine in the melt sheet (similar to the work done for HCN in Hedgepeth et al. (2022)), using the SF2 model and the Chivers et al (2021) thermophysical model. The SF2 model is used to determine how much of the glycine will freeze into the ice for melt concentrations of 1 ppt (0.1%) to 210 ppt (21%, saturation point). We use these results in the Chivers model to consider melt sheets of 10 m, 50 m, 100 m, and 250 m in thickness, at concentrations of glycine between 5 (0.5%) to 100 ppt (10%). This is performed for the same sized crater and floor diameter (80 km and ~55 km respectively) studied in Hedgepeth et al. (2022). We present these in contrast to the HCN results of Hedgepeth et al. (2022) and then take them a step further to consider these emplacement profiles when hydrolysis is actively changing the concentration of the system.

To study how hydrolysis will affect the emplacement of organics into the ice we consider the relationship between HCN and glycine. We use the results of Hedgepeth et al. (2022) for HCN and assume HCN is representative of the initial population of organics in the Selk crater melt sheet. We choose to do this because HCN is one of the most abundant organics on Titan and is known to hydrolyze when mixed with water to produce a range of purines, pyrimidines, and amino acids with glycine being the most abundant biomolecule formed (Coates and Hartshorne, 1931; Ferris et al., 1973, 1974, 1978; Haynes, 2011; Krasnopolsky, 2015;). Each organic found on Titan will have different chemical properties, and they will not all be buoyant like HCN (Haynes, 2011; Hörst, 2017). Therefore, HCN may not reflect the properties of the starting prebiotic mixture in the melt sheet. If we assume the organic material that mixes with the impact melt has the same composition of organics as estimated to form in the Titan atmosphere, the bulk density, based on the 10 most abundant organics, would be $\sim 1150 \text{ kg/m}^3$, or only slightly denser than water (Haynes et al., 2011; Vuitton et al., 2014). Therefore, the initial population of organics may not follow the same pattern as HCN, but the small density difference from water will likely

produce less extreme removal as observed for impurities like salt ($\rho_{salt} > 2000 \text{ kg/m}^3$) or even many biomolecules (e.g., $\rho_{glycine} = 1610 \text{ kg/m}^3$). Many of the biomolecules of life are denser than water (e.g., DNA and its nucleobases, Soukup, 2003). It is therefore likely that the bulk density of the system will increase as hydrolysis occurs. If the bulk density of the initial prebiotic mixture has a density more than that of water, the transition to daughter molecules will likely have a less dramatic impact on the emplacement pattern (i.e., material will preferentially concentrate at the base at increasing amounts). By using HCN, we consider the most extreme transition in impurity properties that should be expected. In contrast to HCN, we consider glycine because it is a major product that forms both from HCN and from other organics that exist on Titan (Ferris et al., 1973, 1974, 1978; Neish et al., 2008, 2010; Cleaves et al. 2014; Hörst et al., 2017; Lee and Choe, 2017). Glycine also presents a contrasting density to HCN that is representative of many other biomolecules ($\rho_{glycine} = 1610 \text{ kg/m}^3$, $\rho_{HCN} = 687 \text{ kg/m}^3$; Haynes et al., 2011).

3.2.2 Modeling Hydrolysis

Past work studying the production of glycine from HCN shows several possible chemical pathways (Lee and Choe, 2017). However, there are two main reaction outcomes, each using three HCN molecules to produce one molecule of glycine (Lee and Choe, 2017). The various pathways use either three or four molecules of H_2O to produce three possible secondary products as shown in **Equations 3.1** and **3.2**,



The production of ammonia (NH_3), carbon dioxide (CO_2), and isocyanic acid (HNCO) in the reactions may further modify the properties of the mixture. Ammonia is known to lower the freezing temperature of water (Croft et al., 1988; Cynn et al., 1989), and carbon dioxide is known to react with ammonia to produce bicarbonate and carbamate (Choi et al., 2012). The production of bicarbonates and carbamates will reduce the pH of the system, as will the addition of isocyanic acid (Belson and Strachan, 1982; Park et al., 2008). Isocyanic acid will also hydrolyze to produce more ammonia and carbon dioxide

(Belson and Strachan, 1982). However, NH_3 increases the pH of the system, and as a major biproduct of the reaction, it may counter the decrease in pH by the other components (Ferris et al., 1973, 1974, 1978; Haynes, 2011). It is therefore unclear what effect the reaction will have on the net pH of the system, but any change may affect the rate of the reaction.

The rate of hydrolysis will be dependent on both the pH and temperature of the system (Ferris et al. 1978; McDonald et al. 1994; Neish et al. 2010; Hörst et al. 2012; Ruiz-Bermejo et al. 2021). Hydrolysis is often characterized by its half-life, or the time it takes for one-half of the parent product to evolve into the daughter products. At temperatures of $>60^\circ\text{C}$, the half-life is in the range of weeks to minutes if the pH is balanced (Miyakawa et al. 2002). As the pH is lowered, the half-life increases exponentially to between years and centuries. The half-lives are similarly lowered even at reasonable pH values when we approach the freezing temperature of water at Titan conditions (i.e., $\sim 0^\circ\text{C}$). These are the temperatures Hedgepeth et al. (2022) assumed with their model, where the melt began the freezing process at 0°C . However, the melt will likely reach very warm temperatures during the crater formation process (up to the boiling point; Artemieva and Lunine, 2005), and this may facilitate very short half-lives during the initial stages of freezing. It also may lead to the vaporization or destruction of HCN and other organics (Coates and Hartshorne, 1931; Haynes, 2011).

We track hydrolysis within the Chivers thermophysical model by running two independent melt sheets, one with HCN that has a mass sink and one with glycine that has a mass source fueled by the HCN sink. We estimate the rate of hydrolysis as a function of exponential decay based on past experimental work studying the rate of hydrolysis of Titan tholins (Neish et al., 2008, 2009). We begin by estimating the decay of the parent product, HCN, at each timestep (n) in **Equation 3.3**,

$$S_{parent_n} = (S_{parent_{n-1}} - c) * e^{-\frac{t}{\tau}} + c \quad \text{Equation 3.3}$$

Where S_{parent_n} and $S_{parent_{n-1}}$ are the respective concentrations of HCN in the current and previous timesteps, c is the critical concentration needed for HCN to hydrolyze or HCN at $t=\infty$, t is time, and τ is the half-life of HCN. Past work has defined the decay of the parent

product using a fixed constant for $(S_{parent_{n-1}} - c)$, but we are working in a freezing system where the impurities are concentrating independent of the hydrolysis process. Therefore, the rate of hydrolysis will change as the concentration of the impurities changes. The rate of hydrolysis, or half-life, varies widely depending on the conditions, so we have modeled half-lives from 1 to 50 yrs. Similarly, the value of c is also dependent on other factors, namely temperature. The value of c likely relates to the chemical pathways available to it. That is, 3 molecules of HCN are needed to react with water to form one molecule of glycine, and as the concentration of HCN decreases, the probability of 3 HCN molecules being close enough to react decreases. We consider a range of c values, defined as a fraction of the initial concentration of HCN in the melt (from 0% to 100%). The growth of glycine ($S_{daughter_n}$) is directly connected to the decay of HCN (S_{parent_n}) in this model. However, conservation of mass requires the conversion of HCN to glycine to be chemically balanced. The mass of HCN lost at each timestep (ΔS_{parent_n}) can be found with **Equation 3.4**,

$$\Delta S_{parent_n} = (S_{parent_{n-1}} - c) * e^{-\frac{t}{\tau}} \quad \text{Equation 3.4}$$

The mass of glycine that is produced from the amount of HCN lost at each timestep can be found by converting the mass of the lost HCN to the number of moles where the chemical balance of the HCN to glycine reaction is known to be 3:1. This gives the solution for the mass of glycine that is produced at each timestep ($\Delta S_{daughter_n}$) in **Equation 3.5**,

$$\Delta S_{daughter_n} = \frac{\Delta S_{parent_n}}{m_{parent}} * \frac{m_{daughter}}{3} \quad \text{Equation 3.5}$$

Where m is the molar mass of the parent and daughter products. The growth curve for glycine can then be found with **Equation 3.6**,

$$S_{daughter_n} = \Delta S_{daughter_n} + S_{daughter_{n-1}} \quad \text{Equation 3.6}$$

Where $S_{daughter_n}$ and $S_{daughter_{n-1}}$ are the respective concentrations of glycine in the current and previous timesteps.

3.3 Results and Discussion

3.3.1 Glycine Distribution

We have modeled the distribution of glycine freezing into a liquid water melt sheet on Titan. We present the distribution of glycine ($C_2H_5NO_2$) in contrast to the HCN results of Hedgepeth et al (2022). Unlike HCN, glycine is a molecule that is denser than water, thereby inverting the buoyancy driven forces that affect impurity emplacement into ice. The denser glycine moves the domain of the SF2 mushy layer model to the upper freeze front of the melt sheet (Buffo et al., 2020; Hedgepeth et al., 2022). The SF2 model assumes the impurities are concentrated in an infinite ocean rather than the closed system of a melt lens (Buffo et al., 2018, 2020). Therefore, we characterize all the possible states (i.e., melt concentrations and thermal gradients) that will exist within the actual melt sheet by creating entrainment concentration profiles for concentrations of glycine within the melt from 1 ppt (0.1%) to 210 ppt (21%, saturation point) (**Figure 3.1**).

These entrainment profiles are not a true representation of how glycine will freeze into a melt lens, but instead represent what sea ice forming over an infinite ocean would look like at these conditions. Instead, they form a catalog of data points that represent the range of *possible* states in which a glycine rich Titan melt lens will freeze (Hedgepeth et al., 2022). We present them here to study how glycine will freeze into the ice across these different states (i.e., at different depths/thermal gradients with various melt concentrations), and then we will use these outputs to model a 2D melt lens. The outputs of the SF2 model are quantitatively characterized by fitting them to the constitutive equations determined by Buffo et al. (2020) to relate the amount of glycine entrained into the ice for a range of thermal gradients (or analogously, depth) given an assumed initial concentration in the melt (**Table 3.2**). The constitutive equations represent three unique domains: 1) the concentration as a function of depth, 2) the shallow (or high thermal gradient) domain as a function of thermal gradient, and 3) the deep (or low thermal gradient) domain as a function of thermal gradient (Buffo et al., 2020).

The glycine concentration profiles show similar patterns as those observed in the HCN concentration profiles (Hedgepeth et al., 2022). For high thermal gradients ($T_{grad} \geq$

40 K/m), larger melt concentrations will lead to more glycine freezing into the ice. The same is true at more moderate thermal gradients ($10 \leq T_{grad} \leq 40$ K/m) where the jump in glycine concentration in the ice is roughly the same magnitude as the jump seen at the higher thermal gradients. This contrasts with the HCN profiles where higher melt concentrations produced steadily smaller gains of HCN concentration in the ice with smaller thermal gradients. In other words, the glycine emplacement profiles are parallel to each other at moderate to high thermal gradients, but the HCN emplacement profiles are not parallel to each other, instead converging upon one another. The exact reason for this dichotomy is unclear. It may be that the HCN emplacement profiles are transitioning into the linear domain a more rapidly (i.e., at higher thermal gradients). Nevertheless, it demonstrates how the emplacement profile is unique to the organic molecule being studied. Nevertheless, the glycine concentration profiles do eventually converge but only after reaching the linear domain of the emplacement profile (**Table 3.1**) (Buffo et al., 2018, 2020; Hedgepeth et al., 2022). The transition from the shallow (high thermal gradient) to linear (low thermal gradient) domain is more consistent with what was observed in the HCN results, with a characteristic spike in concentration as we reach the linear domain. However, the constitutive equations do not capture the spike that we see in the outputs of the SF2 model, which may imply the spikes are artifacts or that the constitutive equations do not capture the complete picture at the *boundary* of these domains. Each of these trends, and the precision to which the constitutive equations can capture them, will govern the pattern that we see within the 2D melt lens. Therefore, the outputs of the SF2 model provide insight into why we see the patterns we do in the 2D melt lens.

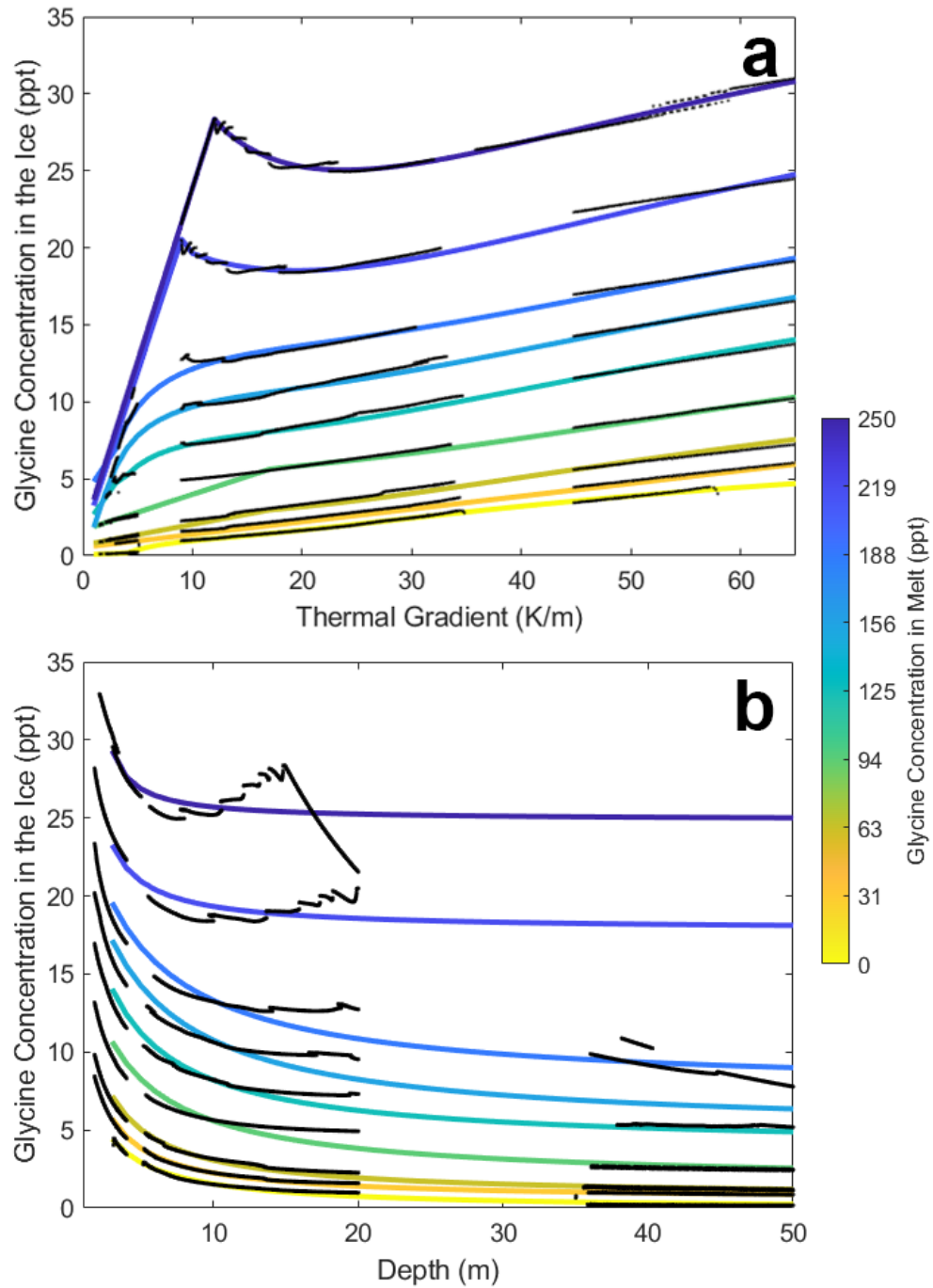


Figure 3.1. The concentration of glycine (ppt) in ice forming over an infinite ocean, for initial concentrations of 1 ppt (0.1%, yellow) to 210 ppt (21%, saturation point, dark blue), at thermal gradients (a), and depths (b) observed at the surface of Titan. The SF2 model results are shown with black points (they appear as disjointed lines because the spatial resolution is so fine). The analytical fits from Buffo et al. (2020) are applied to our data, where solid lines are fits formed using SF2 results (see Table 3.1)

The ultimate intent of fitting the SF2 results to these constitutive equations is to import them into a more realistic 2D model of a melt lens on Titan. The constitutive equations allow the results of the 1D SF2 model to be imported into the 2D heat transfer model of Chivers et al. (2021), which solves the 2D melt sheet as a finite closed system rather than the infinite ocean scenario that the SF2 model is designed to model (Hedgepeth et al., 2022). With the constitutive equations, the temperature, impurity concentration, and phase are modeled through time to produce the final emplacement profile within the melt sheet (**Figure 3.2**). The domain of the SF2 mushy layer model exists for only one of the freeze fronts (i.e., the upper freeze front for glycine) because it is driven by buoyancy differences. As in past work studying freezing melt lenses (i.e., Chivers et al., 2021; Hedgepeth et al., 2022), we assume the contrasting freeze front (i.e., the base of the melt sheet) will retain all of the glycine that was in the melt at the time of freezing because the same buoyancy forces that drive glycine out of the upper freeze front will force the glycine to remain emplaced in the basal freeze front.

The Chivers model is executed for melt sheets of thicknesses (h) from 10 m to 250 m and over glycine concentrations (S) from 5 ppt (or 0.5 %) to 100 ppt (or 10%) (**Figure 3.2**). The results are largely as expected, with orders of magnitude more glycine freezing at the base of the melt lens than at the top. More interesting is the leveling out of glycine in the top portion of the melt sheet as the system concentrates. This occurs in all simulations, except for concentrations of ≥ 50 ppt in melts ≥ 50 m thick. This is reflective of how higher concentrations reach the linear domain (i.e., the dramatic drop in glycine in the ice) sooner, while the lower concentrations (5 ppt and 10 ppt) have a much more gradual drop (**Figure 3.1**). What's more, we can see how 50 ppt and 100 ppt converge in the linear domain, leading to about the same amount of glycine in the ice. Lastly, there is plateau in the concentration every time the system reaches 210 ppt because it is the saturation point of glycine. This suggests there may be layers of precipitated glycine within the melt lens like the precipitated salt layers that are expected in melt lens on Europa (Schmidt et al., 2011; Chivers et al., 2021).

Table 3.2. The constitutive equations developed by Buffo et al. (2020) with the corresponding constants used to fit to our glycine results from the SF2 model. Each equation represents a specific domain of the data set (Buffo et al., 2020; Chivers et al., 2021; Hedgepeth et al., 2022). The first equation represents the concentration as a function of depth. The second equation represents the shallow (or high thermal gradient) domain of the results as a function of thermal gradient. The third equation represents the deep (or low thermal gradient) domain of the results as a function of thermal gradient. These equations are fit to the data for 1 ppt (0.1%) to 210 ppt (21%, saturation point).

Constitutive Equations	a	b	c	d
$S_{tot}(z) = a + \frac{b}{c - z}$	$a_1 = -0.05889$ $a_5 = 0.5031$ $a_{10} = 0.7577$ $a_{25} = 1.767$ $a_{50} = 3.857$ $a_{75} = 5.911$ $a_{100} = 7.552$ $a_{150} = 17.82$ $a_{210} = 24.86$	$a_1 = -18.22$ $a_5 = -18.26$ $a_{10} = -25.38$ $a_{25} = -47.96$ $a_{50} = -53.41$ $a_{75} = -59.58$ $a_{100} = -77.15$ $a_{150} = -14.57$ $a_{210} = -7.246$	$a_1 = -1.113$ $a_5 = -0.5014$ $a_{10} = -0.9553$ $a_{25} = -2.391$ $a_{50} = -2.213$ $a_{75} = -2.381$ $a_{100} = -3.420$ $a_{150} = 0.3273$ $a_{210} = 1.376$	
$S_{tot}\left(\frac{\partial T}{\partial z}\right) = a + b \frac{\partial T}{\partial z}$	$a_1 = -0.06602$ $a_5 = 0.5478$ $a_{10} = 0.5928$ $a_{25} = 1.460$ $a_{50} = 2.723$ $a_{75} = 1.654$ $a_{100} = 3.765$ $a_{150} = 1.094$ $a_{210} = 1.395$	$a_1 = 0.1000$ $a_5 = 0.08094$ $a_{10} = 0.1898$ $a_{25} = 0.3452$ $a_{50} = 0.6230$ $a_{75} = 1.477$ $a_{100} = 1.053$ $a_{150} = 2.163$ $a_{210} = 2.247$		
$S_{tot}\left(\frac{\partial T}{\partial z}\right) = a + \frac{b\left(\frac{\partial T}{\partial z} + c\right)}{1 + \frac{\partial T}{\partial z}} \left[1 - \exp\left(-\frac{d}{\frac{\partial T}{\partial z}}\right) \right]$	$a_1 = 10.75$ $a_5 = 18.95$ $a_{10} = 22.32$ $a_{25} = 27.64$ $a_{50} = 32.54$ $a_{75} = 35.51$ $a_{100} = 40.96$ $a_{150} = 45.05$ $a_{210} = 48.53$	$a_1 = -9.068$ $a_5 = -15.76$ $a_{10} = -17.85$ $a_{25} = -20.90$ $a_{50} = -22.91$ $a_{75} = -23.65$ $a_{100} = -25.85$ $a_{150} = -28.64$ $a_{210} = -30.78$	$a_1 = 1.822$ $a_5 = 2.134$ $a_{10} = 2.367$ $a_{25} = 1.970$ $a_{50} = 2.193$ $a_{75} = 2.013$ $a_{100} = 2.267$ $a_{150} = -0.2384$ $a_{210} = -3.387$	$a_1 = 68.75$ $a_5 = 104.6$ $a_{10} = 112.9$ $a_{25} = 110.8$ $a_{50} = 105.5$ $a_{75} = 98.64$ $a_{100} = 111.8$ $a_{150} = 83.17$ $a_{210} = 62.26$

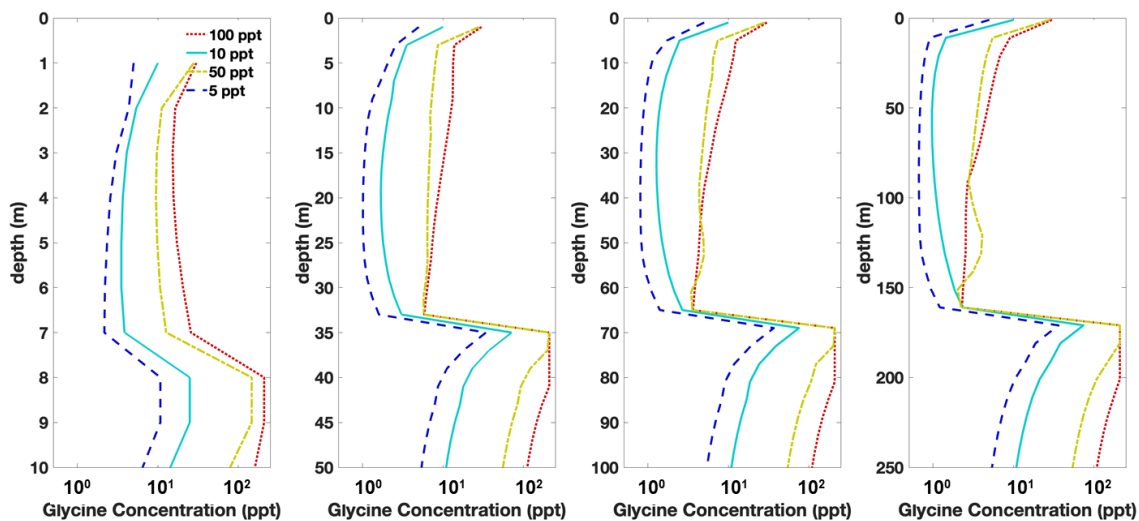


Figure 3.2. The results of the Chivers et al. (2021) model showing the concentration of glycine frozen into the ice with depth. The melt sheet is modeled for initial glycine concentrations of 5 ppt (0.5%, blue dashed line), 10 ppt (1%, turquoise solid line), 50 ppt (5%, yellow double-dashed line), and 100 ppt (or 10%, red dotted line) and for melt thicknesses of 10 m, 50 m, 100 m, and 250 m. Results are taken for an 80 km diameter crater (with a crater floor that is ~55 km in diameter).

3.3.2 Hydrolysis

We next model a system in which the HCN has a mass sink that sources the glycine system via hydrolysis (**Figure 3.3**). Each system is still assumed to be independent of the other, with the impurity properties defined as an aqueous mixture of water with HCN and water with glycine respectively (**Figure 3.3**). The Chivers et al. (2021) model is modified and executed with an added mass flux while all other factors are kept the same (Hedgepeth et al., 2022). The mass flux is determined by assuming the hydrolysis of HCN causes an exponential decay in that molecule, and the subsequent production of glycine follows a first-order growth curve. We consider a range of half-lives from 1 to 50 years (Neish et al., 2008). We use a broad range of half-lives because the rate of hydrolysis may vary due to temperature, pH or other properties (Miyakawa et al. 2002). We chose 1 to 50 years specifically because, for a 50 m melt sheet, it produces a range of systems between one where almost all the HCN hydrolyzes immediately to a system where only a fraction of HCN (~10%) hydrolyzes over the melt sheets lifespan (~10 yrs.). We have also considered

three possible constants that the system may converge to: 1) where all of the HCN is eventually lost to hydrolysis ($c = 0\%$), 2) where half of the initial HCN concentration is lost to hydrolysis ($c = 50\%$), and 3) where none of the initial concentration of HCN is lost to hydrolysis ($c = 100\%$). To be clear, these limits are based on the *initial* concentration of HCN, so as the melt lens concentrates, the HCN will begin to hydrolyze once it passes the set threshold. We consider up to 100% of the initial concentration, but the threshold could be higher, with hydrolysis only beginning once (or if) the threshold is met.

The concentration of HCN in the ice is not significantly altered for most of the scenarios we studied. For $c = 50\%$, the melt concentration reaches the 50% limit about a fourth of the way into the melt sheet, and for $c = 100\%$, the melt concentration does not significantly change until about third of the way into the melt sheet. This limit on the hydrolysis of HCN leads to an emplacement pattern at the base of the melt sheet that varies little in most cases studied. Even for $c = 0\%$, the emplacement pattern at the base of the melt sheet only begins to significantly change for half-lives less than 10 yrs. It also appears that when the melt drops to concentrations below ~ 1 ppt (0.1 %) HCN, its emplacement at the base and top of the melt sheet is about the same concentration, rather than the orders of magnitude difference we observe without hydrolysis. That is to say, there seems to be a point where the removal of impurities from the ice becomes negligible for critically low concentrations ($S < 1$ ppt). This is consistent with the results of Hedgepeth et al. (2022), who showed that the rejection of HCN slowed once the concentration became very low. This contrasts with glycine, which appears to demonstrate more variance at low concentrations.

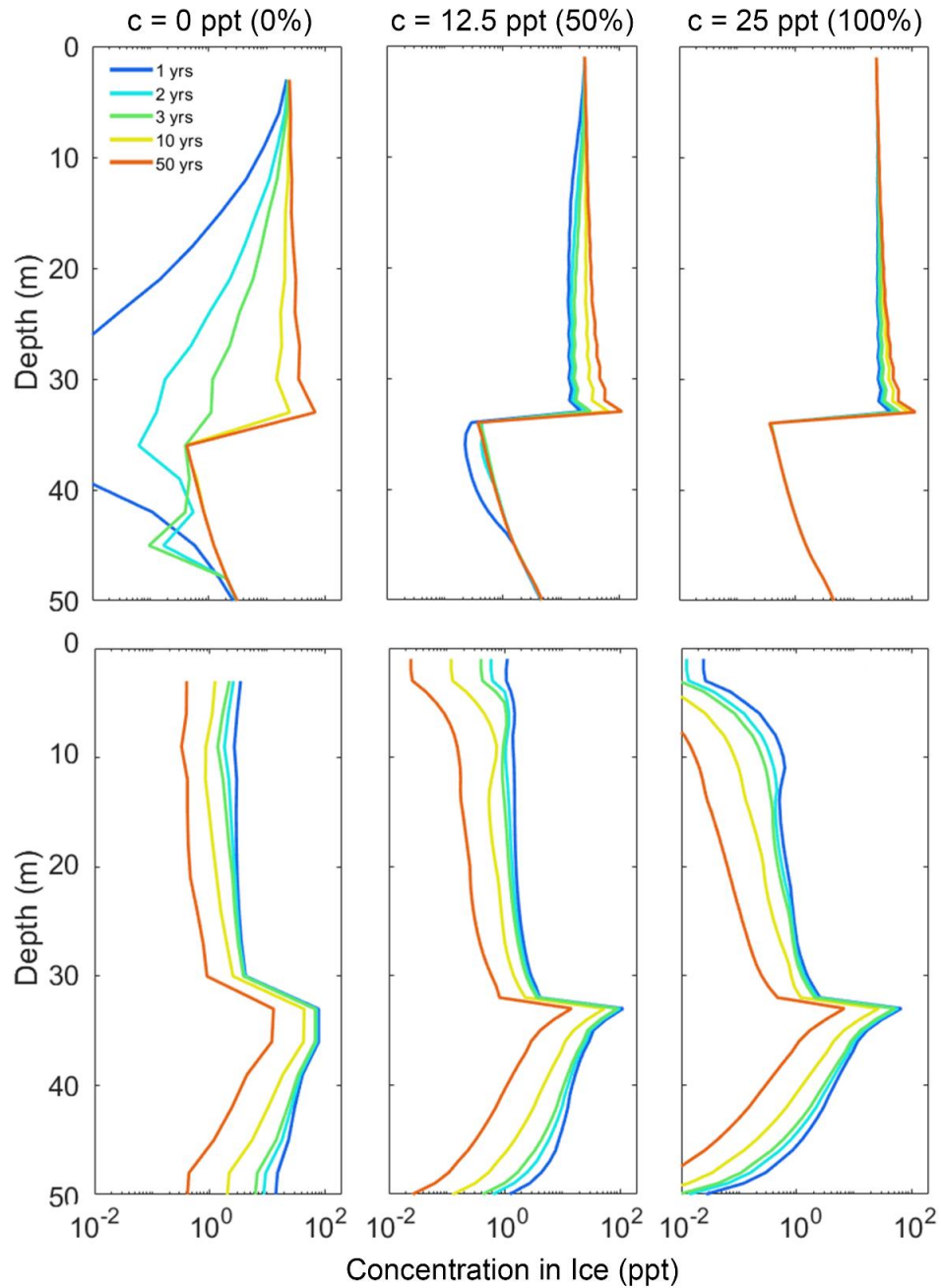


Figure 3.3. The Chivers et al. (2021) model is ran for HCN (top) and glycine (bottom) with an added mass flux representing the hydrolysis of HCN into glycine (i.e., mass is removed from the HCN model and added to the glycine model through time). We consider a range of half-lives from 1 year in blue to 50 years in orange, and a threshold concentration for HCN to hydrolysis into glycine of 0% (left), 50% (middle), and 100% (right) of the initial 25 ppt (2.5%) concentration. Results are taken for an 80 km diameter crater (with a crater floor of diameter ~ 55 km).

The concentration of HCN in the ice is not significantly altered for most of the scenarios we studied. For $c = 50\%$, the melt concentration reaches the 50% limit about a fourth of the way into the melt sheet, and for $c = 100\%$, the melt concentration does not significantly change until about third of the way into the melt sheet. This limit on the hydrolysis of HCN leads to an emplacement pattern at the base of the melt sheet that varies little in most cases studied. Even for $c = 0\%$, the emplacement pattern at the base of the melt sheet only begins to significantly change for half-lives less than 10 yrs. It also appears that when the melt drops to concentrations below ~ 1 ppt (0.1 %) HCN, its emplacement at the base and top of the melt sheet is about the same concentration, rather than the orders of magnitude difference we observe without hydrolysis. That is to say, there seems to be a point where the removal of impurities from the ice becomes negligible for critically low concentrations ($S < 1$ ppt). This is consistent with the results of Hedgepeth et al. (2022), who showed that the rejection of HCN slowed once the concentration became very low. This contrasts with glycine, which appears to demonstrate more variance at low concentrations.

The concentration of glycine increases steadily for higher rates of hydrolysis, even at high convergent constants (i.e., $c \geq 50\%$). However, there is a lag in the rise of glycine for very slow half-lives and very high convergent constants (i.e., $\tau \geq 3$ yrs, $c = 100\%$). The minimum abundance needed for detection by Dragonfly is 500 ppb (Grubisic et al., 2021), or 0.0005 ppt. This threshold is met near the top of the melt sheet for every scenario except $\tau = 50$ yrs, which reaches the critical threshold ~ 5 meters below the surface. This suggest there should be sufficient biomolecules present for Dragonfly to detect. However, if the concentration of glycine we have modeled here represents a mixture of biomolecules, it may not be enough to distinguish any one molecule because the abundance of individual molecules may be below the threshold, even if the total organic concentration is above the threshold. The chance of identifying any specific molecule increases as the abundance increases. For example, above ~ 0.01 ppt, up to 20 individual molecules might be identified (if each was 500 ppb). This threshold is met, even for the slowest half-life we consider, 8 m below the surface. For more liberal half-lives, we see an easily detectable amount of glycine within 1 m of the surface. This suggests Dragonfly will very likely be able to detect biomolecules throughout the depth of the melt sheet. However, the largest increase in

concentration occurs within the first 10 m of the ice sheet, suggesting it would be ideal to target below the 10 m mark. Furthermore, the initial concentration of the melt and the threshold concentration needed to trigger hydrolysis may be different than what we have studied in this work. This would alter how deep Dragonfly must target to detect the daughter products. Therefore, we recommend future experimental work is done to constrain what the threshold concentration is for HCN to hydrolyze into biomolecules. This will provide a more precise limit on how deep into the melt sheet Dragonfly should target. The most ideal depth to target is about 75% into the ice sheet, consistent with what Hedgpeeth et al. (2022) found for HCN. However, that depth will vary depending on the initial temperature of the melt and the amount of heating of the surrounding ice; more realistic initial melt and ice temperatures would likely drive the highest concentration of glycine toward the base of the crater, making it more difficult to sample.

Note, we are studying a 50 m melt sheet, but these patterns should also hold for thicker melt sheets depending on the rate of hydrolysis. The biggest change for a thicker melt sheet is that it may begin more diluted, which may produce a delay in the start of hydrolysis. However, once the critical concentration for hydrolysis to start is reached, biomolecules should arise.

3.3.3 Modeling Mixtures

The conversion from HCN to glycine does not significantly reduce the total concentration of organic impurities in the melt, despite some of the HCN being lost to secondary products. The production of the secondary products NH_3 , CO_2 , and HNCO may increase the total concentration of impurities within the water. However, we do not account for these because we consider the two systems to be independent of one another and their secondary products. For the primary parent and daughter products, the bulk concentration doesn't change much because the molar mass of $3\text{HCN} \cong \text{C}_2\text{H}_5\text{NO}_2$. What's more, we do not consider the interaction of the two primary products (or the secondary products) in our modeling. The change in chemistry will likely affect the rate of hydrolysis. If the pH drops, the rate of hydrolysis will slow with time, but if it increases, the rate of hydrolysis is unlikely to change (Miyakawa et al., 2002). More work is needed to understand how dramatically the change in pH will affect hydrolysis. Ammonia may significantly depress

the freezing temperature of the system and prolong the lifespan of the melt, but ammonia has also been shown to induce faster hydrolysis rates even at low temperatures (0 °C, Neish et al., 2009, 2010). This demonstrates how the addition of other chemistry complicates the physics controlling the freezing process. To truly consider an HCN-glycine mixture, laboratory work is needed to understand how complex organic mixtures affect the physical and chemical properties of an aqueous mixture. Until such work is done, we are limited to study this process as two independent mixtures, but these results provide boundary conditions for a buoyant vs dense organic mixture.

The complexity of Titan's surface makes it virtually impossible to study the exact chemistry that will be found there prior to the Dragonfly mission. Therefore, we recommend a broad exploration of how prebiotic and biomolecular mixtures affect the properties of an aqueous mixture (i.e., the bulk density, the freezing temperature, and the mixture thermal properties, Buffo et al., 2018, 2020; Hedgepeth et al., 2022). For example, the abundance of organics known to exist on Titan can be used to create a Titan-like aqueous mixture to examine in the laboratory. A contrasting mixture may be created using a range of oxygenated biomolecules that are expected to form via hydrolysis on Titan. The fraction of oxygenated to nonoxygenated organics can be controlled to study how the properties change and to judge whether hydrolysis is likely to significantly alter the chemical properties of the mixture. The problem can be expanded by the inclusion of salts and ammonia to study how these affect the mixture properties.

3.4 Conclusions

We expand on the work of Hedgepeth et al. (2022) to model the emplacement of glycine within a freezing melt sheet on Titan. We begin by modeling glycine as HCN was modeled in Hedgepeth et al. (2022), demonstrating how its density inverts the emplacement profile observed with HCN, with the highest concentrations being found near the base of the melt sheet. We then assume HCN hydrolyzes to produce glycine and introduce a mass flux within the model that removes HCN and creates glycine. In this set up, HCN remains above the Dragonfly detection limit for most scenarios, only becoming undetectable when the threshold concentration for HCN (the concentration at $t = \infty$) approaches zero, meaning all the HCN has left the system. Alternatively, glycine becomes detectable almost

immediately in all scenarios. Even at very low concentrations (i.e., $S < 1$ ppt), it remains detectable at both the surface and base of the melt sheet. In fact, once the concentration in the melt becomes very low (< 1 ppt), the emplacement at the top and base of the melt sheet becomes about equal for both HCN and glycine. This suggests that once the concentration of an impurity in the melt gets very low, the buoyancy forces driving the removal of impurities have a much smaller impact on how much impurity freezes into the ice. Therefore, the biggest factor determining whether Dragonfly will be able to detect the daughter products is how amenable the aqueous mixture is to hydrolysis. For the thresholds we tested, glycine becomes detectable within the top 10 m of the ice sheet, with the highest concentrations near the base of the crater. We recommend more work is done (1) to constrain the threshold concentration of HCN needed to hydrolysis into glycine, and (2) to study the chemical properties of a realistic mixture in a Titan melt sheet. This information will improve the results of future modeling efforts and provide the Dragonfly team with more realistic constraints for their sampling efforts.

3.5 References

- Artemieva, N., Lunine, J.I., 2005. Impact cratering on Titan II. Global melt, escaping ejecta, and aqueous alteration of surface organics. *Icarus* 175, 522–533. <https://doi.org/10.1016/j.icarus.2004.12.005>
- Barnes, J.W., Turtle, E.P., Trainer, M.G., Lorenz, R.D., MacKenzie, S.M., Brinckerhoff, W.B., Cable, M.L., Ernst, C.M., Freissinet, C., Hand, K.P. and Hayes, A.G., 2021. Science goals and objectives for the Dragonfly Titan rotorcraft relocatable lander. *The Planetary Science Journal*, 2(4), p.130.
- Belson, D.J. and Strachan, A.N., 1982. Preparation and properties of isocyanic acid. *Chemical Society Reviews*, 11(1), pp.41-56.
- Buffo, J., Schmidt, B., and Huber, C., 2018. Multiphase reactive transport and platelet ice accretion in the sea ice of McMurdo sound, Antarctica. *Journal of Geophysical Research: Oceans* 123, 324-345.
- Buffo, J., Schmidt, B., and Huber, C., Walker, C., 2020. Entrainment and dynamics of ocean-derived impurities within Europa's ice shell. *Journal of Geophysical Research*. <https://doi.org/10.1002/essoar.10502079.2>.
- Buffo, J.J., Schmidt, B.E., Huber, C. and Meyer, C.R., 2021. Characterizing the ice-ocean interface of icy worlds: A theoretical approach. *Icarus*, 360, p.114318.
- Chivers, C. J., Buffo, J. J., & Schmidt, B. E. (2021). Thermal and chemical evolution of small, shallow water bodies in Europa's ice shell. *Journal of Geophysical Research: Planets* 126. <https://doi.org/10.1029/2020JE006692>.
- Choi, B.G., Kim, G.H., Yi, K.B., Kim, J.N. and Hong, W.H., 2012. Influence of operating temperature on CO₂-NH₃ reaction in an aqueous solution. *Korean Journal of Chemical Engineering*, 29(4), pp.478-482.

- Cleaves, H. J., Neish, C., Callahan, M. P., Parker, E., Fernández, F. M., and Dworkin, J. P. (2014). Amino acids generated from hydrated Titan tholins: Comparison with Miller-Urey electric discharge products. *Icarus* 237:182–189.
- Coates, J.E., and Hartshorne, N.H., 1931. Studies on Hydrogen Cyanide. Part III. The Freezing Points of Hydrogen Cyanide-Water Mixtures. *Journal of Chemistry Society*, 657-665.
- Croft, S.K., Lunine, J.I. and Kargel, J., 1988. Equation of state of ammonia-water liquid: Derivation and planetological applications. *Icarus*, 73(2), pp.279-293.
- Cynn, H.C., Boone, S., Koumvakalis, A., Nicol, M. and Stevenson, D.J., 1989. Phase diagram for ammonia-water mixtures at high pressures: implications for icy satellites.
- El-Sharkawy, A.A., Dakroury, A.Z. and Osman, M.B.S., 1992. Thermal properties of some α -amino acids in aqueous solutions. *International journal of thermophysics*, 13(5), pp.827-835.
- Feltham, D., Untersteiner, N., Wettlauger, J.S., Worster, M.G., 2006. Sea ice is a mushy layer. *Geophysical Research Letters* 33, L14501. doi:10.1029/2006GL026290.
- Ferris, J.P., Donner, D.B. and Lobo, A.P., 1973. Possible role of hydrogen cyanide in chemical evolution: investigation of the proposed direct synthesis of peptides from hydrogen cyanide. *Journal of Molecular Biology*, 74(4), pp.499-510.
- Ferris, J.P., Wos, J.D., Ryan, T.J., Lobo, A.P. and Donner, D.B., 1974. Biomolecules from HCN. *Origins of life*, 5(1), pp.153-157.
- Ferris, J.P., Joshi, P.C., Edelson, E.H. and Lawless, J.G., 1978. HCN: A plausible source of purines, pyrimidines and amino acids on the primitive earth. *Journal of molecular evolution*, 11(4), pp.293-311.
- Forsberg-Taylor, N.K., Howard, A.D. and Craddock, R.A., 2004. Crater degradation in the Martian highlands: Morphometric analysis of the Sinus Sabaeus region and

simulation modeling suggest fluvial processes. *Journal of Geophysical Research: Planets*, 109(E5).

Griewank, P.J. and Notz, D., 2013. Insights into brine dynamics and sea ice desalination from a 1-D model study of gravity drainage. *Journal of Geophysical Research: Oceans* 118, 3370-3386.

Grubisic, A., Trainer, M.G., Li, X., Brinckerhoff, W.B., van Amerom, F.H., Danell, R.M., Costa, J.T., Castillo, M., Kaplan, D. and Zacny, K., 2021. Laser Desorption Mass Spectrometry at Saturn's moon Titan. *International Journal of Mass Spectrometry*, 470, p.116707.

Haynes, W.M., 2011. *CRC Handbook of Chemistry and Physics*, (Internet Version 2011). Taylor Francis Group: Boca Raton, FL.

He, C., Smith, M.A., 2014. Identification of nitrogenous organic species in Titan aerosols analogs: Implication for prebiotic chemistry on Titan and early Earth, *Icarus* 238, 86-92, <https://doi.org/10.1016/j.icarus.2014.05.012>.

Hedgepeth, J.E., Neish, C.D., Turtle, E.P., Stiles, B.W., Kirk, R., & Lorenz, R.D, 2020. Titan's impact crater population after Cassini. *Icarus* 344, 113664. <https://doi.org/10.1016/j.icarus.2020.113664>.

Hedgepeth, J.E., Buffo, J.J., Chivers, C.J., Neish, C.D. and Schmidt, B.E., 2022. Modeling the Distribution of Organic Carbon and Nitrogen in Impact Crater Melt on Titan. *The Planetary Science Journal*, 3(2), p.51.

Hörst, S.M., Yelle, R.V., Buch, A., Carrasco, N., Cernogora, G., Dutuit, O., Quirico, E., Sciamma-O'Brien, E., Smith, M.A., Somogyi, A., Szopa, C., Thissen, R., and Vuitton, V., 2012. Formation of amino acids and nucleotide bases in a Titan atmosphere simulation experiment. *Astrobiology* 12: 809–817.

Hörst, S.M., 2017. Titan's atmosphere and climate. *Journal of Geophysical Research: Planets* 122, 432–482. <https://doi.org/10.1002/2016JE005240>.

- Huber, C., Parmigiani, A., Chopard, B., Manga, M., & Bachmann, O., 2008. Lattice Boltzmann model for melting with natural convection. *International Journal of Heat and Fluid Flow* 29, 1469–1480. <https://doi.org/10.1016/j.ijheatfluidflow.2008.05.002>.
- Hunke, E.C., Notz, D., Turner, A.K., and Vancoppenolle, M., 2011. The multiphase physics of sea ice: A review for model developers. *The Cryosphere* 5(4), 989–1009. <https://doi.org/10.5194/tc-5-989-2011>.
- Kerr, J.A., 1999. *CRC Handbook of Chemistry and Physics* 79th edn ed DR Lide. p. 3-173.
- Kouvaris, L.C., Flasar, F.M., 1991. Phase equilibrium of methane and nitrogen at low temperatures: Application to Titan. *Icarus* 91, 112–124. [https://doi.org/10.1016/0019-1035\(91\)90131-C](https://doi.org/10.1016/0019-1035(91)90131-C).
- Krasnopolsky, V.A., 2014. Chemical composition of Titan's atmosphere and ionosphere: Observations and the photochemical model. *Icarus* 236, 83-91. <https://doi.org/10.1016/j.icarus.2014.03.041>.
- Lee, H.M. and Choe, J.C., 2017. Formation of glycine from HCN and H₂O: A computational mechanistic study. *Chemical Physics Letters*, 675, pp.6-10.
- Lindal, G.F., Wood, G.E., Hotz, H.B., Sweetnam, D.N., Eshleman, V.R., Tyler, G.L., 1983. The atmosphere of Titan: An analysis of the Voyager 1 radio occultation measurements. *Icarus* 53, 348–363. [https://doi.org/10.1016/0019-1035\(83\)90155-0](https://doi.org/10.1016/0019-1035(83)90155-0).
- Lopes, R. M.C., Mitchell, K.L., Stofan, E.R., et al., 2007. Cryovolcanic features on Titan's surface as revealed by the Cassini Titan Radar Mapper, *Icarus* 186, 395–412, [doi:10.1016/j.icarus.2006.09.006](https://doi.org/10.1016/j.icarus.2006.09.006).
- Lorenz, R.D., Wall, S., Radebaugh, J., Boubin, G., Reffet, E., Janssen, M., Stofan, E., Lopes, R. M.C., Kirk, R.L., Elachi, C., Lunine, J., Mitchell, K., Paganelli, F., Soderblom, L., Wood, C., Wye, L., Zebker, H., Anderson, Y., Ostro, S., Allison, M., Boehmer, R., Callahan, P., Encrenaz, P., Ori, G. G., Francescetti, G., Gim, Y.,

- Hamilton, G., Hensley, S., Johnson, W., Kelleher, K., Muleman, D., Picardi, G., Posa, F., Roth, L., Seu, R., Shaffer, S., Stiles, B., Vetrella, S., Flamini, E., West, R., 2006. The Sand Seas of Titan: Cassini RADAR Observations of Longitudinal Dunes. *Science* 312, 724–727. <https://doi.org/10.1126/science.1123257>
- Lorenz, R.D., Mitchell, K.L., Mitchell, K.L., Kirk, R.L., Hayes, A.G., Aharonson, O., Zebker, H.A., Paillou, P., Radebaugh, J., Lunine, J.I., Janssen, M.A., Wall, S.D., Lopes, R.M., Stiles, B., Ostro, S., Mitri, Giuseppe, Stofan, E.R., 2008. Titan's inventory of organic surface materials. *Geophys. Res. Lett.* 35, doi:10.1029/2007GL032118. L02206
- Lorenz, R.D., Zimbelman, J.R., 2014. *Dune Worlds: How Windblown Sand Shapes Planetary Landscapes*, 1st ed. Springer-Verlag Berlin Heidelberg.
- Lorenz, R.D., Turtle, E.P., Barnes, J.W., Trainer, M.G., Adams, D.S., Hibbard, K.E., Sheldon, C.Z., Zancy, K. Peplowski, P.N., Lawrence, D.J., and Ravine, M.A., 2018. Dragonfly: A rotorcraft lander concept for scientific exploration at Titan. *Johns Hopkins APL Technical Digest*, 34(3), p14.
- Lorenz, R.D., MacKenzie, S.M., Neish, C.D., Le Gall, A., Turtle, E.P., Trainer, M.G., Barnes, J.W., Werynski, A., Hedgepeth, J., Karkoschka, E., 2021. Selection and Characteristics of the Dragonfly Landing Site near Selk Crater, Titan. *Planetary Science Journal*.
- MatWeb, 2018. Hydrogen Cyanide, HCN - MatWeb. http://www.matweb.com/search/datasheet_print.aspx?matguid=95207a948b2c4d6ab6bed897a6c0a0d4&n=1 (accessed 2018)
- McDonald, G.D., Corlies, P., Wray, J.J., Horst, S.M., Hofgartner, J.D., Liuzzo, L.R., Buffo, J., and Hayes, A. G., 2015. Altitude-dependence of Titan's methane transmission windows: Informing future missions. In: 46th Lunar and Planetary Science Conference Abstracts, The Woodlands, Texas, USA.

- Melosh, H.J., 1989. *Impact Cratering: A Geologic Process*, Oxford monographs on geology and geophysics. Oxford University Press.
- Miller, S.L., 1953. A production of amino acids under possible primitive earth conditions. *Science* 117, 528-529.
- Miyakawa, S., James Cleaves, H. & Miller, S.L. The Cold Origin of Life: A. Implications Based On The Hydrolytic Stabilities Of Hydrogen Cyanide And Formamide. *Orig Life Evol Biosph* 32, 195–208 (2002). <https://doi.org/10.1023/A:1016514305984>
- Neish, C.D., Lorenz, R.D., O'Brien, D.P., and the Cassini RADAR Team, 2006. The potential for prebiotic chemistry in the possible cryovolcanic dome Ganesa Macula on Titan. *Int J Astrobiol* 5, 57–65.
- Neish, C.D., Somogyi, A., et al., 2008. Rate measurements of the hydrolysis of complex organic macromolecules in cold aqueous solutions: Implications for prebiotic chemistry on the early Earth and Titan. *Astrobiology* 8 (2), 273–287.
- Neish, C.D., Somogyi, A., and Smith, M.A., 2009. Low temperature hydrolysis of laboratory tholins in ammonia-water solutions: implications for prebiotic chemistry on Titan. *Icarus* 201, 412–421.
- Neish, C.D., Somogyi, A., and Smith, M.A., 2010. Titan's primordial soup: formation of amino acids via low-temperature hydrolysis of tholins. *Astrobiology* 10, 337–347.
- Neish, C.D., Kirk, R.L., Lorenz, R.D., Bray, V.J., Schenk, P., Stiles, B.W., et al., 2013. Crater topography on Titan: implications for landscape evolution. *Icarus* 223, 82–90.
- Neish, C.D., Molaro, J.L., Lora, J.M., Howard, A.D., Kirk, R.L., Schenk, P., Bray, V.J., Lorenz, R.D., 2016. Fluvial erosion as a mechanism for crater modification on Titan. *Icarus* 270, 114–129. <https://doi.org/10.1016/j.icarus.2015.07.022>
- Neish, C.D., Lorenz, R.D., Turtle, E.P., Barnes, J.W., Trainer, M.G., Stiles, B., et al., 2018. Strategies for detecting biological molecules on Titan. *Astrobiology* 18, 571-585.

- O'Brien, D.P., Lorenz, R.D., and Lunine, J.I. (2005) Numerical calculations of the longevity of impact oases on Titan. *Icarus* 173:243–253.
- Osinski, G.R., Tornabene, L.L., and Grieve, R.A. 2011. Impact ejecta emplacement on terrestrial planets. *Earth and Planetary Science Letters*, 310, 167-181.
- Park, H., Jung, Y.M., You, J.K., Hong, W.H. and Kim, J.N., 2008. Analysis of the CO₂ and NH₃ reaction in an aqueous solution by 2D IR COS: Formation of bicarbonate and carbamate. *The Journal of Physical Chemistry A*, 112(29), pp.6558-6562.
- Ruiz-Bermejo, M.; de la Fuente, J.L.; Pérez-Fernández, C.; Mateo-Martí, E. A Comprehensive Review of HCN-Derived Polymers. *Processes* 2021, 9, 597. <https://doi.org/10.3390/pr9040597>
- Rumble, J.R. (2020). *CRC Handbook of Chemistry and Physics*, 101st Edition (Internet Version 2020). Taylor Francis Group: Boca Raton, FL.
- Sagan, C., and Khare, B.N., 1979. Tholins—Organic chemistry of interstellar grains and gas, *Nature* 277, 102–107, doi:10.1038/277102a0.
- Sagan, C., and Thompson, W.R., 1984. Production and condensation of organic gases in the atmosphere of Titan, *Icarus*, 59, 133–161, doi:10.1016/0019-1035(84)90018-6.
- Schmidt, B.E., Blankenship, D.D., Patterson, G.W. and Schenk, P.M., 2011. Active formation of ‘chaos terrain’ over shallow subsurface water on Europa. *Nature*, 479(7374), pp.502-505.
- Soderblom, J.M., Brown, R.H., Soderblom, L.A., Barnes, J.W., Jaumann, R., Mouélic, S.L., Sotin, C., Stephan, K., Baines, K.H., Buratti, B.J., 2010. Geology of the Selk crater region on Titan from Cassini VIMS observations. *Icarus* 208, 905–912. <https://doi.org/10.1016/j.icarus.2010.03.001>
- Soukup, G.A., 2001. *Nucleic acids: General properties*. e LS.

- Steeffel, C., DePaolo, D., Lichtner, P., 2005. Reactive transport modeling: An essential tool and a new research approach for the Earth sciences. *Earth and Planetary Science Letters* 240, 539-558.
- Thompson, W.R. and Sagan, C. (1992). Organic chemistry on Titan: surface interactions. In: *Proceedings of the Symposium on Titan, 9–12 September 1991, Toulouse, France. ESA SP-338*, pp. 167–176.
- Tobie, G., Lunine, J.I. and Sotin, C., 2006. Episodic outgassing as the origin of atmospheric methane on Titan. *Nature*, 440(7080), pp.61-64.
- Tomasko, M.G., Archinal, B., Becker, T., Bézard, B., Bushroee, M., Combes, M., Cook, D., Coustenis, A., De Bergh, C., Dafoe, L.E. and Doose, L., 2005. Rain, winds and haze during the Huygens probe's descent to Titan's surface. *Nature*, 438(7069), pp.765-778.
- Trainer, M.G., Pavlov, A.A., DeWitt, H.L., Jimenez, J.L., McKay, C.P., Toon, O.B., and Tolbert, M.A., 2006. Organic haze on Titan and the early Earth. *Proceedings of the National Academy of Sciences* 103(48), 18035-18042.
- Vuitton, V., O. Dutuit, M. A. Smith, and N. Balucani, 2014. Chemistry of Titan's Atmosphere, in *Titan*, edited by I. Müller-Wodarg et al., Cambridge Univ. Press, Cambridge, U. K., 224– 271.
- Wald, G., 1954. The Origin of Life. *Scientific American* 191, 44-53.
- Weissenberger, J., Dieckmann, G., Gradinger, R. and Spindler, M., 1992. Sea ice: a cast technique to examine and analyze brine pockets and channel structure. *Limnology and Oceanography*, 37(1), pp.179-183.
- Worster, M.G., 1992. The dynamics of mushy layers. In *Interactive dynamics of convection and solidification* (pp. 113-138). Springer, Dordrecht.
- Worster, M.G., 1997. Convection in mushy layers. *Annual Review of Fluid Mechanics* 29, 91-122.

Chapter 4

4 Impact Crater Degradation on Pluto

4.1 Introduction

In 2015, the New Horizons spacecraft showed that Pluto exhibits a wide array of landscapes of differing ages. Some regions are as old as the planet itself, while others appear as young as 500 kyr (i.e., Sputnik Planitia, McKinnon et al., 2016; Moore et al., 2016; Buhler and Ingersoll, 2017). Much of the surface modification on Pluto comes from the evolution of volatile ice through sublimation, deposition, and relaxation (Stern et al., 2015a; Moore et al., 2017; Bertrand et al., 2018, 2019; Moore and Howard, 2021; Young et al., 2021). The three dominant volatiles are carbon monoxide (CO), methane (CH₄), and nitrogen (N₂) (Grundy et al., 2016; Cruikshank et al., 2021). Of these, nitrogen is the most volatile, being the least stable at Pluto conditions (Stern et al., 2015a; Bertrand et al., 2018, 2019; Umurhan et al., 2021; Young et al., 2021). CO is similarly volatile, but far less abundant on Pluto (Umurhan et al., 2021; Young et al., 2021). The CH₄ cycle is not well understood on Pluto, but it is generally more stable than N₂ (Umurhan et al., 2021; Young et al., 2021). Pluto's orbit creates large changes in its climate, which drives the cycling (i.e., sublimation and deposition) of its volatile ices (Bertrand et al., 2018; Moore and Howard, 2021; Young et al., 2021). This drives much of the landscape evolution on its surface (Moore and Howard, 2021; Young et al., 2021), resulting in a planetary body with a varied and unique geologic history (White et al., 2021).

New Horizons imaged ~78% of Pluto's surface at varying resolutions. The side of Pluto facing the sun during the closest approach was dubbed Pluto's nearside, imaged at scales ranging from 76 to 850 m/pixel; it also imaged 25% of the farside at 2.2 – 31 km/pixel (Weaver et al., 2008; Stern et al., 2015; Stern et al., 2021). A stereophotogrammetric DEM was created using the images of the nearside, with vertical precision from 100 – 800 m, allowing for more detailed analysis of Pluto's surface processes (Schenk et al., 2018). Volatiles significantly affect the state of the surface (Bertrand and Forget, 2016; Binzel et al., 2017; Forget et al., 2017; Bertrand et al., 2018, 2019; Lewis et al., 2021), creating stark differences between the very young, volatile-rich

regions (e.g., Sputnik Planitia) and the very old, volatile-poor regions (e.g., Cthulhu Macula) (Singer et al., 2021; White et al., 2021). Thus, by understanding Pluto’s surface history, we can better constrain its volatile history and vice versa. Attempts to understand Pluto’s surface history have thus far been made by studying the surface geology at large (Moore et al., 2015, 2016; Stern et al., 2015; White et al., 2021) and the age of the surface through impact cratering (Robbins et al., 2017, 2021; Singer et al., 2019, 2021).

A detailed history of Pluto’s surface and the volatile processes that act upon it has been constructed by relating crater age dating to the geomorphology of its surface (Moore et al., 2016, 2017; Singer et al., 2019, 2021; Moore and Howard, 2021; White et al., 2021). Focused studies have used crater morphologies to understand localized processes (e.g., cryovolcanism, glaciation, haze production, etc.) (Bertrand and Forget, 2016; Howard et al., 2017a, 2017b; Grundy et al., 2018; Schenk et al., 2018; Ahrens and Chevrier, 2021; Moore and Howard, 2021; White et al., 2021; Earle et al., 2022), and multiple works have looked at Pluto’s crater population as a whole (Robbins et al., 2017, 2021; Singer et al., 2019, 2021), even creating depth to diameter fits for visually best-preserved craters (Robbins et al., 2021). However, a global analysis of the morphology of Pluto’s more degraded craters has yet to be completed. A large-scale crater morphology analysis can provide quantitative, statistically significant constraints on the extent of surface modification across Pluto. In this work, we present the results of a global analysis of Pluto’s crater morphologies to constrain the amount of surface modification. We also study regional variations in crater modification, using crater relative depths ($R = 1 - d_{pristine}/d_{current}$) as a metric of crater degradation. We compare our results to the geologic groups identified by White et al. (2021). Using this approach, we seek to constrain Pluto’s geologic history and strengthen our understanding of the volatile processes that continue to modify Pluto’s surface. In the subsequent sections, we review Pluto’s geologic history and the types of crater modification that were predicted to exist on Pluto (i.e., Stern et al., 2015). Note that our study is limited to the nearside (and the entirety of the north pole), where the highest resolution imaging and topographic data are available. We present the type of crater morphologies that could have formed on Pluto and use these to quantify the effect of the volatile processes on its surface. In doing so, we improve our understanding the degradation of Pluto’s surface.

4.1.1 Geologic History

Sputnik Planitia has been identified as the youngest terrain on Pluto and shows no confirmed impact craters (**Figure 4.1**). It is filled with a layer of solid N₂ and CO that is thick enough to induce convection in the volatile ice deposit (Schenk et al., 2018; McKinnon et al., 2016). Convection and sublimation lead to a resurfacing age of less than 500 ky, explaining the lack of craters in the region (McKinnon et al., 2016; Robbins et al., 2017, 2021; Singer et al., 2019, 2021). South of Sputnik Planitia lies another young surface, the Wright group (Singer et al., 2021). Its observed topography and surface roughness suggest that erosion is not the primary cause for its youthful appearance (Moore et al., 2016; Schenk et al., 2018; White et al., 2021). Its young age is instead interpreted to be the result of Wright Mons and its surrounding regions, a suspected cryovolcanic province (Nimmo and McKinnon, 2021; White et al., 2021; Singer et al., 2022). The paucity of impact craters suggests that a cryovolcanic event(s) must have happened in the past (as young as 1 Gy) (Singer et al., 2021, 2022). North of Sputnik Planitia, the surface shows signs of glaciation with otherwise minor modification (Bertrand and Forget, 2016; Moore et al., 2016; Howard et al., 2017a; White et al., 2019). It likely dates to soon after Sputnik Planitia formed, when N₂ ice is predicted to have migrated into the impact basin (Bertrand and Forget, 2016; Howard et al., 2017a; White et al., 2019).

To the east of Sputnik Planitia is the Tartarus group, which is a combination of different rough surface regions that are interpreted to be the next youngest features on Pluto (Robbins et al., 2017; Singer et al., 2019, 2021; White et al., 2021). The region is split into the Eastern Tombaugh Regio (ETR) and the bladed terrain, formally called Tartarus Dorsa (Singer et al., 2019, 2021; White et al., 2021). Craters are sparse in both terrains and are particularly hard to identify in the heavily pitted ETR, but the craters that are identified show signs of erosion. The bladed terrain is likely the younger of the two terrains at about 200 – 300 My old. ETR may be several hundred million years old up to a 2 Gy old.

North of the Tartarus group lies the Hayabusa group. The most characteristic feature of this region is its rounded topography and flat floored craters and valleys (Howard et al., 2017b; White et al., 2021). Compositional data shows signs of volatile ices like N₂ and CH₄, which is consistent with long term mantling of CH₄ ice in the region (Grundy et

al., 2016; Howard et al., 2017b; Lewis et al., 2021). In the southeast region of the group, more jagged terrain suggests that this area may have undergone more sublimation erosion than the upper region (Howard et al., 2017b). The eastward side of the group shows more signs of smoothing, which has been suggested as evidence of alternating deposition and sublimation there (Stern et al., 2021). While it is not the oldest geologic group, the mantling of the Hayabusa group has been noted to have caused the most crater modification in the region (Singer et al., 2021; White et al., 2021). The mantle formation is interpreted to have occurred as late as Pluto's Middle Ages, with its precise age unclear (Howard et al., 2017b). Singer et al. (2019, 2021) did not produce an estimated age for the Hayabusa group, instead including it in the overall age of the northern polar region with ages that range from 0.5 – ~4 Gy old. This is consistent with the large variation in sublimation and deposition observed in this group.

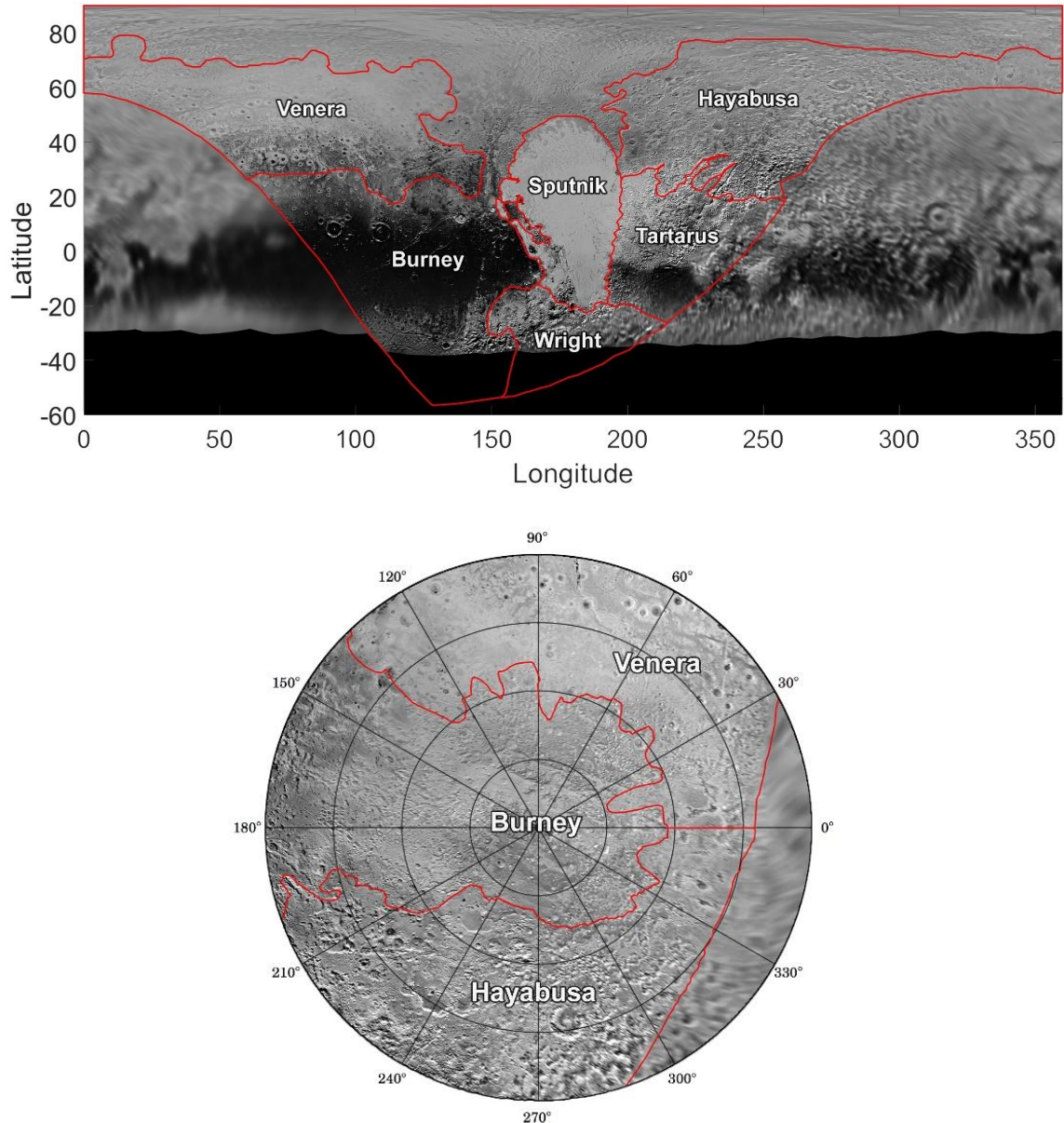


Figure 4.1. A cylindrical (top) and polar (bottom, *latitude* $\geq 50^\circ$) projection of Pluto from the “Pluto New Horizons LORRI MVIC - Global Mosaic” (300 mpp). It is overlain with red outlines of its geologic terrains as defined by White et al. (2021). Image courtesy New Horizons Team, USGS Astrogeology Science Center, https://astrogeology.usgs.gov/search/map/Pluto/NewHorizons/Pluto_NewHorizons_Global_Mosaic_300m_Jul2017

The polar uplands also show signs of modification largely dominated by erosion (Howard et al., 2017b) and appear younger than the rest of the group with fewer craters (Singer et al., 2019, 2021). There is a distinct presence of methane in the uplands (Protopapa et al., 2017; Earle et al., 2018). It has been suggested that the uplands are composed of a thick (3 km) methane mantle (Howard et al., 2017b), but this is not consistent with global volatile ice models (Binzel et al., 2017; Bertrand et al., 2019). Instead, the polar uplands should be steadily losing their methane ice (Bertrand et al., 2019). Obliquity cycling could induce periods of methane ice deposition, thickening by meters rather than kilometers (Binzel et al., 2017). Such cycling has been suggested as a means of weakening and eroding the bedrock (Moore et al., 1996, 1999; White et al., 2021). Alternatively, methane glaciation may have eroded the existing methane and water ice bedrock (Howard et al., 2017b).

The Venera group lies to the west of Sputnik Planitia, at about the same latitude as the Hayabusa group. The region's old age is reflected by its large population of craters with distinct rims and flat floors (Robbins et al., 2017; Singer et al., 2019, 2021). Venera appears less smoothed than Hayabusa, which suggests mantling is less prominent, although still present (Howard et al., 2017b; White et al., 2021). Dark regions within Venera appear to have lost most of their mantle, with water ice being detectable, but patches of the mantle remain partially preserved in the adjacent brighter regions (Grundy et al., 2016; Protopapa et al., 2017; White et al., 2021). Further west ($< 90^\circ$ longitude) in Vega Terra, bright deposits with methane signatures coat the rims of craters (Earle et al., 2022; Protopapa et al., 2017; Grundy et al., 2016). However, these are only interpreted to be a thin layer of methane ice coating the structure, rather than a thick mantle (Earle et al., 2022). Further north ($> 45^\circ$ latitude) in Venera Terra, a layer of nitrogen is detected, but shows little evidence for mantling (e.g., there is no observed ponding) (Grundy et al., 2016; Protopapa et al., 2017; Earle et al., 2022). South of Venera Terra, Piri Plinitia has a paucity of impact craters, and this has been interpreted to be evidence of significant erosion, removing the craters that had formed within the once overlying mantle layer (Singer et al., 2019, 2021). The primary composition of the Venera group mantle is thought to be methane (Grundy et al., 2016; Protopapa et al., 2017; Cruikshank et al., 2021), but it is suggested that stronger water ice is mixed into it as methane alone is too weak support the features observed in the

region (Moore et al., 2017; White et al., 2021). Overall, Venera is considered one of the oldest terrains on Pluto, estimated to be 3.5 to 4.5 Gy old. The mantle is estimated to have formed after the bedrock ice of the Burney group (Singer et al., 2019, 2021).

The Burney group dates to Pluto's earliest period, during its high impact era more than ~4 Gy ago (White et al., 2021). The Burney group contains the largest impact basin to form after the impact that created Sputnik Planitia, named the Burney Basin (Schenk et al., 2018; Singer et al., 2021).

The southern portion of the Burney group, which extends down into Cthulhu Macula (Moore et al., 2016; White et al., 2021), shows few signs of modification (Schenk et al., 2018; Singer et al., 2019; White et al., 2021). It is thought to be the oldest terrain in Pluto's nearside and one of the most heavily cratered (Singer et al., 2019, 2021; Robbins et al., 2017, 2021). In fact, no regional-scale deposition seems to have occurred across the Burney group, leaving Pluto's water ice crust exposed (Howard et al., 2017b; White et al., 2021). Cthulhu Macula has a uniquely low albedo due to a surface covering of precipitated haze particles and lack of volatile ices (Grundy et al., 2018; Cruikshank et al., 2021; Earle et al., 2022). The haze deposit overlaying the water ice crust is estimated to be up to 14 m thick and composed of molecules of prebiotic interest (i.e., tholins, Sagan and Khare, 1979; Grundy et al., 2018; Cruikshank et al., 2019a; Johnson et al., 2021). Apart from the modest haze particle deposition, crater morphologies within Cthulhu Macula appear relatively well-preserved. With its limited surface modification, craters within Cthulhu Macula are a prime astrobiological target, similar to those being targeted by the Dragonfly mission to Titan (Lorenz et al., 2018, 2021). There, tholins may mix with impact melt deposits to produce biological molecules like amino acids (Neish et al., 2010, 2018; Hedgepeth et al., 2021).

4.1.2 Crater Modification

Pluto's craters are degraded by a range of processes, some observed even on terrestrial planets, such as sublimation of volatile ices (Moore et al., 1996, 1999; Stern et al., 2015; Howard et al., 2017b; Moore and Howard, 2021; Singer et al., 2022), and some common on other icy worlds, such as viscous relaxation (Parmentier and Head, 1981; Dombard and McKinnon, 2006; Stern et al., 2015; Schurmeier and Dombard, 2017).

Viscous relaxation is the slow creep of ice driven by gravity to an equilibrium state (Parmentier and Head, 1981). This process isn't observed on rocky bodies because the viscosity of the rock is too high, and on some icy satellites, the extremely low temperatures significantly slow the rate of relaxation. For example, relaxation is very slow on Titan's cold surface (94 K), but sand deposition can provide added insulation and moderately enhance the process (Schurmeier and Dombard, 2018). Even then, the timescales are too long to compete with the much faster fluvial and depositional processes observed there (Neish et al., 2013, 2016; Hedgepeth, et al., 2020). Similarly, Pluto is probably too cold (< 50 K, Earle et al., 2017) for water ice to relax on the timescale of the solar system (Kamata and Nimmo, 2014; Nimmo and McKinnon et al., 2021). Nonetheless, there is evidence of potential relaxation on Pluto (McKinnon et al., 2018), even though other craters of similar size have not relaxed (Nimmo and McKinnon et al., 2021). Nitrogen ice is known to act as an insulator in some parts of Pluto (e.g., Sputnik Planitia, McKinnon et al., 2016), so there may be instances where a water ice crater could relax if insulated by sufficient volatiles. Viscous relaxation of craters may also play a significant role in craters that form in thick mantles of volatile ices on Pluto (i.e., CH_4 and N_2), which relax on much shorter timescales than water ice (Stern et al., 2015; Howard et al., 2017b; Moore and Howard, 2021).

Stern et al. (2015) studied the role of escape erosion (i.e., sublimation) and relaxation of craters on Pluto in N_2 and CH_4 ices. Theoretically, a crater on Pluto formed in N_2 ice would relax on very fast timescales (< 1 My, at $T \geq 40$ K). Even at very cold temperatures (~ 35 K), the smallest craters formed in N_2 ice would relax in less than a billion years. Thus, it is very likely that most craters formed in a mantle of N_2 ice would be completely relaxed by the time of New Horizon's flyby (i.e., ~ 4.5 Gy post formation). However, relaxation is a large wavelength process, so smaller wavelength features like rims would theoretically be retained (Parmentier and Head, 1981), unless later erosion erases these features (Stern et al., 2015; Moore et al., 2017; Bertrand et al., 2018, 2019). In contrast, CH_4 ice is more viscous, with relaxation times on the order of the age of the solar system at 40 K and < 1 Gy at 45 K (Yamashita et al., 2010; Stern et al., 2015). At more extreme conditions (i.e., 35 K), relaxation is longer than the age of the solar system (Stern et al., 2015), but estimates of Pluto's surface temperatures suggest temperatures will stay

above 40 K even with the variations that occur in Pluto's orbit (Earle et al., 2017). Therefore, craters that formed in CH₄ ice may be preserved on Pluto but likely with significant signs of ongoing degradation via relaxation. Erosion by sublimation may speed up this process (Stern et al., 2015; Moore et al., 2017; Bertrand et al., 2018, 2019; Moore and Howard, 2021), but CH₄ is generally less volatile than N₂ on Pluto (Umurhan et al., 2021). The range of geologic landscapes across Pluto suggests that these volatile processes might occur to varying degrees depending on the abundance of volatile ice, which may be reflected in the regional crater morphologies. What's more, the crater morphologies may preserve evidence of past volatile ice distributions; for example, Pluto's conditions are suspected to have changed significantly after the Sputnik impact, possibly even undergoing polar wander (Rubincam, 2003; Keane and Matsuyama, 2016; McGovern et al., 2020). To appreciate the types of crater morphologies that should exist on Pluto, we must consider how craters would form in different environmental conditions (**Figure 4.2**).

One major factor that will affect how a crater evolves over time is the composition and depth of the ices at an impact site. Complex craters ($D > 13 \text{ km}$) on Pluto reach depths of 1-4 km (Robbins et al., 2021). If a crater forms in a water ice target prior to volatile ice mantle formation (i.e., CH₄ and/or N₂), all crater modification would likely be by depositional erasure alone, unless insulation exacerbates viscous relaxation (Forsberg-Taylor and Howard, 2004; Howard et al., 2017b; Moore and Howard, 2021). Cyclical deposition and escape erosion may further erode the crater (Moore et al., 1996, 1999; Stern et al., 2015). Predicting the morphology of craters that form after mantle formation is more complicated (**Figure 4.2**). Craters that form in a sufficiently thick volatile ice layer (i.e., $h > \text{depth}$) are assumed to form with a heterogeneous composition and a crater shape that is defined by the volatile ice properties of the top layer rather than water ice bedrock (Melosh, 1989; Bray et al., 2008; Senft and Stewart, 2008; Umurhan et al., 2021). To constrain the morphology of craters that form into a thin mantle over water ice bedrock (i.e., $h < d$, where h is volatile ice thickness and d is crater depth), we consider two potential analogues: sedimentary rock layers and rock-ice layers on Earth and Mars. First, impact craters that form into stratified rock on Earth do not exhibit significant morphological differences from impacts that form into heterogeneous bedrock because the material properties do not differ significantly (e.g., Barringer crater, Shoemaker and

Kieffer, 1974; Kring, 2007; Collins et al., 2008; Kenkmann et al., 2014). Stratified layers react uniformly as material is excavated and folded back to form the rim and ejecta blanket (Melosh, 1989; Senft and Stewart, 2007; Collins et al., 2008; Osinski and Pierazzo, 2012; Silber et al., 2021). In contrast, work on crater formation into ice layers on Mars do not follow the same template because the material properties (specifically, the pressure melting point of ice and rock) differ significantly (Pierazzo et al., 1997; Senft and Stewart, 2008; Silber et al., 2021). Modeling by suggests that the ejected basalt bedrock overlays the water ice layer to form the rim when the ice layer is thin (i.e., $h \sim \leq 0.5 * depth$). Thicker ice layers (i.e., $h \sim > 0.5 * depth$) eject and form the entire rim, but the weak ice flows back into the basin, covering the crater, completely shielding any evidence that it formed similar to marine impacts on Earth or Titan (e.g., Neish et al., 2014; Bray et al., 2022). We expect craters formed in ice-rock layers on Earth and Mars are likely the best analogue for crater formation into significantly layered volatile-water ice on Pluto (Bray et al., 2008; Senft and Stewart, 2008; Silber et al., 2021; Umurhan et al., 2021). More work is needed to fully understand the morphology of complex craters formed in layers of two or more different ices. However, until more work is done, we present these two crater structures as end points for the type of crater morphologies that may form when an impactor strikes layered ices on Pluto (Eluszkiewicz and Stevenson, 1990; Schenk and Zahnle, 2007; Schenk et al., 2021).

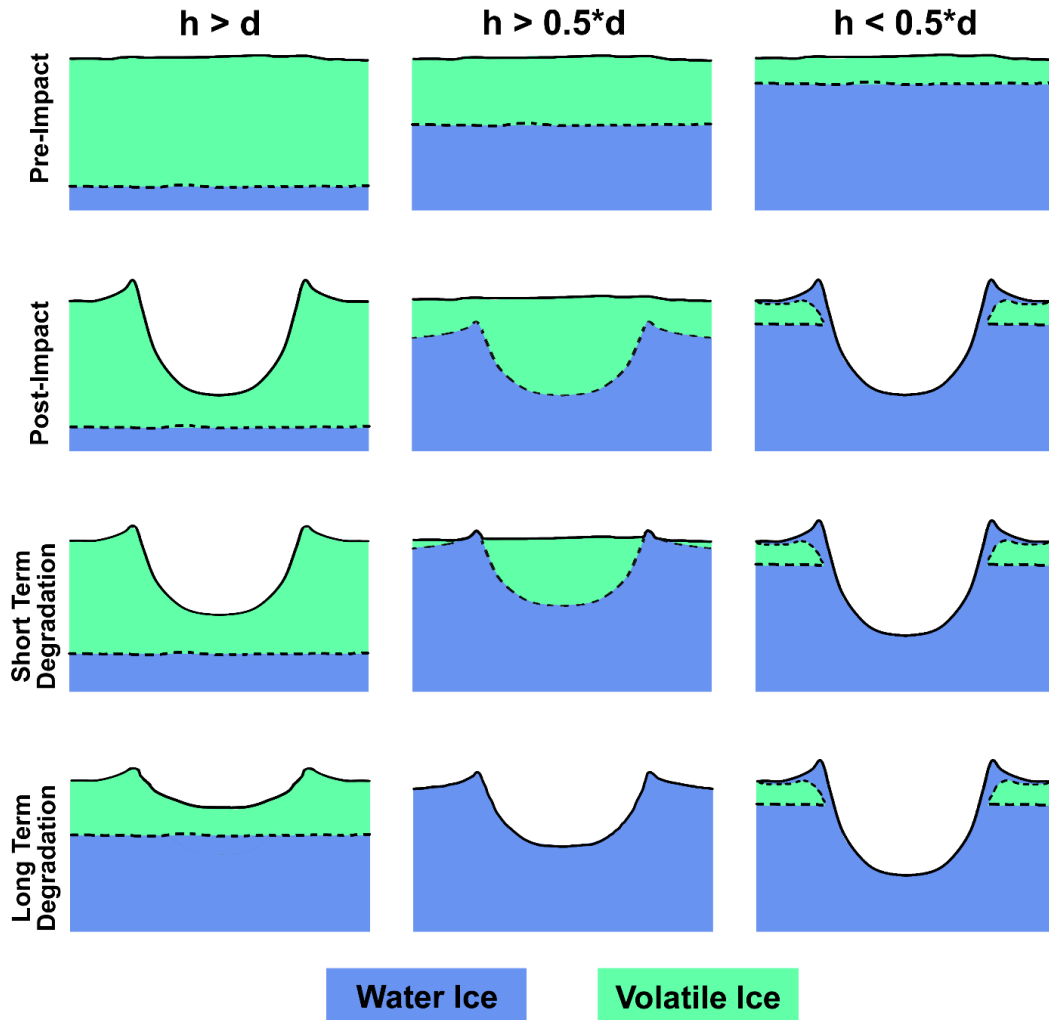


Figure 4.2. Expected crater morphologies proposed for layered ice on Pluto, assuming different volatile ice layer thicknesses. The immediate post-impact morphologies are compared to the surface before impact and after short- and long-term degradation by escape erosion and relaxation. Note that “short” and “long” are relative terms, which vary based on the volatile ice (e.g., the long-term relaxation stage of N_2 will occur much faster than CH_4 ; Stern et al., 2015). Craters that form in a sufficiently thick volatile ice layer (i.e., $h > d$, where h is volatile ice thickness and d is crater depth) are assumed to form a traditional crater shape. Craters that form in thinner volatile ice layers are assumed to act like craters forming in water ice overlaying the much stronger basalt bedrock on Mars (see text for more details; Senft and Stewart, 2008). Escape erosion may degrade every crater, but it will most significantly affect craters that form into thicker volatile ice layers ($h > 0.5 * d$). For a moderate volatile thickness ($d > h > 0.5 * d$), the weaker volatile ice is expected to flow back and cover the more rigid water ice basin. Escape erosion would eventually reveal a shallower than normal water ice crater. For very thick volatile layers ($h > d$), escape erosion will act in conjunction with relaxation to degrade the crater.

Understanding the modification of a crater is most straightforward if it forms within a mantle composed of only one type of ice that is greater than or equal to the crater depth (**Figure 4.2 - left column**). However, mantle ices may not be pure (Stranberry et al., 1996; Protopapa et al., 2017; Cuikshank et al., 2021), and the strength of the layer may be altered by impurities in the ice (Pierazzo et al., 1997; Senft and Stewart, 2011). Water ice craters are unlikely to be modified in the same way as the more volatile ices because of its strength at Pluto temperatures (Stern et al., 2015; Umurhan et al., 2021), but water ice craters may still undergo degradation through other means (Moore et al., 1996, 1999; Howard et al., 2017a, 2017b). For example, observations suggest N₂ ice glaciation in the high latitudes may have eroded water ice craters there (Howard et al., 2017a). The cyclical deposition and sublimation of volatile ices may also weaken water ice (Moore et al., 1996, 1999). Therefore, degraded craters on Pluto may form in one of three ways: (1) they may be the remnants of a crater formed in a moderately thick mantle of volatile ice, which has since relaxed and/or undergone sublimation, (2) craters that formed into a moderately thick mantle of volatile ice may have formed anomalously shallow as can happen in marine impacts on Earth (Bray et al., 2022), or (3) water ice craters that have been modified by external degradation. This latter scenario is possible, but the terrains where these processes have been proposed are rare. Therefore, it is unlikely to affect most water ice craters on Pluto.

4.2 Methodology

4.2.1 Crater Mapping

We constructed two maps of Pluto using data from the LORRI instrument on New Horizons and the associated digital elevation model (DEM): a cylindrical projection of the equatorial region ($\sim 40^{\circ}\text{S}$ to 50°N) and a northern polar projection ($\geq 50^{\circ}\text{N}$) (**Figure 4.1**) (Schenk et al., 2018; Stern, 2018). We mapped all complex craters (> 15 km in diameter, slightly above the 13 km estimate to avoid transitional craters) on the nearside of Pluto (and north pole), where topographic data is available (**Figure 4.3**) (Schenk et al., 2018). Craters at $\geq 50^{\circ}\text{N}$ latitude were mapped in a polar projection centered at 90° latitude and 0° longitude, and all other craters were mapped in the cylindrical projection. Craters, preserved and degraded, were identified using key characteristics such as their circular

shape, elevated rims (both visibly and topographically), ejecta material, central peaks and pits, and topographic depression (**Figure 4.3**) (Bierhaus and Dones, 2015; Robbins et al., 2014, 2017; Singer et al., 2019). The mapping was mirrored after the techniques described in Robbins et al. (2017; 2021), but our topographic analysis did not segregate craters by how pristine they are (**Figure 4.3**).

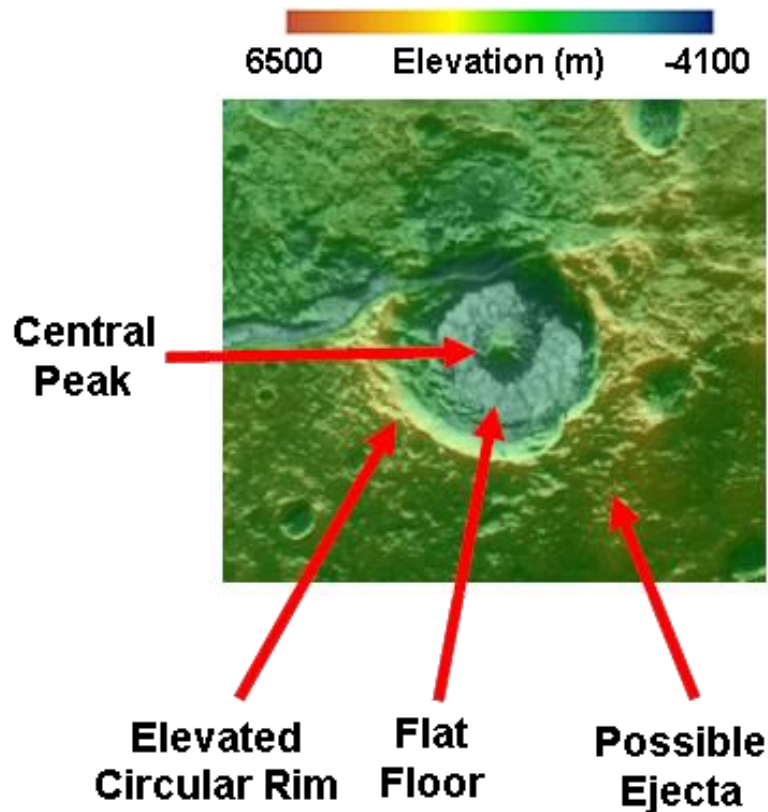


Figure 4.3. An example impact crater shown in the LORRI mosaic of Pluto overlaid with the DEM. The craters were identified by their circular shape, elevated rims, central peaks, flat floor, and ejecta (if present).

4.2.2 Crater Morphology

Approximately 300 crater depths were measured using the 8-profile technique (**Figure 4.4**) (Robbins et al., 2018). The 8-profile technique takes 8 topographic profiles through the center of the crater, each equally spaced, up to 5 radii from the crater center (Bray et al., 2012; Hedgepeth et al., 2020). After removing any regional slope, we find the maximum rim and minimum floor positions on each side of center, confirming that a superimposed impact crater is not leading to an anomalously low minimum value, and

compute the difference between the two points to find the crater depth. The depths are then averaged across all 16 radial measurements to arrive at a mean value. The relative depth ($R(D) = 1 - \frac{d_{pluto}(D)}{d_{pristine}(D)}$) of each crater is then found using the predicted depths ($d_{pristine}$) of a well-preserved crater, based on depths derived by Robbins et al. (2021). Robbins et al. (2021) identified morphologically pristine craters across Pluto and used them to determine the depth to diameter relationship of craters. Robbins et al. (2021) used several approaches for fitting the data, but we used the weighted mean fit because it achieved the lowest error. Note that Robbins et al. (2021) measured their depths using a statistical approach that utilized the topography of the entire crater, not just eight profiles (Robbins et al, 2018), and the different approach may give different measurements for depth. However, past studies have shown that the variation between this statistical approach and the 8-profile technique is minor (Hedgepeth et al., 2020), so it is unlikely to be a major source of error.

A larger concern for error exists within the DEM itself (Schenk et al., 2018). Schenk et al. (2018) used the high-resolution observations of the nearside to construct a topographic map via stereogrammetric analysis, but there is still a large degree of vertical uncertainty. Vertical uncertainty in the DEM's height measurements range from 100 to 800 m (Schenk et al., 2018), which is nonnegligible compared to the well-preserved crater depths (i.e., 3 to 4 km, Robbins et al., 2021). Furthermore, error propagation in depth calculations can lead to significant error in the final value. This is especially true for the most degraded craters, where the actual depth measurements are similar to or smaller than the actual error. This error is unavoidable, but it is generally systematic (Schenk et al., 2018, Cook et al., 1996). In other words, the absolute topography in a region may exhibit error, but the local differences in crater topography are likely more reliable. Therefore, the derived depth measurements (which are measured as differences in topography) are likely to be representative of the level of degradation within the geologic regions studied.

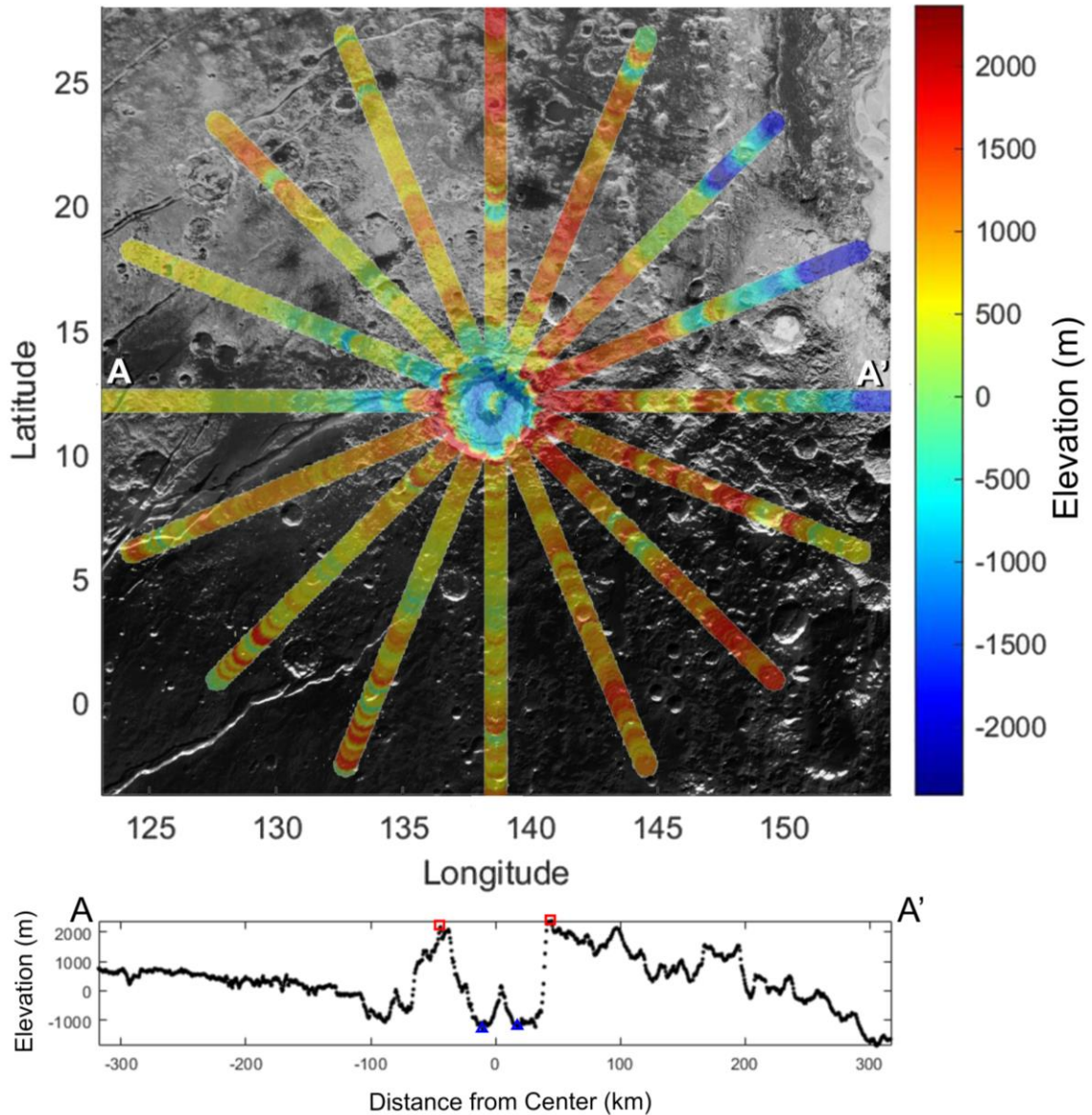


Figure 4.4. Crater topography is mapped using the 8-profile technique (top). An example topographic plot of profile A-A', where the x axis is distance from the crater center (bottom). The red square identifies the rim, and the blue triangle indicates the crater floor.

4.3 Results

Here we present the relative depths of Pluto's impact craters and use them as a metric of surface modification in different geologic regions. We focus on the different geologic groups identified by White et al. (2021) (**Table 4.1**), providing equatorial (**Figure**

4.5) and north polar maps (**Figure 4.6**) of crater relative depths in Pluto's nearside. We can make several broad conclusions from these maps. First, there appears to be a relationship between relative depth and longitude. On Pluto's westernmost limb is a population of very degraded craters ($R \cong 1.0$). As we move eastward, we transition to craters that are only lightly to moderately degraded ($R \cong 0.4$). Continuing to the southeast, craters show only a small amount of degradation ($R \cong 0.2$), with a patch of nearly pristine craters ($R \cong 0.0$) southwest of Sputnik Planitia.

These patterns do not match up exactly with the geologic groups defined by White et al., (2021) but do strongly correlate with them (**Table 4.1**). The most degraded region of craters exists within the Venera group, the second oldest group on Pluto after the Burney group. As a result, the Venera group has the highest average relative depth of any group on Pluto ($R_{avg} = 0.595$), with only moderate variance ($R_{std} = 0.264$), and a max relative depth indicative of complete degradation ($R_{max} = 1.110$). Cthulhu Macula (within the Burney group) is thought to be the oldest terrain on Pluto, but it has a lower average relative depth compared to the Venera group ($R_{avg} = 0.286$). Still, its average relative depth is the second largest on Pluto, and it is the reason the Burney Group's overall average is similarly high ($R_{avg} = 0.275$). Cthulhu Macula exhibits the highest level of variance of any group ($R_{std} = 0.313$), with contrasting regions of very degraded craters ($R \cong 1.0$) and regions of anomalously deep craters ($R < 0.0$, **Figure 4.7**). Interestingly, this region of especially deep craters extends into the Wright group, which is the youngest group on Pluto and has the lowest average relative depth ($R_{avg} = 0.110$). It is not without degraded craters ($R_{max} = 0.577$), however, and its apparent pristine nature may be due to the anomalously deep craters within it (as illustrated by the high variance in the group, $R_{std} = 0.269$).

The other geologic groups show minimal degradation, including the polar region of the Burney Group. Despite being one of the oldest terrains, the north polar region has a comparatively low average relative depth ($R_{avg} = 0.229$) with the lowest amount of variance ($R_{std} = 0.200$). The younger Hayabusa and Tartarus groups show a similar level of degradation ($R_{avg} = 0.188$ and $R_{avg} = 0.197$, respectively) with only slightly more variance ($R_{std} = 0.236$ and $R_{std} = 0.239$, respectively).

Table 4.1. Relative depth statistics by geologic group, ranked by estimated surface age (oldest to youngest). N is the number of craters in that group, R is the relative depth, avg is the average, std is the standard deviation measured using the ‘std’ function in MATLAB, and max is the maximum.

Geologic Regions	N	R_{avg}	R_{std}	R_{max}
<i>Burney Group</i>	218	0.275	0.296	1.034
Cthulhu Macula*	177	0.286	0.313	1.034
North Pole*	41	0.229	0.200	0.640
<i>Venera Group</i>	111	0.595	0.264	1.110
<i>Hayabusa Group</i>	45	0.188	0.236	0.729
<i>Tartarus Group</i>	5	0.197	0.239	0.465
<i>Wright Group</i>	8	0.110	0.269	0.577

*Burney Group is split into the northern region ($\geq 30^\circ$ *Latitude*) and Cthulhu Macula ($< 30^\circ$ *Latitude*).

There is inherent uncertainty in our approach that stems from the vertical error in the original height measurements of Schenk et al. (2018). The associated errors of 100-800 m are smaller than the expected crater depths of craters of this size ($D \geq 15$ km, $depth > 1.5$ km), but the errors grow as we propagate them when calculating the crater relative depth. To approximate the final error, we propagate the errors in quadrature:

$$\delta d = \sqrt{\delta H_{rim}^2 + \delta H_{floor}^2} \quad \text{Equation 4.1}$$

where H is height, d is depth, and δ is error. This error is carried into the relative depth error,

$$\delta R = \sqrt{\left(\frac{\delta d_{measured}}{d_{measured}}\right)^2 + \left(\frac{\delta d_{predicted}}{d_{predicted}}\right)^2} \quad \text{Equation 4.2}$$

where R is relative depth computed using the error in measured depth and the error in the predicted depth fits from Robbins et al. (2021). For the highest vertical errors in the DEM

($\delta = 800 \text{ m}$) the relative depth error approaches $\delta R \geq 1$. Similarly, the most degraded craters (i.e., $R \cong 1$) reach the same level of error even in the regions of lowest DEM error because the measured values are so small. This is an inherent limitation in these results. However, these are also the most conservative error estimates with the vertical errors typically being systematic (Cook et al., 1996; Schenk et al., 2018), so calculating the depth measurements as differences between heights in localized regions should be more reliable. Therefore, we posit that these results are likely representative of regional geologic patterns.

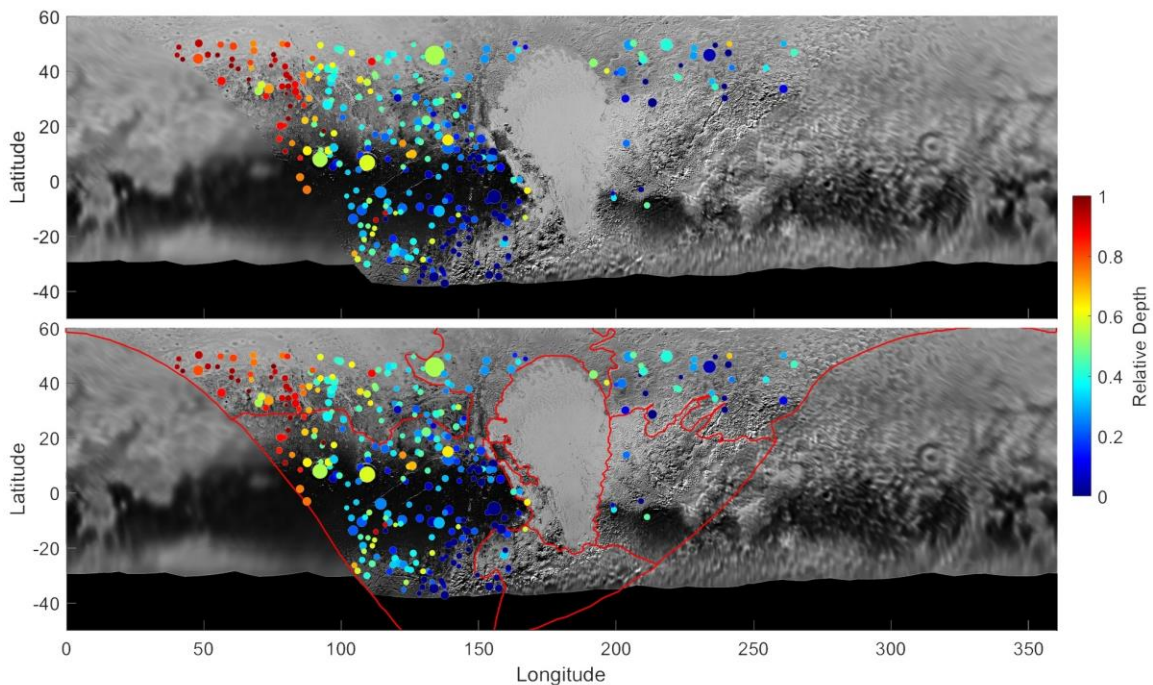


Figure 4.5. Global mosaic of Pluto's complex impact craters ($D \geq 15 \text{ km}$) near the equator ($-50^\circ < \textit{Latitude} < 50^\circ$) colorized by relative depth where redder (higher R) are the most degraded and bluer craters are the most well-preserved. The map is shown without (top) and with (bottom) the geologic group boundaries. Crater diameters are proportional to circle size but are not to scale. Note, craters with $R < 0$ are shown as 0 (see Figure 4.7 and text for details).

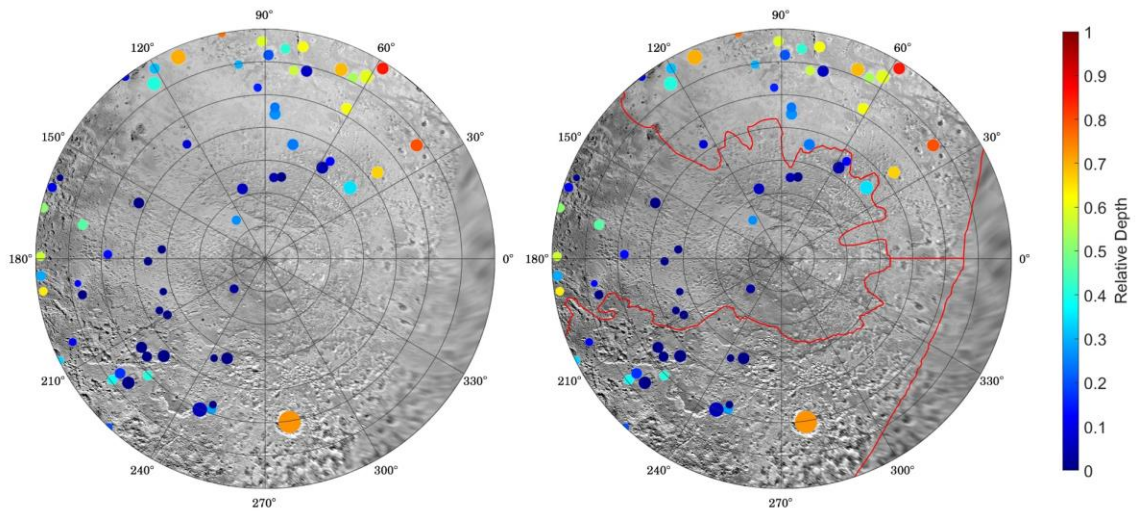


Figure 4.6. Polar map (50°N to 90°N latitude) of Pluto's north pole with impact craters ($D \geq 15$ km) mapped and colorized by relative depth. The map is shown without (left) and with (right) the geologic group boundaries. Redder (higher R) craters are the most degraded and bluer craters are the most well-preserved. Crater diameters are proportional to dot size but not to scale.

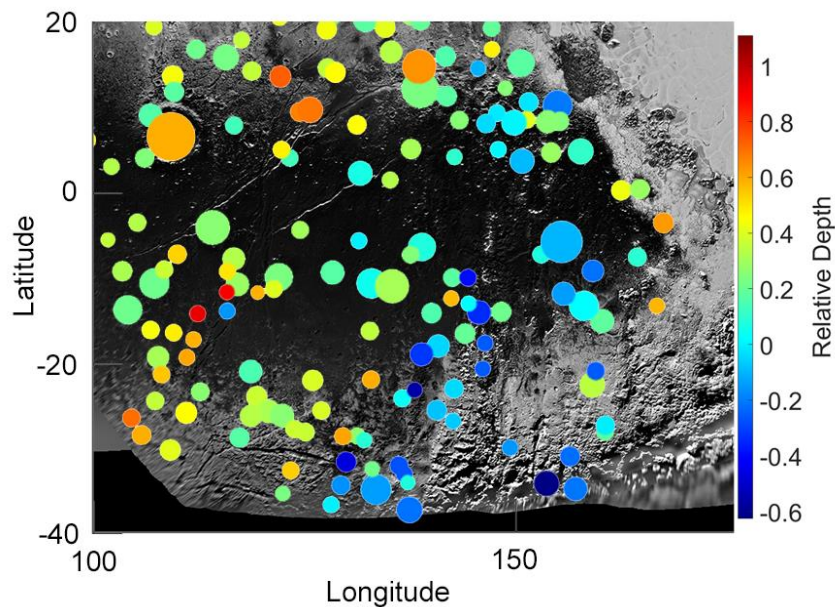


Figure 4.7. Relative depths of craters in the southeast region of Cthulhu Macula and the western region of the Wright group, with relative depths less than 0 shown to demonstrate the cluster of anomalously deep craters in this region

4.4 Discussion

Overall, the most degraded geologic groups (i.e., with the most degraded craters) are some of the oldest, but that trend does not hold true in every geologic group. This is indicative of a surface that has undergone localized degradational processes rather than a single global process. The extent of crater degradation reflects the type of processes that are acting upon the surface in each region. We considered volatile ices as the primary driver of modification, but the relationship between the volatile ices and the level of degradation is not obvious. For example, there is a distinct latitudinal variation in volatile ices, particularly methane (Grundy et al., 2016; Cruikshank et al., 2021), but this is just a thin coating rather than a thick mantle that exists (or existed) across Pluto (Earle et al., 2022). If these global distributions were thicker now, or in the past, a fraction of the crater population would show much larger levels of degradation by any combination of relaxation and erosion (Stern et al., 2015). Instead, this type of mantling is known to occur in localized regions on the surface (Howard et al., 2017b). However, there is a distinct longitudinal trend with degradation. This may be coincidental, but it may also be evidence of a very different surface in that past that has since changed significantly (e.g., by polar wander, Rubincam, 2003; Keane and Matsuyama, 2016; McGovern et al., 2020). This would also explain why degradation still exists in regions where mantling isn't hypothesized.

4.4.1 The Mantling of the Venera and Hayabusa Groups

The Venera group and the Hayabusa group represent two contrasting histories of mantling. The Hayabusa group is suggested to have a thicker mantle that may be undergoing periods of deposition and erosion (Howard et al., 2017b; Stern et al., 2021), which may have modified its craters (Singer et al., 2021; White et al., 2021). However, our results suggest the modification is minimal, with relative depths suggestive of well-preserved crater forms ($R < 0.2$) (**Table 4.1**). In fact, it appears to be among the least modified groups, comparable to younger regions such as the Tartarus group. In contrast, craters in the Venera group exhibit much more degradation, with the highest relative depths of any group ($R \sim 0.6$). This suggests the effects of mantling are much more significant here. The Venera group appears to be bifurcated into two distinct regions, one of extreme degradation and one of moderate degradation (**Figure 4.5, 4.6**). The most degraded craters

are found in Vega Terra where a thin mantle of methane is suspected (Howard et al., 2017b; Moore et al., 2017). McKinnon et al. (2021) suggested the overall degraded topography is representative of the type of topography associated with tidally heated satellites Europa and Triton, hinting that relaxation is the cause. However, it seems unlikely to be a direct example of crater relaxation because the most degraded craters are the smallest, and relaxation occurs more quickly on larger depressions (Parmentier and Head, 1981). That would suggest the craters didn't form in a thick ($h > d$) volatile ice mantle where relaxation would be a dominant form of degradation.

Alternatively, this may be a unique scenario where the thickness of the mantle was thicker than the depth of the smaller craters but thinner than the depth of the larger craters (**Figure 4.2**). In this scenario, smaller craters would relax (left panel in **Figure 4.2**) while larger craters would penetrate deeper into the bedrock ice (right panel in **Figure 4.2**). This would require escape erosion, theoretically, for the water ice basin to become exposed because the moderately thick volatile ice mantle would shield the water ice basin, but the lack of rims across the region suggests something more is at play because rims should be the last feature to decay in both relaxation and escape erosion (Parmentier and Head, 1981; Howard et al., 2012; Moore et al., 2017). It is possible that a particular depth of mantle deposit has impeded rim and ejecta deposition in these regions in the geologic past, similar to marine craters on Earth (e.g., Bray et al., 2022). Ultimately, the combination of these processes complicates attempts to understand the evolution of the craters in this region. Relaxation will degrade larger craters more quickly than smaller craters (Parmentier and Head, 1981), but sublimation seems to degrade smaller craters more quickly than larger craters (Howard et al., 2012). This is further complicated by the possibility that the ices may not be pure water ice or methane ice (Cruikshank et al., 2021; Umurhan et al., 2021). Nevertheless, it is likely that some combination of escape erosion and relaxation is at play in the Venera group, in addition to consideration that various crater morphologies will be created by impact into mantles of different thickness. Ultimately, more work is needed to understand crater degradation within multiple layers of ice.

4.4.2 The Degraded Craters of Cthulhu Macula

The complexity of crater degradation on Pluto is further demonstrated within Cthulhu Macula (the Burney group at *latitude* $< 30^\circ$). Here, very little mantling is suspected but moderate degradation has occurred in what is likely Pluto's oldest terrain (Howard et al., 2017b; Singer et al., 2019, 2021). Like the Venera group, Cthulhu contains distinct populations of craters; to the east along the boundary of the Wright group are especially well-preserved craters while to the west are moderately degraded craters. There is some evidence of light mantling of nitrogen ice in the north of Cthulhu Macula (Howard et al., 2017b; White et al., 2021), but this cannot account for the degraded craters in the southwest of Cthulhu Macula. One possibility is that a larger deposition and sublimation event has occurred than suspected within Cthulhu Macula. This would explain why it has fewer small craters ($D < 10 \text{ km}$) than expected with those that are present exhibiting degradation (Robbins et al., 2017; Singer et al., 2019, 2021). The potential for polar wander in response to the Sputnik basin forming, could provide a means by which the western longitudes could have accumulated thicker mantling deposits in their deep history than would be expected during the current epoch. However, the buildup of the thick layer of dark tholin material suggests the surface has undergone very little change, and remained at its current latitude band, for a very long time (Protopapa et al., 2017; Grundy et al., 2018). McKinnon et al. (2021) noted the same muted topography observed within Vega Terra exists within Cthulhu Macula, suggesting relaxation as a potential degradation mechanism. While the rims are more retained in this terrain, the level of degradation is yet again higher for smaller craters. Nevertheless, if relaxation is at play, it may speak to heating in the early Pluto system, or the material properties of the ice may be different. It has been proposed that the ice in this terrain may be a mix of tholins and water ice (Cruikshank et al., 2021). This could alter the material properties of the ice in a way that would affect its relaxation rates (Umurhan et al., 2021), but the same problem has not been considered on Titan where a similar mix of organics and ice may exist (Neish et al., 2016; Hedgepeth et al., 2020). Instead, the organic sand deposits on Titan have been shown to facilitate relaxation in its craters by insulating the bedrock ice (Schurmeier and Dombard, 2018). If the degradation is driven by the presence of tholins, however, there is not an obvious correlation between the tholin layer and crater degradation, with some of these degraded craters extending down

beyond the tholin terrain. What's more, some of the anomalously deep craters near the Wright group extend into the tholin terrain as well, so the cause of the deep craters may have affected both groups.

4.4.3 The Anomalously Deep Craters of Cthulhu Macula and the Wright Group

One of the more perplexing discoveries is the existence of especially deep craters ($R < 0$) in the southeast region of Cthulhu Macula (**Figure 4.7**) (Robbins et al., 2021). Impact velocity can affect the depth of a 'pristine' crater (Silber et al., 2017), but the fact that there is a cluster of deep craters suggests it is a regional effect (e.g., material properties, Chandnani et al., 2019). Robbins et al. (2021) noted the presence of these anomalously deep craters and excluded them when developing their depth to diameter fits. They noted that these are indicative of unique target properties (e.g., increased porosity) (Chandnani et al., 2019; Robbins et al., 2021). Most of the deep craters are outside the primary dark region of Cthulhu Macula, which may suggest the effect is related to the neighbor Wright Group such as cryovolcanism (Singer et al., 2022). Alternatively, it could be related to the mountains in the region (Moore et al., 2015; Schenk et al., 2018). If this is the case, the existence of some of these deep craters within the dark tholin terrain may be evidence of more ancient events (cryovolcanic or otherwise) that altered the bedrock that has since become coated with the haze material (Grundy et al., 2018; Moore and Howard, 2021). One flaw in this hypothesis, however, is the lack of anomalously deep craters in other regions where cryovolcanism is suggested to have occurred (i.e., NW Cthulhu Macula; Cruikshank et al., 2019b, 2021). However, these craters do exhibit a pristine morphology, if not especially deep, and as such, they may be slightly modified by other means, such as further cryovolcanism. This explanation seems consistent with the crater morphologies in the Wright group.

The Wright group's low average relative depth is indicative of the anomalously deep craters ($R < 0$) within it, but amongst those craters are slightly degraded craters ($R \sim 0$). This illustrates how cryovolcanism could alter the surface properties while still actively modifying the features preceding it (Cruikshank et al., 2019b, 2021; Umurhan et al., 2021; Singer et al., 2022). However, the level of degradation is not as widespread as it

would have to be for every crater near the other cryovolcanic events to have a crater depth that is not anomalously deep. The lack of widespread degradation within the Wright group, however, likely relates its young age, the youngest among the groups we studied (Singer et al., 2019; 2021).

4.4.4 The Lightly Degraded Terrains of Pluto

The next youngest group after the Wright group, Tartarus, exhibits slightly more degradation to match its slightly older surface. However, the same correlation between age and degradation does not exist within the north polar region which, despite being one of the oldest terrains, exhibits very little degradation ($R_{avg} = 0.229$) (Singer et al., 2019, 2021). In contrast, the north polar region (the Burney group at $latitude \geq 30^\circ$) exhibits about the same level of degradation as the younger Wright and Tartarus groups despite being one of the oldest surfaces. In fact, the polar uplands ($70^\circ \leq latitude \leq 90^\circ$) are the most pristine (**Figure 4.6**), highlighting that minimal degradation has occurred. In areas where degradation is observed in the polar uplands, sublimation-deposition cycling has been suggested to weaken the water ice bedrock allowing for degradation (Moore et al., 1996, 1999; White et al, 2021). However, if this was a significant form of degradation, we would expect to see more degraded craters within the region. Ultimately, the region exhibits minimal degradation. The polar uplands may be especially pristine with its average relative depth skewed by the slightly degraded craters in the middle of the Burney group (i.e., $30^\circ \leq latitude < 70^\circ$). Overall, however, the north polar region is very similar to the Tartarus group, which itself is not dissimilar to the slightly older Hayabusa group (Singer et al, 2019, 2021). If the anomalously deep craters within the Wright group were assumed to be a relative depth of 0, its average relative depth becomes like these slightly more degraded groups ($R_{avg} = 0.162$), and if removed entirely, the average degradation becomes slightly more modified than the rest ($R_{avg} = 0.259$). This suggests that degradation is independent of age, and each of these groups (i.e., Tartarus, Hayabusa, the north polar region, and maybe Wright) have experienced roughly the same level of degradation, or consequentially, minimal modification since the surfaces were last active.

4.4.5 Summary

We approached this problem under the expectation that volatile ices would drive the modification of craters on Pluto. There seem to be cases where this occurring (i.e., Venera group), but the volatile processes alone are insufficient to explain the observed degradation, since degraded craters are found in regions where there is little evidence of significant volatile ice mantling, now or in the past (i.e., Cthulhu). Furthermore, regions where significant volatile ice mantling has occurred exhibit roughly the same level of degradation as regions where volatile ice mantling has not occurred, again suggesting other forces are at play. Complicating this investigation is the potential changes to the material properties of the bedrock that may be altered by volatile ices, cryogenic flows, or organic haze material. Nevertheless, the existence of a larger longitudinal trend hints that Pluto may have undergone significant changes in its past (e.g., polar wander after the Sputnik impact, Rubincam, 2003; Keane and Matsuyama, 2016; McGovern et al., 2020).

4.5 Conclusions

In this work, we studied the degradation of impact craters across Pluto. We used relative crater depths to constrain how Pluto's surface has been modified and discussed the implications of these results on Pluto's geologic history. We showed that the Venera group has undergone the largest amount of degradation since it formed early in Pluto's history. The observed degradation is inconsistent with viscous relaxation alone, because larger craters are generally less degraded, and while escape-erosion will erase the smallest craters first, the rims should be the last feature to decay. The cause of this degradation is likely a combination of the two. Cthulhu Macula, within the Burney group, also shows a significant amount of crater degradation, but no volatile ices are present. The primary degradation process in this region appears to be relaxation, but the conditions that facilitated relaxation are unclear (e.g., heating in the past, tholin-water ice material properties, and/or insulation by the haze layer). In contrast to the degraded craters within Cthulhu Macula are the anomalously deep craters that extend into the Wright group, suggesting variations in material properties in this region. The rest of Pluto exhibits minimal degradation, even the ancient polar uplands. Overall, this array of degradational states suggests that volatile ice processes are not the only driver of crater degradation, with regions currently rich in

volatile ice appearing insignificantly degraded (i.e., the Hayabusa group). Nevertheless, this interpretation would be improved with a more robust understanding of how sublimation and relaxation act to modify craters, and how craters are formed in layered ice.

4.6 References

- Ahrens, C. J., and Chevrier, V. F. 2019. Compressional ridges on Baret Montes, Pluto as observed by New Horizons. *Geophys. Res. Lett.*, 46, 14328–14335.
- Bertrand, T., and Forget, F. 2016. Observed glacier and volatile distribution on Pluto from atmosphere-topography processes. *Nature*, 540, 86–89.
- Bertrand, T., Forget F., Umurhan, O. M., et al. 2018. The nitrogen cycles on Pluto over seasonal and astronomical timescales. *Icarus*, 309, 277–296.
- Bertrand T., Forget F., Umurhan O. M., et al. 2019. The CH₄ cycles on Pluto over seasonal and astronomical timescales. *Icarus*, 329, 148–165.
- Bierhaus, E. B., and Dones, L. 2015. Craters and ejecta on Pluto and Charon: Anticipated results from the New Horizons flyby. *Icarus*, 246, 165–182.
- Binzel, R. P., Earle, A. M., Young, L. A., et al. 2017. Climate zones on Pluto and Charon. *Icarus*, 287, 30–36, DOI: 10.1016/j.icarus.2016.1007.1023.
- Bray, V.J., Collins, G.S., Morgan, J.V.m and Schenk, P.M. 2008. The effect of target properties on crater morphology: Comparison of central peak craters on the Moon and Ganymede. *Meteoritics & Planetary Science*, 4312, pp.1979-1992. <https://doi.org/10.1111/j.1945-5100.2008.tb00656.x>
- Bray V. J., Schenk P. M., Melosh, H. J., Morgan, J. V., and Collins, G. S. 2012. Ganymede crater dimensions: Implications for central peak and central pit formation and development. *Icarus*, 217, 115–129, DOI: 10.1016/j.icarus.2011.10.004.
- Bray, V.J., Hagerty, J.J. and Collins, G.S. 2022. “False peak” creation in the Flynn Creek marine target impact crater. *Meteorit Planet Sci.* <https://doi.org/10.1111/maps.13822>
- Buhler, P.B., and Ingersoll, A.P. 2017. Sublimation Pit Distribution Indicates Convection Cell Surface Velocity of 10 Centimeters per Year in Sputnik Planitia, Pluto. In 48th Annual Lunar and Planetary Science Conference, No. 1964, p. 1746.

- Collins, G.S., Kenkmann, T., Osinski, G.R., and Wünnemann, K. 2008. Mid-sized complex crater formation in mixed crystalline-sedimentary targets: Insight from modeling and observation. *Meteoritics & Planetary Science*, 4312, pp.1955-1977.
- Cook, A., Oberst, J., Roatsch, T., Jaumann, R., Acton, C. 1996. Clementine imagery: selenographic coverage for cartographic and scientific use. *Planet. Space Sci.* 44, 1135–1148.
- Cruikshank, D. P., Materese, C. K., Pendleton, Y. J., et al. 2019a. Prebiotic chemistry of Pluto. *Astrobiology*, 197, 831–848.
- Cruikshank, D. P., Umurhan, O. M., Beyer, R. A., et al. 2019b. Recent cryovolcanism in Virgil Fossae on Pluto. *Icarus*, 330, 155–168.
- Cruikshank, D. P., Grundy, W. M., Protopapa, S., Schmitt, B., and Linscott, I. R. 2021. Surface composition of Pluto. In *The Pluto System After New Horizons*, pp. 165–193. Univ. of Arizona, Tucson, DOI: 10.2458/azu_uapress_9780816540945-ch009.
- Dombard, A. J., and McKinnon, W. B. 2006. Elastoviscoplastic relaxation of impact crater topography with application to Ganymede and Callisto. *J. Geophys. Res.*, 111, E01001, DOI: 10.1029/2005JE002445.
- Earle, A. M., Binzel, R. P., Young, L. A., et al. 2017. Long-term surface temperature modeling of Pluto. *Icarus*, 287, 37–46.
- Earle, A. M., Grundy, W., Howett, C. J. A., et al. 2018. Methane distribution on Pluto as mapped by the New Horizons Ralph/MVIC instrument. *Icarus*, 314, 195–209.
- Earle, A.M., Binzel, R.P., Keane, J.T., et al. 2022. Tracing seasonal trends across Pluto's craters: New Horizons Ralph/MVIC results. *Icarus*, 373, p.114771. <https://doi.org/10.1016/j.icarus.2021.114771>
- Eluszkiewicz, J., and Stevenson, D. J. 1990. Rheology of solid methane and nitrogen: Applications to Triton. *Geophys. Res. Lett.*, 17, 1753–1756.

- Forget, F., Bertrand, T., Vangvichith, M., et al. 2017. A post-New Horizons global climate model of Pluto including the N₂, CH₄, and CO cycles. *Icarus*, 287, 54–71.
- Forsberg-Taylor, N. K., Howard, A. D., and Craddock, R. A. 2004. Crater degradation in the Martian highlands: Morphometric analysis of the Sinus Sabaeus region and simulation modeling suggest fluvial processes, *J. Geophys. Res.*, 109, E05002, doi:10.1029/2004JE002242.
- Grundy, W. M., Binzel, R. P., Buratti, B. J., et al. 2016. Surface compositions across Pluto and Charon. *Science*, 3516279, aad9189.
- Grundy, W. M., Bertrand, T., Binzel, R. P., et al. 2018. Pluto's haze as a surface material. *Icarus*, 314, 232–245.
- Hedgepeth, J.E., Buffo, J.J., Chivers, C.J., Neish, C.D., and Schmidt, B.E. 2022. Modeling the Distribution of Organic Carbon and Nitrogen in Impact Crater Melt on Titan. *The Planetary Science Journal*, 3, p.51.
- Hedgepeth, J. E., Neish, C. D., Turtle, E. P., et al. 2020. Titan's impact crater population after Cassini. *Icarus*, 344, 113664.
- Howard, A.D., Moore, J.M., Schenk, P.M., White, O.L. and Spencer, J. 2012. Sublimation-driven erosion on Hyperion: Topographic analysis and landform simulation model tests. *Icarus*, 2201, pp.268-276.
- Howard, A. D., Moore, J. M., Umurhan, O. M., et al. 2017a. Present and past glaciation on Pluto. *Icarus*, 287, 287–300.
- Howard, A. D., Moore, J. M., White, O. L., et al. 2017b. Pluto: Pits and mantles on uplands north and east of Sputnik Planitia. *Icarus*, 293, 218–230.
- Johnson P. E., Young L. A., Protopapa S., et al. 2021, Modeling Pluto's minimum pressure: Implications for haze production. *Icarus*, 356, 114070.
- Kamata, S., and Nimmo, F. 2014, Impact basin relaxation as a probe for the thermal history of Pluto. *J. Geophys. Res.–Planets*, 119, 2272–2289.

- Keane, J.T. and Matsuyama, I., 2016, March. Pluto followed its heart: True polar wander of Pluto due to the formation and evolution of Sputnik Planum. In 47th Annual Lunar and Planetary Science Conference (No. 1903, p. 2348).
- Kenkmann, T., Poelchau, M.H., and Wulf, G. 2014, Structural geology of impact craters. *Journal of Structural Geology*, 62, pp.156-182. <https://doi.org/10.1016/j.jsg.2014.01.015>
- Kring, D.A. 2007, Guidebook to the geology of barringer meteorite crater, arizona aka Meteor Crater. p. 150. Houston: Lunar and Planetary Institute.
- Lewis, B. L., Stansberry, J. A., Holler B. J., et al. 2021, Distribution and energy balance of Pluto's nitrogen ice, as seen by New Horizons in 2015. *Icarus*, 356, 113633.
- Lorenz, R.D., Turtle, E.P., Barnes, J.W., et al. 2018, Dragonfly: A rotorcraft lander concept for scientific exploration at Titan. *Johns Hopkins APL Technical Digest*, 343, p.14.
- Lorenz, R.D., MacKenzie, S.M., Neish, C.D., et al. 2021, Selection and Characteristics of the Dragonfly Landing Site near Selk Crater, Titan. *The Planetary Science Journal*, 21, p.24.
- McGovern Jr, P.J., White, O.L. and Schenk, P., 2020, December. Global Tectonics of Pluto: The Roles of Basin Infill Loading and True Polar Wander. In AGU Fall Meeting Abstracts (Vol. 2020, pp. P031-08).
- McKinnon, W. B., Nimmo, F., Wong, T., et al. 2016, Convection in a volatile nitrogen-ice-rich layer drives Pluto's geological vigour. *Nature*, 534, 82–85.
- McKinnon, W. B., Schenk, P. M., Bland, M. T., et al. 2018, Pluto's heat flow: A mystery wrapped in an ocean inside an ice shell. In *Lunar and Planetary Science XLIX*, Abstract #2715. LPI Contribution No. 2083, Lunar and Planetary Institute, Houston.
- McKinnon, W.B., Glein, C.R., Bertrand, T. and Rhoden, A.R. 2021, Formation, Composition, and History of the Pluto System: A Post-New-Horizons Synthesis.

The Pluto System After New Horizons, pp. 507–543. Univ. of Arizona, Tucson, DOI: 10.2458/azu_uapress_9780816540945-ch022.

Melosh, H. J. 1989, *Impact Cratering: A Geologic Perspective*. Oxford Univ., New York. 245 pp.

Moore, J. M., Mellon, M. T., and Zent, A. P. 1996, Mass wasting and ground collapse in terrains of volatile-rich deposits as a solar systemwide geological process: The pre-Galileo view. *Icarus*, 122, 63–78.

Moore, J. M., Asphaug, E., Morrison, D., et al. 1999, Mass movement and landform degradation on the icy Galilean satellites: Results of the Galileo nominal mission. *Icarus*, 140, 294–312.

Moore, J. M., Howard, A. D., Schenk, P. M., et al. 2015, Geology before Pluto: Pre-encounter considerations. *Icarus*, 246, 65–81.

Moore, J. M., McKinnon, W. B., Spencer, J. R., et al. 2016, The geology of Pluto and Charon through the eyes of New Horizons. *Science*, 3516279, 1284-1293.

Moore, J. M., Howard, A. D., Umurhan, O. M., et al. 2017, Sublimation as a landform-shaping process on Pluto. *Icarus*, 287, 320–333, DOI: 310.1016/j.icarus.2016.1008.1025.

Moore, J. M., and Howard, A. D. 2021, The landscapes of Pluto as witness to climate evolution. In *The Pluto System After New Horizons*. pp. 105–120. Univ. of Arizona, Tucson, DOI: 10.2458/azu_uapress_9780816540945-ch006.

Neish, C.D., Somogyi, Á., and Smith, M.A. 2010, Titan's primordial soup: formation of amino acids via low-temperature hydrolysis of tholins. *Astrobiology* 10, 337–347.

Neish, C.D., Kirk, R.L., Lorenz, R.D., et al. 2013, Crater topography on Titan: Implications for landscape evolution. *Icarus*, 2231, pp.82-90.

Neish, C.D., Molaro, J.L., Lora, J.M., et al. 2016, Fluvial erosion as a mechanism for crater modification on Titan. *Icarus*, 270, pp.114-129.

- Neish, C.D., Lorenz, R.D., Turtle, E.P., et al. 2018. Strategies for detecting biological molecules on Titan. *Astrobiology*, 185, pp.571-585.
- Nimmo, F., and McKinnon, W.B. 2021, Geodynamics of Pluto. *The Pluto System After New Horizons*, pp. 89–103. Univ. of Arizona, Tucson, DOI: 10.2458/azu_uapress_9780816540945-ch005.
- Osinski, G.R., and Pierazzo, E. 2012, *Impact cratering: Processes and products*. John Wiley & Sons.
- Parmentier, E., and Head, J. 1981, Viscous relaxation of impact craters on icy planetary surfaces: Determination of viscosity variation with depth. *Icarus*, 47, 100-111.
- Pierazzo, E., Vickery, A.M., and Melosh, H.J. 1997, A reevaluation of impact melt production. *Icarus*, 1272, pp.408-423.
- Protopapa, S., Grundy, W. M., Reuter, D. C., et al. 2017, Pluto's global surface composition through pixel-by-pixel Hapke modeling of New Horizons Ralph/LEISA data. *Icarus*, 287, 218–228.
- Robbins, S.J., Antonenko, I., Kirchoff, M.R., et al. 2014, The variability of crater identification among expert and community crater analysts. *Icarus*, 234, pp.109-131.
- Robbins, S.J., Singer, K.N., Bray, V.J. 2017, Craters of the Pluto-Charon system. *Icarus*, 287, 187–206. DOI: 10.1016/j.icarus.2016.09.027.
- Robbins, S.J., Watters, W.A., Chappelow, J.E., et al. 2018, Measuring impact crater depth throughout the solar system. *Meteoritics & Planetary Science*, 534, pp.583-637.
- Robbins, S.J., Schenk, P.M., Riggs, J.D., et al. 2021, Depths of Pluto's and Charon's craters, and their simple-to-complex transition. *Icarus*, 356, p.113902.
- Rubincam, D.P., 2003. Polar wander on Triton and Pluto due to volatile migration. *Icarus*, 163(2), pp.469-478.

- Sagan, C., and Khare, B. N. 1979, Tholins: Organic chemistry of interstellar grains and gas. *Nature*, 277, 102–107.
- Schenk, P.M. and Zahnle, K. 2007, On the negligible surface age of Triton. *Icarus*, 192, 135–149.
- Schenk, P. M., Beyer, R. A., McKinnon, W. B., et al. 2018, Basins, fractures, and volcanoes: Global cartography and topography of Pluto from New Horizons. *Icarus*, 314, 400–433.
- Schenk, P.M., Beddingfield, C.B., Bertrand, T., et al. 2021. Triton: Topography and Geology of a Probable Ocean World with Comparison to Pluto and Charon. *Remote Sensing*, 13, p.3476.
- Schurmeier, L.R., and Dombard, A.J. 2018, Crater relaxation on Titan aided by low thermal conductivity sand infill. *Icarus*, 305, pp.314-323.
- Senft, L.E., and Stewart, S.T. 2007, Modeling impact cratering in layered surfaces. *Journal of Geophysical Research: Planets*, 112.
- Senft, L.E., and Stewart, S.T. 2008, Impact crater formation in icy layered terrains on Mars. *Meteoritics & Planetary Science*, 43, pp.1993-2013.
- Senft, L. E. and Stewart, S.T. 2011, Modeling the morphological diversity of impact craters on icy satellites, *Icarus*, 214, 67-81. 10.1016/j.icarus.2011.04.015
- Shoemaker, E.M., Kieffer, S.W., and Sutton, R.L. 1974, Guidebook to the geology of Meteor Crater, Arizona. Guidebook, pp.i-66.
- Silber, E. A., Osinski, G. R., Johnson, B. C., & Grieve, R. A. (2017). Effect of impact velocity and acoustic fluidization on the simple-to-complex transition of lunar craters. *Journal of Geophysical Research: Planets*, 122(5), 800-821.
- Silber, E. A., Johnson, B. C., Bjornes, E., MacGregor, J. A., Larsen, N. K., & Wiggins, S. E. (2021). Effect of ice sheet thickness on formation of the Hiawatha impact crater. *Earth and Planetary Science Letters*, 566, 116972.

- Singer, K. N., McKinnon, W. B., Gladman, B., et al. 2019, Impact craters on Pluto and Charon indicate a deficit of small Kuiper belt objects. *Science*, 363, 955–959.
- Singer, K. N., Greenstreet, S., Schenk, P. M., Robbins, S. J., and Bray, V. J. 2021, Impact craters on Pluto and Charon and terrain age estimates. In *The Pluto System After New Horizons*. DOI: 10.2458/azu_uapress_9780816540945-ch007.
- Singer, K.N., White, O.L., Schmitt, B., et al. 2022, Large-scale cryovolcanic resurfacing on Pluto. *Nat Commun* 13, 1542. <https://doi.org/10.1038/s41467-022-29056-3>
- Stern, S. A., Porter S., and Zangari, A. 2015a, On the roles of escape erosion and the viscous relaxation of craters on Pluto. *Icarus*, 250, 287–293.
- Stern, S. A., Bagenal, F., Ennico, K., et al. 2015b, The Pluto system: Initial results from its exploration by New Horizons. *Science*, 350, aad1815.
- Stern, S.A., White, O.L., McGovern, P.J., et al. 2021, Pluto's far side. *Icarus*, 356, p.113805.
- Stern, A., 2018, V1.0. NASA Planetary Data System.
- Stansberry, J. A., Spencer, J. R., Schmitt, B., et al. 1996, A model for the overabundance of methane in the atmospheres of Pluto and Triton. *Planet. Space Sci.*, 44, 1051–1063.
- Umurhan, O.M., Ahrens, C.J., and Chevrier, V.F. 2021, Rheological and Thermophysical Properties and Some Processes Involving Common Volatile Materials Found on Pluto's Surface. *The Pluto System After New Horizons*, pp. 195–255. Univ. of Arizona, Tucson, DOI: 10.2458/azu_uapress_9780816540945-ch010.
- Weaver, H.A., Gibson, W.C., Tapley, M.B., Young, L.A., Stern, S.A. 2008, Overview of the New Horizons Science Payload. *Space Science Reviews* 140,75{91.doi:10.1007/s11214-008-9376-6, arXiv:0709.4261.
- White, O. L., Moore, J. M., Howard, A. D., et al. 2019, Washboard and fluted terrains on Pluto as evidence for ancient glaciation. *Nature Astron.*, 3, 62–68.

- White, O. L., Moore, J. M., Howard, A. D., et al. 2021, The geology of Pluto. In *The Pluto System After New Horizons*, pp. 55–87. Univ. of Arizona, Tucson, DOI: 10.2458/azu_uapress_9780816540945-ch004.
- Yamashita, Y., Kato, M., and Arakawa, M. 2010, Experimental study on the rheological properties of polycrystalline solid nitrogen and methane: Implications for tectonic processes on Triton. *Icarus*, 207, 972–977.
- Young, L. A., Bertrand, T., Trafton, L. M., et al. 2021, Pluto’s volatile and climate cycles on short and long timescales. In *The Pluto System After New Horizons*, pp. 321–361. Univ. of Arizona, Tucson, DOI: 10.2458/azu_uapress_9780816540945-ch014.

Chapter 5

5 Discussions and Conclusions

5.1 Discussion

In this work, we have investigated the role of carbon- and nitrogen-containing molecules on the geology and astrobiology of icy bodies in the solar system. We focused on the icy bodies Pluto and Titan because they are rich in organic molecules, and these molecules play a unique and distinct role on each of these worlds. We began, in Chapter 2, by investigating the habitability of liquid impact melt on Titan and how organic molecules will become emplaced within the melt lens as it freezes (Hedgepeth et al., 2022). In Chapter 3, we expand on this problem to consider a more complex system where simple organic molecules are evolving into biomolecules. We study how quickly the biomolecules become detectable by the Dragonfly mission for a variety of hydrolysis scenarios. In Chapters 2 and 3, we use our results to guide Dragonfly in where to target for samples of astrobiological interest at Titan. In Chapter 4, we transition to Pluto to study the degradation of its surface, as it is reflected in Pluto's crater population, and how volatile nitrogen and methane ice affect the crater morphology.

5.1.1 The emplacement of organics into a freezing ice layer.

In Chapters 2 and 3, we studied the entrapment of organics into a freezing melt lens on Titan by adapting a model that was originally designed for sea ice and later adapted to study European ice (Buffo et al., 2018, 2020; Chivers et al., 2021; Hedgepeth et al., 2022). We began our study using HCN as a representative molecule of the larger population of organics that will exist in the Titan melt. This work, with its focus on HCN, was presented as a first order approximation of the freezing of organics into the ice as the melt lens froze. A Titan melt lens, however, is likely to be much more chemically complex, both initially and through time. The composition of the surface organics on Titan is not well constrained (Lorenz et al., 2008), but the atmosphere is known to have a wide range of organic molecules (Krasnopolsky, 2014; Vuitton et al., 2014). HCN is among the ten most abundant of these organics. There is also existing laboratory work that constrains 1) the chemical properties that are needed to use HCN in the sea ice model and 2) the yields of

biomolecules when it hydrolyzes in water (Hartshorne, 1931; Ferris et al., 1973, 1974, 1978; Haynes, 2011). The chemical properties of the impurity in the water are a key component needed to model how the organic becomes emplaced into the ice, and the lack of experimental constraints on the chemical properties of complex mixtures is a major reason why we do not consider mixtures in our work (Buffo et al., 2018, 2020).

There are larger questions to be answered about how a mixture of impurities will freeze into ice. The terrestrial analogue that our work is built on, while composed of multiple salts, models a single salt at a time (Buffo et al., 2018, 2020; Chivers et al., 2021). Questions remain about whether the presence of one salt effects the emplacement of another, or if the salts will all be driven by the bulk properties of the mixture. The mechanism of emplacement implies it should be driven by bulk properties (Feltham et al., 2006; Buffo et al., 2018, 2020). As the water ice lattice forms, the impurities and the remaining liquid fraction of the melt become concentrated into centimeter scale veins that eventually become pockets once a critical porosity is reached (~ 0.05). Until critical porosity is met, the impurity rich liquid fraction can freely flow out of the ice, into the melt lens, driven by the physics of the sea ice model. The process is therefore not happening on the molecular level, so it is likely driven by the bulk properties of the mixture. This suggests that studying a single organic is likely a good proxy for a more complex mixture.

The system is made even more complex as the chemistry (and the properties of the mixture) will evolve through time. It is even more difficult to constrain the chemical properties of an evolving mixture because the chemical properties will become time dependent. Instead, we consider glycine in contrast to HCN to demonstrate how two very different chemistries can affect the emplacement process. The buoyancy differences between the two organics and water drive the forces that determine the pattern of emplacement, and each work as proxies of two possible mixtures (i.e., one that is either more or less buoyant than water). We use glycine in this work because it is a major byproduct of HCN hydrolysis (Ferris et al., 1973, 1974, 1978; Cleaves et al. 2014; Hörst et al., 2017; Lee and Choe, 2017).

In the last stage of this work, we consider how hydrolysis will affect the concentration of the parent and daughter products, with HCN and glycine acting as proxies

for each respectively. Two melt lenses are modeled independently, one with HCN and the other with glycine. There is no assumed mixing of chemistry (and the consequential changing of the chemical properties), but the two systems are connected by the estimated loss of HCN and the subsequent gain of glycine in each system. The ultimate result illustrates how quickly biomolecules will become detectable by the Dragonfly spacecraft (at >500 parts per billion, ppb). Furthermore, the relative abundance of HCN and glycine in each system reflects how the chemical properties of the mixture will shift as HCN hydrolyses to form glycine.

The emplacement of the organics studied in this work follow similar patterns but are inverted based on the buoyancy of the organic. We found that the inversion occurs about 75% into the depth of the melt sheet, where the highest concentration of organic is found for both glycine and HCN. However, the position of maximum concentration will vary depending on the initial conditions of the melt lens. Warmer melt than what we modeled ($>0^{\circ}\text{C}$) and warmer basal ice (from heating during impact) will slow the freezing at the base. Even with a melt of 0°C and ice assumed not be heated (i.e., 94 K), the heat loss at the surface is much higher because it is exposed to the atmosphere where the temperature remains 94 K while the underlying ice quickly becomes warmer insulating ice. This suggests the highest concentration will be shifted even further into the original depth of the melt lens. However, if a methane clathrate layer were to form at the surface of the melt, it would increase the insulation of the melt from the atmosphere, and the highest concentration would be shifted toward the surface. Outside of the most concentrated region, the patterns of HCN and glycine are inverted, with the highest concentrations of HCN being near the surface and the highest concentrations of glycine being near the base. When buoyancy is driving the organic out of the ice (i.e., at the base for HCN and at the upper boundary for glycine), the concentration of organics in the ice is on the order of 1-10 parts per thousand (ppt). The precise amount varies, with higher thermal gradients producing higher concentrations in the ice, but even at the same thermal gradients and melt concentrations, there is variation between glycine and HCN because the other thermal chemical properties (beyond buoyancy) effect the emplacement process as well.

The addition of hydrolysis does not affect this overall pattern of emplacement in most cases. Even for large half-lives (the time taken for half of the HCN to hydrolyze into glycine), a detectable fraction of HCN undergoes hydrolysis almost immediately, unless the melt lens lacks a minimum concentration of HCN. We consider that minimum concentration (c) as a function of the initial concentration, because it is not well constrained. At the temperatures (up to boiling) in the melt, c is likely to be small compared to the concentrations of HCN and other parent products that we predict to be in the melt (Artemieva and Lunine, 2005; Krasnopolsky, 2014; Vuitton et al., 2014; Hedgepeth et al., 2022). If the volume of melt is much higher than expected (Wakita et al., 2022), the initial concentrations may be lower because the HCN and other organics become more diluted at the start of the melt. However, in **Chapter 2**, we estimate that HCN would still be on the order of parts per thousand even in the most liberal melt estimates by Artemieva and Lunine (2005). Assuming this is still above the critical concentration needed for HCN to hydrolyze, our results suggest even long half-lives (i.e., $\tau = 50$ yrs.) will produce glycine at 2 to 3 orders of magnitude below the concentration of HCN within the first meter of ice freezing. This equates to glycine concentrations of 10^{-3} ppt or higher in the melt (if we assume initial concentration of ~ 1 ppt HCN), which would likely result in negligible rejection of glycine from the ice, even at the top of the melt sheet, because we have shown how glycine will freeze into the ice at about the melt concentration when the melt concentration is $\ll 1$ ppt.

5.1.2 Impact Crater Degradation on Pluto

In Chapter 4, we studied the degradation of craters on Pluto to improve our understanding of the geologic history of Pluto. Crater morphology provides a reflection of how the surface is changing; the extent of surface modification can be constrained, quantitatively, by calculating the deviation of the crater morphology from pristine crater morphology. Robbins et al. (2021) used the population of pristine craters to ascertain the depth to diameter relationship of fresh craters on Pluto. Unlike similar work (e.g., Neish et al., 2013; Hedgepeth et al., 2020) we don't have to use crater depths from an analogue world, removing one source of error. However, our work is limited by a stereophotogrammetric DEM with high levels of vertical error in places (Schenk et al.,

2018). While this error is unavoidable, such error is generally systematic, so the localized relative depths we take are assumed to be representative of the degradation in the region.

We began by identifying all the complex craters in the region with topography (i.e., the nearside, Schenk et al., 2018), setting a threshold diameter of 15 km to avoid craters in the transition zone (the transition from simple to complex craters is ~ 13 km on Pluto, Robbins et al., 2021). Once identified, we used the 8-profile technique to measure the crater morphology. This technique uses 8 topographic profiles taken through the center of the crater, up to 5 radii from the crater center (Bray et al., 2012; Hedgpeeth et al., 2020). The crater depth is measured on each side of each profile, thus producing 16 measurements for the radius, rim height, and depths, with the final measurements taken as the average of each. Once the depths are measured, the relative depth is taken by comparing the crater depth to the expected depth of a crater of that size ($R(D) = 1 - \frac{d_{Pluto}(D)}{d_{pristine}(D)}$). Relative depth measures whether a crater is entirely degraded ($R = 1$) versus one that is entirely pristine ($R = 0$). We present our results in terms of relative depth because it allows for us to extract regional trends, where the intent of degradation is more reflective than the raw depth measurement, which can vary significantly with diameter. However, it should be noted that the pristine crater depth may vary depending on the surface composition and crater velocity.

We approached this problem under the assumption that increased volatile activity would produce more degradation. Our biggest finding is that the causes of degradation seem to be much more nuanced than first assumed. The Venera group is a region where a thick mantle (i.e., layer) of volatile ice has been proposed (Howard et al., 2017, and our results supports our original hypothesis with significant levels of degradation, specifically within Vega Terra. We consider several possible causes, each suggestive of a different geologic history. We find that viscous relaxation is not consistent with our observations because the smallest craters show the highest levels of degradation, even though smaller features should be the most resistant to relaxation. The degraded rims observed there are inconsistent with both relaxation and escape erosion but may be a result of the volatile ice mantle limiting the deposition of rim and ejecta material during formation, like terrestrial marine craters (Bray et al., 2022). Outside of Venera group, there is not as strong

connection between volatile ice and crater degradation. There are two lines of evidence that suggest the degradation cause is more complicated: 1) there is a lack of significant degradation in the other significantly mantled group, Hayabusa, and 2) there is significant degradation of craters within Cthulhu Macula, where there is minimal evidence of significant mantling.

Cthulhu Macula, located in the southern Burney Group, is the next most degraded region. However, the degradation is not clustered in a specific region, as it is in Vega Terra. In fact, Cthulhu Macula exhibits the highest variance in crater degradation followed by the Venera group. This variance may speak to the rate of degradation, where slow degradation would produce high variance on an ancient surface and fast degradation of a young surface would have low variance. Cthulhu Macula's variance comes from a range of entirely degraded craters, partially degraded craters, and anomalously deep craters (i.e., they appear distinctly deeper than predicted for craters of that size, Robbins et al., 2021). The most degraded craters are a unique anomaly because the water ice crust that they formed in should not relax on the age of the solar system (Stern et al., 2015), nor should sublimation be affecting the morphology. It suggests some form of localized heating, perhaps tidally driven, to allow for relaxation to take place (McKinnon et al., 2021). Alternatively, the geologic past of Cthulhu Macula may be more complicated. This is evidenced by the broader trend of decreasing degradation from the southwest toward the southeast of Cthulhu Macula.

Recent work has suggested polar wander may have occurred after the formation of Sputnik basin, and this may have significantly altered the distribution of surface materials. Thus, the degradational trend may reflect the state of the surface before the polar wander event. Our work can only observe the region of the surface that was captured by New Horizons, but it suggests such a trend exists. Outside of Venera group and Cthulhu Macula, the level of degradation is surprisingly constant among the other groups. This suggests the extent of degradation is not directly related to the ages of the surface (Singer et al., 2019, 2021). If what we are observing is caused by polar wander, the similarities between the other groups may suggest they were under similar conditions before the event. The variance that is observed within each group may also be due to the superposition of craters formed

in different eras. However, the Sputnik impact is suggested to have occurred very early in the history of Pluto ($\geq 4 G.y.$, Singer et al., 2019, 2021), so unless the properties of the pre-polar wander surface is sustained, we should expect newer craters to begin to form representing the new surface conditions.

Overall, the patterns of degradation demonstrate that Pluto has a complex geologic history. It hints at localized events, particularly in Cthulhu Macula and Vega Tera, but the exact cause for the degradation is still not well constrained. More work is needed to understand the juxtaposition of the different factors modifying its surface.

5.2 Future Work

5.2.1 Experimental studies on organics in a Titan melt sheet

In this dissertation, I present HCN and glycine as representative, respectively, of the parent population of Titan organics and the daughter population of biomolecules that may form in the melt sheet on Titan. I demonstrate how these can guide Dragonfly in their mission, but there is much more work that can be done to prepare for the upcoming Dragonfly mission. Furthermore, the work I present here is applicable beyond Dragonfly, to any mission looking for biomolecules in the ice of an ocean world (e.g., Enceladus, Cable et al., 2021). I propose two main experimental investigations that need to be pursued: 1) testing the assumptions of the model, and 2) identifying the chemical properties of complex organic mixtures.

I first propose three of the major model assumptions are investigated. First, we assume buoyancy is the driving factor in the model. Just as it will drive out material at one boundary, it will hold it in place at the other boundary. It is important to demonstrate that this assumption is valid, especially for the chemistry that is being explored. In sea ice, buoyancy forces dominate, but other factors may dominate once the buoyancy of the impurity becomes approximately equal with that of water. In cases where buoyancy forces become negligible, it is important to understand the impact of the other forces (e.g., by volumetric changes or thermally induced convection forces, Buffo et al., 2018, 2021). Secondly, we assume that organic impurities will freeze like salty brine in terrestrial ice.

This should be reproducible experimentally. Furthermore, the scale and distribution of vein pockets should be studied to inform how Dragonfly samples the ice. Lastly, I have treated HCN and glycine as acting independent of one another, but it is likely that mixtures of impurities will be driven by the bulk properties of the mixture. This assumption should be investigated to understand whether the impurities will act as a bulk mixture in the ice or segregate. This directly impacts how a complex mixture would be modeled because it may require modeling individual chemistries rather than a bulk mixture if the impurities segregate. However, even if impurities segregate, the freezing temperature of the total mixture needs to be constrained.

The second piece of work I propose is that the chemical properties of complex Titan mixtures be constrained through further experimental work. There are limited constraints on the exact distribution of the chemistry that will exist within a Titan melt sheet, but Titan-like mixtures can be created. Even limited chemical properties of such mixtures would allow for more robust modeling. These properties are those outlined in Chapters 2 and 3, but the principal constraint needed is the freezing temperature of a mixture. Each mixture can be altered to study how the bulk properties are impacted by mixtures of parent and daughter products. These results would create a new parameter space of chemical properties for a mixture as a function of parent to daughter abundance. This approach will allow for more robust predictions and will reveal how significantly the chemical properties that dominate the freezing process would be altered by changes in the mixture composition.

Similar problems have been explored by others in the past. There is a breadth of work recreating terrestrial sea ice in the lab (Feltham et al., 2006; Worster and Rees Jones, 2015), and such experimental work can lay the groundwork for how to approach a Titan melt lens investigation. Similarly, existing experimental approaches exist to investigate chemical properties of organic-water mixtures (e.g., Coates and Hartshorne, 1931; Shimoyamada et al., 1994), but this work would be limited by the practicality of working with the toxic organics that likely exist on Titan. Fortunately, we would not need to recreate the extreme temperature conditions on Titan in the lab. The model is making predictions based only on the melt concentration and the thermal gradient when the ice freezes. The temperatures that will exist within the melt will be near or above the freezing temperature

of water, so most standard freezers would likely replicate the temperatures and thermal gradients that would exist at the ice-water boundary once significant insulation by freezing has occurred.

5.2.2 Modeling impacts into heterogeneous ice layers

In this work, I present the degradation of Pluto's craters and relate them to the types of processes that are modifying Pluto's surface. However, this work could be improved in two major ways: 1) understanding the morphology of craters that form in stratified ice layers, and 2) how relaxation, sublimation, and deposition combine to affect the morphology of craters. The first problem can be investigated using impact crater models that consider different types of ice. This type of work has been done for analogous scenarios (i.e., marine and impacts on Earth and Mars, Senft and Stewart, 2008; Silber et al., 2021; Bray et al., 2022), but it is not clear that these are perfect analogues for the stratified ices on Pluto, since the material properties are not the same. Furthermore, these problems should be considered for more complex ices, such as water ice mixed with nitrogen and/or methane (Cruikshank et al., 2021). The initial morphology is necessary to constrain the level of crater degradation, but it also lays the groundwork for the landscape modeling that I propose is needed to address the second major limitation of our work.

There is a unique combination of processes acting upon Pluto's surface, and landscape modeling would help constrain what processes could produce the types of morphologies that are observed on Pluto. Stern et al. (2015) studied how the crater population would be diminished by a combination of sublimation (i.e., escape erosion) and relaxation, but did not study the detailed morphology because they were only interested in the total crater count. However, the landscape evolution cannot be reduced to just studying erosion or relaxation of the ice because there may be variations of ice compositions and layer thicknesses that will affect the long-term modification of the crater. This highlights the importance of constraining the starting morphologies to adequately model the landscape's evolution. In principle, we know the shape of pristine craters on Pluto, but these assume the craters are forming into the same water-ice bedrock. Craters that form into different bedrock (that may vary by composition or internal structure) may form different pristine crater morphologies.

5.3 Conclusions

There are many ways carbon- and nitrogen-containing molecules can present themselves across the solar system. On Earth and Titan, nitrogen dominates the atmosphere, but beyond the ice giants, nitrogen begins to form as an ice. As carbon and nitrogen combine with each other and other atoms, more complex chemistry forms. From Earth to Pluto, these can lead to complex organics collecting in a planet's atmosphere and on its surface. These same worlds have an abundance of water, whether stored as ice or as an unstable liquid on its surface, and that draws the attention of astrobiologists interested in understanding the origin of life. Simultaneously, this prebiotic chemistry feeds into the geology that shapes these different planets, from the rivers of Titan to the meters thick haze layer on Pluto (and likely other Kuiper belt objects). In this work, we have studied the role of these organic molecules as both geologic agents and precursors to life. Furthermore, we have studied how the geology intersects with the origin of life to guide and inform future astrobiological missions.

NASA's Dragonfly mission is going to Titan, and we have presented evidence to guide the mission in its sampling strategy. We demonstrated how some molecules may be less accessible than others. Our results suggest that biomolecules will be present in detectable quantities within the first meter of the melt sheet. However, specific molecules may not be easy to detect if the parent products produce a wide range of daughter products that dilute the concentration of any one molecule. Therefore, deeper samples are more likely to have undergone advanced hydrolysis because more time has passed, and the samples will also become increasingly concentrated. Our results are a guide for Dragonfly, but more work is still needed to understand more complex systems. This will provide a more robust set of recommendations for Dragonfly, and it will enable the larger chemical system to be recreated based off the samples that are taken.

While we are unlikely to sample a Pluto impact crater melt lens, my Titan work is also applicable to Pluto. One of the many ways carbon and nitrogen rich molecules present themselves on Pluto is in the form of an organic haze in the atmosphere and as an organic

deposit in Cthulhu Macula (Cruikshank et al., 2019a, 2021). Craters that form in this region are likely to have the same temporary habitable environment conducive to the formation of biomolecules like they are hypothesized to on Titan, and there are also several suspected cryovolcanic flows around Cthulhu Macula that could be another environment where biomolecules could form (Cruikshank et al., 2019b; Singer et al., 2022). There is a very compelling case to be made to send a similar mission to Pluto where we could target Pluto's haze material and search for biomolecules in impact melt and cryovolcanic flows. Furthermore, the cryovolcanic flows may provide evidence of Pluto's ocean conditions (current or past) which is fascinating both geologically and astrobiologically. Such a mission would also reveal more about Pluto's geologic history.

I have outlined how Pluto's geologic history is much more complex than the depositional processes in Cthulhu Macula. Volatile ices form thin layers across the surface, and in localized regions, thicker deposits form. However, the degradation that we observe across the surface is not directly linked to the presence of volatile ice. There is, in fact, a longitudinal trend (west to east) of decreasing degradation that may have resulted from polar wander after the Sputnik impact. There is also no correlation between surface age and the level of degradation, which may be a product of the polar wander. Where there is high degradation, there is more variance that could be due to the superposition of more recent craters. However, our results are limited to the nearside of Pluto, and the data we use has large error in places. Nevertheless, our results provide constraints on how Pluto's surface is changing.

The work I have presented is only the beginning of an ongoing exploration of icy worlds. Our melt sheet results will inform not only Dragonfly, but any mission seeking to study biomolecules on the surface of icy worlds (e.g., Pluto, Enceladus, or Europa). It also highlights the areas where more work is needed leading up to these missions. While a mission to Pluto in the near future is unlikely, there are calls for missions to similar worlds orbiting the ice giants (e.g., Triton, National Academies of Sciences, Engineering, and Medicine, 2022). These missions can test the ideas explored in this work, but this work should also inform those missions on the type of questions that need to be studied more thoroughly (e.g., crater morphologies into volatile ice layers).

5.4 References

- Artemieva, N., Lunine, J.I., 2005. Impact cratering on Titan II. Global melt, escaping ejecta, and aqueous alteration of surface organics. *Icarus* 175, 522–533. <https://doi.org/10.1016/j.icarus.2004.12.005>
- Bray, V.J., Schenk, P.M., Melosh, H.J., Morgan, J.V. and Collins, G.S., 2012. Ganymede crater dimensions—Implications for central peak and central pit formation and development. *Icarus*, 217(1), pp.115-129.
- Bray, V.J., Hagerty, J.J. and Collins, G.S., 2022. “False peak” creation in the Flynn Creek marine target impact crater. *Meteoritics & Planetary Science*.
- Buffo, J., Schmidt, B., and Huber, C., 2018. Multiphase reactive transport and platelet ice accretion in the sea ice of McMurdo sound, Antarctica. *Journal of Geophysical Research: Oceans* 123, 324-345.
- Buffo, J., Schmidt, B., and Huber, C., Walker, C., 2020. Entrainment and dynamics of ocean-derived impurities within Europa’s ice shell. *Journal of Geophysical Research*. <https://doi.org/10.1002/essoar.10502079.2> .
- Cable, M.L., Porco, C., Glein, C.R., German, C.R., MacKenzie, S.M., Neveu, M., Hoehler, T.M., Hofmann, A.E., Hendrix, A.R., Eigenbrode, J. and Postberg, F., 2021. The science case for a return to Enceladus. *The planetary science journal*, 2(4), p.132.
- Chivers, C. J., Buffo, J. J., & Schmidt, B. E. (2021). Thermal and chemical evolution of small, shallow water bodies in Europa’s ice shell. *Journal of Geophysical Research: Planets* 126. <https://doi.org/10.1029/2020JE006692>.
- Cleaves, H. J., Neish, C., Callahan, M. P., Parker, E., Fernández, F. M., and Dworkin, J. P. (2014). Amino acids generated from hydrated Titan tholins: Comparison with Miller-Urey electric discharge products. *Icarus* 237:182–189.

- Coates, J.E., and Hartshorne, N.H., 1931. Studies on Hydrogen Cyanide. Part III. The Freezing Points of Hydrogen Cyanide-Water Mixtures. *Journal of Chemistry Society*, 657-665.
- Cruikshank, D. P., Materese, C. K., Pendleton, Y. J., et al. 2019a. Prebiotic chemistry of Pluto. *Astrobiology*, 197, 831–848.
- Cruikshank, D. P., Umurhan, O. M., Beyer, R. A., et al. 2019b, Recent cryovolcanism in Virgil Fossae on Pluto. *Icarus*, 330, 155–168.
- Cruikshank, D.P., Grundy, W.M., Protopapa, S., Schmitt, B. and Linscott, I.R., 2021. Surface composition of Pluto. *The Pluto System After New Horizons*, p.165.
- Feltham, D., Untersteiner, N., Wettlauger, J.S., Worster, M.G. , 2006. Sea ice is a mushy layer. *Geophysical Research Letters* 33, L14501. doi:10.1029/2006GL026290.
- Ferris, J.P., Donner, D.B. and Lobo, A.P., 1973. Possible role of hydrogen cyanide in chemical evolution: investigation of the proposed direct synthesis of peptides from hydrogen cyanide. *Journal of Molecular Biology*, 74(4), pp.499-510.
- Ferris, J.P., Wos, J.D., Ryan, T.J., Lobo, A.P. and Donner, D.B., 1974. Biomolecules from HCN. *Origins of life*, 5(1), pp.153-157.
- Ferris, J.P., Joshi, P.C., Edelson, E.H. and Lawless, J.G., 1978. HCN: A plausible source of purines, pyrimidines and amino acids on the primitive earth. *Journal of molecular evolution*, 11(4), pp.293-311.
- Haynes, W.M., 2011. *CRC Handbook of Chemistry and Physics*, (Internet Version 2011). Taylor Francis Group: Boca Raton, FL.
- Hedgpeeth, J.E., Neish, C.D., Turtle, E.P., Stiles, B.W., Kirk, R. and Lorenz, R.D., 2020. Titan's impact crater population after Cassini. *Icarus*, 344, p.113664.
- Hedgpeeth, J.E., Buffo, J.J., Chivers, C.J., Neish, C.D. and Schmidt, B.E., 2022. Modeling the Distribution of Organic Carbon and Nitrogen in Impact Crater Melt on Titan. *The Planetary Science Journal*, 3(2), p.51.

- Hörst, S.M., 2017. Titan's atmosphere and climate. *Journal of Geophysical Research: Planets* 122, 432–482. <https://doi.org/10.1002/2016JE005240>.
- Howard, A.D., Moore, J.M., White, O.L., Umurhan, O.M., Schenk, P.M., Grundy, W.M., Schmitt, B., Philippe, S., McKinnon, W.B., Spencer, J.R. and Beyer, R.A., 2017. Pluto: Pits and mantles on uplands north and east of Sputnik Planitia. *Icarus*, 293, pp.218-230.
- Krasnopolsky, V.A., 2014. Chemical composition of Titan's atmosphere and ionosphere: Observations and the photochemical model. *Icarus* 236, 83-91. <https://doi.org/10.1016/j.icarus.2014.03.041>.
- Lee, H.M. and Choe, J.C., 2017. Formation of glycine from HCN and H₂O: A computational mechanistic study. *Chemical Physics Letters*, 675, pp.6-10.
- Lorenz, R.D., Mitchell, K.L., Mitchell, K.L., Kirk, R.L., Hayes, A.G., Aharonson, O., Zebker, H.A., Paillou, P., Radebaugh, J., Lunine, J.I., Janssen, M.A., Wall, S.D., Lopes, R.M., Stiles, B., Ostro, S., Mitri, Giuseppe, Stofan, E.R., 2008. Titan's inventory of organic surface materials. *Geophys. Res. Lett.* 35, doi:10.1029/2007GL032118. L02206
- National Academies of Sciences, Engineering, and Medicine, 2022. *Origins, Worlds, and Life: A Decadal Strategy for Planetary Science and Astrobiology 2023-2032*. doi: <https://doi.org/10.17226/26522>.
- Neish, C.D., Kirk, R.L., Lorenz, R.D., Bray, V.J., Schenk, P., Stiles, B.W., Turtle, E., Mitchell, K., Hayes, A. and Cassini RADAR Team, 2013. Crater topography on Titan: Implications for landscape evolution. *Icarus*, 223(1), pp.82-90.
- Robbins, S.J., Singer, K.N., Bray, V.J., Schenk, P., Lauer, T.R., Weaver, H.A., Runyon, K., McKinnon, W.B., Beyer, R.A., Porter, S. and White, O.L., 2017. Craters of the Pluto-Charon system. *Icarus*, 287, pp.187-206.

- Robbins, S.J., Schenk, P.M., Riggs, J.D., Parker, A.H., Bray, V.J., Beddingfield, C.B., Beyer, R.A., Verbiscer, A.J., Binzel, R. and Runyon, K.D., 2021. Depths of Pluto's and Charon's craters, and their simple-to-complex transition. *Icarus*, 356, p.113902.
- Schenk, P.M., Beyer, R.A., McKinnon, W.B., Moore, J.M., Spencer, J.R., White, O.L., Singer, K., Nimmo, F., Thomason, C., Lauer, T.R. and Robbins, S., 2018. Basins, fractures and volcanoes: Global cartography and topography of Pluto from New Horizons. *Icarus*, 314, pp.400-433.
- Senft, L.E. and Stewart, S.T., 2008. Impact crater formation in icy layered terrains on Mars. *Meteoritics & Planetary Science*, 43(12), pp.1993-2013.
- Shimoyamada, M., Shibata, M., Ishikawa, K.I., Fukuta, Y., Ishikawa, S. and Watanaba, K., 1994. Freezing and eutectic points of an aqueous amino acid solution containing ethanol, and the effect of ethanol addition on the freeze concentration process. *Bioscience, biotechnology, and biochemistry*, 58(5), pp.836-838.
- Silber, E. A., Johnson, B. C., Bjonnes, E., MacGregor, J. A., Larsen, N. K., & Wiggins, S. E. (2021). Effect of ice sheet thickness on formation of the Hiawatha impact crater. *Earth and Planetary Science Letters*, 566, 116972.
- Singer, K.N., McKinnon, W.B., Gladman, B., Greenstreet, S., Bierhaus, E.B., Stern, S.A., Parker, A.H., Robbins, S.J., Schenk, P.M., Grundy, W.M. and Bray, V.J., 2019. Impact craters on Pluto and Charon indicate a deficit of small Kuiper belt objects. *Science*, 363(6430), pp.955-959.
- Singer, K.N., Greenstreet, S., Schenk, P.M., Robbins, S.J. and Bray, V.J., 2021. Impact craters on Pluto and Charon and terrain age estimates. *The Pluto System After New Horizons*, p.121.
- Singer, K.N., White, O.L., Schmitt, B., et al. 2022. Large-scale cryovolcanic resurfacing on Pluto. *Nat Commun* 13, 1542. <https://doi.org/10.1038/s41467-022-29056-3>
- Stern, S.A., Porter, S. and Zangari, A., 2015. On the roles of escape erosion and the viscous relaxation of craters on Pluto. *Icarus*, 250, pp.287-293.

- Vuitton, V., O. Dutuit, M. A. Smith, and N. Balucani, 2014. Chemistry of Titan's Atmosphere, in Titan, edited by I. Müller-Wodarg et al., Cambridge Univ. Press, Cambridge, U. K., 224– 271.
- Wakita, S., Johnson, B.C., Soderblom, J.M., Shah, J. and Neish, C.D., 2022. Methane-saturated layers limit the observability of impact craters on Titan. *The Planetary Science Journal*, 3(2), p.50.
- Worster, M. G., & Rees Jones, D. W. (2015). Sea-ice thermodynamics and brine drainage. *Philosophical Transactions of the Royal Society A*, 373(2045), 20140166. <https://doi.org/10.1098/rsta.2014.0166>

Curriculum Vitae
Josh Hedgepeth
 Department of Earth Sciences
 The University of Western Ontario
 1151 Richmond St, London, ON N6G 2V4

Education

- | | |
|-------------|--|
| 2018 – 2022 | University of Western Ontario
PhD Student in Geophysics and Planetary Science |
| 2016 – 2018 | University of Western Ontario
MSc. in Geophysics and Planetary Science |
| 2015 – 2016 | Georgia Institute of Technology
B.Sc. in Earth and Atmospheric Sciences |
| 2012 – 2015 | Georgia Institute of Technology
B.Sc. in Mechanical Engineering |

Professional Experience

- | | |
|------------------------------|---|
| January 2019 – April 2019 | Teaching Instructor
Department of Earth Sciences, University of Western Ontario |
| September 2016 – August 2022 | Graduate Research and Teaching Assistant
Department of Earth Sciences, University of Western Ontario |
| January 2015 – December 2016 | Undergraduate Teaching and Research Assistant
Department of Earth and Atmospheric Sciences,
Georgia Institute of Technology |

Field Experience

- | | |
|----------------|--|
| October 2018 | Course: Meteor Crater Field Course
<i>Location:</i> Barringer Meteorite Crater, Arizona, United States
<i>Features:</i> Impact Cratering |
| September 2017 | Course: Impact Cratering Short Course and Field School
<i>Location:</i> Sudbury, Ontario, Canada
<i>Features:</i> Impact cratering |
| May 2017 | Course: Planetary Surfaces Field School
<i>Location:</i> Arizona and Utah
<i>Features:</i> Impact cratering, volcanism, glaciation |

Conference Presentations

Hedgepeth, J. E. (2022, May). The Role of Hydrolysis in the

Emplacement of Organic Molecules in Impact Melt on Titan. In *AbSciCon* (No. 204-07).

Hedgepeth, J. E., Neish, C. D., & Bray, V. J. (2021, March). Nitrogen's Role in the

Degradation of Craters on Pluto. In *Lunar and Planetary Science Conference* (No. 2548, p. 2555).

Udell, K., Schmidt, B., Washam, P., Walker, C. C., **Hedgepeth, J. E.**, & Wood, A. G.

(2020, December). Constraints on the Hydrologic Systems of Three Tidewater Glaciers using High Temporal and Spatial Resolution Satellite Imagery. In *AGU Fall Meeting Abstracts* (Vol. 2020, pp. C043-0008).

Hedgepeth, J. E., Buffo, J., Neish, C., & Schmidt, B. (2021, October). Modeling the

Emplacement of Amino Acids in Impact Melt on Titan. In *AAS/Division for Planetary Sciences Meeting Abstracts* (Vol. 53, No. 7, pp. 405-07).

Hedgepeth, J. E., Buffo, J., Neish, C., Schmidt, B., & Chivers, C. (2020, December).

Tracking HCN Molecules in Crater Melt Ponds on Titan. In *AGU Fall Meeting Abstracts* (Vol. 2020, pp. P067-0012).

Hedgepeth, J. E., Buffo, J., Neish, C., Schmidt, B., Chivers, C. (2020, March). Tracking Organic Molecules in Crater Melt Ponds on Titan. *51st Annual Lunar and Planetary Science Conference* (Vol. 2020, pp. 2326).

Hedgepeth, J. E., Buffo, J., Neish, C., & Schmidt, B. (2020, October). Tracking HCN

Molecules in Crater Melt Ponds on Titan. In *AAS/Division for Planetary Sciences Meeting Abstracts* (Vol. 52, No. 408.04D).

Hedgepeth, J. E., Buffo, J., Neish, C., Schmidt, B., & Chivers, C. (2019, June).

Tracking HCN Molecules in Crater Melt Ponds on Titan. In *TEPS 2019 Summer School Workshop*.

Skills

MATLAB, Excel, ArcGIS, ISIS, JMars, Photoshop, Python, ENVI, LabVIEW, and Illustrator